UM-HSRI-76-11-2
Contract No. DOT-HS-4-00943

EFFECTS OF TIRE PROPERTIES ON TRUCK AND BUS HANDLING

R.D. Ervin
C.B. Winkler
J.E. Bernard
R.K. Gupta

Technical Final Report

June 1976

Highway Safety Research Institute
The University of Michigan

Prepared for:

National Highway Traffic Safety Administration
U. S. Department of Transportation

Prepared for the Department of Transportation, National Highway Traffic Safety Administration, under Contract No. DOT-HS-4-00943. The opinions, findings, and conclusions expressed in this publication are those of the authors and not necessarily those of the National Highway Traffic Safety Administration.

Technical Report Documentation Page

1. Report No.	2. Government Accession No.	3. Recipient's Catalog No.
UM-HSRI-76-11		

4. Title and Subtitle	5. Report Date
EFFECTS OF TIRE PROPERTIES ON TRUCK AND BUS HANDLING	June 1976
	6. Performing Organization Code
7. Author(s)	8. Performing Organization Report No.
R.D. Ervin, C.B. Winkler, J.E. Bernard, R.K. Gupta	UM-HSRI-76-11
9. Performing Organization Name and Address	10. Work Unit No. (TRAIS)
Highway Safety Research Institute The University of Michigan Huron Parkway & Baxter Road Ann Arbor, Michigan 48109	11. Contract or Grant No. DOT-HS-4-00943
	13. Type of Report and Period Covered Final Report 6/28/74 - 12/31/75
12. Sponsoring Agency Name and Address National Highway Traffic Safety Administration U. S. Department of Transportation Washington, D.C. 20590	14. Sponsoring Agency Code

15. Supplementary Notes

16. Abstract

The principal thrust of this project was to identify the importance of tire traction properties of truck tires in determining the steering and braking response of light and heavy commercial vehicles. The study generated a large quantity of parametric data describing the commercial vehicle and, especially, its tires. Tire tests on a large sample of light and heavy truck tires were conducted using two laboratory and one over-the-road tire test device. A computerized simulation study providing a mechanistic understanding of the response sensitivity of the open-loop vehicle to tire properties was conducted. Full-scale vehicle tests permitted validation of the simulation as reinforcement to the basic findings obtained through computerized analysis.

Findings of this study include the illumination of significant differences in the qualitative performance characteristics of truck tires relative to passenger car tires, and the manner in which these unique truck tire properties may affect the yaw stability of the commercial vehicle. Potential problems of vehicle stability were dramatically illustrated by a rollover incident which occurred during testing of a heavy truck.

17. Key Words	18. Distribution Statement
tires, heavy truck, light truck, van, bus, testing, parameters, simulation, stability, yaw divergence, rollover	Unlimited

19. Security Classif. (of this report)	20. Security Classif. (of this page)	21. No. of Pages	22. Price
None	None		

Form DOT F 1700.7 (8-72) Reproduction of completed page authorized

* U. S. GOVERNMENT PRINTING OFFICE : 1973 725-504/328

ACKNOWLEDGEMENTS

The Contract Technical Manager on this project was Mr. Lloyd Emery of NHTSA's Crash Avoidance Research Division. The subcontracted test program at the Texas Transportation Institute was directed by Mr. Monroe White. Testing of commercial vehicle tires on the Tire Research Facility of Calspan Corporation was arranged through Mr. King Bird. Mobile traction experiments conducted using the Dana Truck Test Center were arranged through Mr. Gary Franz. Computer simulation of truck and bus behavior at the Applied Physics Laboratory of Johns Hopkins University was directed by Mr. Paul Bohn.

Mr. J. Boissonneault of HSRI was responsible for preparation of vehicles employed in full-scale testing.

Mr. M. Deering was responsible for conduct of all mobile tire traction measurements, while Mr. D. Brown conducted all flat-bed (laboratory) traction measurements.

The processing of mobile traction data was the responsibility of Mr. C. MacAdam.

Tireless assistance in producing this report was provided by Ms. Jeannette Nafe.

Assistance and special cooperation in the conduct of this study was also received from the following organizations:

White Motors, Inc.
B. F. Goodrich Company
Greyhound Lines, Inc.
Motor Wheel Corporation
The Firestone Tire & Rubber Company
The Goodyear Tire & Rubber Company
Uniroyal, Inc.
Michelin Tire Company
The General Tire & Rubber Company

The Mobile Truck Tire Dynamometer, recently completed at HSRI and employed in this study, was constructed under support by the Motor Vehicle Manufacturers Association.

TABLE OF CONTENTS

1.0 INTRODUCTION

This document constitutes the final report on a research study entitled "Effects of Tire Properties on Truck and Bus Handling" which was conducted by the Highway Safety Research Institute of The University of Michigan. The study was supported by the National Highway Traffic Safety Administration of the U.S. Department of Transportation under contract DOT-HS-4-00943.

This research is based upon the application of the fundamentals of tire and vehicle mechanics to specific considerations of the control behavior of light and heavy commercial vehicles. In this regard, the tire properties of interest are those which determine shear forces and moments such as are generated during steering and braking maneuvers.

Shear force and moment properties, hereinafter referred to as "traction properties," are confined in definition, here, to highway operating conditions—specifically involving nondeformable pavement-type surfaces. Vehicle maneuvering conditions are not limited in their treatment and cover the full range from low-level path-keeping tasks to severe accident-avoidance maneuvers.

To the extent that this study examines vehicle maneuvering only in reference to the physical characteristics of the (open loop) tire/vehicle system, the term "handling" in the project title may be judged a misnomer since, to many, "handling" implies the closed-loop control performance of the driver/vehicle system. For the commercial vehicle very little, if indeed any, research has ever been reported describing examination of closed-loop behavior. This contrasts with a substantial, though by no means comprehensive, body of literature pertaining to passenger car handling.

Examination of the open-loop behavior of heavy commercial vehicles preceded the study reported here, particularly in the

form of a DOT-sponsored study entitled "Truck and Bus Handling" [1]* in which "handling" again was employed to title an investigation of open-loop properties. The "Truck and Bus Handling" study developed a set of heavy-vehicle test procedures which were employed in full-scale experiments conducted during the project reported here. As will be discussed in Section 4.0, the unplanned rollover of a large truck during application of these test procedures led to subsequent findings on truck yaw stability which are not known to have been reported previously.

The principal thrust of this project was to identify the importance of tire traction properties in determining the steering and braking responses of trucks and buses. To that extent, this study can be viewed as the extension, for commercial vehicles, of another recently completed DOT-sponsored project entitled "Effects of Tire Properties on Passenger Car Handling" [2]. The contrast between cars and trucks is indeed significant, however, despite a commonality in the basic physics involved. Since the commercial vehicle's mission implies that payload constitutes the raison d'etre for such vehicles, we find loaded-to-unloaded weight ratioes for heavy trucks, for example, to be on the order of 2:1 to 5:1 as compared to a 1.3:1 value of the same measure for a typical mid-sized passenger sedan. As will be shown, commercial vehicle payloads profoundly influence basic vehicle properties and impose severe demands on the performance of the commercial vehicle tire. Additionally, suspension and axle configuration differences between cars and trucks provide a number of contrasting mechanisms and levels of sensitivity which render the tire's role in the performance of the respective vehicle classes to be worthy of independent study.

In further contrast between passenger and commercial vehicle systems, it should be noted that the published data base describing the traction properties of car tires is immensely greater than

---

*Numbers in brackets refer to References listed at the end of this report.

that describing truck tires. Accordingly, it was necessary, in this study, to conduct a large number of truck tire measurements thereby establishing a data base for use in computerized simulations of truck and bus response. Thus, this report includes a body of findings which derive merely from examination of the substantial data base of traction properties which was gathered here.

The report is configured to provide, in Section 2.0, a summary of the various experimental and analytical methods employed, while detailed descriptions of methodology, simulation models, and test apparatus are presented in Appendices A, B, D, and H. Findings elucidating the basic traction properties of truck and bus tires are presented in Section 3.0, while detailed presentations of the overall traction data base are provided in Appendix C. Findings relating tire properties to commercial vehicle maneuvering behavior are presented in Section 4.0 as derived from the vehicle test data and from simulation results which are detailed in Appendices E and F, respectively.

2.0 RESEARCH METHODOLOGY

2.1 Introduction to the Methodology

The study was designed so as to generate a large quantity of parametric data describing commercial vehicles and, especially, their tires. The parameter measurements were obtained to permit a computerized simulation study which provides a mechanistic understanding of the response sensitivity of the open-loop vehicle to tire properties. Full-scale vehicle tests were also conducted to permit validation of the simulation and to provide a reinforcement, wherever possible, to the basic findings obtained through computerized analysis.

The focus of the study was on the commercial vehicle tire as a force and moment producing mechanism. Thus the relevant parametric characterizations derived from the use of traction testing apparatuses especially suited to measurement of the shear force and moment response of heavy tires. These test machines are comparable to apparatuses employed in the traction measurement of passenger car tires, but are appropriately scaled up in load capacities. Since machinery for measuring truck tire traction has only been available recently, the literature documenting such measurements is relatively scarce, thus the need in this study to obtain, through direct experiment, data exemplifying even the more fundamental truck tire properties.

Similarly, the mathematical modeling of a specific truck or bus requires that a large array of generally unavailable design parameters be obtained through direct measurement. Thus, various laboratory apparatuses were employed to directly measure inertial properties of the sprung and unsprung masses as well as the kinematic and compliance characteristics of steering and suspension systems.

Prediction of the nonlinear behavior of truck and bus vehicles is a sufficiently complex analytical task that only computerized calculations are feasible. Accordingly, two "state-of-the-art" simulations were employed to permit a general study of vehicle response sensitivities to tire properties and to provide a means for more specific investigation of truck directional stability.

In this section, methodologies which were employed in the study will be summarized. Appendices are provided later to document experimental and analytical methods in more detail.

2.2 Methods Employed to Measure Tire Traction Properties

Direct measurements of the traction characteristics of light and heavy commercial vehicle tires were obtained using three different test systems. Data obtained with each machine pertain to the shear force and moment response of the specimen tires under conditions of dry, uncontaminated, non-deformable surfaces. Two laboratory machines were employed; one a slow-speed device which was applied only to lateral traction properties, and the other a high-speed machine which was applied to both longitudinal and lateral, as well as combined slip, measurements. The third machine was a mobile device which traveled at highway-type speeds and measured both longitudinal and lateral traction properties.

The low-speed laboratory device was the HSRI flat-bed machine. Shown in Figure 2.1, this apparatus applies the specimen tire to a flat plank which traverses at a rate of 1.4 mph. The test tire is sustained at selected conditions of vertical load, F_z, slip angle, α, and inclination angle, γ, for both right-going and left-going passes of the bed. Insofar as the bed velocity is very low, the data obtained through flat-bed measurement is most suitable for that operating regime in which slip velocities are low. The traction behavior of tires at low values of slip is known

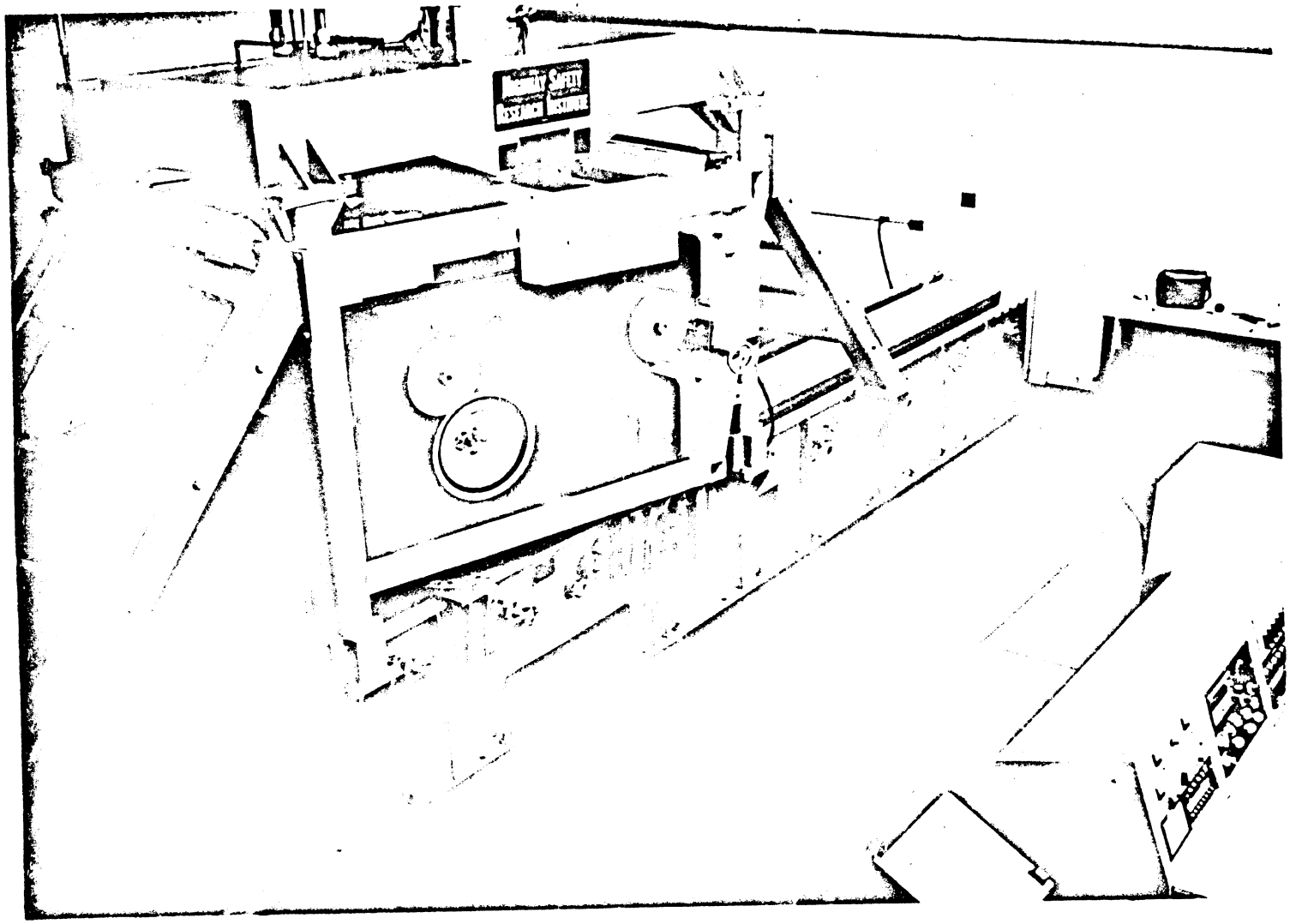

Figure 2.1. UCRI flat-bed tire tester.

to depend primarily upon the structural characteristics of carcass and tread while high slip behavior is principally a function of the frictional coupling between tire and roadway.

Thus, flat-bed measurement can be looked upon as primarily addressed to the examination of structural compliances such as are manifested in force and moment response to angular slip.

A total of 40 tires were tested on the flat-bed machine during this study. Each tire was subjected to a matrix of vertical load and slip angle conditions covering the full operating regime.

The flat-bed machine and each of the other tire test devices to be discussed are described in greater detail in Appendix B. Likewise, data deriving from flat-bed measurement and from application of each of the other test facilities will be summarized in Section 3.0 and presented in detail in Appendix C.

The Calspan Corporation's Tire Research Facility (TIRF) was employed in this study to provide measures of traction sensitivity to velocity and to examine combined slip properties. The TIRF machine, shown in Figure 2.2, employs a flat steel belt as the test surface while exposing the test tire to the desired conditions of slip, load, and velocity.

Two tire types were tested on the TIRF facility—providing a view of light and heavy tire velocity sensitivities as well as an indication of the extent to which such tires alter their traction behavior as a consequence of test-induced wear.

The tire test apparatus employed to measure traction properties "over-the-road" was the HSRI Mobile Truck Tire Dynamometer shown in Figure 2.3. This tractor-trailer device permits measurement of longitudinal behavior by way of the trailer-mounted fixture while lateral properties are obtained using an assembly mounted as an under-carriage to the tractor. As with laboratory machines, the mobile apparatus exposes the tire specimen to controlled

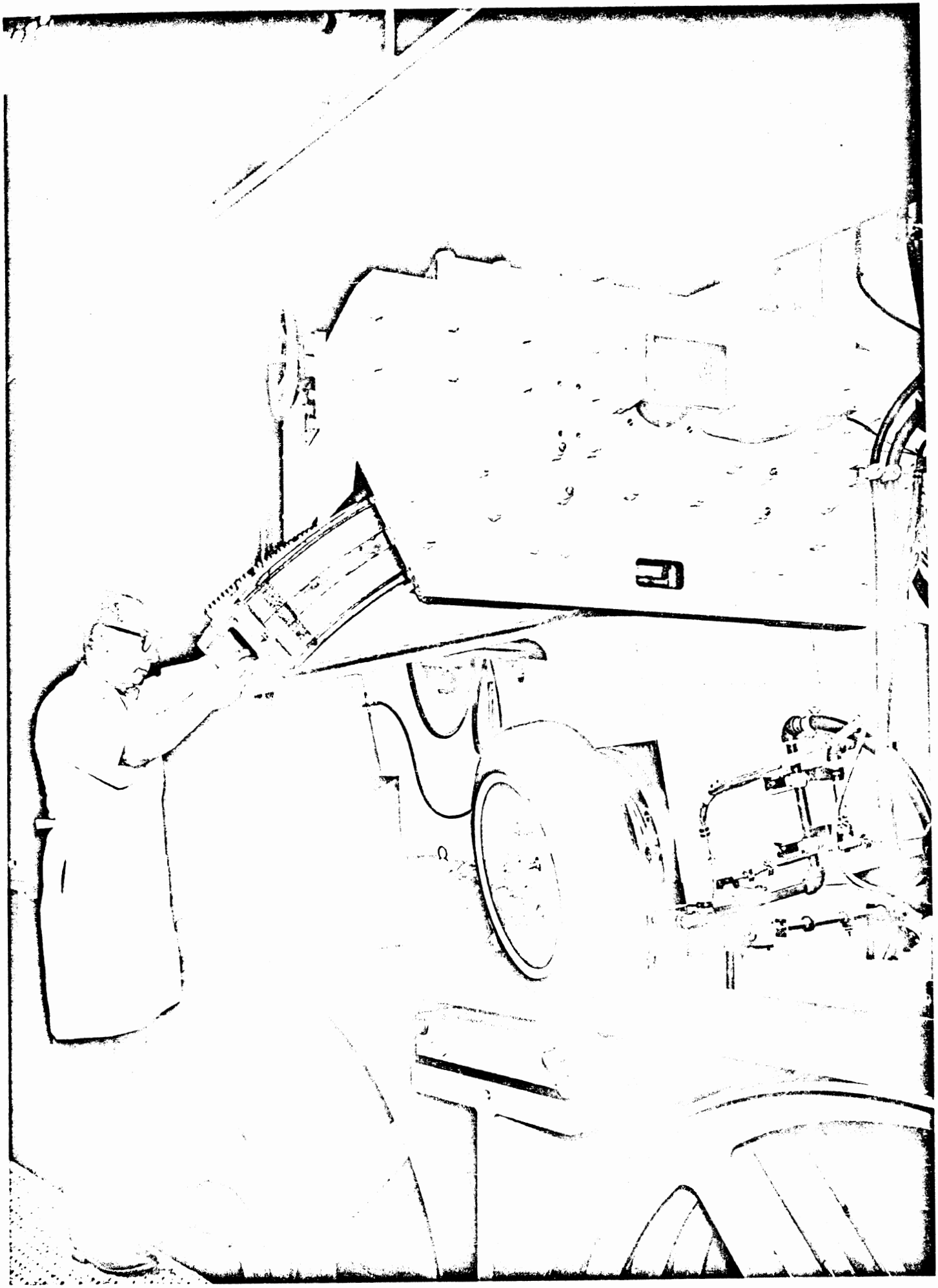

Figure 2.2. Calspan Corporation TIRF machine.

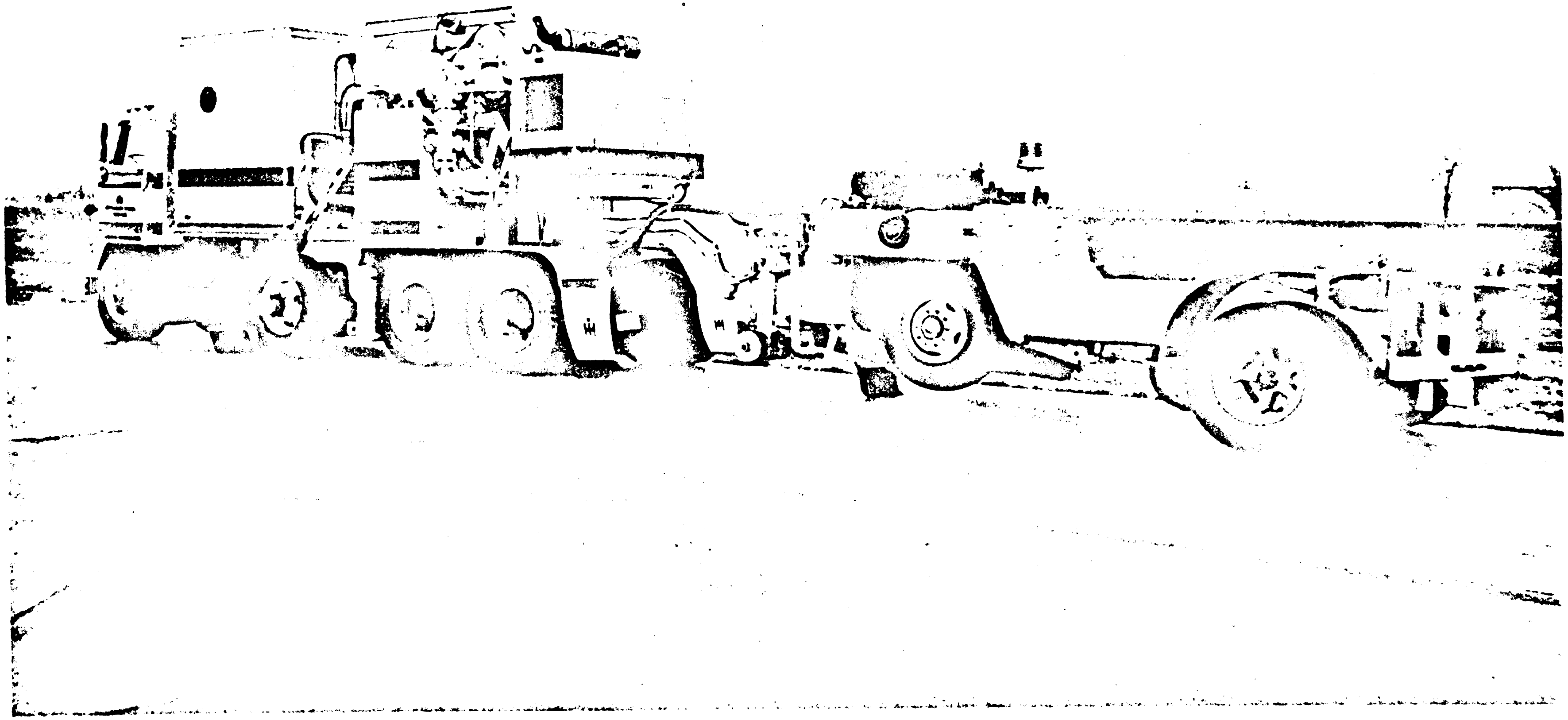

Figure 2. USAF Mobile Truck Fire Demonstrator

conditions of load, slip, and velocity, but with the added realism of representative road surfaces. Thus the device is particularly suited to the characterization of traction performance at elevated levels of slip—for which the frictional coupling between tire and pavement determines the level of developed shear forces.

A total of sixteen light and heavy truck tires were tested on the lateral traction machine and eight heavy tires were also examined in mobile longitudinal tests. All of these tires were mobile tested on the Portland cement concrete track at the Dana Truck Test Center in southeastern Michigan. Additionally, certain mobile tests were conducted at the Texas Transportation Institute (TTI) in order to characterize the surface on which vehicle tests were performed.

A major shortcoming of the tire test effort involved the inability of currently-available apparatuses to obtain a valid characterization of the combined slip behavior of commercial vehicle tires. Thus, the significance of tire properties as an influence upon the braking-in-a-turn response of trucks and buses remains virtually unexplored. While certain data were gathered on Calspan's TIRF facility under combined longitudinal and lateral slip conditions, difficulties in data gathering render the results unusable. Accordingly, it remains for future research activities to probe that most complex domain of tire traction—covering the combined braking and angular slip of the heavy truck tire.

2.3 Methods Employed to Conduct Vehicle Tests

2.3.1 Vehicle Sample. A sample consisting of two light and two heavy vehicles was selected for full-scale test measurement. Shown in Figures 2.4, 2.5, 2.6, and 2.7, these vehicles were chosen to represent light truck and bus (van) classes and heavy truck and bus classes. In addition to being employed in a program of full-scale tests, the sample was also applied in a set of laboratory measurements which provided the design parameters needed to simulate the four vehicle selections.

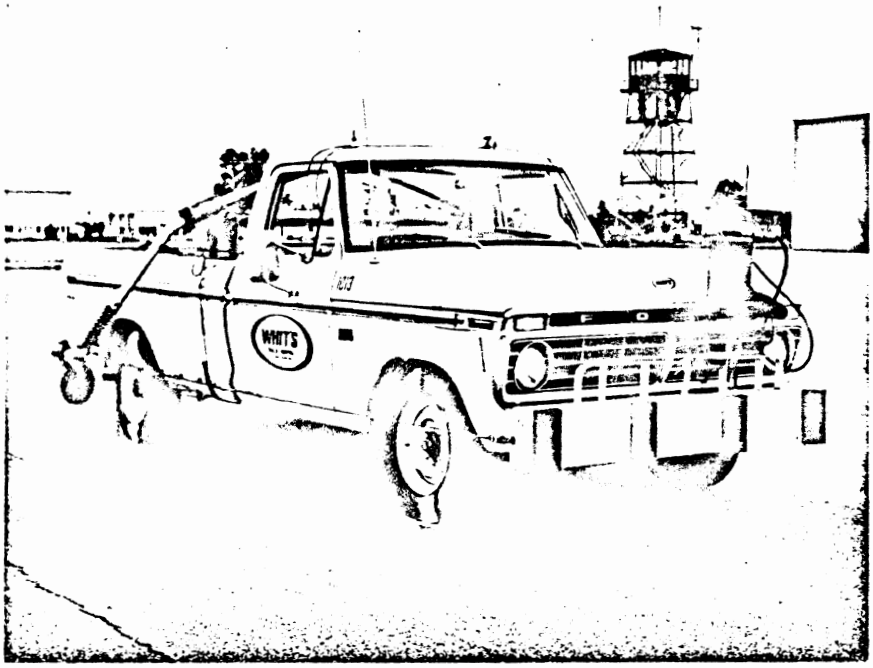

Figure 2.4. Light truck test vehicle.

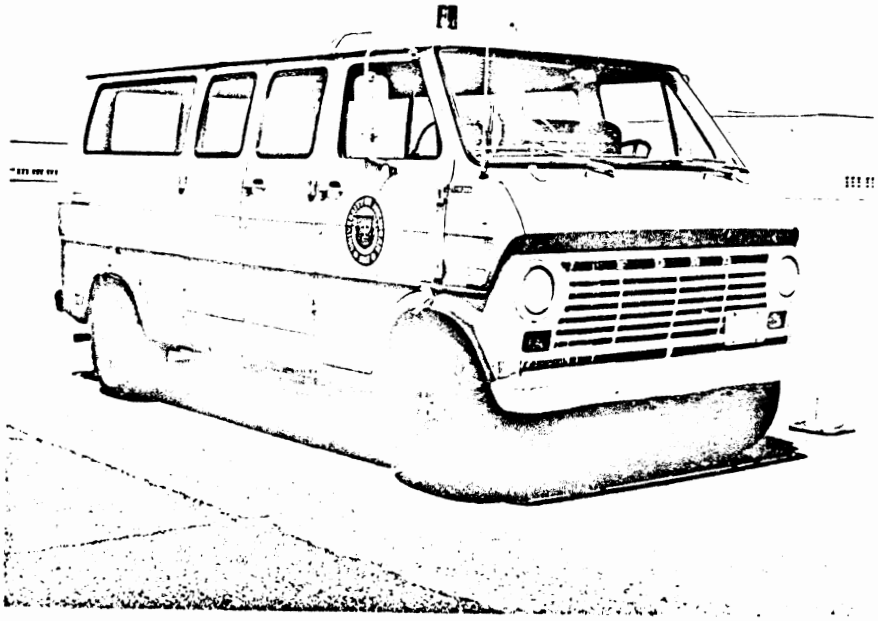

Figure 2.5. Light van test vehicle.

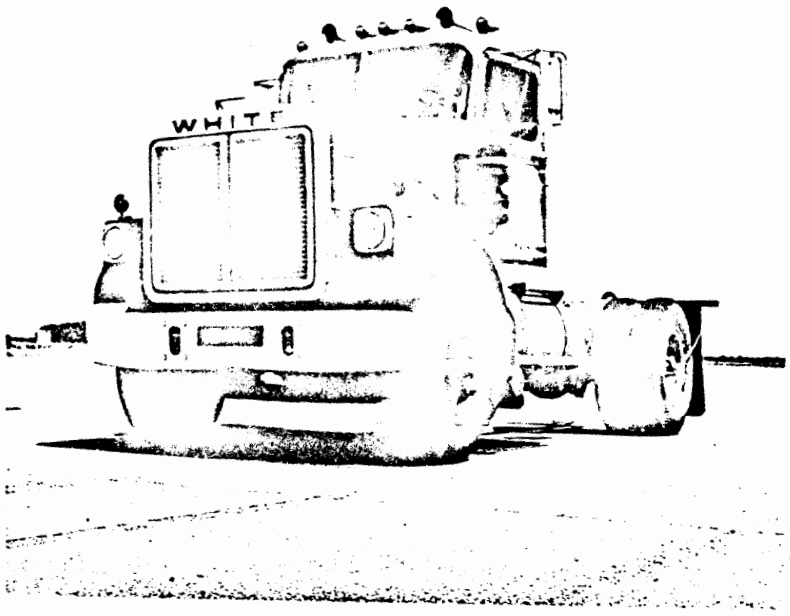

Figure 2.6. Heavy truck test vehicle.

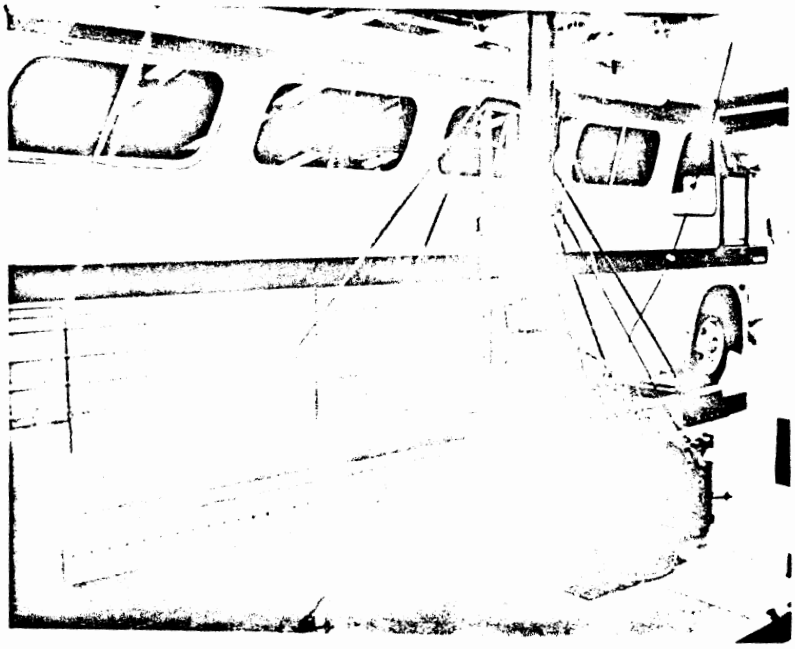

Figure 2.7. Heavy bus test vehicle.

The light vehicle selections were chosen with sufficiently high gvw ratings that "LT Series," rather than passenger car series tires (as defined by the Tire & Rim Association) were provided as original equipment. This selection thus constitutes a narrowing of the interests of the study to include only that portion of the light truck spectrum which employs tires of the higher load rating and higher inflation pressure variety falling in the LT designation (recognizing that many of the light trucks and vans in the "1/2 ton" payload category typically mount passenger car tires).

The selected heavy truck was chosen in the two-axle configuration to provide a simplified system which was more compatible with a program concentrating upon tire properties (although the simulation of many tandem suspension designs is within the current state of the art [3, 4]). The test truck was obtained by loan from the White Motor Corporation and was incorporated in the program as a "straight truck" rather than as a tractor, although vehicles of this type are commonly employed in either role. (A special set of simulation results presented in Section 4.2.4, however, do provide a view of this vehicle's behavior when employed as a tractor with associated semitrailer.) An "original equipment" tire for the heavy truck was selected, rather than specified by the manufacturer, since most of such vehicles are custom-assembled according to the purchaser's request (including tire designation) rather than according to a standard design.

The selected heavy bus was of the "intercity" variety and was leased from the Greyhound Corporation. This was, likewise, obtained in a two-axle configuration to permit simplified isolations of the tire's role in vehicle behavior. Again, as with the heavy truck, the "original equipment" tire was actually a baseline selection made somewhat arbitrarily given that the vehicle user, rather than the original manufacturer, determines which tires shall be employed. Intercity bus fleets generally lease tires on a

mileage basis rather than purchase them. Accordingly, tire usage patterns, as determined through conversations with the major "mileage tire" suppliers, led to the selection of the baseline tire for use on the bus employed in this study.

All tires employed during vehicle tests were operated in their full tread depth condition following only a short (100-mile) break-in period. The heavy bus tires, designed to be regrooved rather than retreaded, were operated likewise in their "uncut" (i.e., full tread depth and original overall diameter) state.

2.3.2 Vehicle Test Methods - Apparatus. Light and heavy test vehicles were subjected to a common set of open-loop test procedures involving steering and braking inputs which were applied through the action of precision servomechanisms. Thus, each test vehicle was outfitted with a complement of test apparatus which applied control displacements to the steering shaft and brake pedal. Additionally, input and response data were gathered using various on-board transducers whose output signals were telemetered for recording at a ground station.

Gathered data included the following:

A_x	longitudinal acceleration
A_y	lateral acceleration
r	yaw rate
V_5	velocity
δ_{sw}	steering wheel angle
δ_1 and δ_2	left and right front wheel steer angles
F_{br}	brake pedal force, for hydraulically-braked vehicles
P_{br}	brake line pressure, for air-braked vehicles.

Component acceleration variables, A_x and A_y, were measured using gyro-stabilized accelerometers.

Wheel rotation information was gathered using wheel-mounted pulse generators. The output signals of these devices was interpreted by a logic circuit module with a light display output indicating the occurrence of wheel lock to the vehicle operator.

While the data acquisition methods employed in this study were contemporary and rather straightforward, the means of applying precision control inputs was closely scrutinized at a time when the test program was partially completed. A brief explanation of this "problem" will be given here, while a more thorough discussion is presented in Appendix G.

For vehicles equipped with manual transmissions, the employment of a fully automatic vehicle controller as a means to obtain precision control inputs is rather impractical. If the basic controller is such as to involve a driverless operation (requiring apparatus such as developed for passenger car research—see Reference [5]) the mechanical difficulties associated with servo-controlled gear-changing generally render the controller inapplicable to manual transmission vehicles. This difficulty was overcome in this study and in the preceding commercial vehicle project funded by NHTSA [1] through the use of a hybrid vehicle controller. By this arrangement, a test driver performs the gear-shifting and other vehicle control functions until programmed inputs of steering and braking are effected at the desired moment by way of overriding servo-actuators. While employing such a hybrid test system in this study the heavy truck test vehicle was rolled over, with injury to the driver. Accordingly, certain data reported herein derive from full-scale tests which were controlled by a hybrid driver/controller system and remaining tests, conducted following the rollover event, employed a fully automatic (driverless) controller. Also as a consequence of the rollover incident, the intercity bus was not incorporated in the full-scale test program, as had been originally planned.

2.3.3 Vehicle Test Methods. Vehicle tests were conducted at the facilities of the Texas Transportation Institute (TTI) in College Station, Texas, according to open-loop test procedures developed under the research contract of Reference [1]. Test procedures encompassed three basic maneuvers: braking in a turn, lane changing, and severe, or J-turn, steering. (Straight-line braking tests were also conducted as a means of measuring brake system parameters.) Each test was performed through the application of precision steering and braking inputs whose functional form renders a maneuver of one of the three described types. The open-loop lane-change and J-turn maneuvers are accomplished through steering waveshapes involving sinusoidal and trapezoidal forms, respectively, which are adjusted to provide prescribed amplitude and frequency content.

In this study, as in the preceding work [1], steering input levels and test velocities were chosen so as to avoid maneuvering severities in the vicinity of each vehicle's rollover limit. Thus the data deriving from full-scale tests represents, in general, the sublimit behavior of the vehicles examined.

The sensitivity of vehicle response to tire properties was examined in a limited way using tire sets which were selected from flat-bed traction test results on the basis of their atypical cornering behavior.

The light van test vehicle was tested using its "OE" tire selection and an "extreme variation" selection comprised of the OE tire on the front axle and a selected snow tire on the rear. Tests were run both loaded and empty on both dry and wet asphalt.

The heavy truck was tested in its OE tire configuration on a wet surface but suffered a demolishing rollover (see Figure 2.8) while attempting certain setup runs in preparation for braking in a turn on dry asphalt.

The pickup truck was subjected to tests with four tire arrangements. In addition to vehicle tests involving the OE tire, the vehicle was operated with three other tire arrangements. The

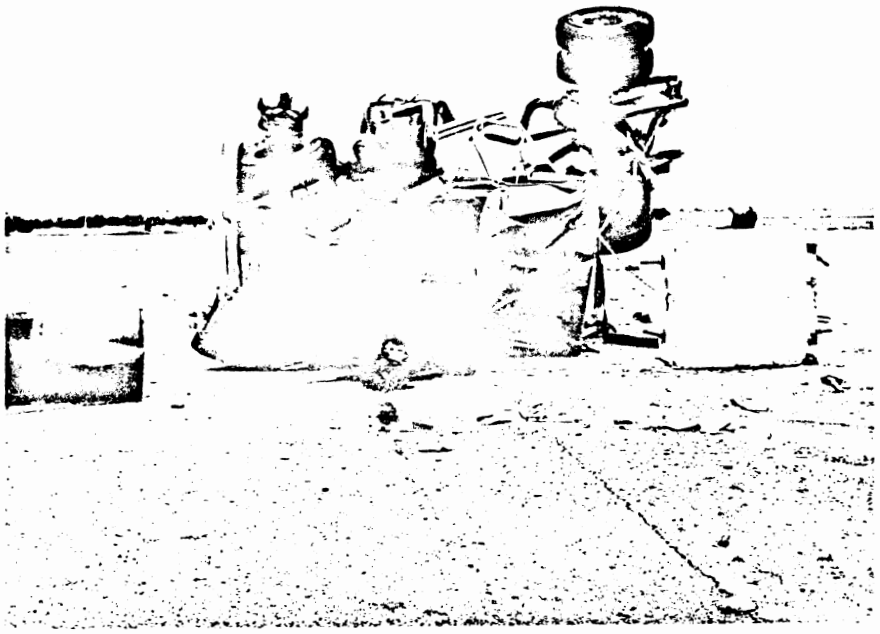

Figure 2.8. Heavy truck following rollover.

three variations covered (a) selected radial and, (b) selected bias-ply rib tires installed at all four wheel positions, and (c) a combination of the OE bias-ply rib-tread tires on the front axle with bias-ply snow-tread tires on the rear axle.

Data resulting from these experiments, interpreted in terms of tire influences on vehicle behavior, are presented in Section 4.1. A tabulation of test results is presented in Appendix E.

2.4 The Simulation of Tire/Vehicle Behavior

Two mathematical simulations of tire/vehicle systems were employed in this study. A major parametric sensitivity study was conducted using the hybrid simulation at the Applied Physics Laboratory of Johns Hopkins University. This computerized tool is based upon a fifteen-degree-of-freedom model and has been documented in Reference [6]. The APL simulation was slightly modified in this study to permit the entry of tire-descriptive data in tabular form.

APL's hybrid model was employed in this study principally as a means to extrapolate beyond the low maneuvering level within which full-scale tests were constrained. Although full-scale tests were limited in severity, a sufficiently broad range was examined to permit simple comparisons between simulated and measured yaw response gain such as is illustrated in Figure 2.9. While a general validity in low maneuver-level predictions was observed, the high-level calculations remain unconfirmed.

Another portion of the study involved computerized simulations employed in the HSRI "Phase II" digital simulation of heavy trucks and tractor-trailers. This thirty-two-degree-of-freedom model was applied in a set of steering-only calculations aimed at examining the sensitivity of truck yaw stability to a variety of vehicle design and loading parameters. The limited study of yaw stability was prompted by the observation that a mild yaw divergency had resulted in the inadvertent rollover of the heavy truck during testing.

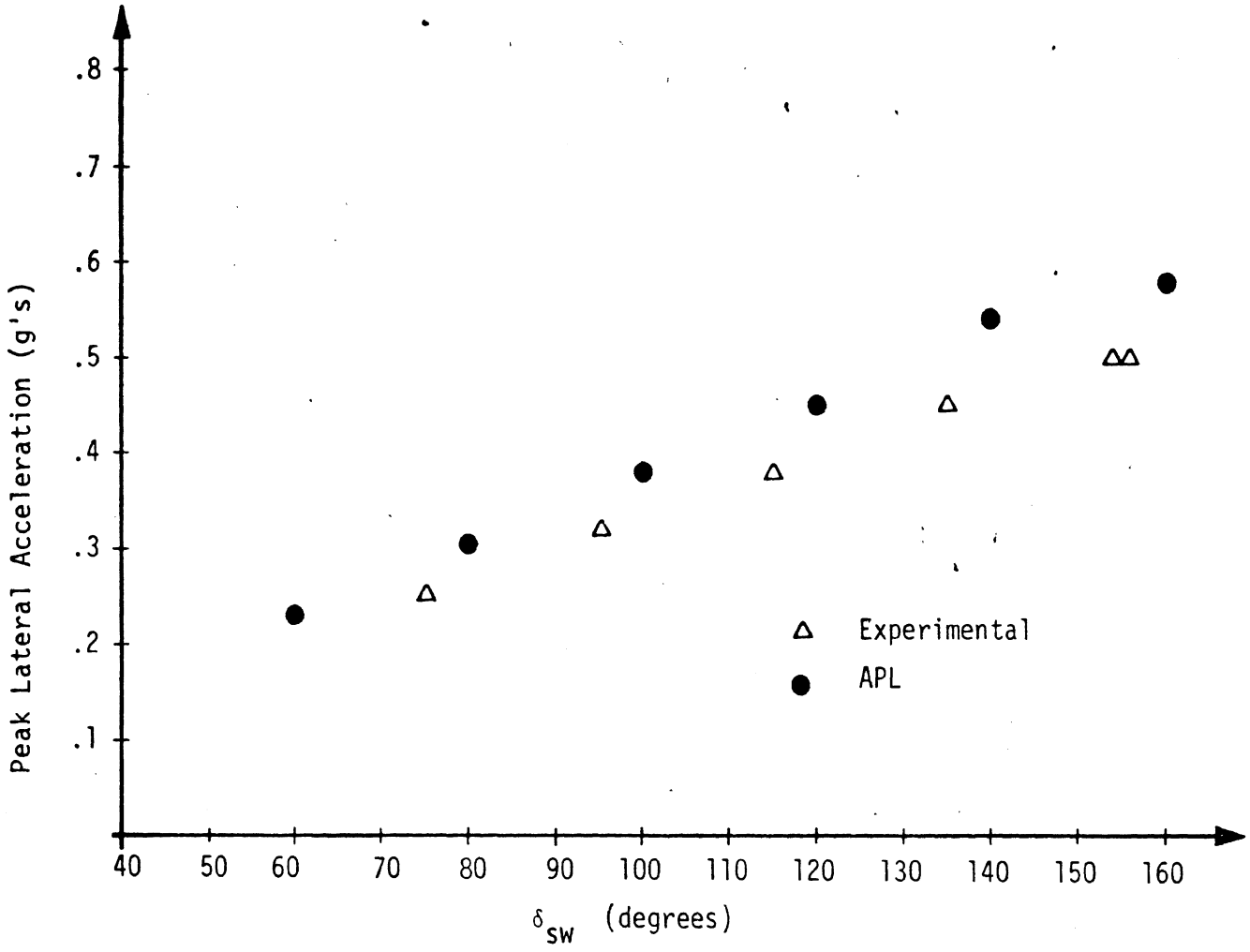

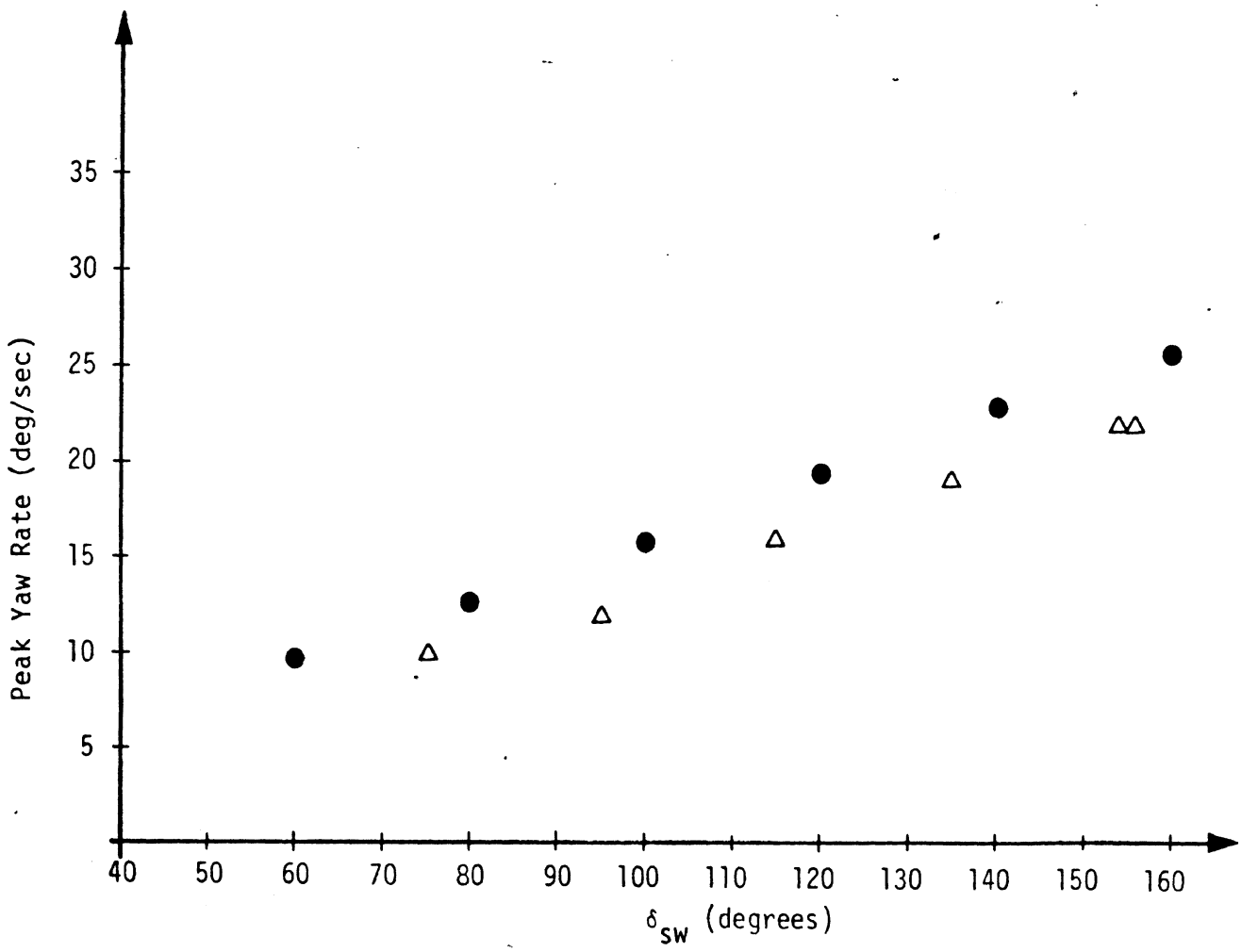

Figure 2.9. Comparison of APL simulation results and full-scale test measurement for Ford F250 pickup truck.

The HSRI simulation, validated during previous efforts [4, 7], was exercised first to examine the extent to which the test incident may have been merely an isolated anomaly, and, secondly, to identify the primary vehicle configuration parameters which influence the directional limits of heavy trucks. As will be discussed in Section 4.2.4, these calculations were not restricted to variations in tire characteristics alone, but rather included the major elements of heavy truck design which might be hypothesized to impinge upon the balancing of the directional moment during a J-turn type of maneuver.

Insofar as the test truck was of the type commonly applied as the tractor of a combination vehicle, additional calculations were run with this truck coupled to a suitably matched semi-trailer to determine the generality of the observed yaw response anomalies. As will be shown, results of this simulation effort are seen to clarify the observations of marginal truck yaw stability and form a basis for the conclusion that a finding of potential significance to traffic safety has been discovered.

3.0 FINDINGS ELUCIDATING THE BASIC TRACTION PROPERTIES OF TRUCK AND BUS TIRES

In this section measurements of commercial tire traction properties are summarized with an emphasis towards identifying characteristic patterns of performance. As stated earlier, traction experiments were conducted using three distinct apparatuses: namely, the HSRI Flat-Bed Tire Tester, the HSRI Mobile Truck Tire Dynamometer, and the Calspan TIRF Facility.

Since the flat-bed machine involves a low velocity, artificial surface condition, the resulting data is employed primarily to characterize linear traction properties. In contrast, the representative velocity and surface conditions characterizing the mobile experiments provides data which authentically characterize friction-limited properties. As a complement to these two extremes, the TIRF measurements provide velocity realism permitting a precision characterization of both operating regimes, albeit in conjunction with an artificial surface condition.

Accordingly, the section is organized into three presentations, considering the measurements obtained on each test machine, in turn. For each machine, both light and heavy tire results are summarized and discussed.

3.1 Flat-Bed Tire Test Findings

3.1.1 Introduction. A total of forty tires were tested on the HSRI Flat-Bed Tire Tester in this study. These tires included twenty heavy truck and bus tires and twenty light truck tires. A complete listing of the tires tested is given in Table 3.1. The tire designations (H-1, H-2....., L-1, L-2.....) given in this table will be referred to throughout this section. Note that H-1 through H-11 are nominally heavy truck sizes while H-12 through H-20 are heavy bus sizes.

TABLE 3.1. FLAT-BED TEST TIRES

Tire No.	Manufacturer	Model	Size
Heavy Truck Tires			
H-1	Uniroyal	Triple Tread	10 x 20F
H-2	Uniroyal	Triple Tread	10 x 20G
H-3	Uniroyal	Triple Tread	11 x 22.5F
H-4	B.F. Goodrich	Milesaver Radial Steel H.D.R.	10 R 20 G
H-5	B.F. Goodrich	Milesaver Radial Steel H.D.B.	10 R 20 G
H-6	Goodyear	Unisteel R-1	10 R 20 G
H-7	Goodyear	Unisteel L-1	10 R 20 G
H-8	Firestone	Power Drive	10 x 20F
H-9	Uniroyal	Unimaster Rib	15 x 22.5H
H-10	Michelin	Radial	10 R 20 G
H-11	Uniroyal	Fleetmaster Superlug	10 x 20F
Heavy Bus Tires			
H-12	Firestone	Hiway Mileage	12.5 x 22.5G
H-13	B.F. Goodrich	Intercity Mileage	12.5 x 22.5G
H-14	B.F. Goodrich	Intercity Mileage	11.5 x 20G
H-15	Uniroyal	Intercity	12.5 x 22.5G
H-16	Uniroyal	MaxRoute I	11.00 R 20H
H-17	Goodyear	Custom Cruiser	12.5 x 22.5G
H-18	Michelin	Radial XZA	11 R 20 H
H-19	Michelin	Radial XZA	11 R 22.5 H
H-20	Michelin	Radial XZA	12 R 22.5H
Light Truck Tires			
L-1	Firestone	Transport 500	8.00 x 16.5D
L-2	Goodyear	Custom HiMiler	8.75 x 16.5E
L-3	Goodyear	Rib HiMiler	8.00 x 16.5D
L-4	Firestone	Transport 110	7.50 x 16.5C
L-5	Goodyear	Super Single HiMiler	10.00 x 16.5E
L-6	Firestone	Town & Country Truck	8.00 x 16.5D
L-7	Goodyear	Custom Flexsteel	8.00 R 16.5E
L-8	Goodrich	Milesaver Radial	8.00 R 16.5D
L-9	Goodyear	Glas Guard XG	8.00 x 16.5D
L-10	Goodyear	Glas Guard XG	8.75 x 16.5E
L-11	Firestone	Town & Country Truck	8.75 x 16.5E
L-12	Goodyear	Custom Flexsteel	8.75 R 16.5E
L-13	Michelin	Radial XCA	8.00 R 16.5E
L-14	Wards	Steel Belted Super Wide	9.50 x 16.5D
L-15	Michelin	Radial XCA	8.75 R 16.5D
L-16	General	Jumbo Power Jet	8.00 x 16.5D
L-17	General	Jumbo Power Jet	8.75 x 16.5E
L-18	Goodyear	Glas Guard	8.00 x 16.5D
L-19	Goodyear	Glas Guard	8.75 x 16.5E
L-20	Goodyear	Rib HiMiler	8.75 x 16.5E

The Flat-Bed Tire Tester was shown in Figure 2.1. This facility allows for traction testing of tires on a flat, artificial road surface which passes beneath the stationary test tire at low speed. In this program, the Flat-Bed was used to examine the lateral force performance of the test tires in the range of 0 to 16° slip angle with variations in normal load and inflation pressure. All tests were performed on freely-rolling tires.

Because of the low speed and artificiality of the test surface, the Flat-Bed machine is best suited for examination of lateral force in the low slip, linear regime. (Tire performance is basically independent of velocity and surface character in this regime.) Nonetheless, results can be informative, at least qualitatively, at higher slip angles, particularly since higher speed, mobile traction experiments conducted on certain of the sample tires indicated little velocity sensitivity (see Section 3.2). Accordingly, the discussion of flat-bed test results (Section 3.1.3) will bear heavily on findings related to cornering stiffness properties (descriptive of linear range performance) with some discussion of performance in the higher slip regime.

Complete listing of the results of flat-bed tests on all forty tires appears in Appendix C.

3.1.2 Test Conditions. The matrix of testing for each of the heavy truck tires was three dimensional, involving slip angle, vertical load, and tire pressure variations. Tests were made measuring side force and aligning moment at slip angles ranging from 0 to ±16° (at a camber angle of zero) under the following conditions of load and inflation pressures.

Inflation Pressure (psi)	Load (lb) 2000	4000	6000	8000
100	X	X	X	X
75		X	X	
50		X	X	

This matrix held for all heavy tires tested except for the 15 x 22.5 wide base tire which was subjected to the following matrix.

Inflation Pressure (psi)	Load (lb) 2500	5000	7500	10,000
120	X	X	X	X
90		X	X	
60		X	X	

The vertical loadings were chosen to be representative of the range of dynamic loads which the tires might experience in handling maneuvers, but within the confines of maximum vertical load rating of the Flat-Bed machine (10,000 lb).

The highest inflation pressure was viewed as the baseline inflation pressure. Generally, this pressure was some 10-15% in excess of T & RA recommended cold inflation pressure. (HSRI mobile tire test experience indicates that the steady-state, "hot" inflation pressure of heavy truck tires operating at rated load and highway velocities typically will be 10-15% above the cold inflation pressure.) Reduced pressures were also tested to observe the effect of this parameter on tire performance.

The twenty light truck tires selected for this program were each Flat-Bed tested at four vertical loads and at slip angles from 0 to ±16°. Load schedules varied depending on rated load of the tire; generally, the four loads used were 0.30, 0.65, 1.00, and 1.35 times rated load. The majority of light tires were tested at one inflation pressure, approximately 10-15% in excess of T & RA recommended cold inflation pressure (and thus representative of typical "hot" inflation pressures). Two tires, L-1 and L-2, were tested at 30, 50, and 75 psi to examine the effects of inflation pressure. In these cases, the highest pressure is viewed as the nominal inflation pressure for the tires.

3.1.3 Flat-Bed Test Results. Figure 3.1 is a summary plot of the cornering stiffness (C_α) properties of all the heavy tires tested. The figure shows C_α plotted against vertical load. All data displayed in this figure was collected at the nominal inflation pressure only. A number of notable findings can be drawn from this plot*, viz.:

1. Unlike passenger car tires, the heavy truck tires showed cornering stiffness to be a strong function of vertical load in the vicinity of rated load. As can be seen, cornering stiffness characteristically increases over the entire load range examined. A few individual tires did show a slight decrease in C_α at the high end of the load range. Some tires displayed a C_α-load relationship which was surprisingly linear and, when extrapolated toward the origin, had a C_α axis intercept very close to zero. (For example, note the wide base tire singled out in the figure.) This finding has important effects on vehicle handling, and will be discussed in that context in Section 4.

2. In this particular tire sample, a remarkably strong delineation between the performance of radial and bias-ply tires is apparent. With few exceptions, the radial tires always display higher C_α values than the bias tires at a given vertical load. Only at lower loads is there significant departure from this generality.

*It should be noted that these findings must be qualified by the tire inflation pressure condition noted.

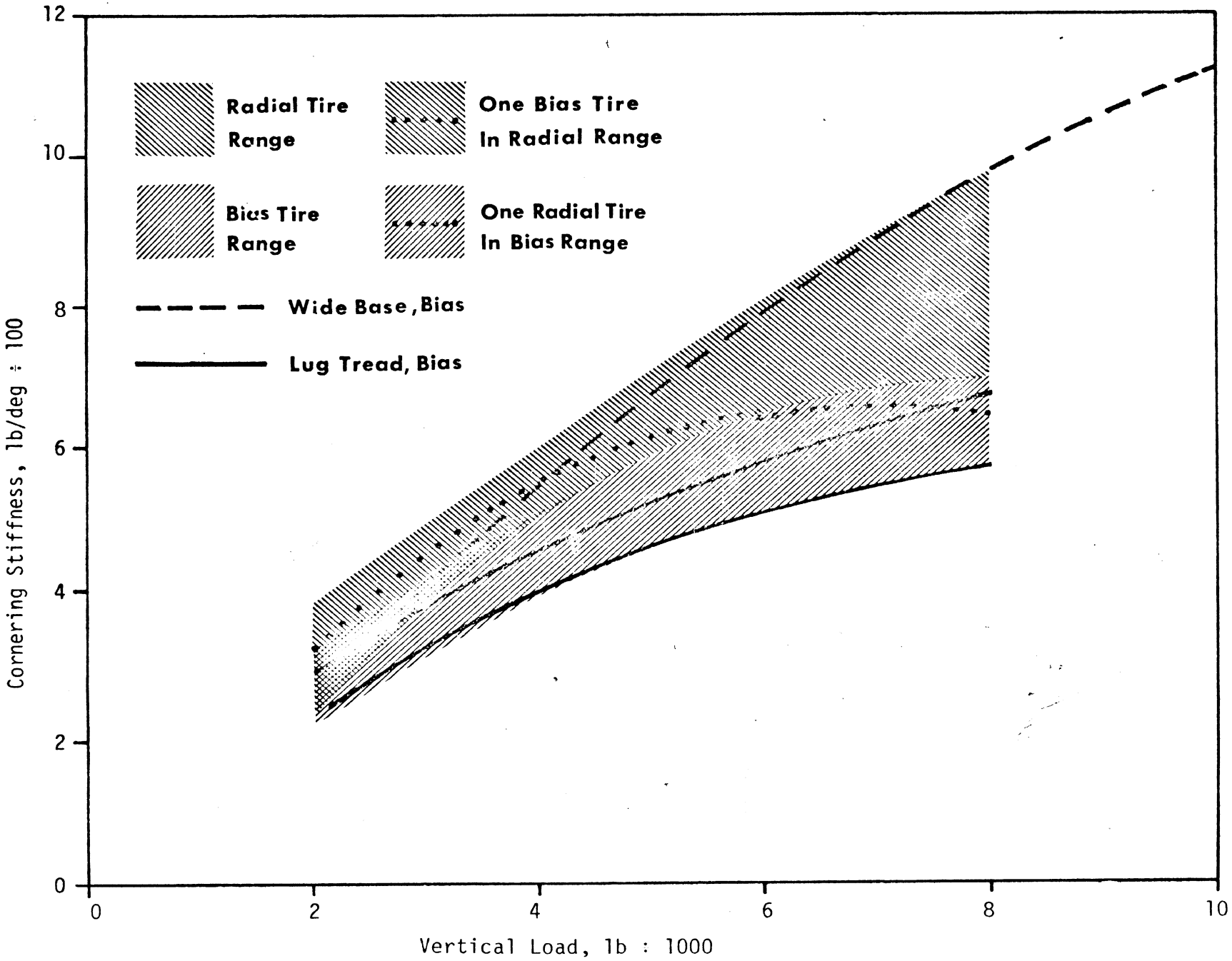

Figure 3.1 The effect of vertical load on cornering stiffness: heavy truck and bus tires.

3. The two bias-ply tires with lug-type tread patterns provided lower C_α values than the characteristic rib-type bias tires.

4. The one wide base single bias tire displayed higher C_α values than other tires in the higher load regime for which it is specifically designed.

Figures 3.2 through 3.5 present a summary of the C_α versus load behavior of the light truck tires tested at their nominal inflation pressures. The four plots show the envelope of all C_α data gathered, while each figure highlights the performance of a particular class of tire (radial, bias-belted, lug, and wide base, respectively). These plots illustrate several basic findings, viz.:

1. As was the case for heavy truck tires, C_α is seen to be a strong function of vertical load, increasing with vertical load. All tires were strictly monotonic in this respect over the range tested. For several individual tires, C_α is remarkably linear in vertical load, and, if the data were extrapolated toward the origin of the plots, would have C_α intercepts quite close to zero.

2. Figure 3.2 indicates that on the average, radial tires were stiffer than the sample in general, but the light truck radial did not demonstrate the strong delineation as was seen with radial heavy truck tires.

3. Taken as a group, the four bias-belted tires tested showed a lower than average cornering stiffness (see Figure 3.3). However, the two "softer" belted tires were also lug-tread type tires. The highway tread, belted tires taken alone showed average or somewhat higher values of C_α.

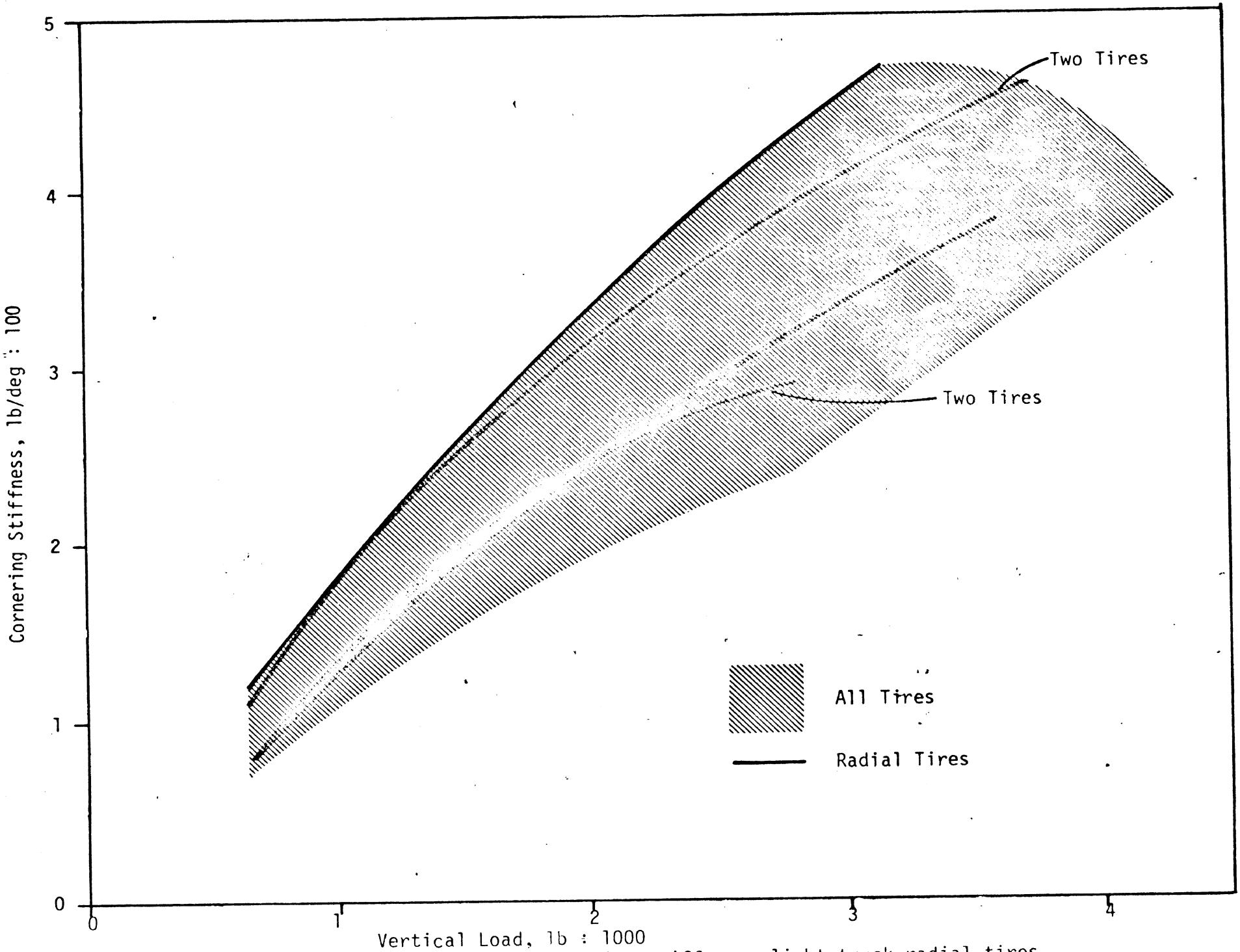

Figure 3. 2 The effect of vertical load on cornering stiffness: light truck radial tires.

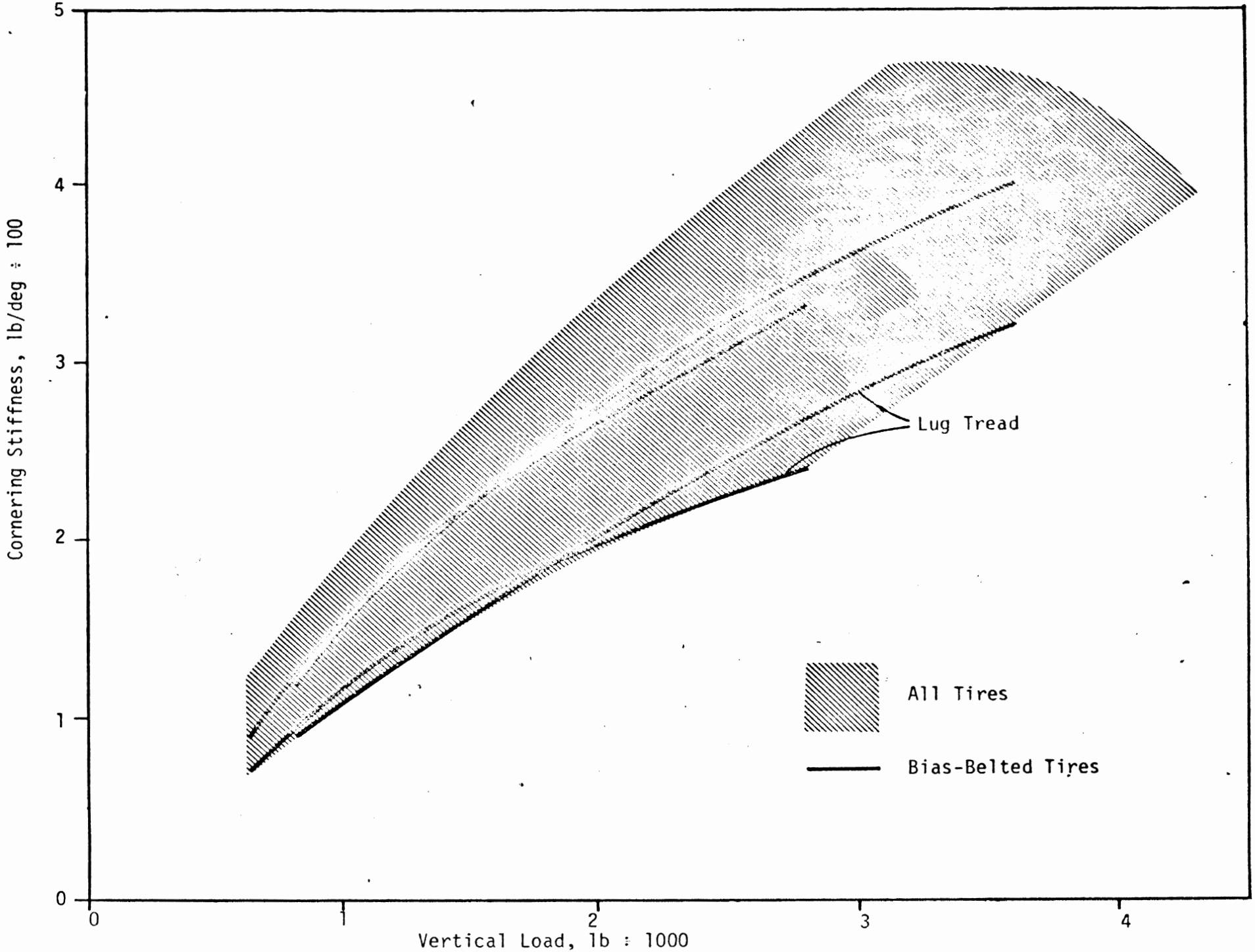

Figure 3.3 The effect of vertical load on cornering stiffness: light truck bias-belted tires.

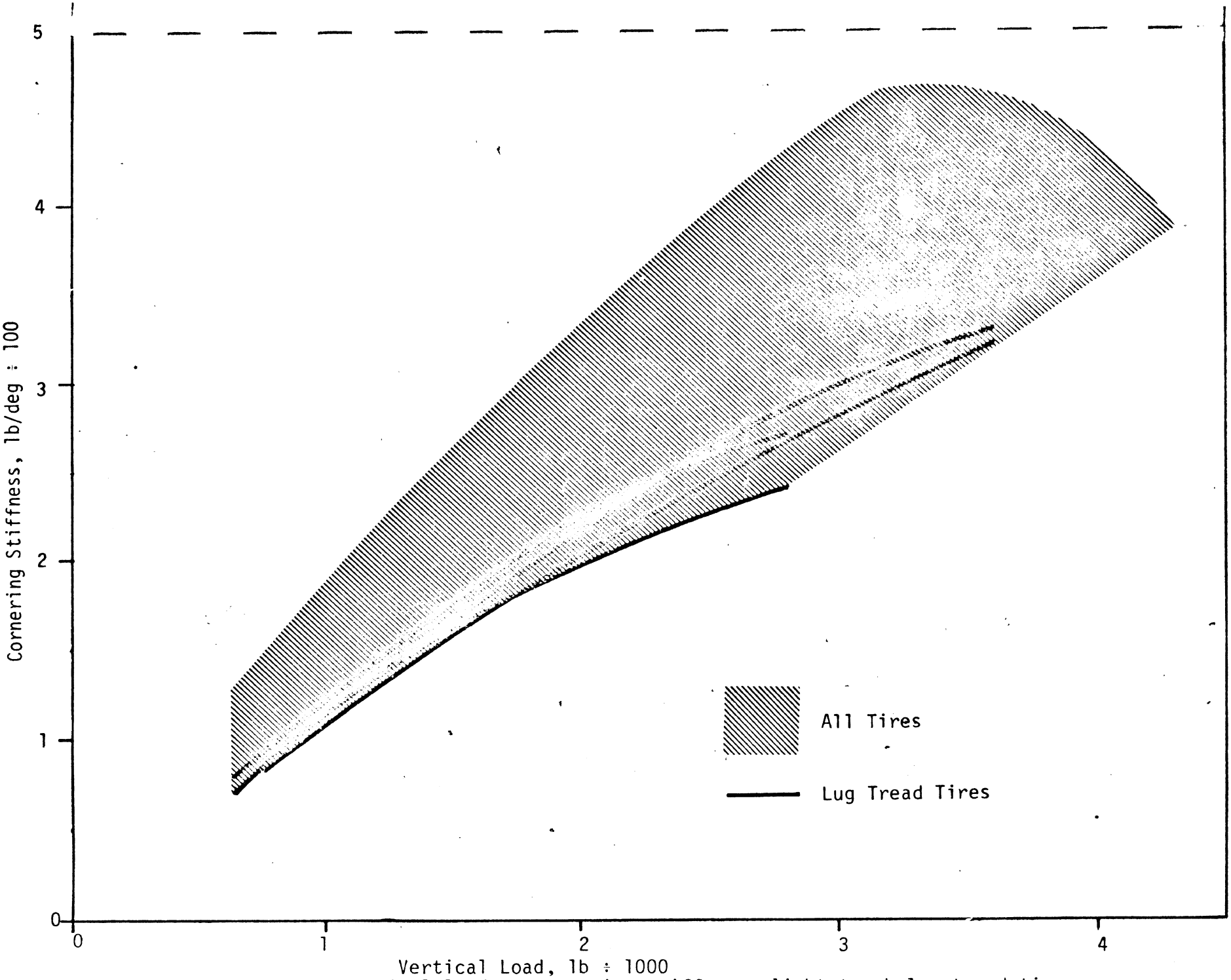

Figure 3.4 The effect of vertical load on cornering stiffness: light truck lug tread tires.

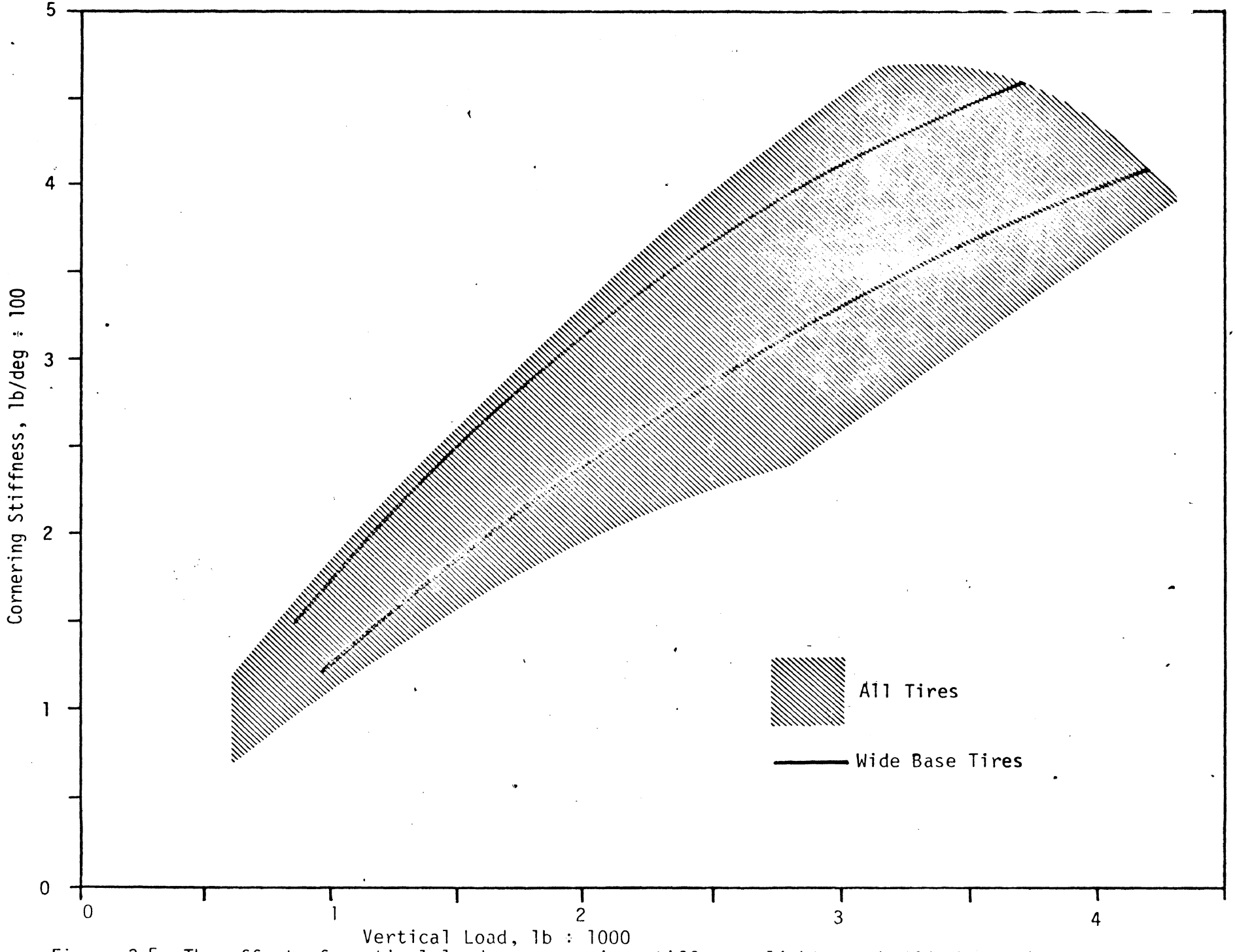

Figure 3.5 The effect of vertical load on cornering stiffness: light truck wide base tires.

4. Figure 3.4 shows that all four tires with lug-type tread patterns had quite "soft" cornering stiffnesses.

5. The two wide base tires tested did not show a consistent trend. (See Figure 3.5.) One was rather "stiff," but the second showed surprisingly low C_α values.

The C_α data presented in Figures 3.1 through 3.5 is, of course, by definition, related only to the low slip, linear regime of tire performance. It is also interesting to examine the manner in which the tire's lateral force response behaves in the transition between the linear regime and the friction-limited condition. Based upon the hypothesis that an abrupt transition might imply an abruptness in the relationship between steer inputs and vehicle yaw responses, a measure has been defined to characterize this property of each of the sample tires. Shown in Figure 3.6 is a plot of side force (F_y) versus slip angle (α) of a hypothetical tire, tested at a constant vertical load. As the figure shows, C_α is, by

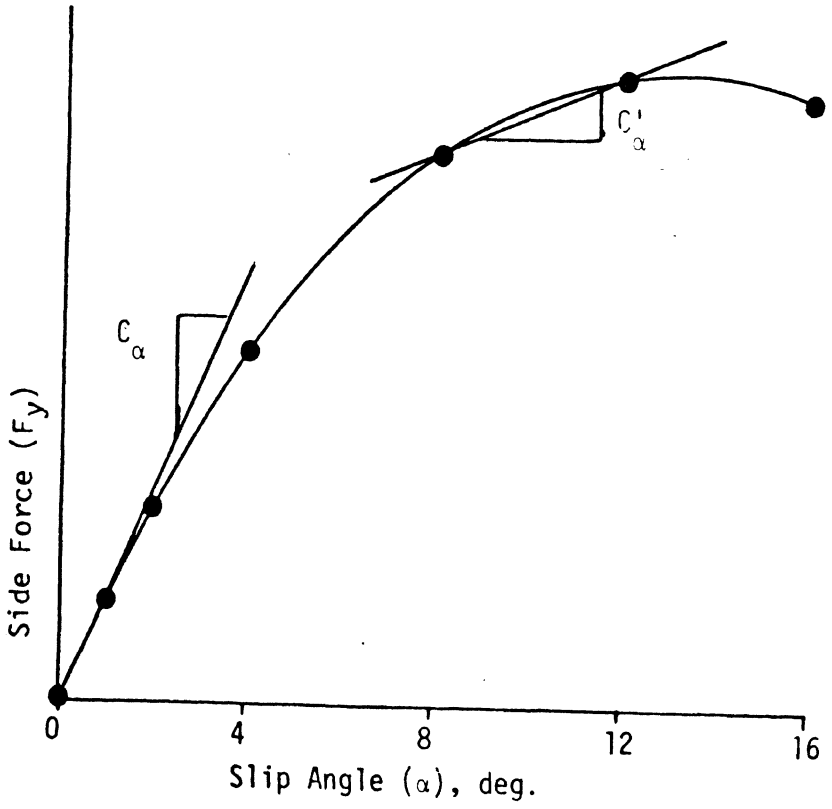

Figure 3.6 Definitions of C_α and C'_α

definition, the slope of this plot at the origin. As α increases, the F_y to α relationship becomes nonlinear such that the slope of the plot is constantly decreasing with increasing α. The ratio of this decreased slope, at some higher value of α, to C_α, is, then, a parameter by which the relative linearity of several tires may be compared. In this instance, the average slope between the 8° and 12° data points has been chosen to demonstrate the transitional behavior in the mid-slip regime. As shown in Figure 3.6, this slope has been defined as C'_α; the ratio of interest is C'_α/C_α.

Figure 3.7 is a plot of the linearity index, $\overline{C}'_\alpha/\overline{C}_\alpha$, versus $\overline{C}_\alpha$ for the heavy truck tires. The notation (viz., $\overline{C}$) indicates that the average has been taken from testing at four vertical loads, all at the nominal inflation pressure. Figure 3.7 contains a data point for each heavy tire except the wide base tire which registers far to the right of $\overline{C}_\alpha$ range shown. Notice the distinct tendency for decreasing linearity index with increasing $\overline{C}_\alpha$. This is not an unexpected result. Assuming that peak available side force is relatively constant among tires tested on a given surface, then those tires with high C_α approach this peak "faster" (in terms of α) and must show greater curvature in their F_y/α behavior at low values of α.

Figure 3.8 is a similar plot for all of the light truck tires. The data here is not quite so orderly, but the tendency for $\overline{C}'_\alpha/\overline{C}_\alpha$ to fall with increasing $\overline{C}_\alpha$ is apparent.

The linearity index plots are introduced here to document the suggested characterization of transitional side force response although no data can be shown attesting specifically to the significance of this measure.

As noted earlier, flat-bed testing on the heavy truck and bus tires was also done at two reduced inflation pressures at the two intermediate loads. Using the results of these tests, C_α is presented as a function of inflation pressure in Figures 3.9 through 3.12. One graph is presented for each tire tested.

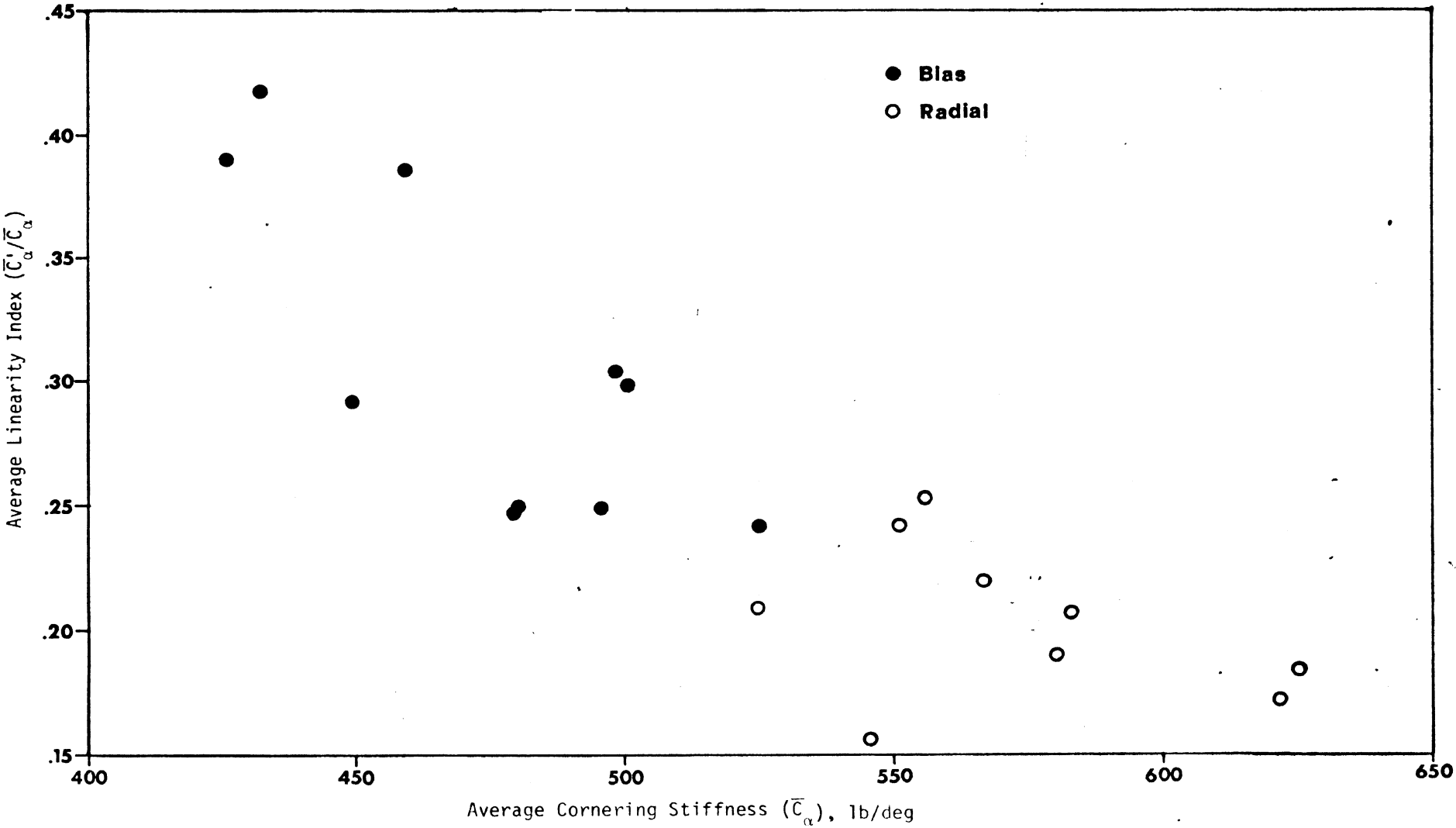

Figure 3.7 The effects of cornering stiffness on the linearity index: heavy truck and bus tires.

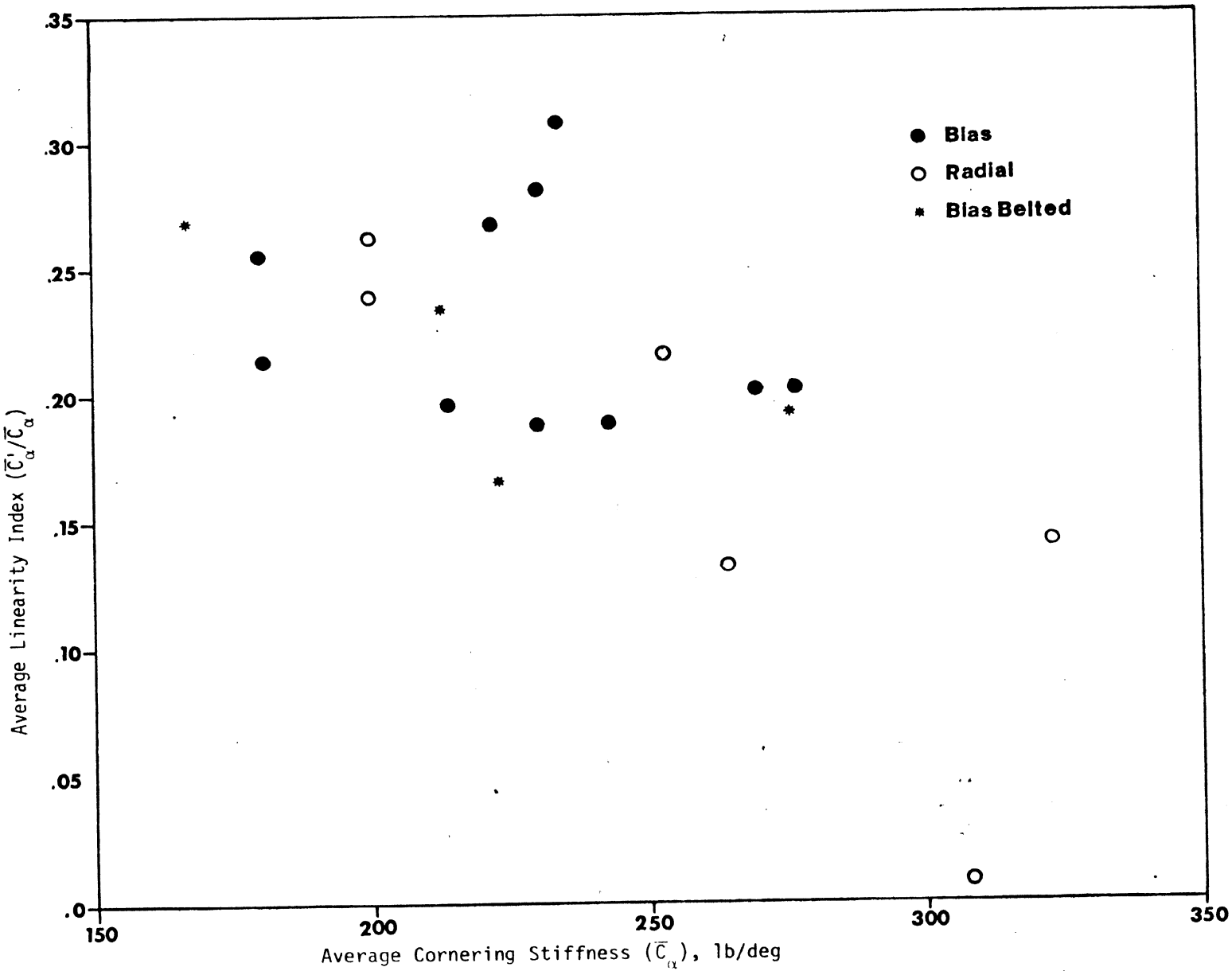

Figure 3.8 The effects of cornering stiffness on the linearity index: light truck tires.

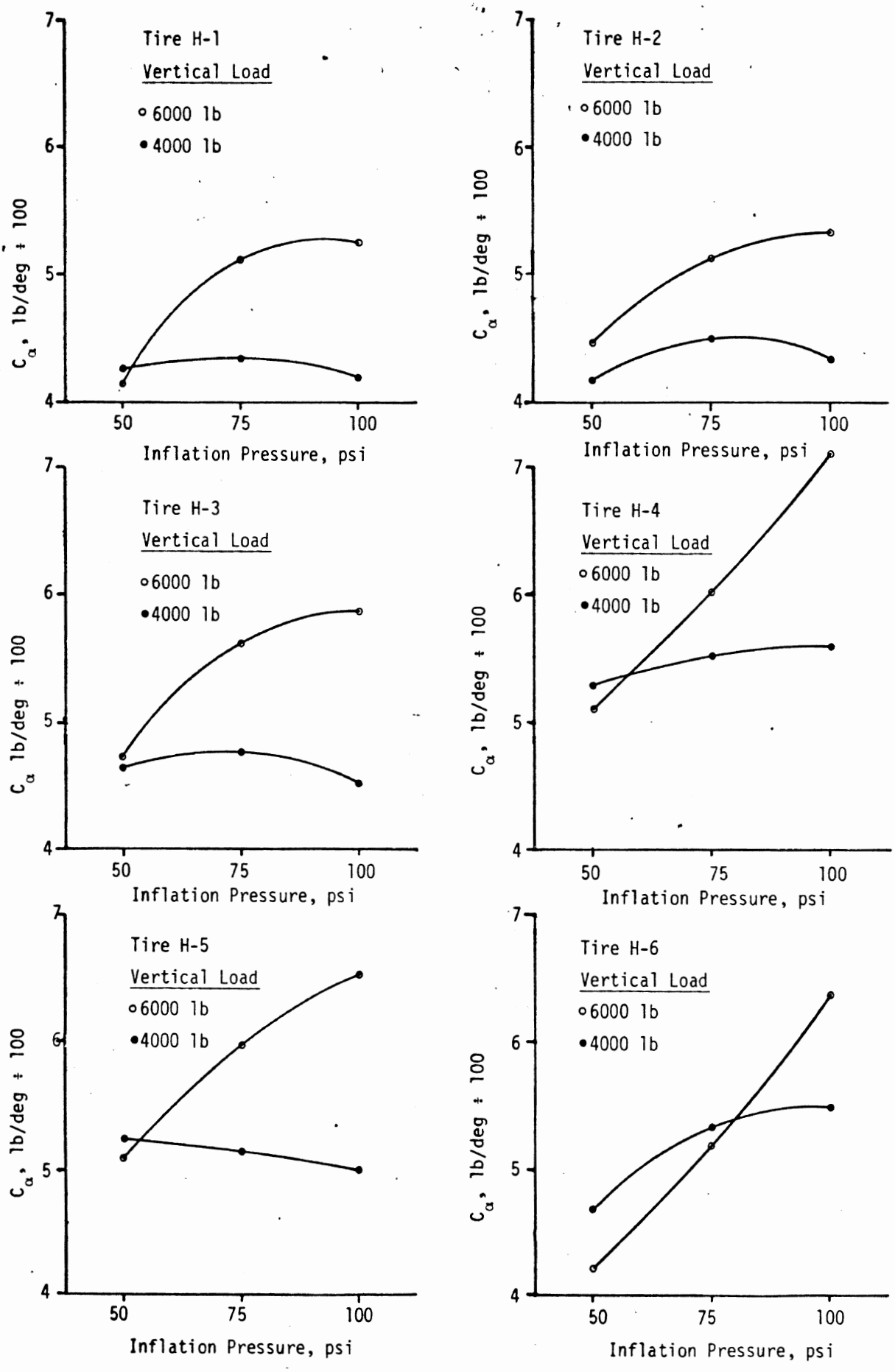

Figure 3.9 The effects of inflation pressure on cornering stiffness: heavy truck tires

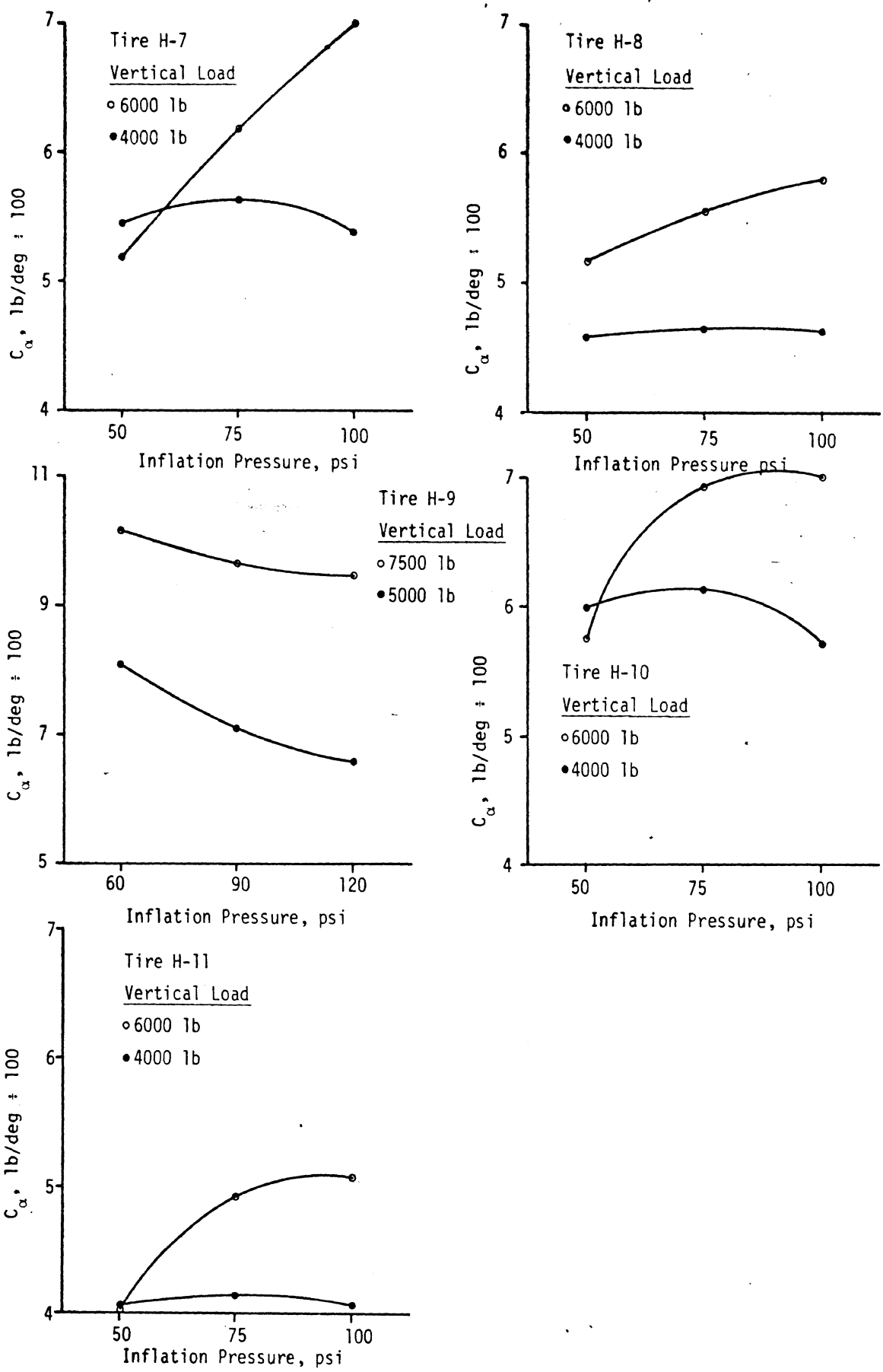

Figure 3.10 The effects of inflation pressure on cornering stiffness: heavy truck tires (cont.).

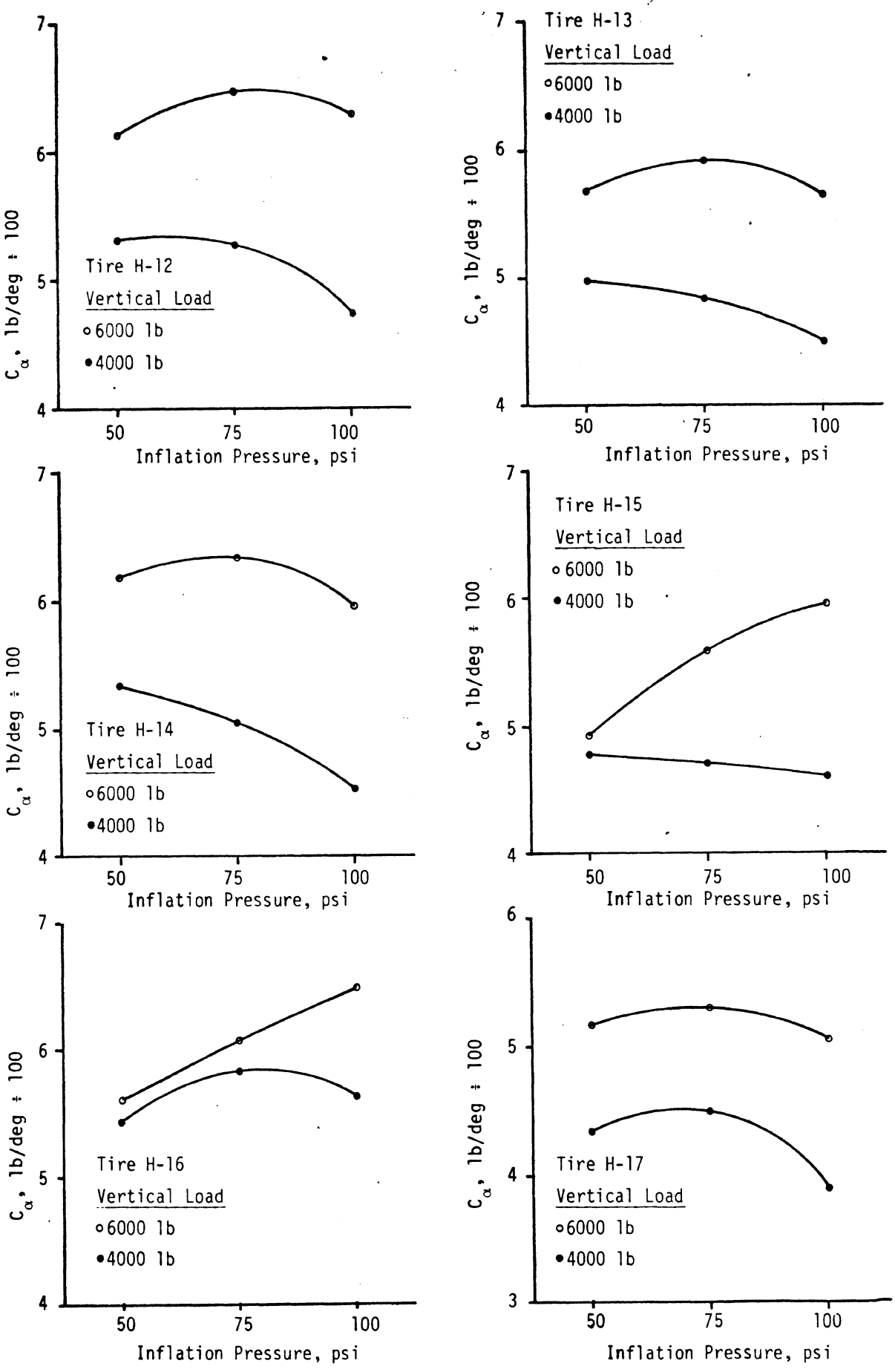

Figure 3.11 The effects of inflation pressure on cornering stiffness: heavy bus tires.

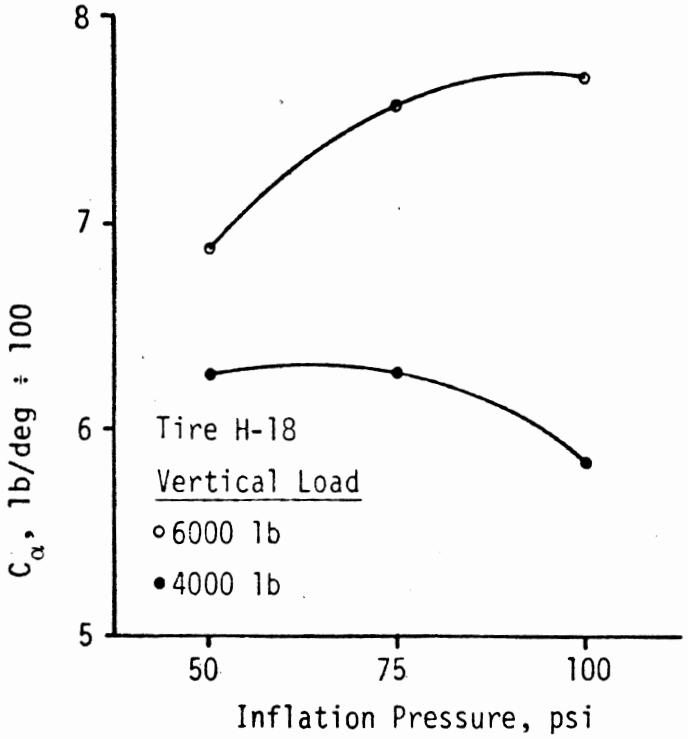

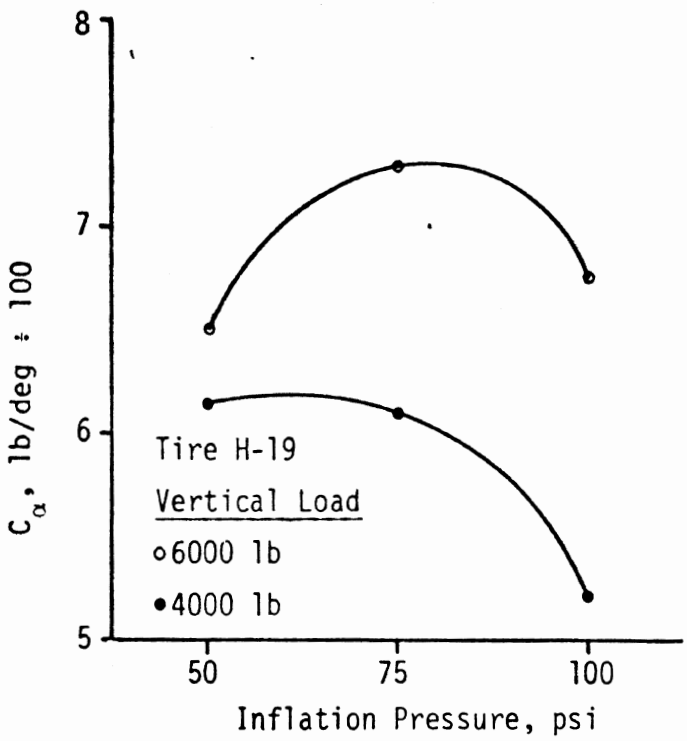

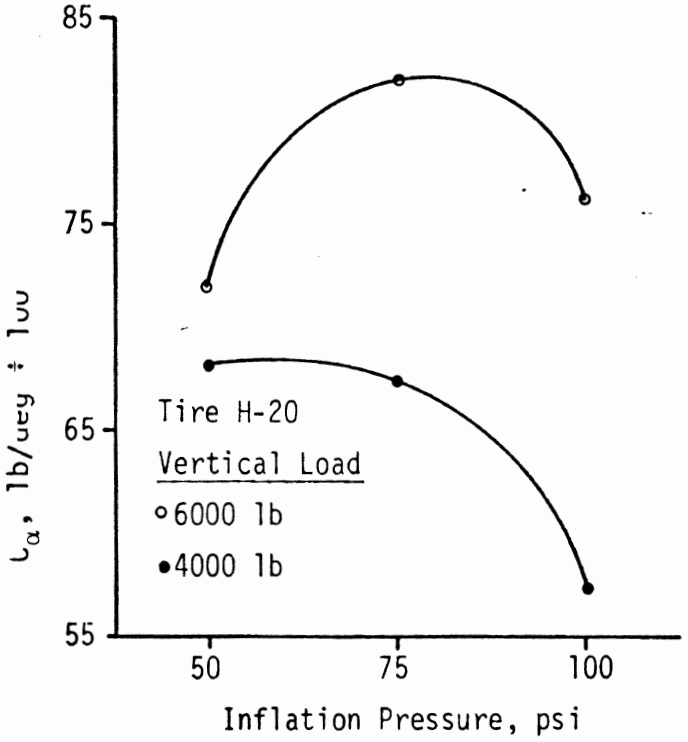

Figure 3.12 The effects of inflation pressure on cornering stiffness: heavy bus tires (cont.).

The data presented in these figures are remarkable in that they indicate that inflation pressure may have a profound effect, quantitatively and qualitatively, on the C_α behavior of these heavy tires. The heavy truck tires (H-1 through H-11) show an increase in C_α with inflation pressure when the tire is operated at the higher load (except for H-9, the wide base tire). At the lower load, behavior is mixed: C_α may rise, fall, or remain quite constant with inflation pressure. For the bus tires (H-12 through H-20) behavior is mixed at both loads. Despite this mix in behavior, it is universally true in this sample of heavy tires that at the higher inflation pressure, C_α is higher at the higher load. However, at reduced inflation pressure, the increase of C_α with load tends to reduce sharply, and, in many cases, at lower inflation pressure, C_α may actually fall with increasing load.

Figure 3.13 is a similar plot for the two light truck tires tested at reduced inflation pressures. At all but one point, C_α is seen to increase with decreasing inflation pressure. For tire L-1, the load sensitivity of C_α is rather independent of inflation pressure, but for L-2, this sensitivity decreases with inflation pressure.

The broad significance of the inflation sensitivity measurements is that light and heavy tires follow no simple rule in their cornering stiffness response to inflation pressure. In marked contrast to the case of passenger car tires, one must be cautious in applying "rules of thumb" relating cornering stiffness dependence upon inflation to the achievement of desirable vehicle understeer quality.

3.2 Mobile Tire Test Findings

3.2.1 Longitudinal Traction - Mobile Measurements. Dry pavement measurements of longitudinal traction performance were conducted on a sample of eight heavy truck tires. These data indicate traction properties which confirm and complement those reported earlier [8, 9]. The data were reduced to so-called

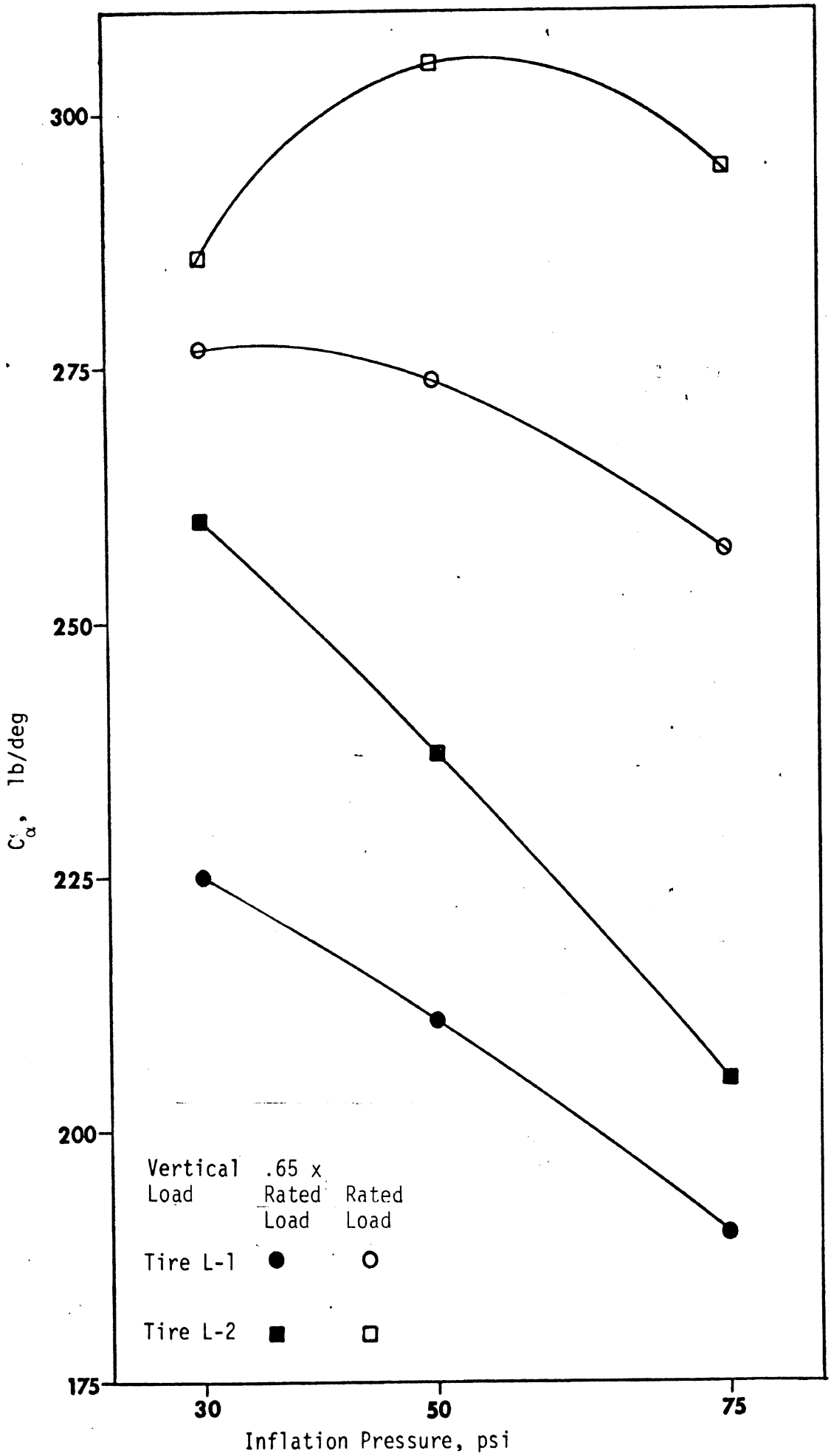

Figure 3.13 The effects of inflation pressure on cornering stiffness: light truck tires.

"μ-slip" plots by way of a digital averaging of the F_x/F_z versus slip relationship over five repeat lockup cycles at each test condition. As shown in Figure 3.14, the typical μ-slip behavior illustrates a steeply rising force response in the low slip regime, reflecting the elastic behavior of the tire structure. At around s = 20%, a peak in F_x/F_z occurs beyond which a monotonic decrease in force output prevails. Finally, at s = 100%, we see that the shear force has dropped by a large increment from the peak value. The large "falloff" in F_x/F_z from the peak to the 100% slip condition is a characteristic which, for dry pavements, clearly distinguishes heavy truck and bus tires from passenger car tires. Thus, while the following data will show truck and bus tires to exhibit peak-to-slide ratios of 1.2 to 2.0, the typical car tire might be seen to register 1.0 to 1.2 under the same conditions.

Shown in Figure 3.15 is a set of μ-slip curves obtained for a single tire over each of three loads and three velocities. By this illustration, it becomes clear that the basic shape of the μ-slip relationship becomes adjusted by both load and velocity. We can review these sensitivities over the sample of tires by considering three typical characteristics for each tire, namely:

1) the slope of F_x/F_z versus slip in the low slip regime,
2) the peak value of F_x/F_z, and
3) the value of F_x/F_z at s = 100%.

First, considering slopes, we see that the sample of tires is remarkably well identified according to construction and tread types in Figure 3.16. This figure presents the value of F_x/F_z at s = 4% as was measured for each tire at a velocity of 40 mph and a load equal to 100% of the T & RA rating. The 4% slip condition is chosen because of a greater accuracy of measurement than can be obtained at lower slip values and because of its representativeness of the positive slope portion of the longitudinal traction response.

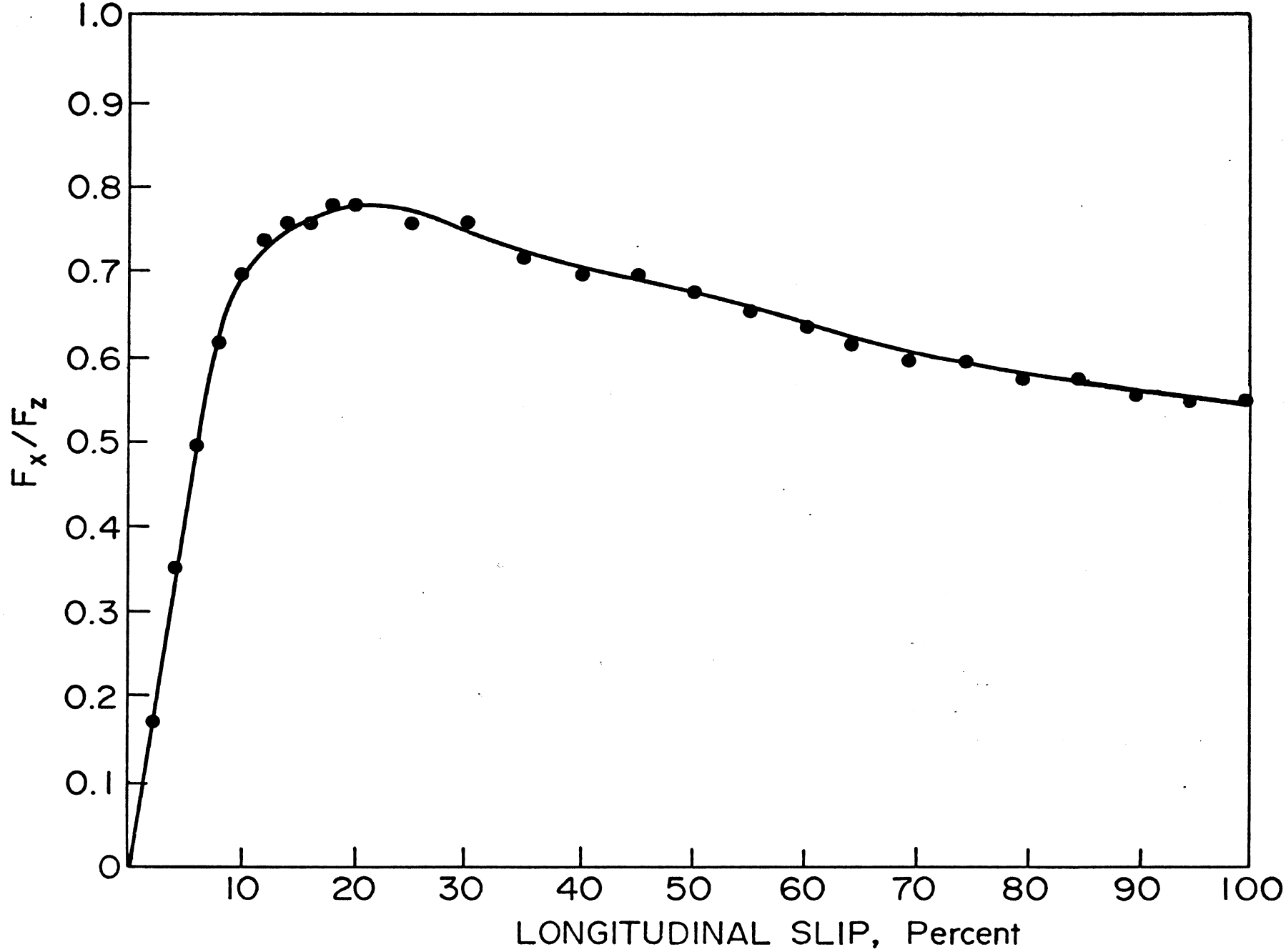

Figure 3.14. Typical μ-slip behavior of a 10.00 x 20/F heavy truck tire--dry pavement, 60 mph.

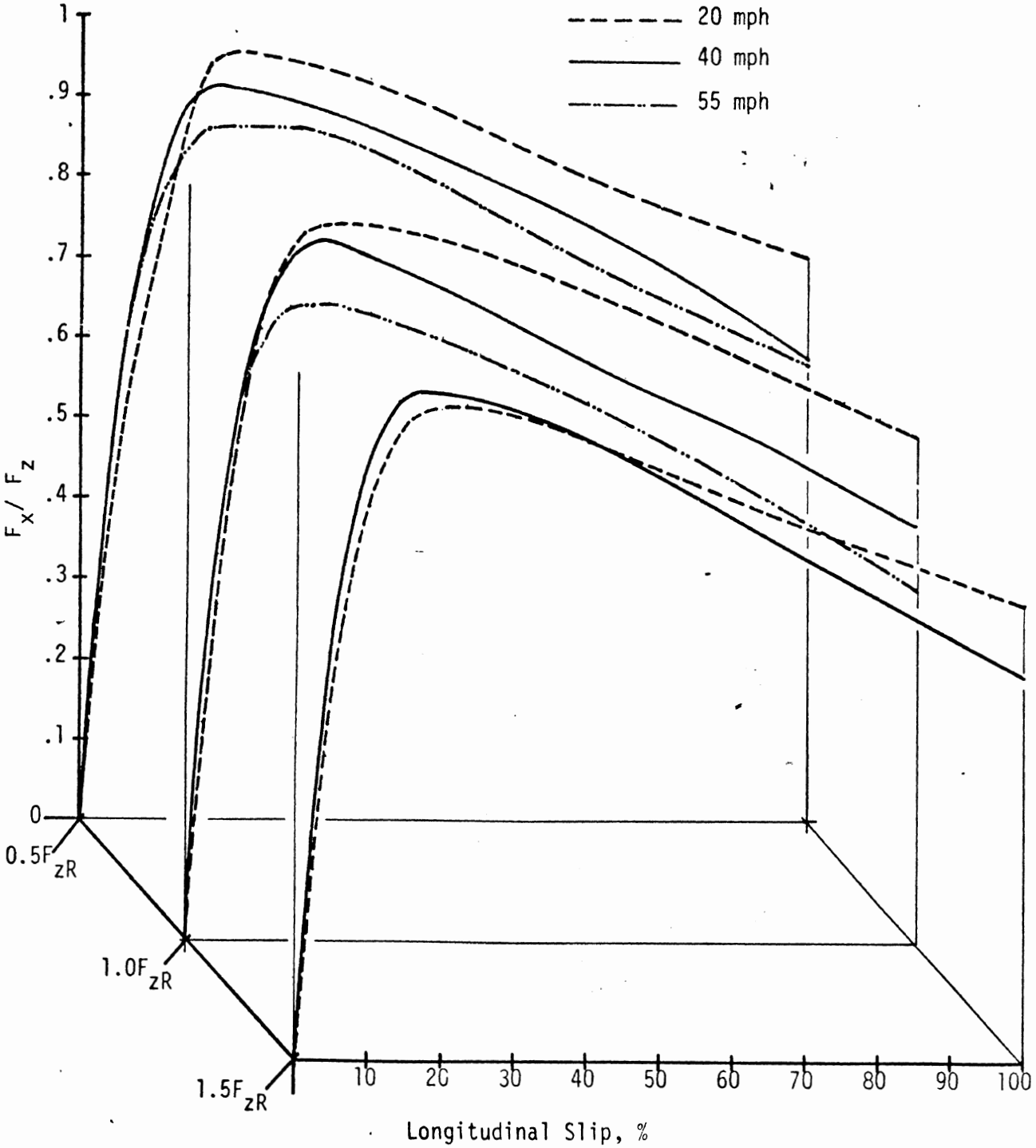

Figure 3.15. Family of μ-slip curves measured for a Goodyear Unisteel R-1 tire, size 10.00 R 20/G, on dry concrete.

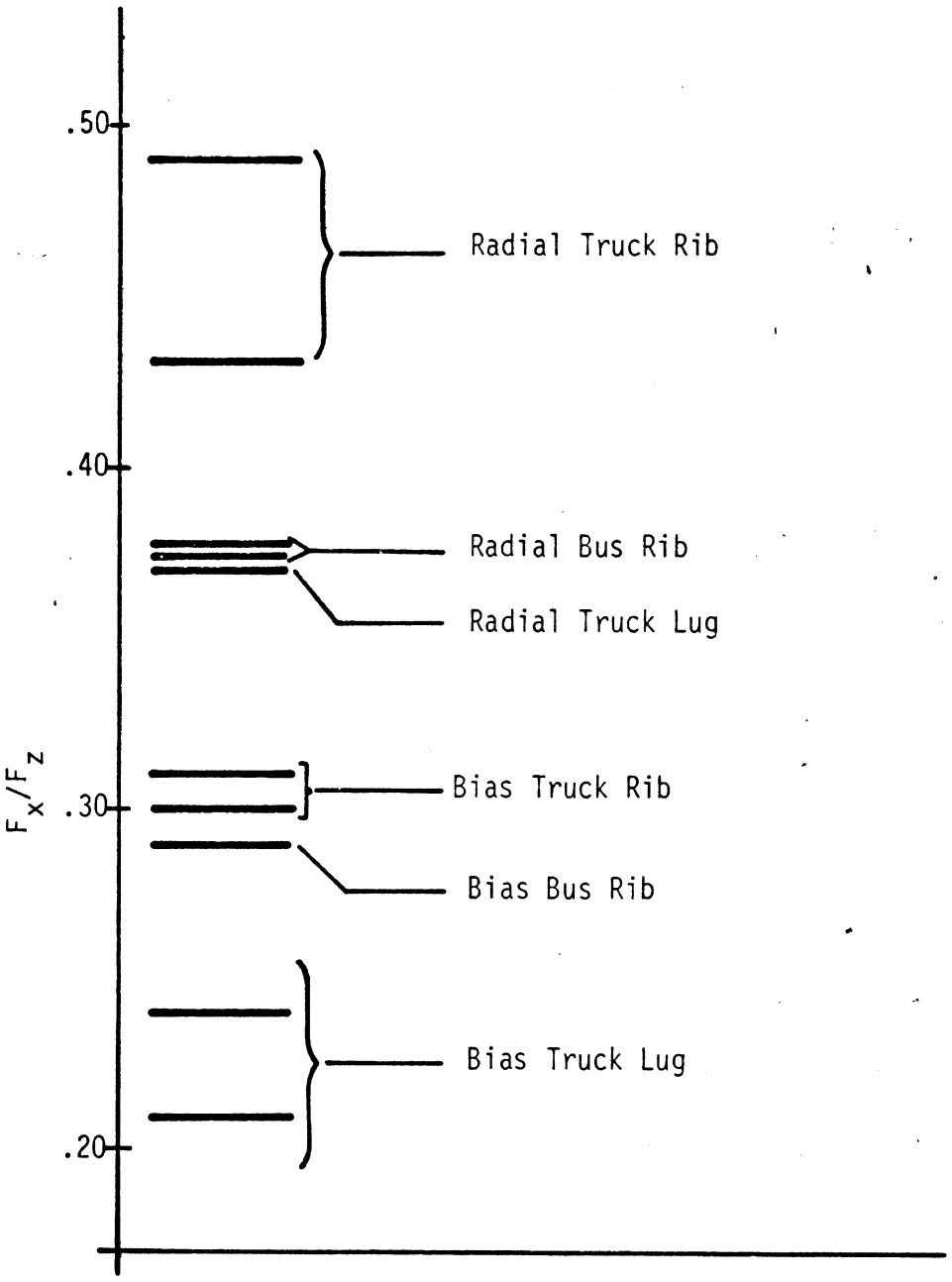

Figure 3.16. Distribution of F_x/F_z values measured at 4% slip, indicating relative longitudinal stiffnesses of various generic types of heavy tires, each tested at rated load.

Figure 3.16 clearly distinguishes between bias- and radial-ply constructions as well as between rib- and lug-type tread patterns. It is also interesting to note that the bus and truck tires in the sample are distinguished from one another in an orderly fashion, although the distinctions are insignificant for the bias-ply varieties.

An interesting separation between radial- and bias-ply tires is found in the cross plot of Figure 3.17. These data illustrate the value of F_x/F_z at s = 4% which was obtained over a range of loading. We find that the radial samples are basically increasing in this normalized stiffness parameter as load increases while the bias-ply samples are uniformly decreasing.

Since the non-normalized longitudinal stiffness of a tire (traditionally described as the slope of F_x versus s at s=0) depends directly on the length of the contact patch, one can approximate influences of load on stiffness by relating load to contact length. Thus, non-normalized longitudinal stiffness rises with increasing load because contact length always increases with load. A normalized stiffness measure, however, such as plotted in Figure 3.17, will increase with load only if contact length increases faster than load or if another carcass or tread-stiffening mechanism acts to augment the contact length mechanism. Thus the finding portrayed in Figure 3.17 can be most suitably explained on the basis of contact-lengthening and carcass-stiffening mechanisms which are significantly sensitive to the differences between bias- and radial-ply configurations.

The longitudinal traction limits afforded by a given tire on a given surface are commonly expressed as "peak and slide" values and are known to be sensitive to both load and velocity. The peak and slide performances of tires tested in this study have been reduced to define envelopes of F_x/F_z behavior as a function of load for each of the three test velocities. While the envelopes have been derived from both bus and truck tires, data are presented

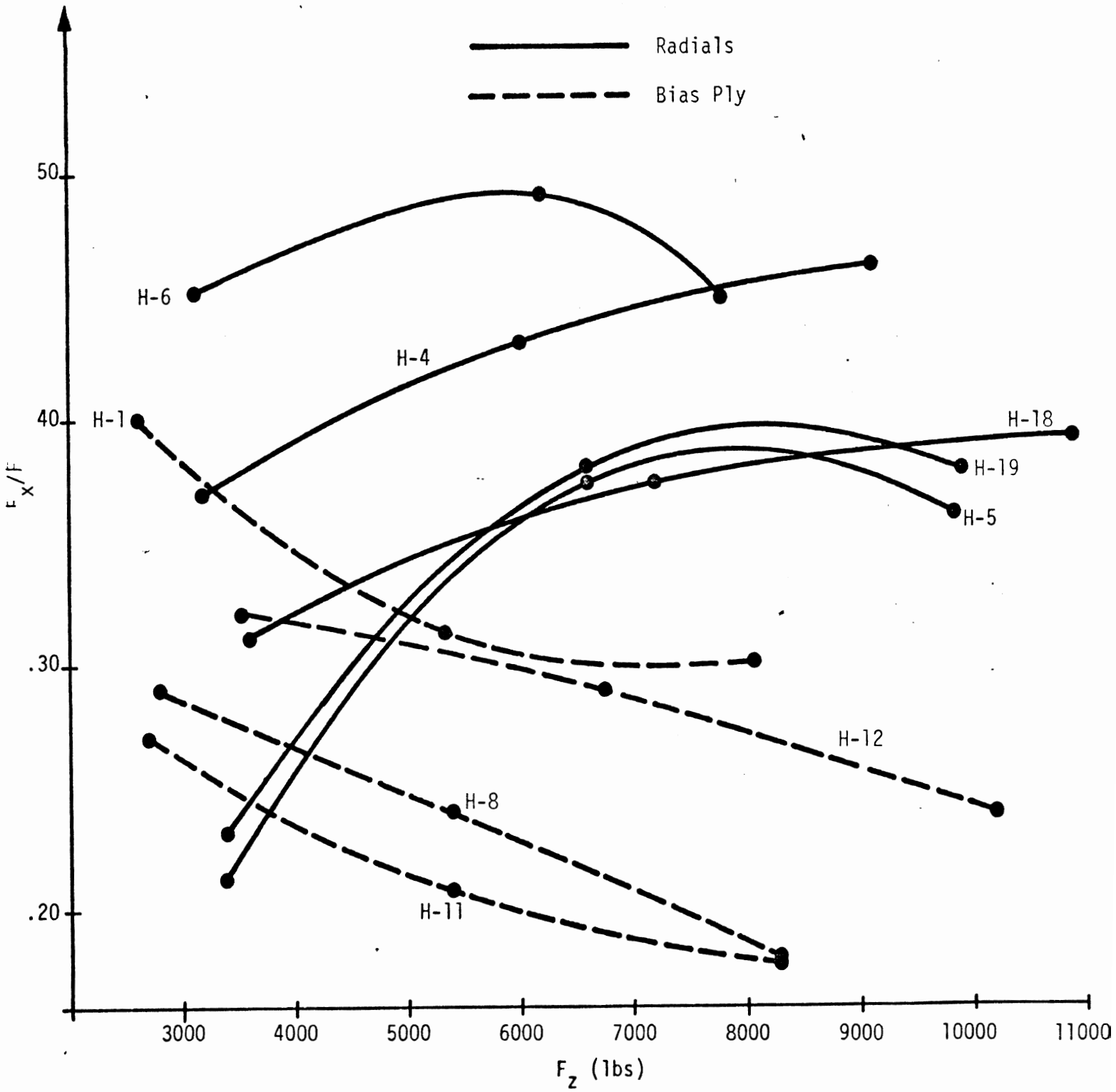

Figure 3.17. The load sensitivity of F_x/F_z values measured at 4% slip for heavy tires of radial and bias-ply construction (tires are identified by code numbers previously listed in Table 3-1).

showing, first, individual bus tires within the bus/truck tire envelope and then individual truck tires within that envelope.

Accordingly, Figures 3.18, 3.19, and 3.20 illustrate peak and slide performances for individual bus tires within the overall envelope for the respective velocities of 20, 40, and 55 mph. In general, the selected bus tires are seen to register low values of peak traction within the indicated envelope. Further, the two radial samples show consistently lower slide traction performance than the single bias-ply sample. Also, the growing spread between peak and slide envelopes as velocity increases is characteristic of commercial tire behavior on dry pavements.

In Figures 3.21, 3.22, and 3.23, the peak and slide performances of individual truck tires are presented for each of the three respective test velocities. These data indicate no clearly defineable distinctions among tire types although the bias-rib tire is a generally superior performer, considering both peak and slide behavior. Also, the radial tires exhibit generally reduced levels of slide traction.

3.2.2 Lateral Traction - Mobile Measurements. A set of eight heavy and eight light truck tires was subjected to a series of lateral traction measurements using the HSRI Mobile Dynamometer. These experiments involved a matrix of load and velocity conditions at each of which a staircase time history of slip angle (α) was applied. All data were gathered on a dry concrete surface and were obtained with each tire inflated to its T & RA-recommended cold inflation pressure. The data was computer processed from the time history format to yield discrete numerics of the tire's normalized side force response, F_y/F_z, at each value of α for which a "dwell" was employed in the staircase time history.

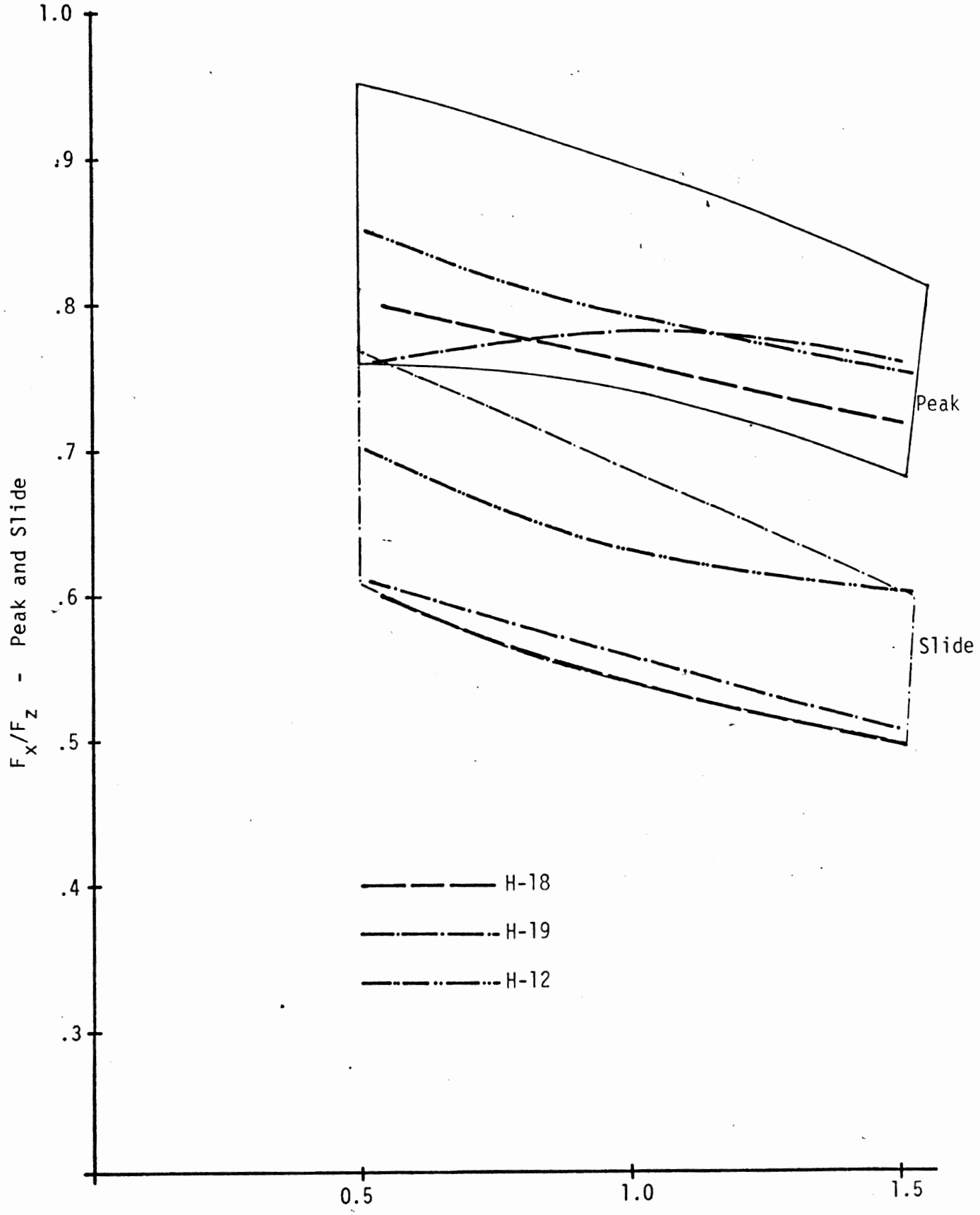

Figure 3.18. "Peak and slide" values of F_x/F_z vs. load for individual

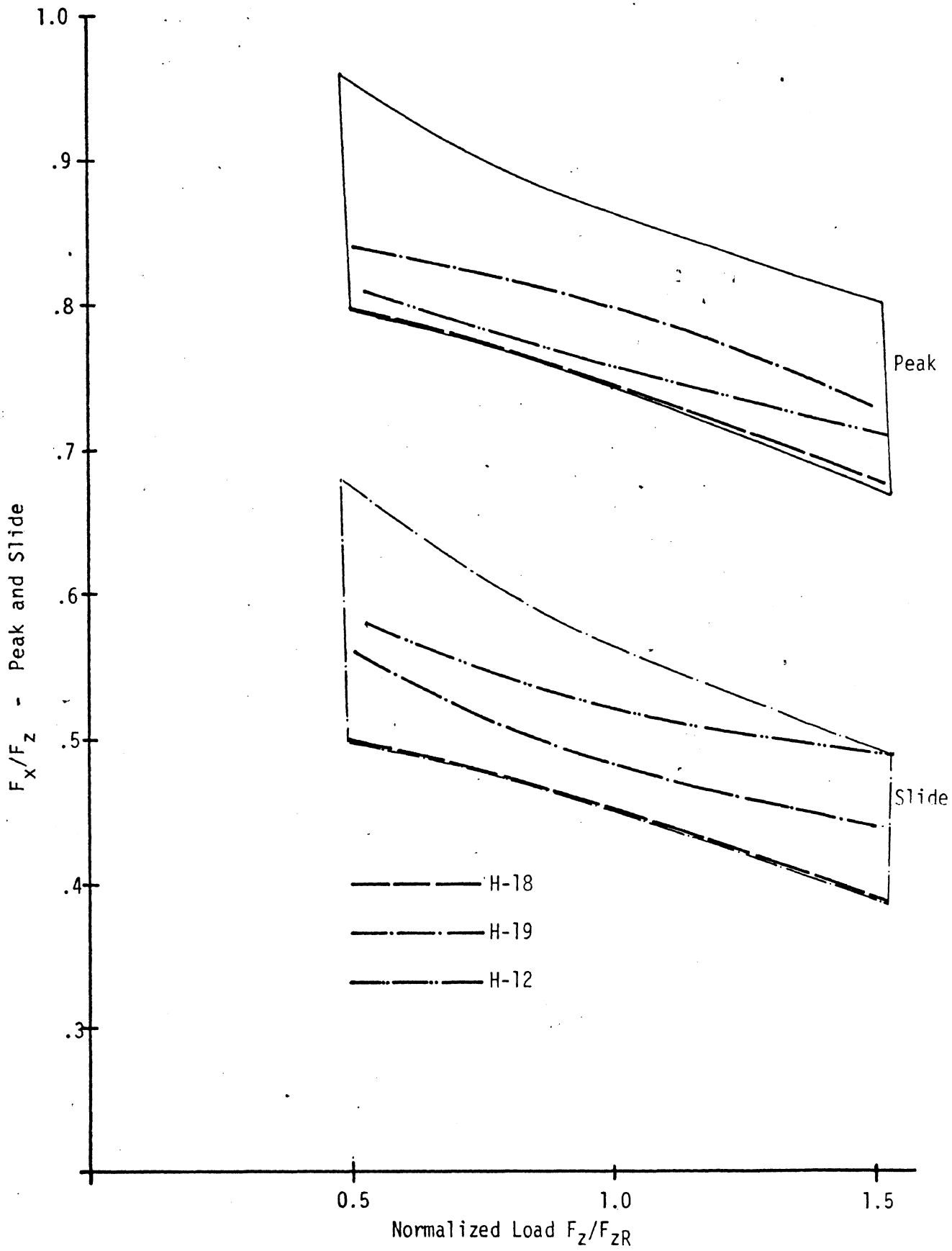

Figure 3.19. "Peak and slide" values of F_X/F_Z vs. load for individual bus tires—superimposed within the envelope of data taken on eight truck and bus tires at 40 mph (for code identifications, see Table 3-1).

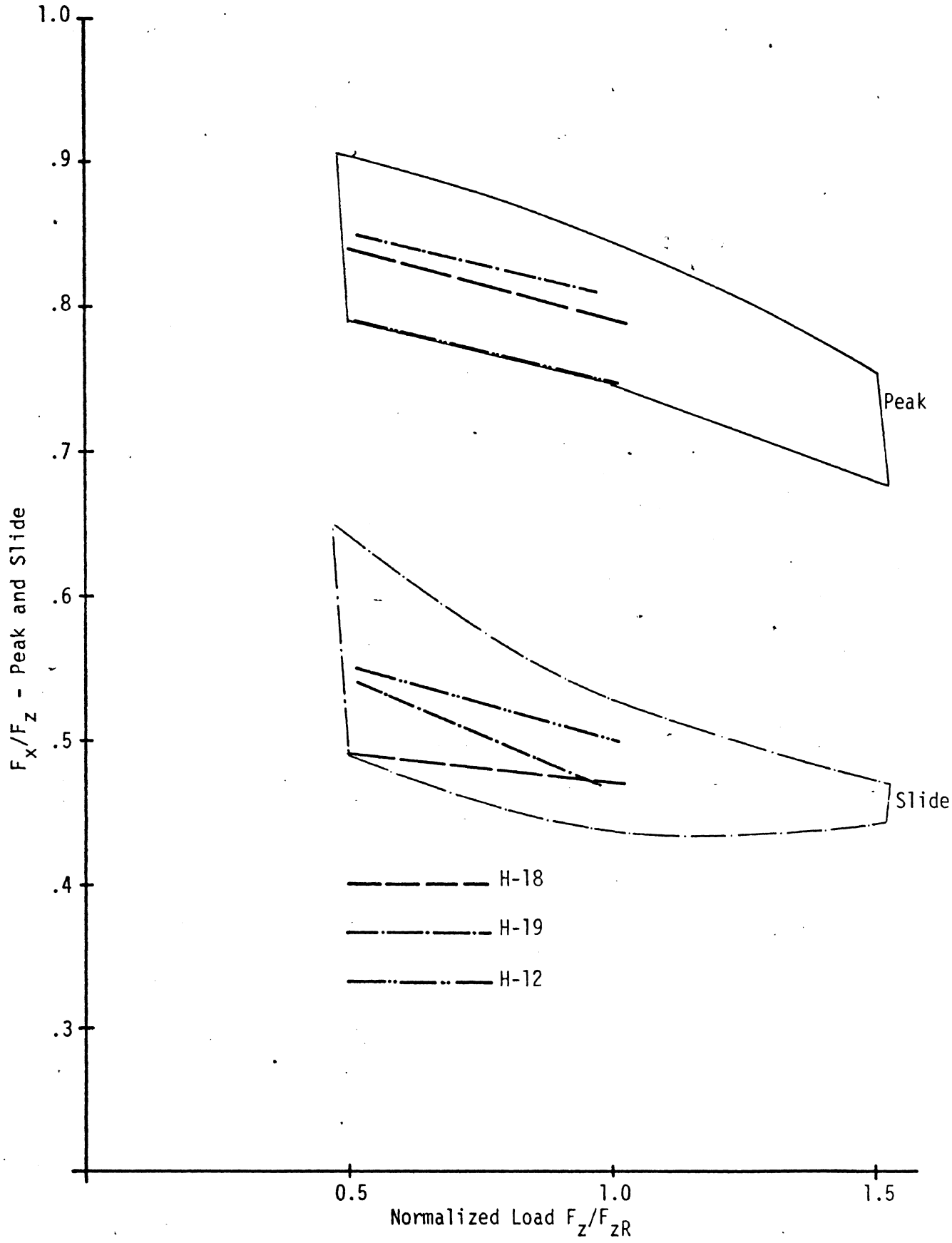

Figure 3.20. "Peak and slide" values of F_x/F_z vs. load for individual bus tires—superimposed within the envelope of data taken on eight truck and bus tires at 55 mph (for code identifications, see Table 3-1).

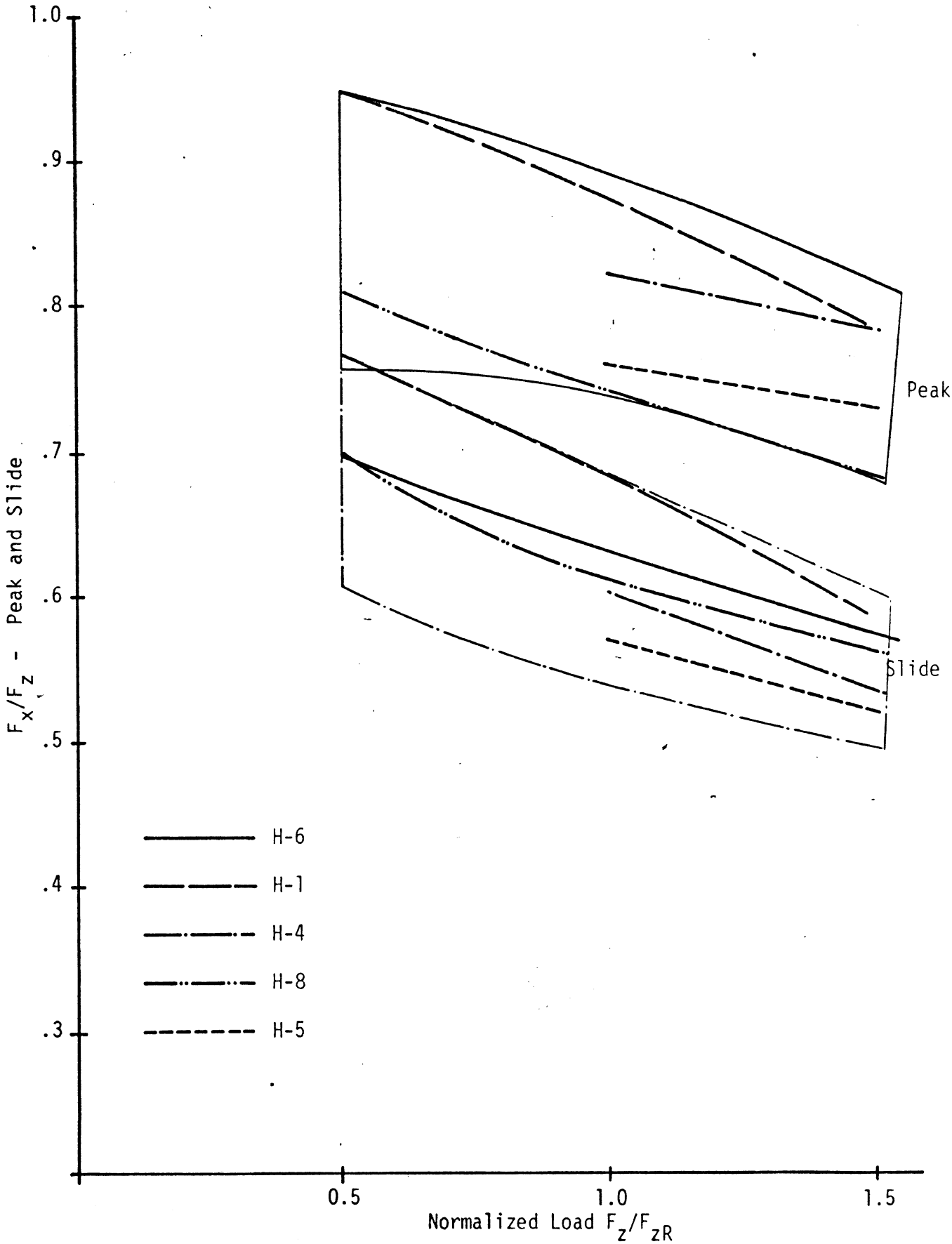

Figure 3.21. "Peak and slide" values of F_x/F_z vs. load for individual truck tires—superimposed within the envelope of data taken on eight truck and bus tires at 20 mph (for code number identifications, see Table 3-1).

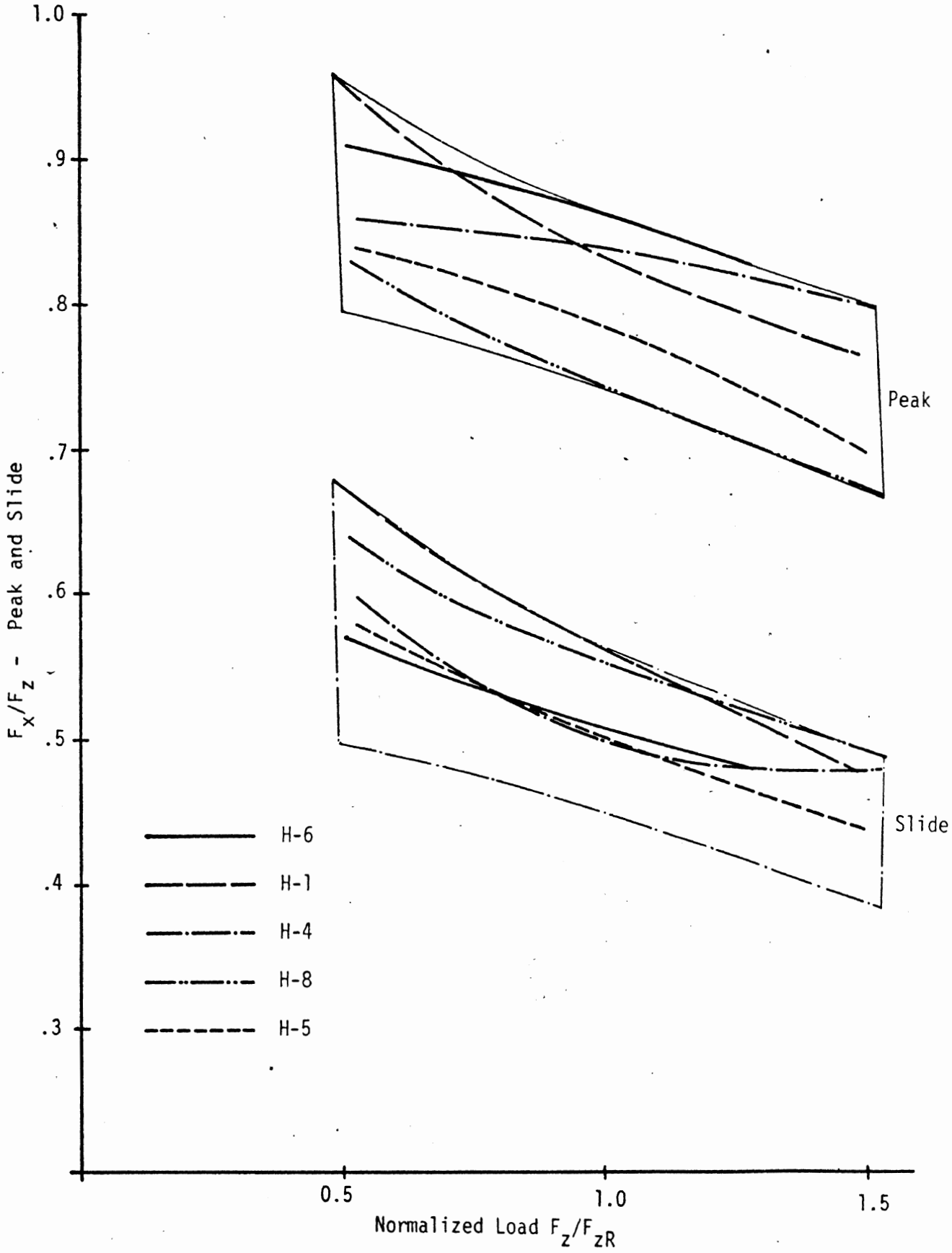

Figure 3.22. "Peak and slide" values of F_x/F_z vs. load for individual truck tires—superimposed within the envelope of data taken on eight truck and bus tires at 40 mph (for code number identifications, see Table 3-1).

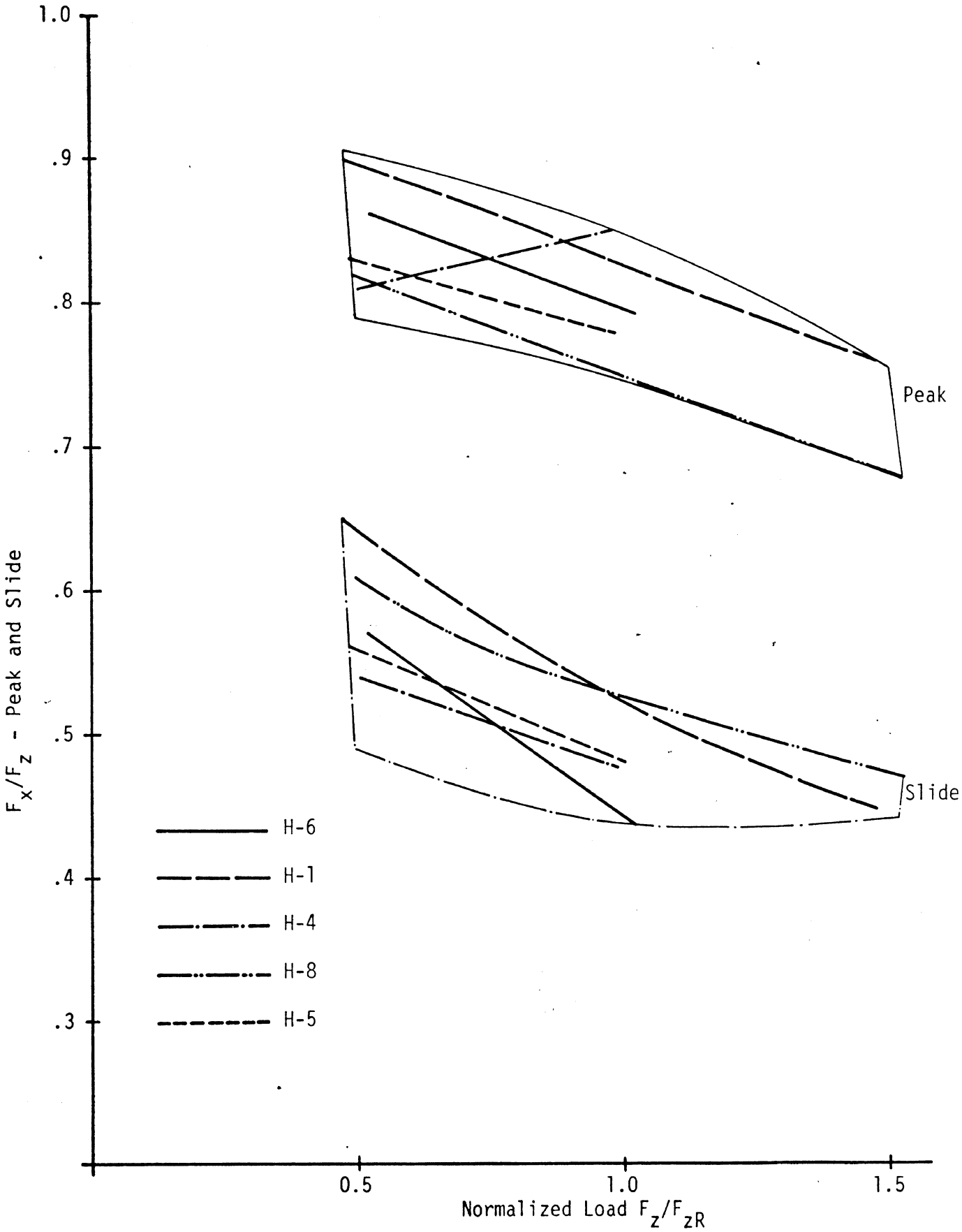

Figure 3.23. "Peak and slide" values of F_x/F_z vs. load for individual truck tires—superimposed within the envelope of data taken on eight truck and bus tires at 55 mph (for code number identifications, see Table 3-1).

As shown in Figures 3.24 and 3.25, the F_y/F_z performance of the heavy truck and bus tire sample at two values of vertical load is summarized. The plots indicate the envelope of responses obtained with all eight tires at the test velocity of 20 mph. The sensitivity of individual tires to changes in vertical load spanning the range from 0.5 to 1.5 times rated load is presented in Appendix C. An example of a typical tire's F_y/F_z performance over the load range is shown in Figure 3.26.

Examination of the envelope summaries and individual load sensitivities reveals a number of findings pertaining to specific tire constructions and to heavy vehicle tires in general. As illustrated in Figures 3.24 and 3.25, we observe that, at the higher load value, the range of behavior of the sample is more condensed and absolute values of normalized lateral traction are reduced over values of slip angle. Clearly, as was established previously with flat-bed measurements, F_y/F_z performance at small slip angles reduces with increasing load as a manifestation of the concave (downward) curvature of the C_α sensitivity to load.

The reduction of F_y/F_z with load at higher slip angles derives from the same sensitivity of the frictional coupling mechanism as influenced the load sensitivity of peak values of longitudinal traction. Indeed, the average reduction in F_y/F_z at $\alpha = 20°$ deriving from the load variation over the 0.5 to 1.5x F_{zR} range is seen to be about -0.12 which compares closely with the average $(F_x/F_z)_{peak}$ reduction of -0.10. Certain tires, however, depart markedly from the average sensitivity of peak F_y/F_z to load. The indicated radial-type bus tire, for example, falls by 0.25 in its F_y/F_z peak value while the bias-ply bus tire shows virtually zero reduction in F_y/F_z over the 0.5 to 1.5 F_{zR} load range.

As can be seen in the specific tire examples overlaid on Figures 3.24 and 3.25, the occurrence of the saturated shear force, or "peak," F_y/F_z condition is not uniquely tied to any given value of slip angle. Thus, for example, certain radial tires have reached their friction-limited condition in the vicinity of $\alpha = 12°$ at the

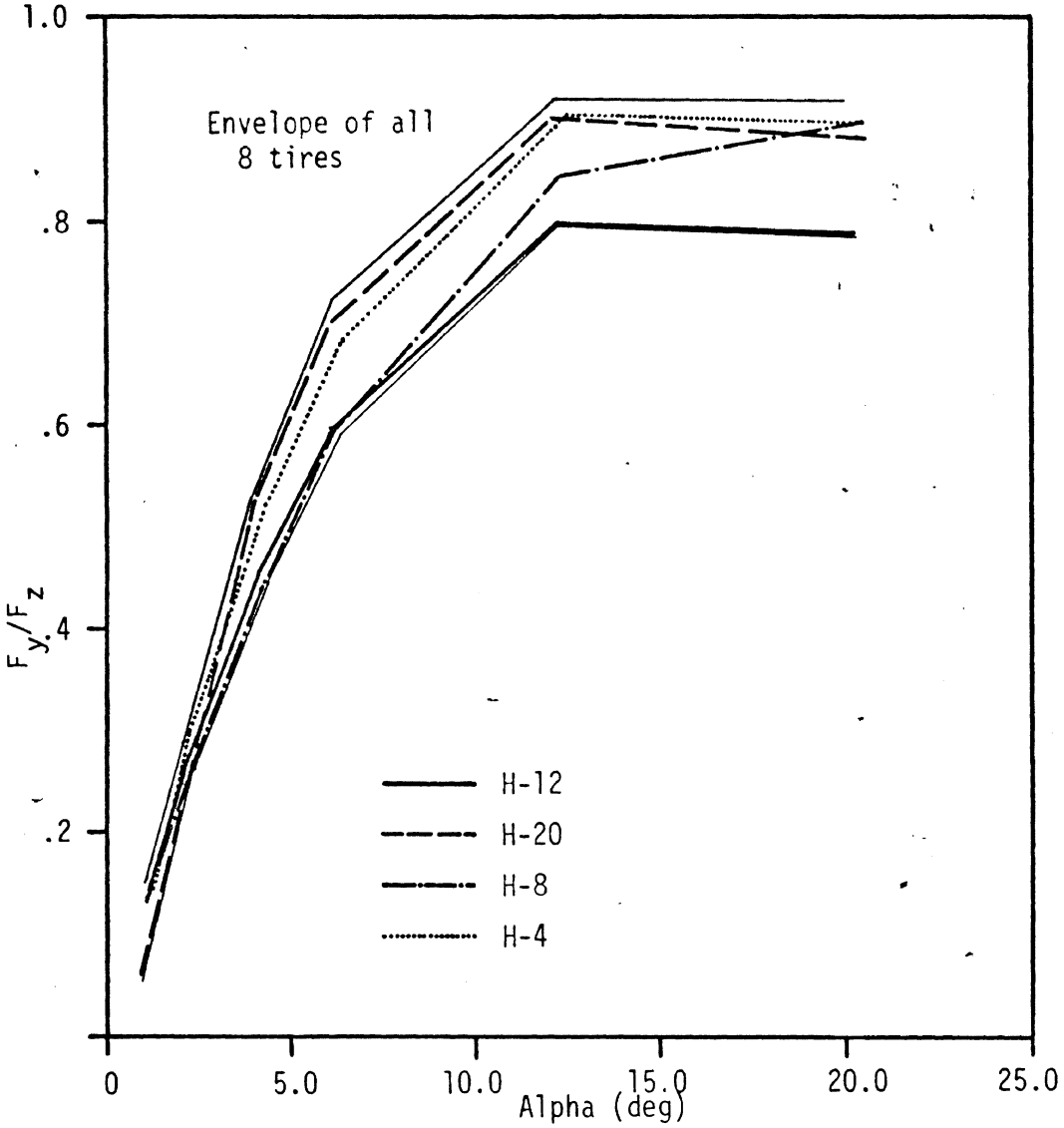

Figure 3.24. Lateral force measurements of heavy truck and bus tires at 20 mph and 0.5 x rated load.

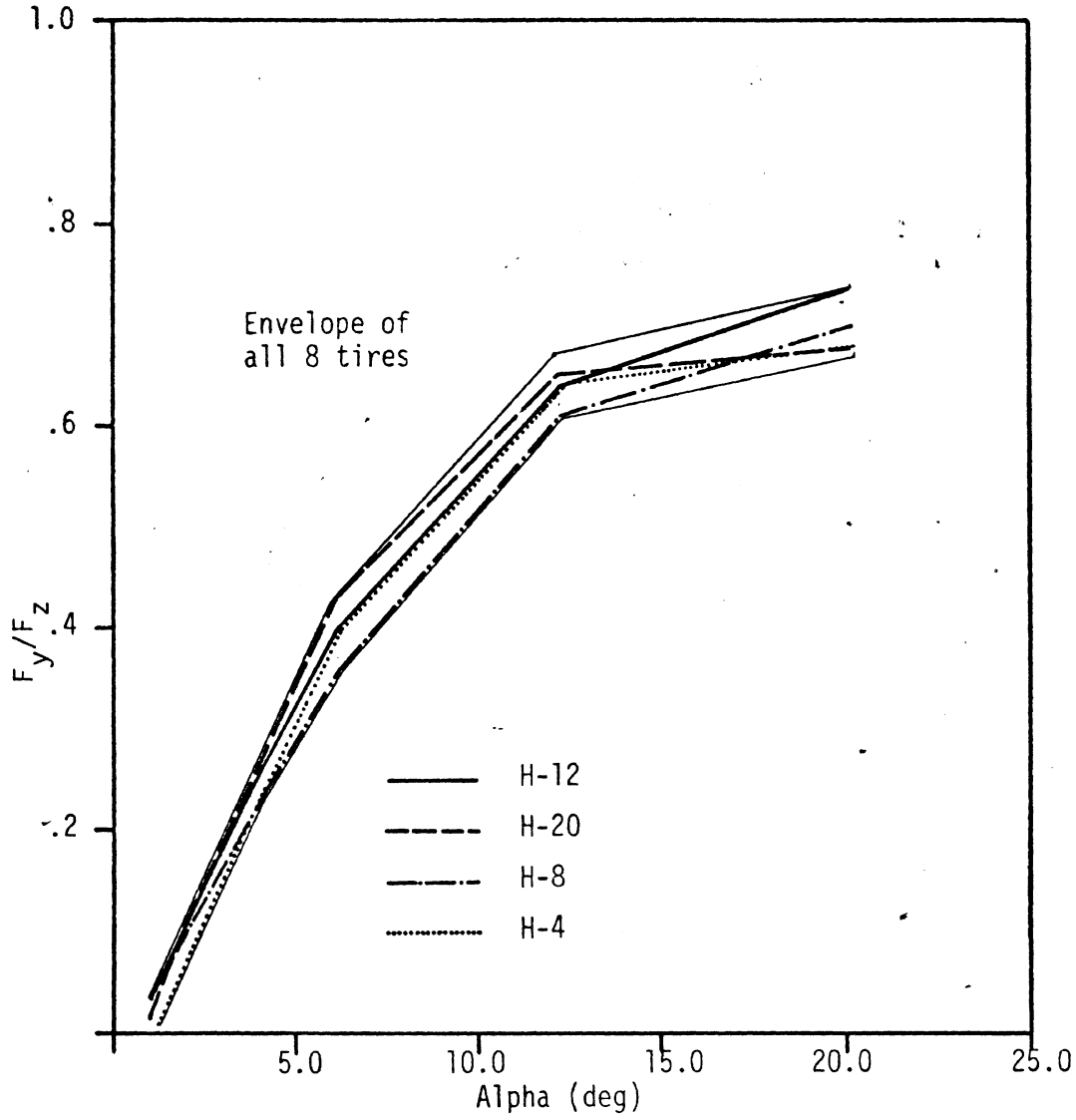

Figure 3.25. Lateral force measurements of heavy truck and bus tires at 20 mph, 1.5 x rated load.

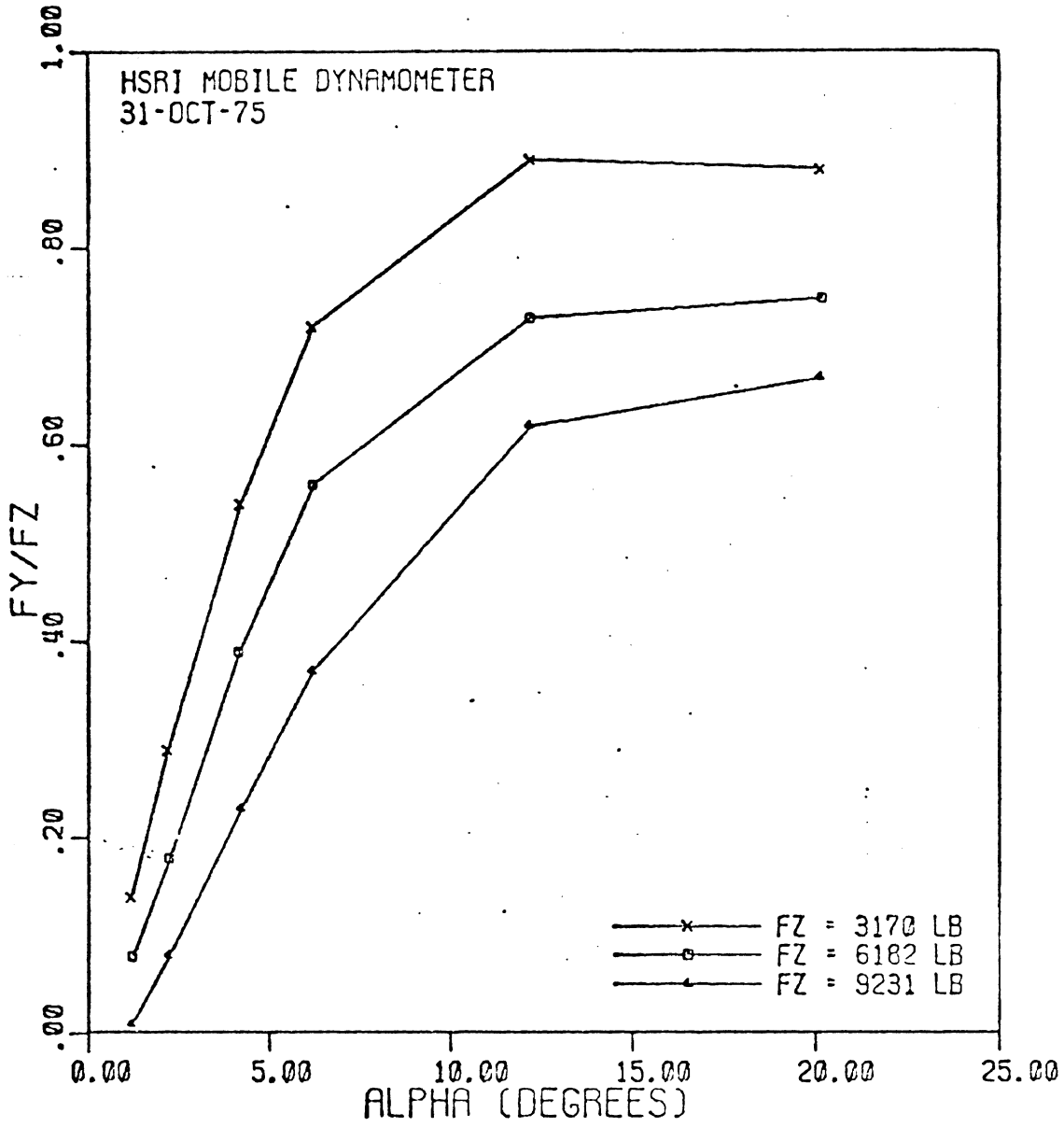

Figure 3.26. Typical array of (F_Y/F_Z vs. α) curves covering the load range from $0.5F_{zR}$ to $1.5\ F_{zR}$.

$F_z = 0.5\ F_{zR}$ condition while the same tire is not yet saturated at $\alpha = 20°$ under the $1.5\ F_{zR}$ load condition. This fundamental property of the side force response of pneumatic tires requires that we pay particular attention to the slip values at which saturation occurs as well as to the limit traction levels themselves.

In this vein, we can draw certain marked distinctions among the limit traction behavior of the various tire types represented. Radial tires in the sample, for example, typically peak in F_y/F_z at lower slip angles than do bias-ply specimens. This performance can be shown to follow directly from the elevated values of cornering stiffness characterizing the radials. Additionally, at the lower vertical load value, the radial samples exhibit a distinct negative slope in their F_y/F_z versus α relationship in the slip angle regime above $\alpha = 12°$. While the various sizes of bias-ply tires exhibit somewhat mixed results, they generally indicate a positive slope in F_y/F_z versus α up to the 20° value of α, at all loads examined. Further, at the $1.5\ F_{zR}$ condition, the bias-ply tires exhibit rather steep slopes indicating that actual side force saturation may not occur until α attains values in the proximity of 30°. In line with this observation, the lug-type tire is particularly notable as a construction variety which, by dint of its compliant tread structure and low C_α behavior, tends to saturate at quite high values of α.

Shown in Figures 3.27, 3.28, and 3.29, the envelopes of F_y/F_z versus α responses obtained at rated load and at three values of velocity are presented. The ranges of traction performance indicated at each value velocity are similar to those observed at each of the two extreme values of vertical load. Going from the 20- to 55-mph velocity condition, the only noticeable feature is that very little, if any, net reduction in F_y/F_z peak results from the velocity increment. Indeed, individual plots of each tire's velocity sensitivity, such as typified by the example of Figure 3.30, indicate remarkably low changes in F_y/F_z behavior with test speed. Additionally, the summary plots of Figures 3.27, 3.28, and 3.29 indicate only minor changes in $F_y/F_z/\alpha$ shape and in the rank order of the illustrated example tires over the velocity range.

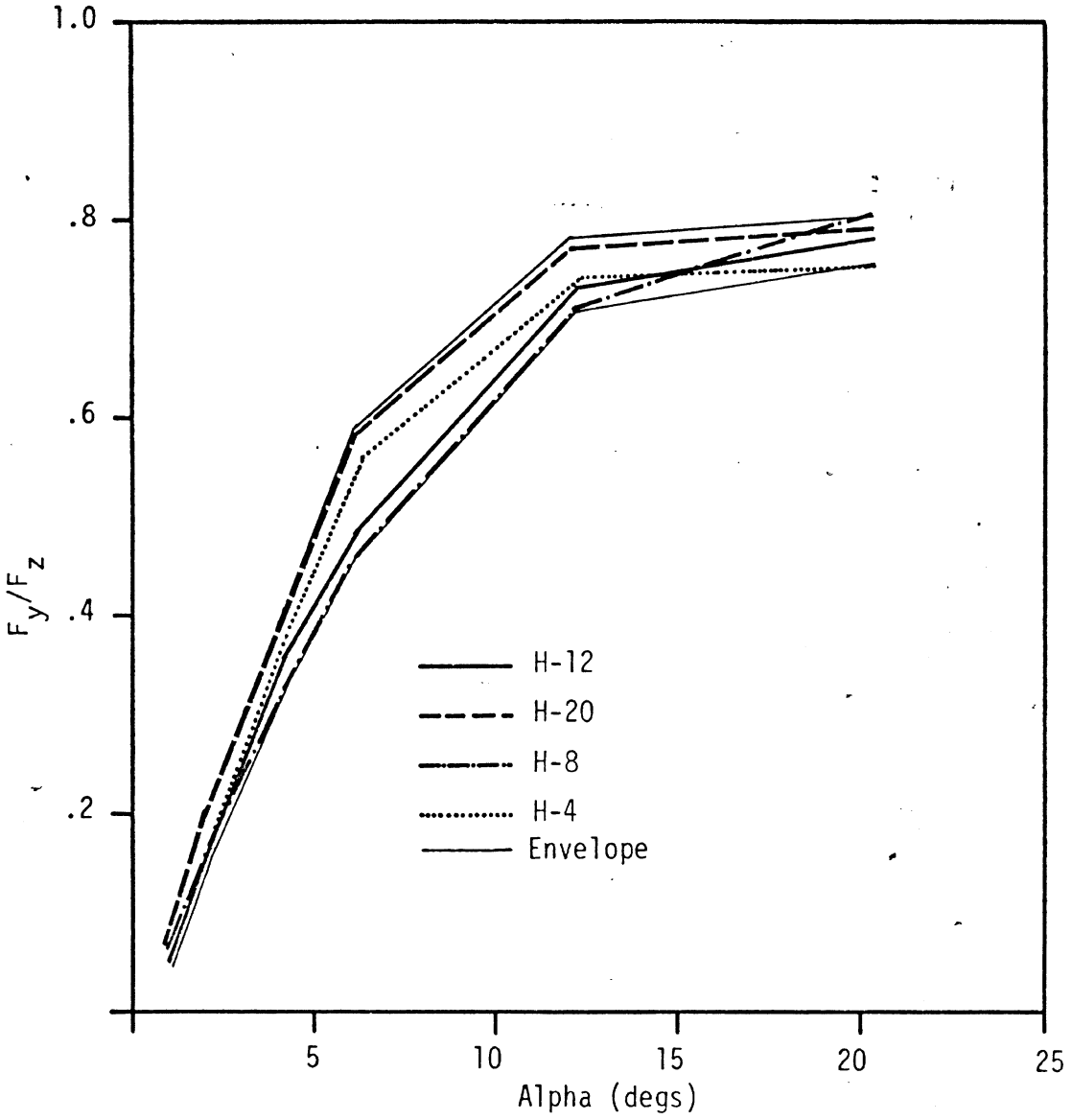

Figure 3.27. Envelope and specific examples of (F_y/F_z vs. α) measurements taken for 8 heavy truck and bus tires at 1.0 F_{zR} and 20 mph.

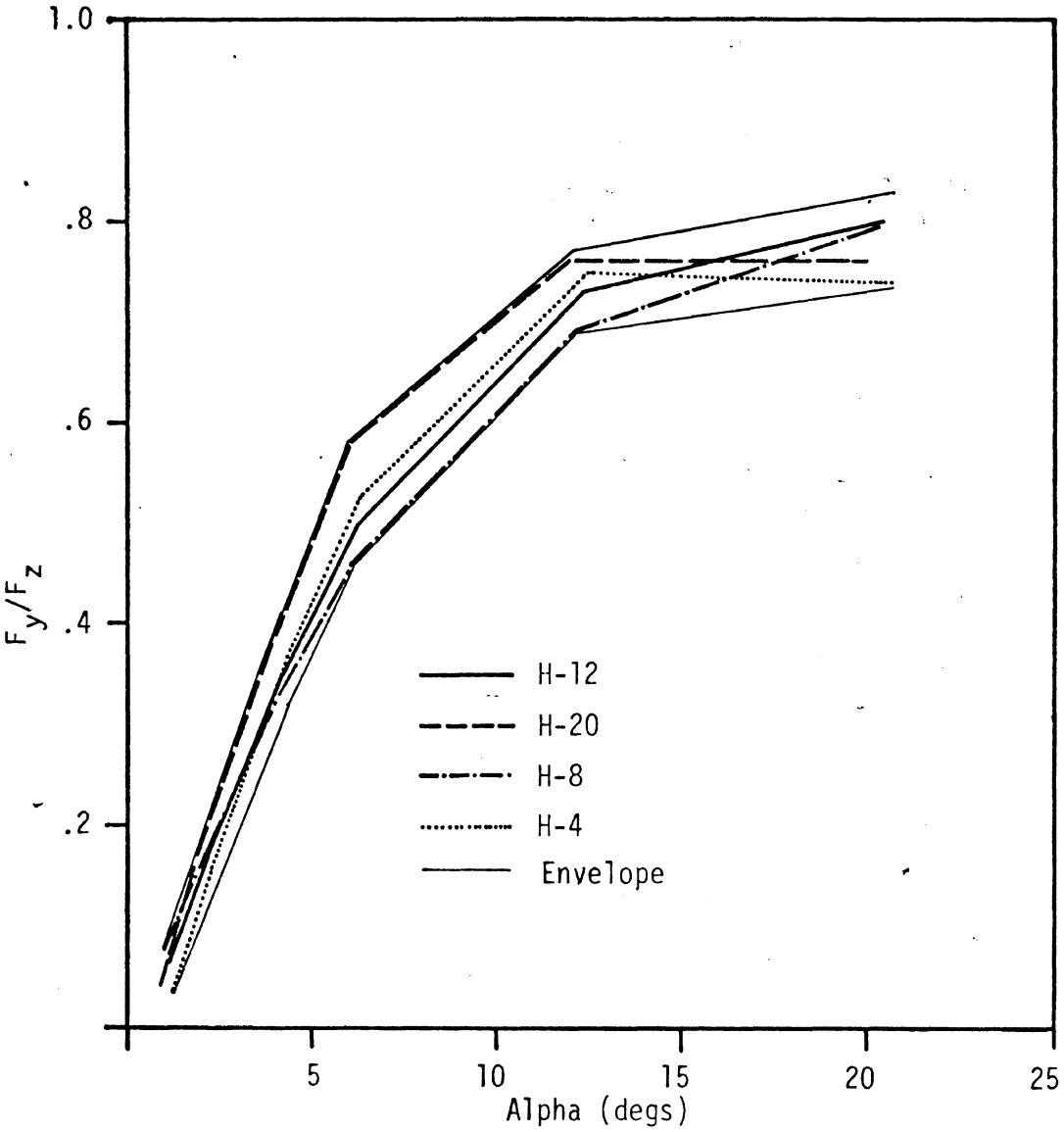

Figure 3.28. Envelope and specific examples of (F_y/F_z vs. α) measurements taken for 8 heavy truck and bus tires at 1.0 F_{zR} and 40 mph.

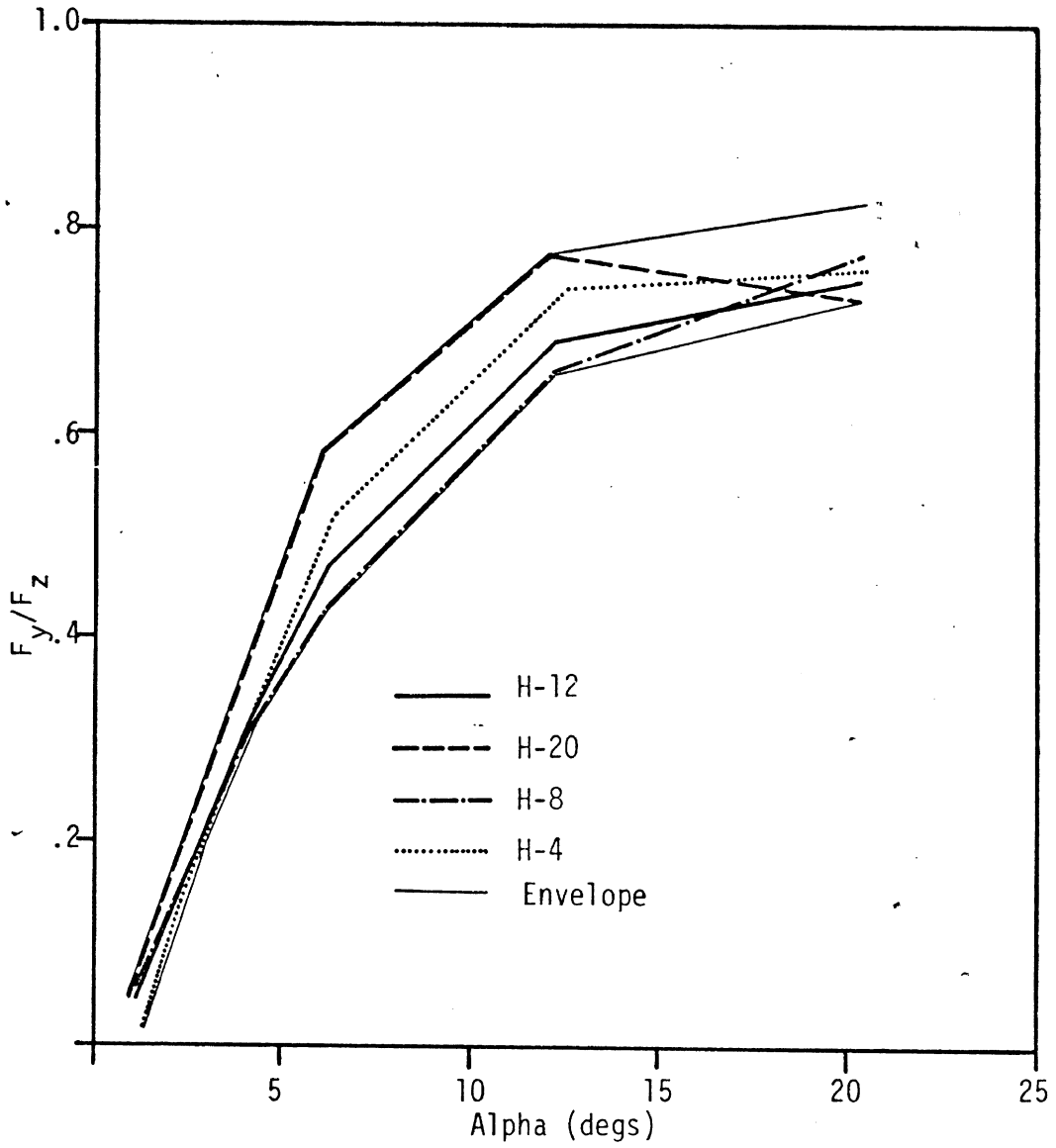

Figure 3.29. Envelope and specific examples of (F_y/F_z vs. α measurements taken for 8 heavy truck and bus tires at 1.0 F_{zR} and 55 mph.

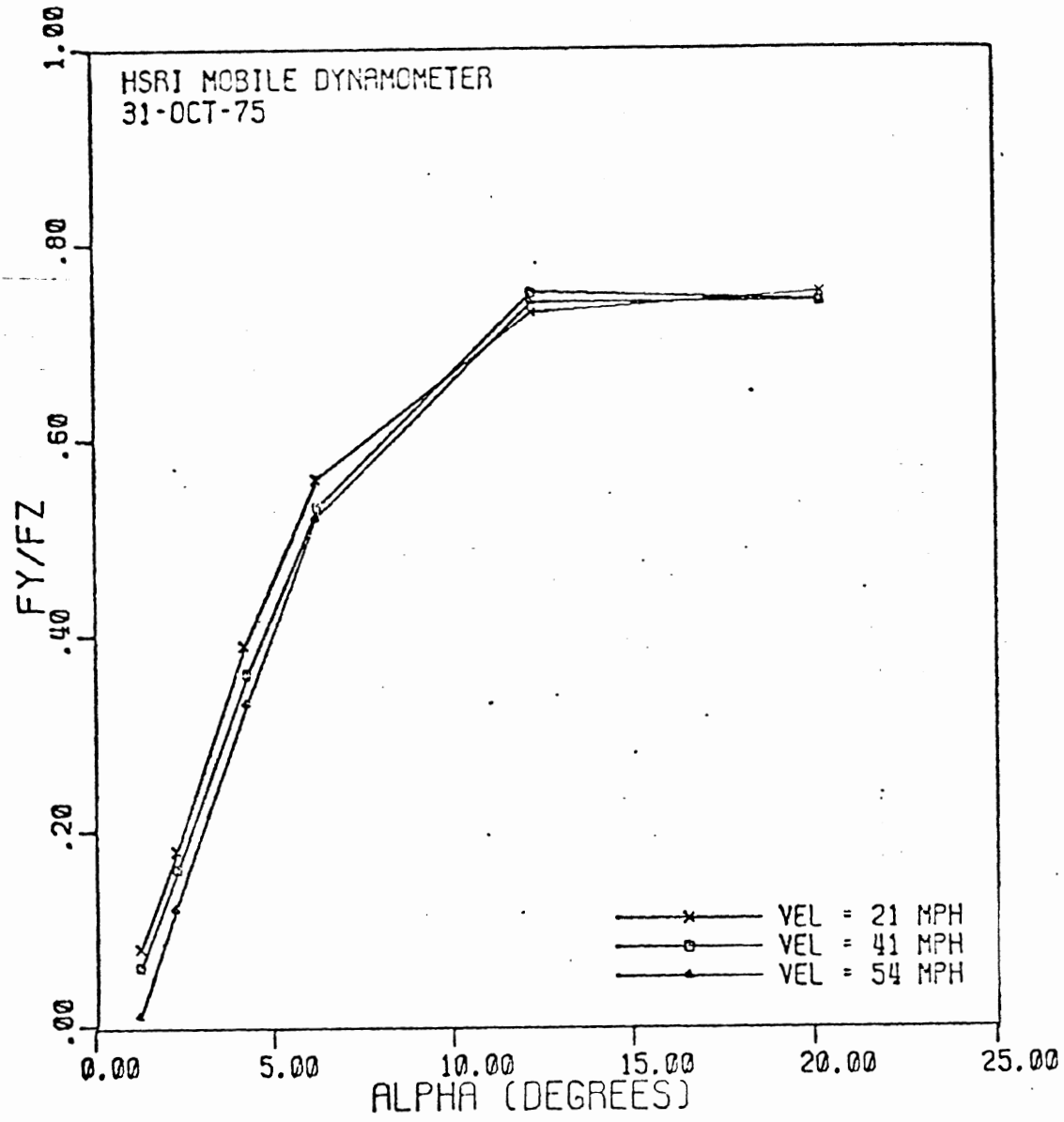

Figure 3.30. Typical array of (F_Y/F_Z vs. α) curves illustrating negligible sensitivity to velocity over the range 20 to 55 mph.

The minimal sensitivity of lateral traction to velocity generally agrees with the low level of velocity sensitivity observed in the previously presented peak longitudinal traction data. Since the $\alpha = 20°$ condition involves a net slip velocity in the contact patch which is comparable to that experienced at the peak of the μ-slip curve (at s = 20 to 25%), these two traction conditions would seem to be analogous from a friction mechanisms point of view.

As a final point summarizing the lateral traction measurements obtained using the mobile machine, Figure 3.31 is presented as a typical indication of the test-induced wear sensitivity of the eight heavy tires tested. The plot illustrates the progressive change in F_y versus α behavior for a single tire specimen subjected to a periodic repeat of the reference condition of rated load and 40-mph test velocity. The changing lateral force response basically illustrates that

1) the test-induced wear tends to increase the peak side force capability of the specimen, and

2) the asymmetry of the wear pattern tends to induce an increased force offset at $\alpha = 0°$.

The result depicted in this example has been observed in measurements of passenger car tire traction involving repeated operation at elevated slip angles and on high friction surfaces [5]. The test wear anomaly—while of no particular significance to heavy vehicle usage—does degrade the quality of mobile lateral traction measurements which are intended to illustrate characteristic sensitivities to operating conditions which are indexed from run to run.

In addition to the lateral traction measurements obtained with heavy truck tires, a sample of eight light truck tires was also examined using the mobile apparatus. In tests of the LT tires, the minimum load limitation of the mobile device prevented the exercise of a test matrix with common fractions of rated load

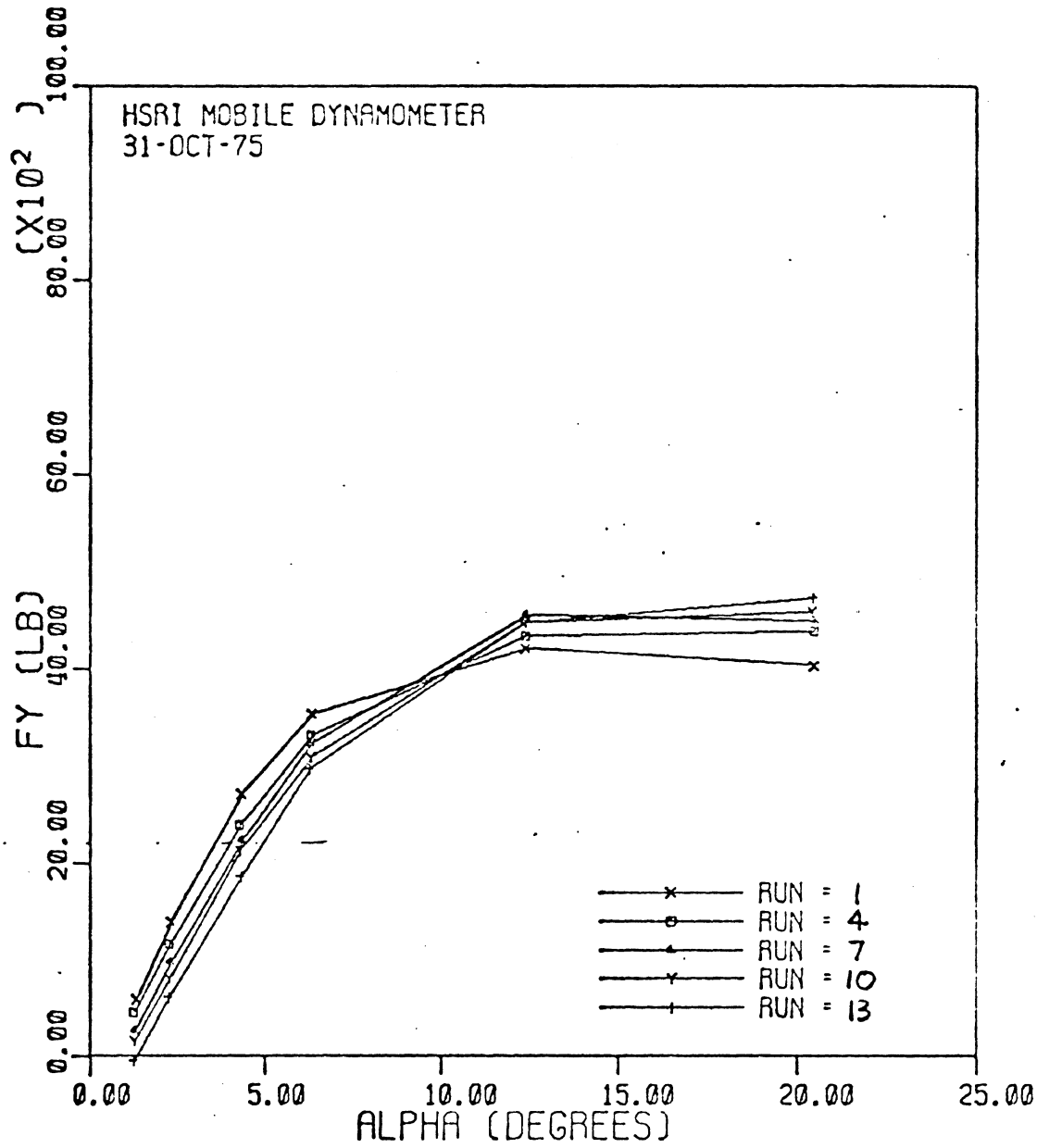

B. F. GOODRICH MILESAVER RADIAL STEEL HDR 10.00R20/G
FZ = 6063 LB VEL = 41 MPH

Figure 3.31. Typical repeat run data for heavy truck tire specimen.

for all samples. Thus, envelopes of lateral traction performance at the previously employed 0.5, 1.0, and 1.5 load fractions are not presented here as data summaries. Shown in Figures 3.32 and 3.33 are examples of load sensitivities for an 8.00R16.5 radial tire and an 8.00 x 16.5 bias-ply sample, respectively. These load sensitivities are typical of the radial and bias-ply constructions which were examined—the bias-ply samples experiencing a larger reduction in F_y/F_z with increasing load than the radial-ply samples.

The envelope of all measurements obtained at velocities of 20, 40, and 55 mph and loaded to 2850-3050 lbs, are shown in Figures 3.34, 3.35, and 3.36. With certain selected examples illustrated within the envelopes, trends comparable to those cited in the heavy tire data are evident, although the two radial-ply samples are remarkably different from one another and, thus, defy any generalization. The overall spread of the envelope is rather large, indicating the light trucks and vans can mount tires spanning a very broad range of shear force properties. When one examines the changes either in the envelopes or in the individual tire behaviors across the three test speeds, a minimal velocity sensitivity is observed. As emphasized by the typical individual velocity sensitivity plot shown in Figure 3.37, the velocity sensitivity of the light truck tire on dry pavement is indeed negligible. An interesting anomaly of the test data obtained on certain tires would suggest a conflict with this finding, however, as illustrated in Figure 3.38. The peak values of F_y/F_z in Figure 3.38 are seen to <u>increase</u> by about 0.08 over the 20- 55-mph range while all other evidence would indicate that, if anything, peak shear forces should <u>reduce</u> with increasing velocity. The conflict is apparently explained by the test-induced wear which progressively influenced the shear force limits exhibited by each tire as the sequence of test conditions was applied. As shown in Figure 3.39, the Michelin radial, which was seen to exhibit minimal velocity sensitivity in the Figure 3.37 plot, is also seen to exhibit a rather small change in its reference F_y/F_z behavior as a result of the wear accrued from repeated testing. In contrast, Figure 3.40 reveals the

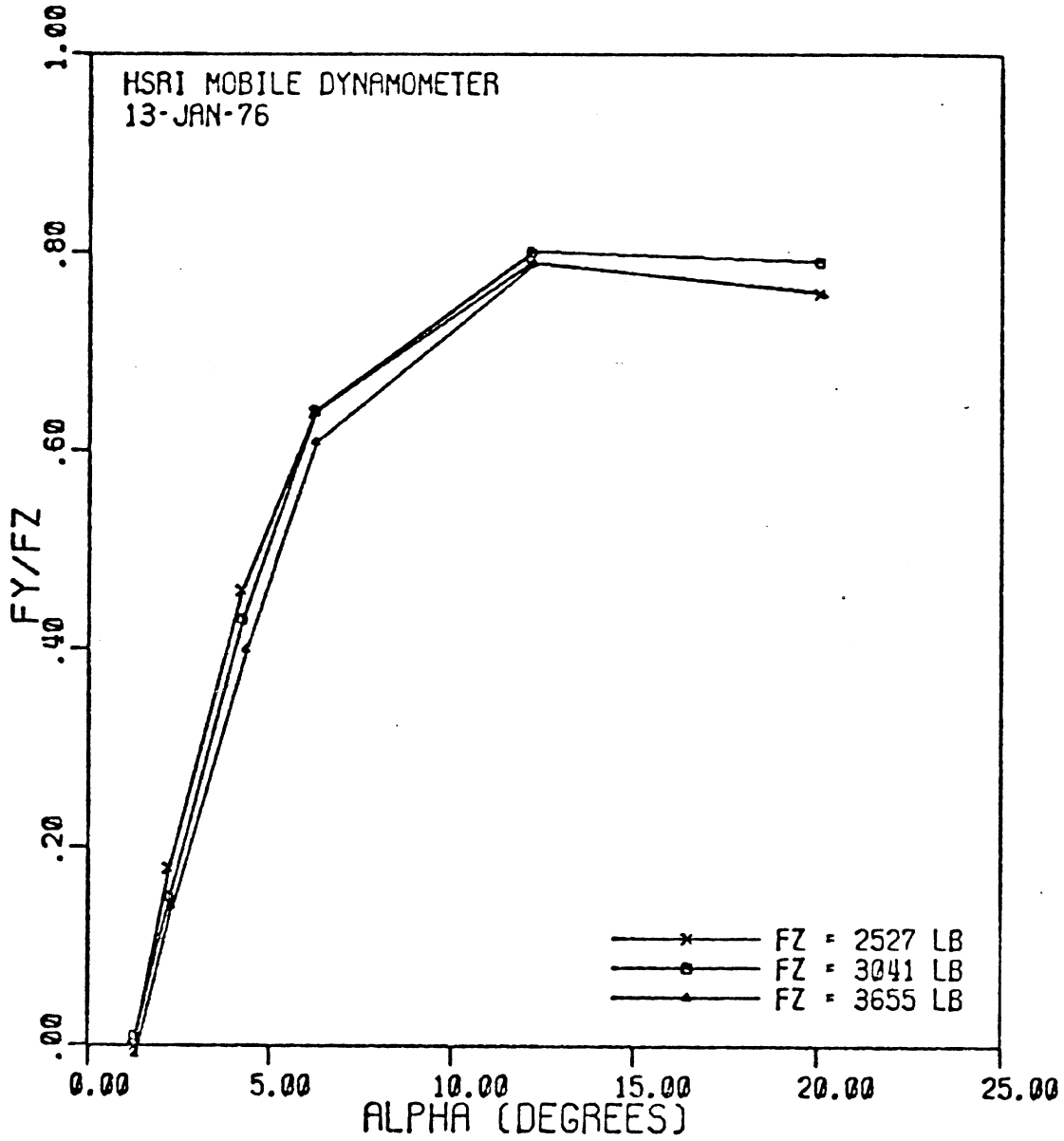

Figure 3.32. Example load sensitivity in the lateral traction performance of a light truck radial.

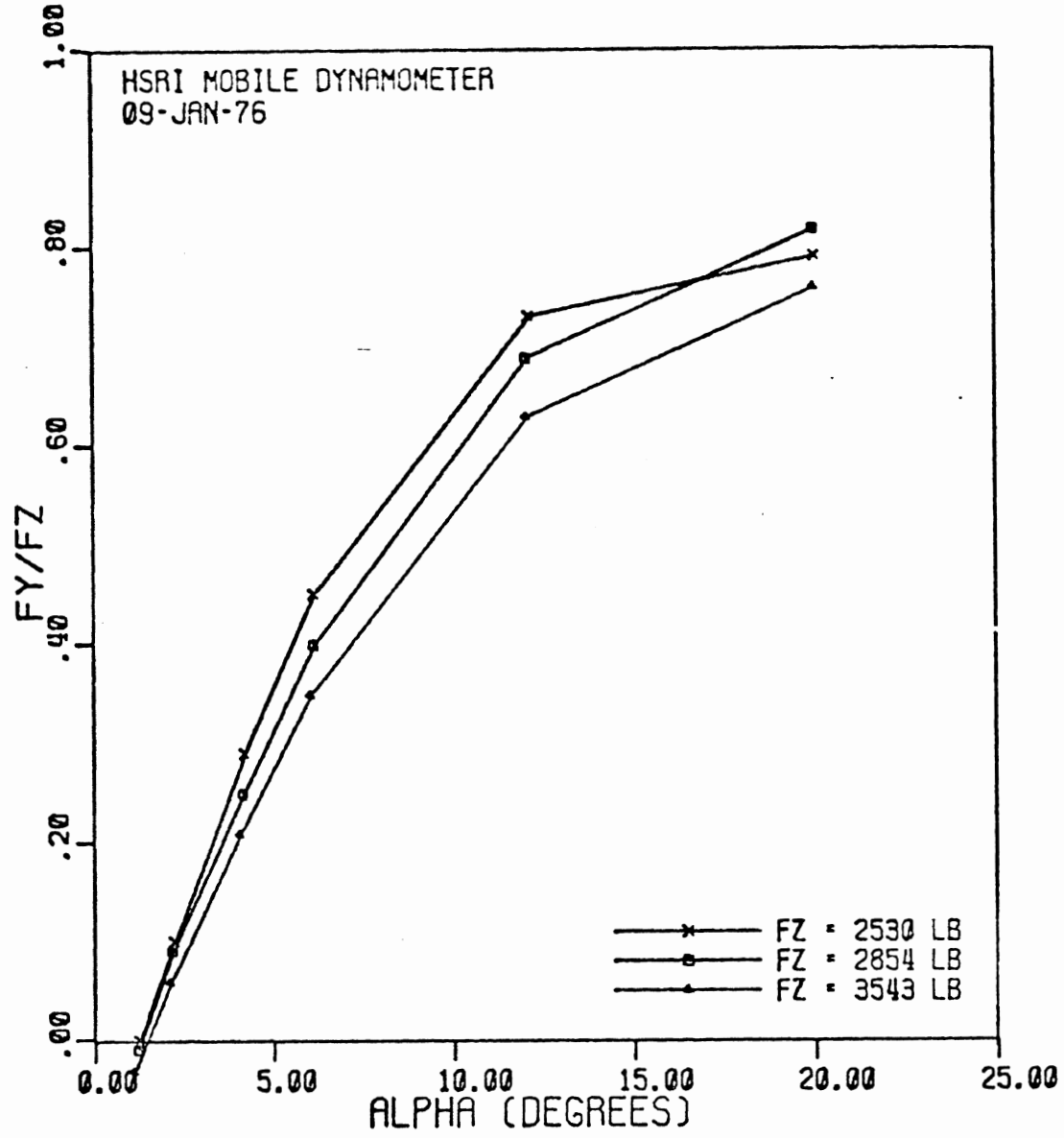

Figure 3.33. Example load sensitivity in the lateral traction performance of a bias-ply light truck tire.

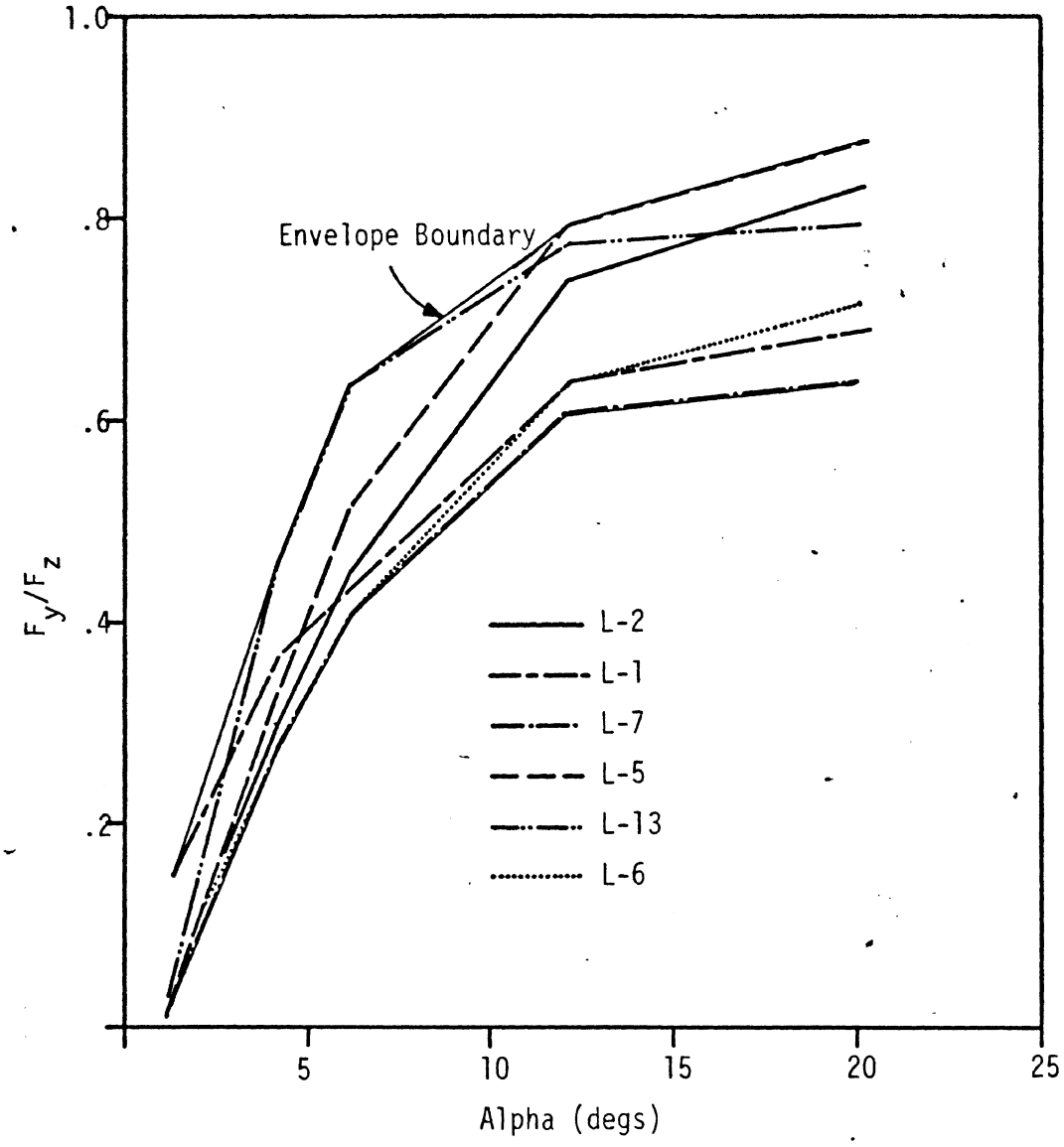

Figure 3.34. Lateral force measurements of light truck tires at rated load, 20 mph.

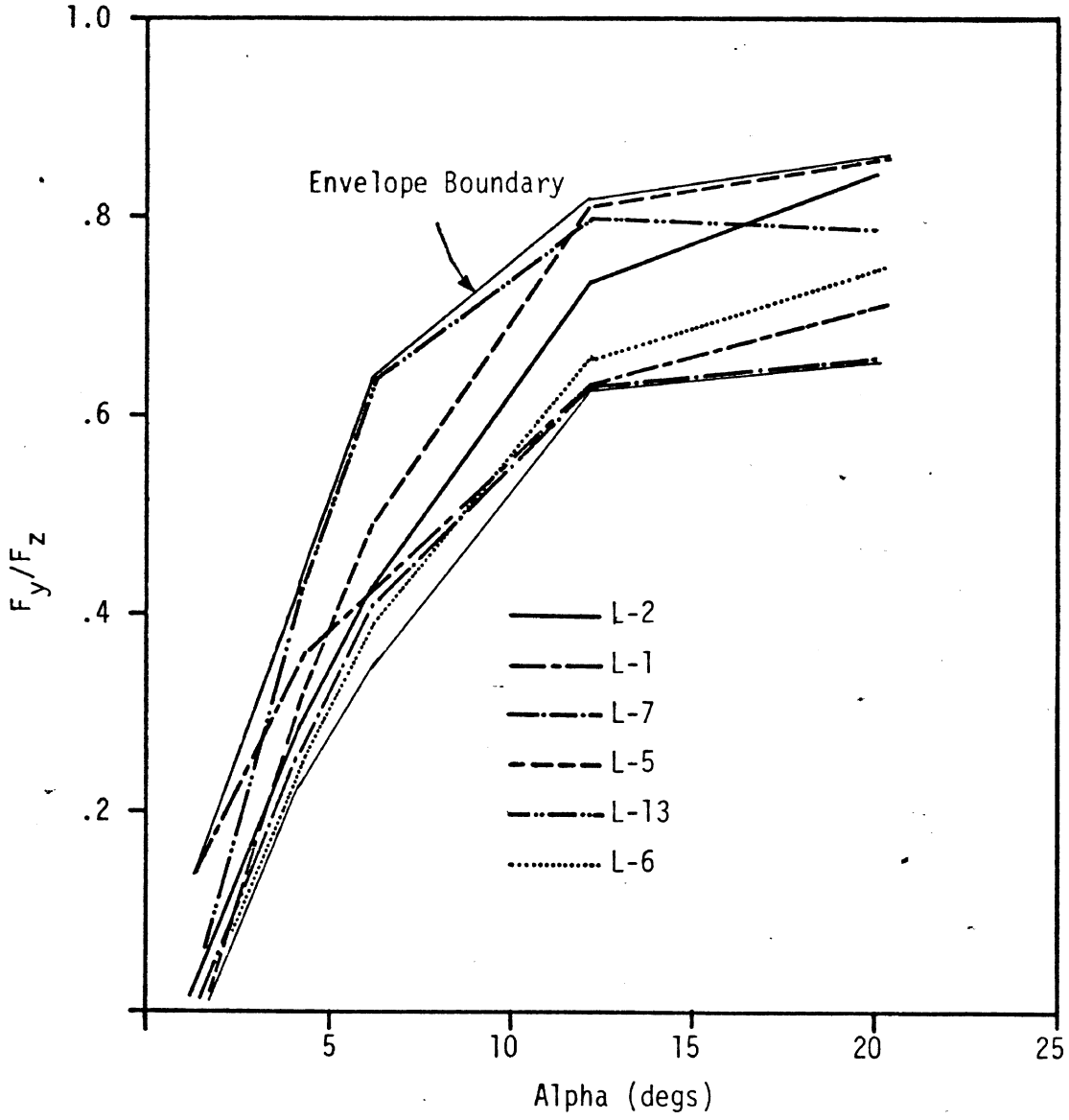

Figure 3.35. Lateral force measurements of light truck tires at rated load, 40 mph.

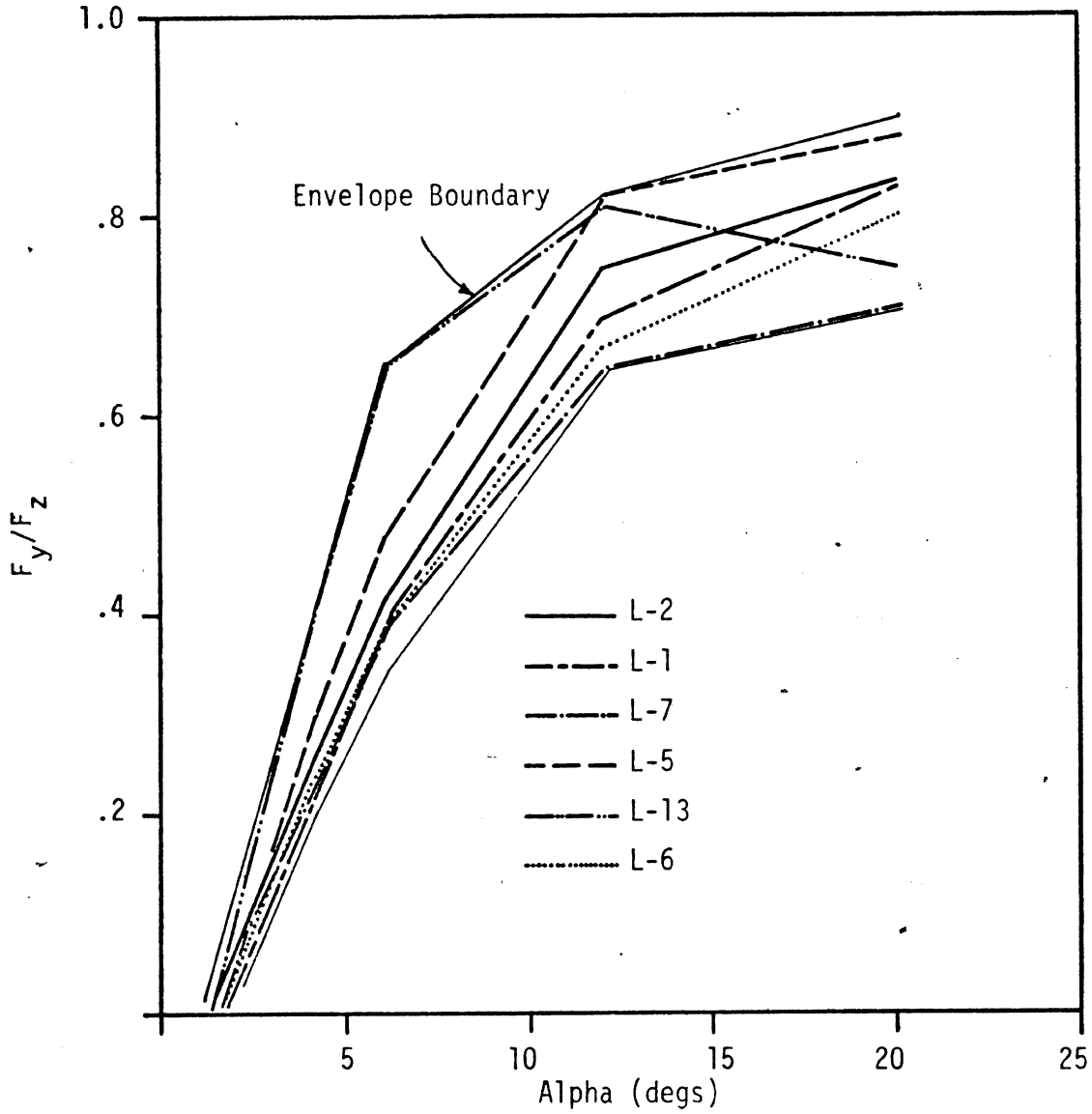

Figure 3.36. Lateral force measurements of light truck tires at rated load, 55 mph.

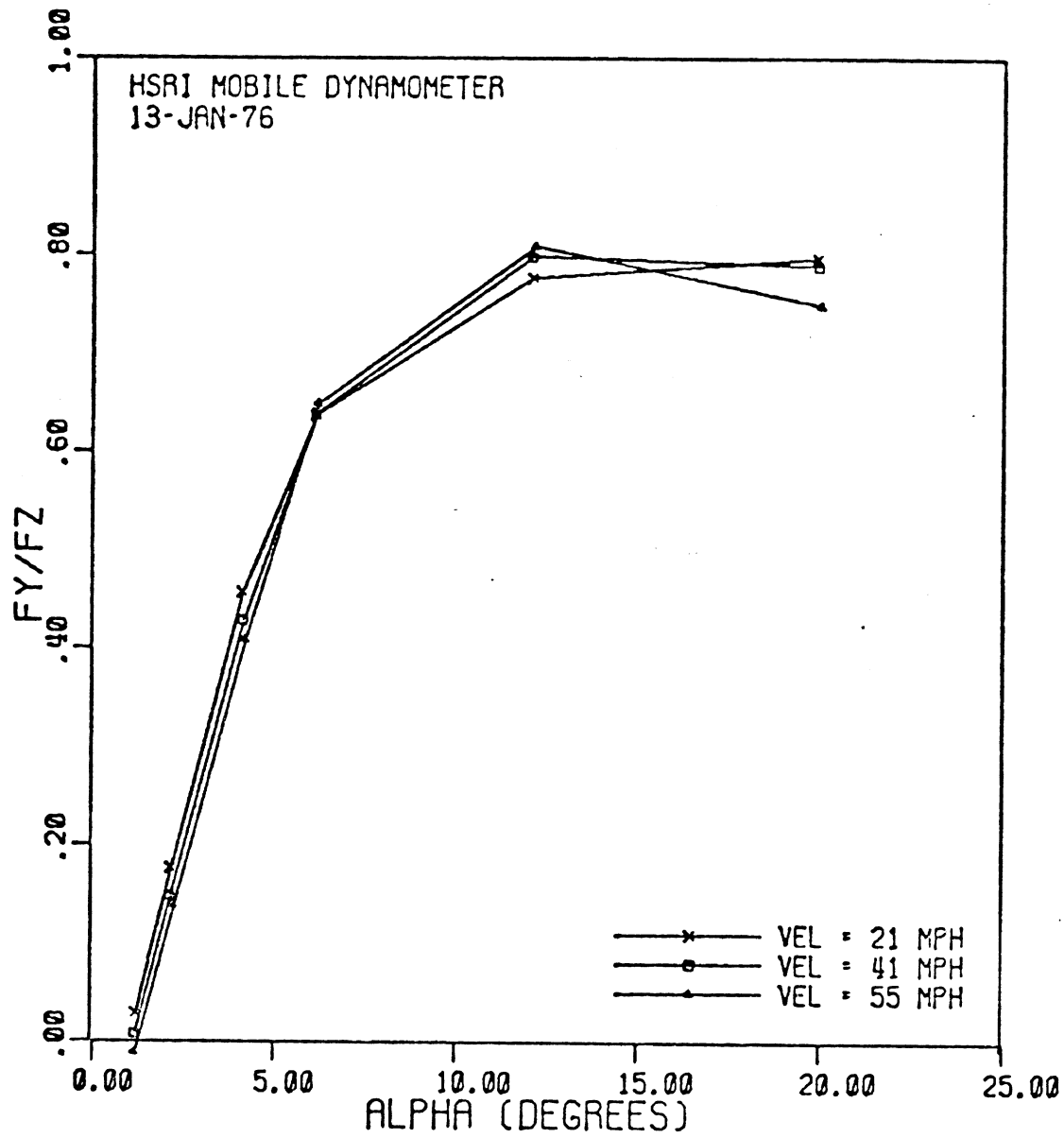

Figure 3.37. Example velocity sensitivity in the lateral traction performance of a Michelin light truck tire.

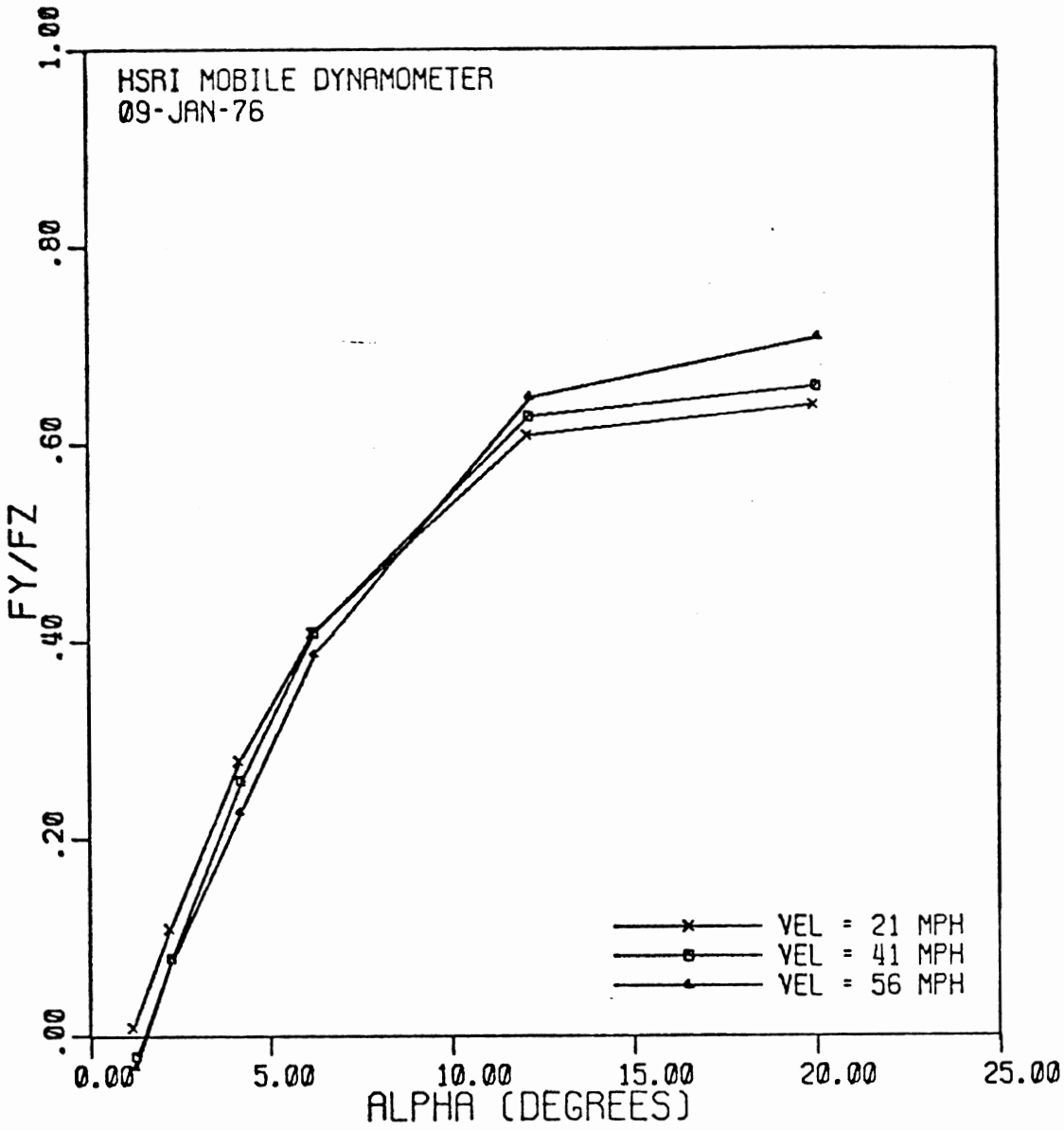

Figure 3.38. Example velocity sensitivity in the lateral traction performance of a Goodyear light truck tire.

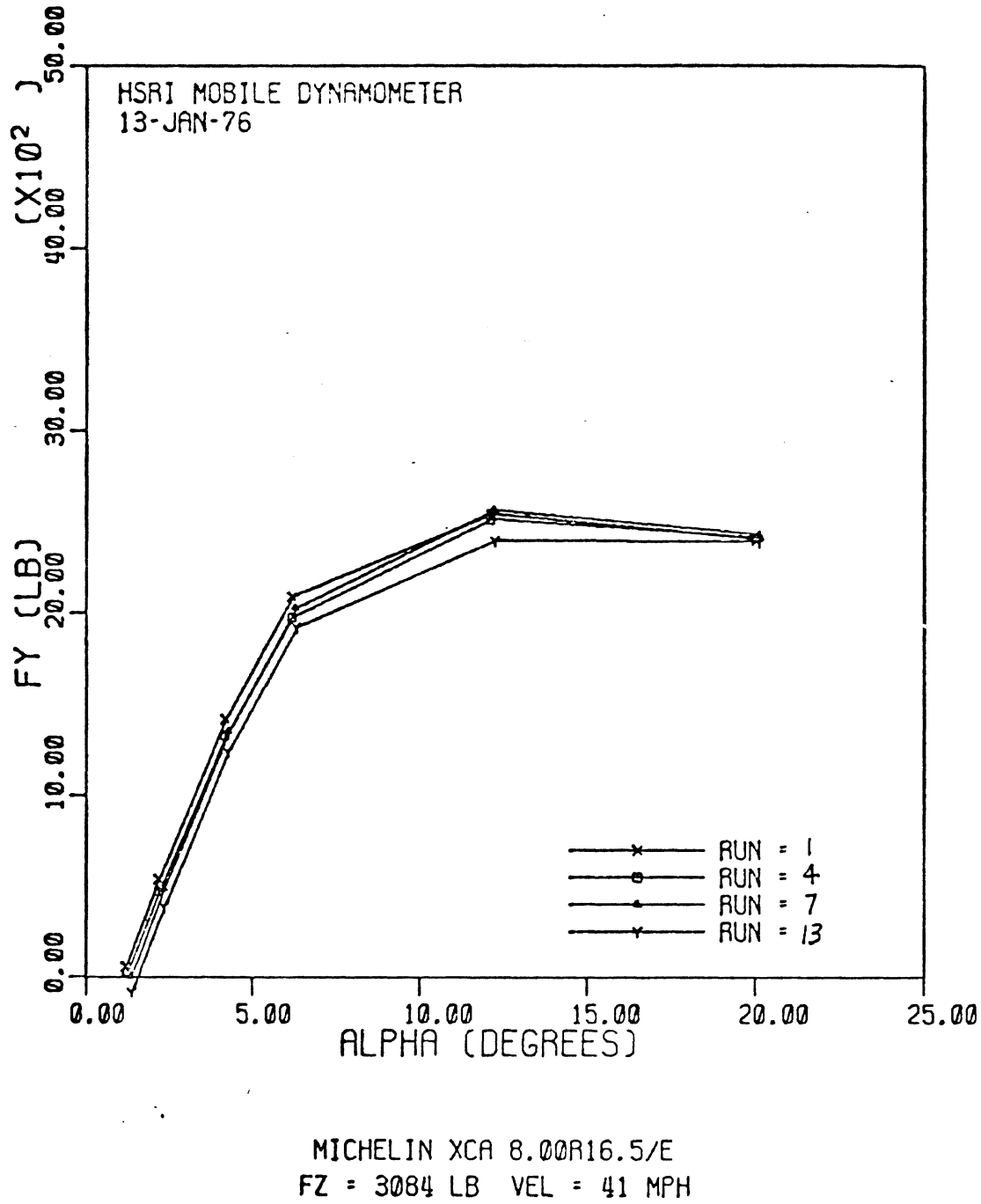

Figure 3.39. Repeat run data for Michelin radial light truck tire.

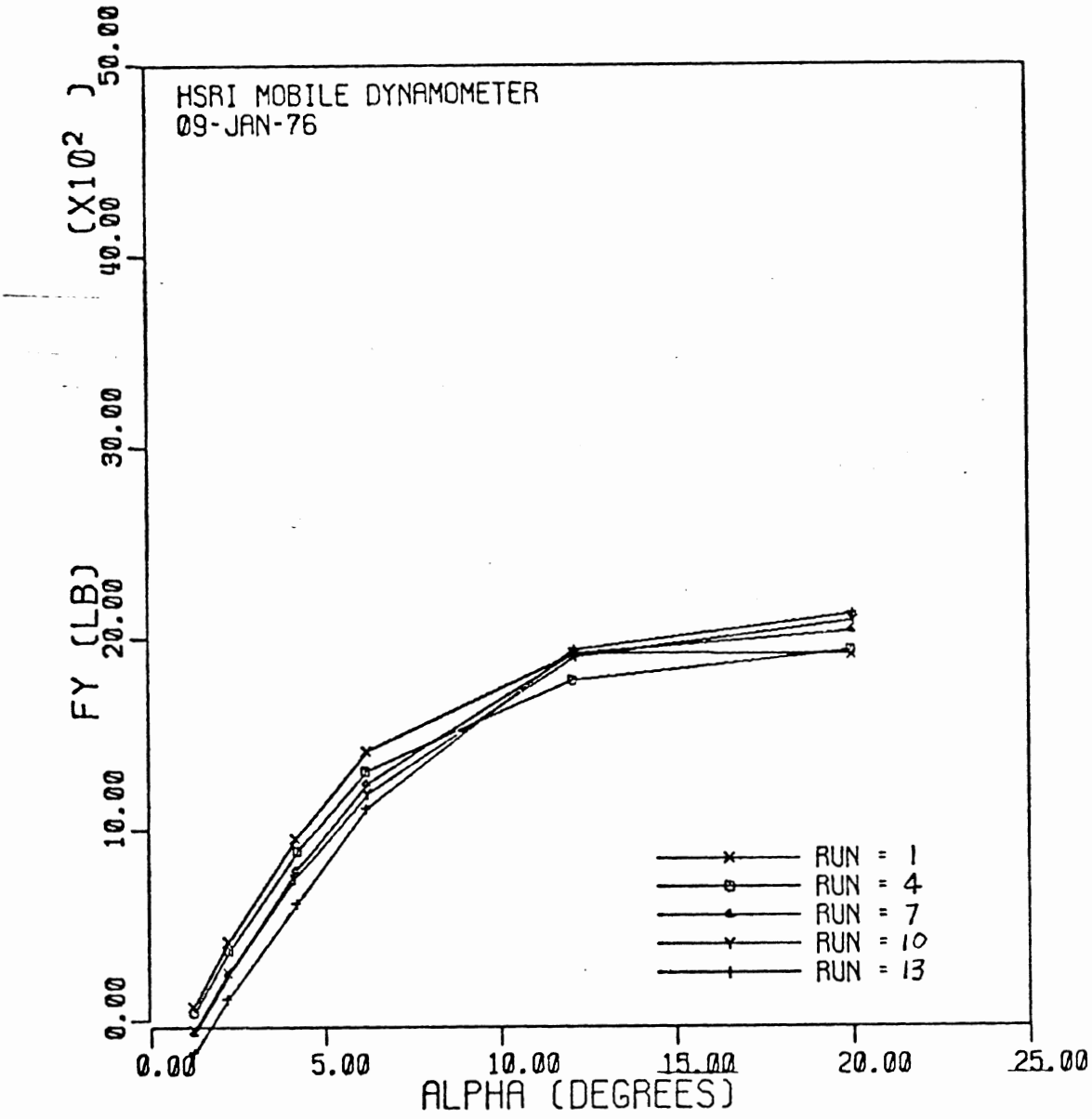

Figure 3.40. Repeat run data for Goodyear radial light truck tire.

Goodyear Flexsteel radial to be yielding the equivalent of a 0.08 increase in its peak F_y/F_z behavior as a result of the wear induced by repeated testing. Since the test runs providing the 20, 40, and 55 mph conditions at rated load were respectively conducted as runs #3, 7, and 11, the velocity sensitivity assessment became monotonically linked to the test-wear sensitivity. Applying this observation to the sample of velocity sensitivities exhibited by the eight-tire sample, we can conclude with confidence that velocity was found to negligibly influence the F_y/F_z behavior of light truck tires.

3.3 TIRF Tire Tests

A program of dry pavement traction measurements was conducted on the Tire Research Facility (TIRF) of the Calspan Corporation, Buffalo, New York. The program involved longitudinal, lateral, and combined traction tests on one light truck tire (Firestone Transport 500 Wide Oval, size 8.00 x 16.5D) and one heavy truck tire (Uniroyal Fleetmaster Triple Tread, size 10.00 x 20F). As originally scheduled, six samples of each tire were to be tested in an effort to minimize wear effects on the results. Due to schedule modifications made during testing, eight light tire samples were used. Details of the test matrix, including chronology of testing, plus a complete listing of the resulting data, are presented in Appendix C.

3.3.1 Longitudinal Traction - TIRF Results. The longitudinal traction data gathered in the test program conducted on TIRF confirm, in large measure, the findings of the mobile traction testing program discussed in the previous section. A notable exception to this, however, is the general shape of the μ-slip curves measured on TIRF. The TIRF data also makes a unique contribution with respect to test-induced wear.

Figure 3.41 presents a number of typical μ-slip curves produced in tests of the Uniroyal Fleetmaster Triple Tread, 10.00 x 20F heavy truck tire. The two curves of similar shape

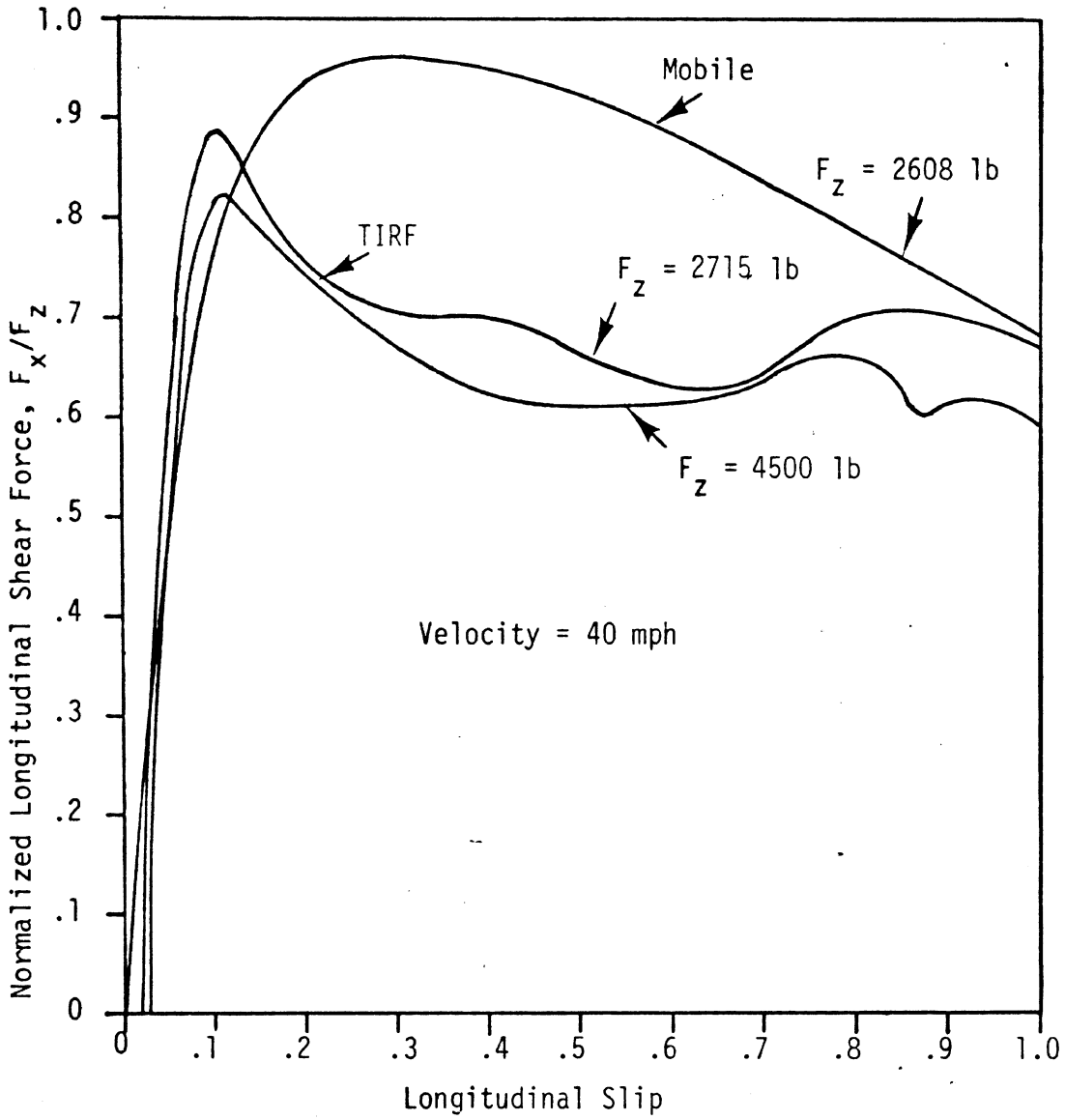

Figure 3.41. Typical μ-slip curves of a heavy truck tire gathered by TIRF and the mobile dynamometer.

were gathered at TIRF while the remaining curve results from HSRI mobile dynamometer testing. We would note firstly that the "mobile" curve derives from the average of five lockup cycles while the TIRF data result from single cycles. Thus, the "ripples" in the TIRF data are not at issue. Further, any differences in peak and slide, F_x/F_z, values between the two data sets are insignificant since the testing was done on different surfaces. However, the obvious difference in the shape of the curves gathered on the two facilities is noteworthy. In particular, three significant points of difference deserve consideration, viz.,

- The marked peakedness of the TIRF data vs. the mobile data
- The occurrence of peak F_x/F_z values at lower slip values in the TIRF data
- The difference of slope of F_x/F_z vs. slip in the low slip regime

The general absence of heavy truck tire data from other sources makes it difficult to comment on the validity of the two data sets. It is quite possible that the observed differences are, to some extent, real, resulting from differences in test conditions. Most obvious is the difference in test surfaces; the mobile data was gathered on a brushed concrete test track, contrasted by the roughed steel belt of the TIRF machine. Additionally, substantial transients can be observed in load and velocity in the TIRF data (Appendix C), particularly during the occurrence of peak F_x/F_z.

With regard to the significance of the observed difference in curve shape, the matter of peakedness is important, particularly due to the emergence of antiskid brake system use on heavy trucks. In general, the more peaked curves probably represent a greater challenge towards achieving good antiskid system performance.

The last two differences highlighted above might be considered as one-in-the same. That is, peak F_x/F_z values occurring at lower values of slip necessitate higher slopes in the low slip regime. Unfortunately, comparison of the low slip regime slopes derived from the two facilities is confused by the fact that the TIRF data does not pass through the origin of the plot. By the definition of longitudinal slip, this is clearly in error, and without a better understanding of the source of this error, evaluation of the data in the low slip regime is difficult.

Contrasting with the differences between TIRF and mobile dynamometer data, is their qualitative agreement regarding peak and slide performance. Figure 3.42 presents peak and slide F_x/F_z values for the Uniroyal 10.00 x 20 tire obtained by TIRF. The large drop in shear force at slide conditions relative to peak values is in general agreement with mobile data as are the general trends of F_x/F_z sensitivity to load and velocity.

A similar presentation of peak and slide data for the light truck tire (Firestone 8.00 x 16.5D) tested at TIRF appears in Figure 3.43. Again, a marked fall off in slide values relative to peak can be seen. Sensitivity of F_x/F_z to load also compliments the findings for heavy truck tires, while velocity sensitivities appear more mixed.

A particularly interesting finding in this data, however, is with regard to test-induced wear. In Figure 3.43, a distinction is drawn between "new" and "worn" tire data. The "new" data points derive from the very first test run experienced by three individual samples (one for each velocity) of the tire type (preceded only by a "break-in" procedure as described in Appendix C). This run consisted of a full longitudinal slip cycle (0-100%) at a zero degree slip angle and at the load and velocity indicated. Following this initial test run, these samples experienced a program of combined slip testing in which full longitudinal slip cycles were conducted at slip angles of 0, 4, 8, and 12° at various loads and velocities. (Precise chronology of test sequences for each tire sample can be

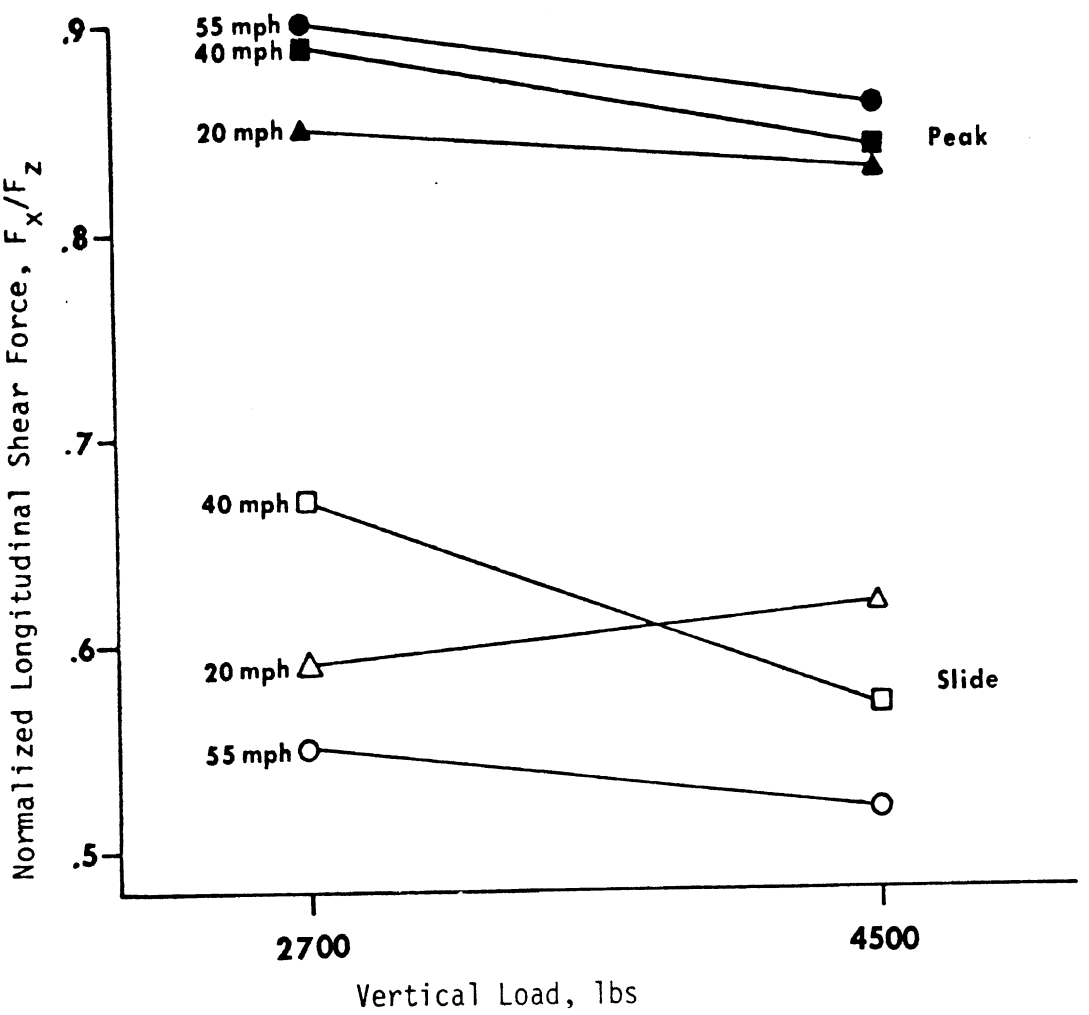

Figure 3.42. Peak and slide longitudinal traction of the heavy truck tire

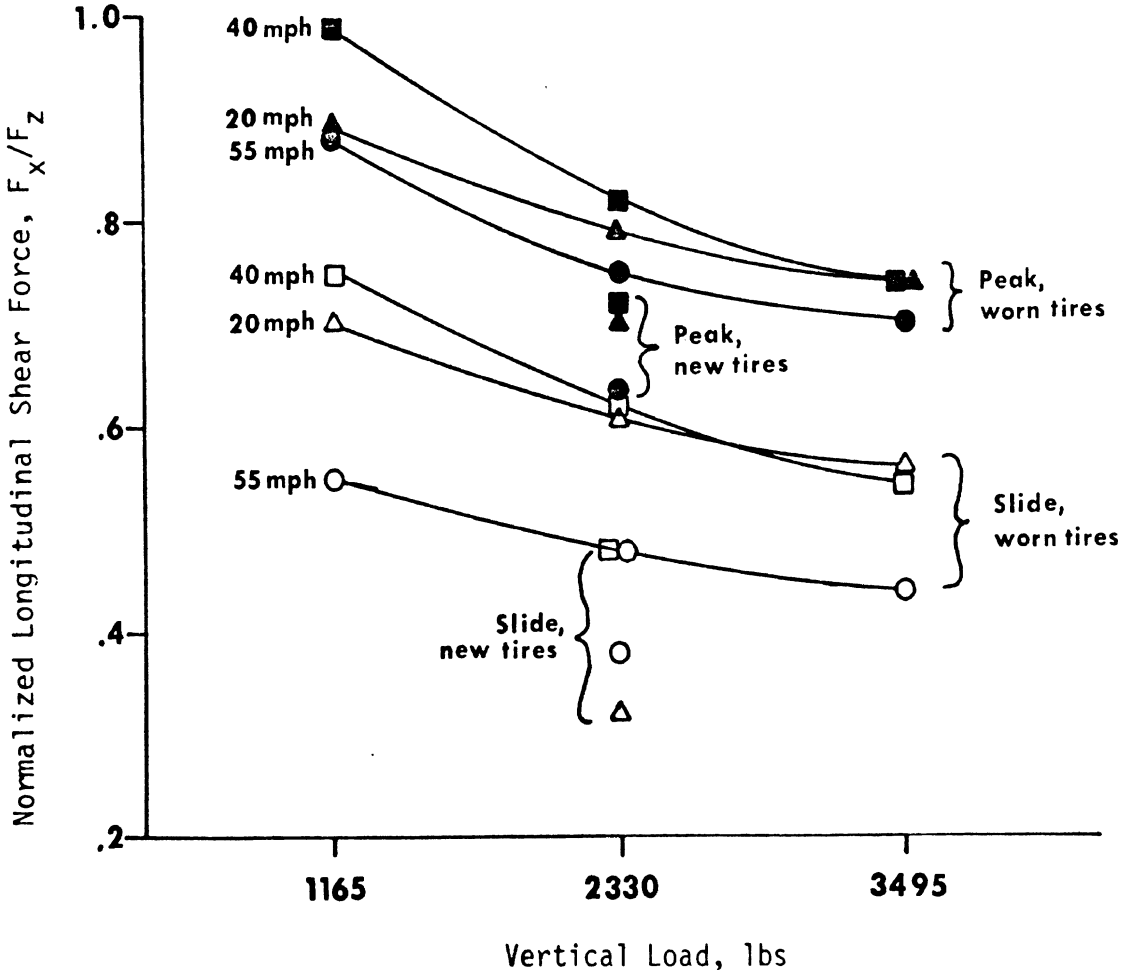

Figure 3.43. Peak and slide longitudinal traction of the light truck tire.

determined from schedules and test results given in Appendix C.) The "worn" data, then, derives from the zero slip angle data of these combined slip tests. The figure indicates a remarkable increase of both peak and slide traction of the worn tires.

We would note further that no such wear-induced changes in longitudinal traction of heavy truck or bus tires were evidenced by data gathered either by TIRF or by the mobile dynamometer.

3.3.2 Lateral Traction - TIRF Results. Both the light and heavy truck tires tested at TIRF were subjected to a lateral force test program. The matrix of test conditions included three loads (appropriate for the tires' rated loads) and three velocities (20, 44, and 55 mph). The light tire was tested at 0, 1, 2, 4, 8, 12, and 16 degree slip angles while in the heavy tire tests, the 16° point was eliminated. The testing was dispersed over several samples of each tire in order to limit and to allow observations of the effects of wear on performance.

Examples of carpet plots resulting from the test data can be found in Appendix C, as can the details of test chronology and division of testing over individual tire samples.

In reviewing the results of these tests, data will be presented in the form of plots of cornering stiffness (C_α), normalized side force (lateral force/vertical load; F_y/F_z), and slip angle (α) versus "wear units."* For our purposes, a wear unit is accrued by a tire when it has been tested over the full range of slip angles, at one load and one velocity, regardless of magnitude. (Clearly, the wear accrued by a tire is dependent on load and velocity, but for our purposes a more precise, and complicated, formula for wear units is not warranted.) In the plots of the following discussion, the wear units indicated are those accrued at the completion of the run from which the data derives.

---

*In the plots presented in this section, the data points derive from the average of all runs conducted at the indicated conditions of load, velocity, and wear. The number of runs averaged range from one to three.

Cornering stiffness data are displayed in Figures 3.44 and 3.45 for the light and heavy truck tires, respectively. The data is plotted as a function of wear with load and velocity influences indicated.

The light tire data indicate, over the range of testing, virtually no sensitivity of C_α to either velocity or wear. However, the strong, monotonic sensitivity of C_α to load, displayed in the flat-bed data in Section 3.1, has been repeated. The heavy tire data of Figure 3.45 shows a similar insensitivity to velocity and a similar sensitivity to load. However, this data also shows a distinct, if slight, trend for C_α to decrease with increasing wear.

In examining peak lateral traction performance, the plot displayed in Figure 3.46 is most interesting. The data is for the light truck tire and is displayed in the form of peak F_y/F_z versus wear as a function of load and velocity. The manner in which wear causes improvement in the peak lateral traction of this tire is most striking. However, the effects of both velocity and load are also evident. Load effects appear to be the strongest with peak F_y/F_z declining as load increases for any fixed velocity and wear conditions. Although not as strongly, increasing velocity also results in a decline of peak F_y/F_x for any given load and wear state.

Other interesting findings for the light tire data appear in Figure 3.47. Here, the sideslip angle at which peak F_y/F_z occurred (α_p) is plotted as a function of the three variables, load, velocity, and wear. It is interesting to note that α_p tends to rise with increasing wear. Further, α_p appears to be influenced by velocity while being quite insensitive to load. We would note in discussing this particular plot that, as shown in Figure 3.48, α_p is a measure which is extremely sensitive to small changes in shape of the F_y/F_z versus α relationship. Because we are concerned with the nearly horizontal peak region of the curve, α_p can be very sensitive to test noise. The data presented in Figure 3.47 should be interpreted in this light.

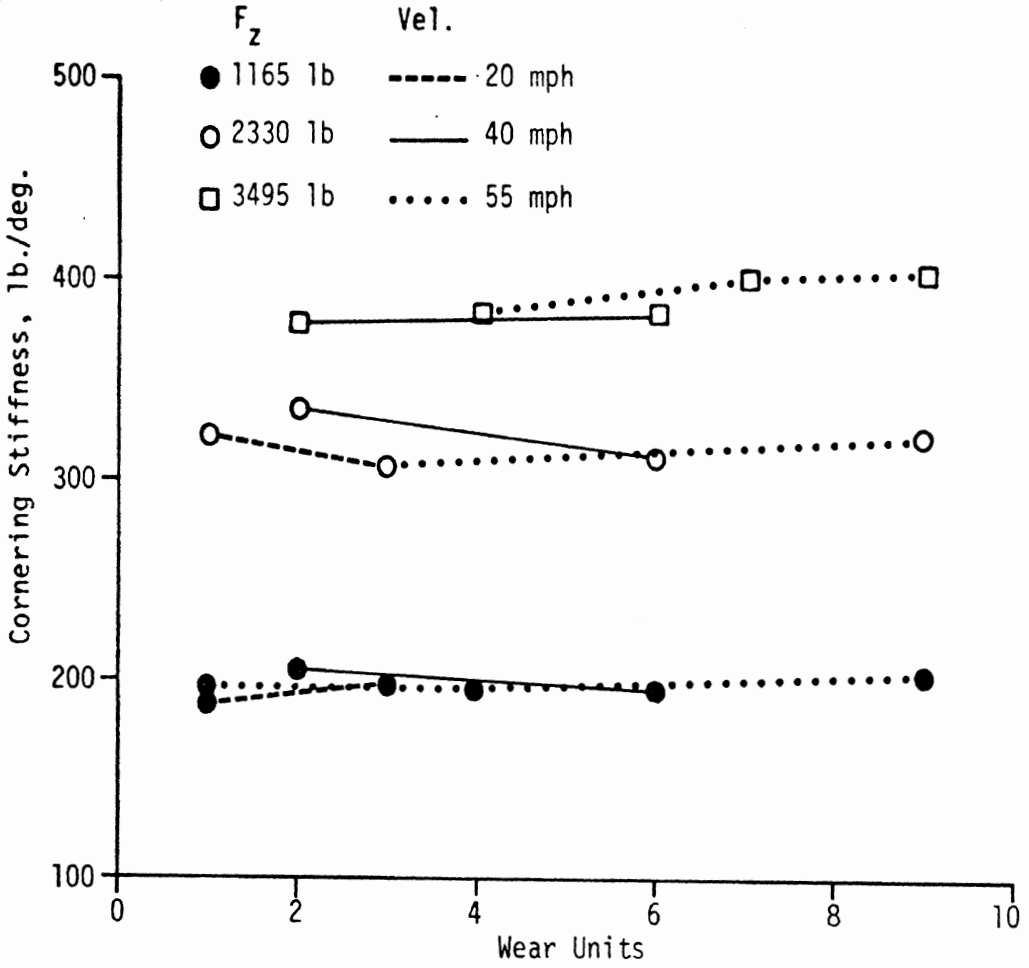

Figure 3.44. Cornering stiffness properties of the light truck tire.

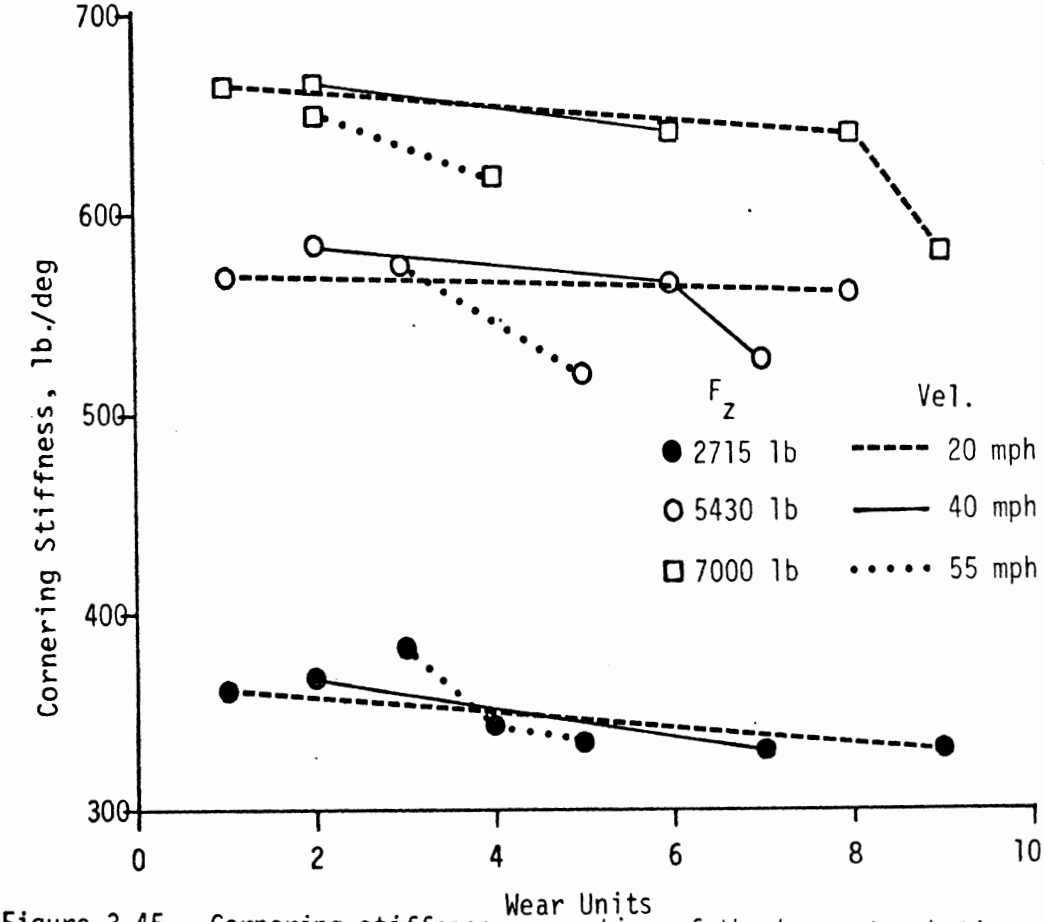

Figure 3.45. Cornering stiffness properties of the heavy truck tire.

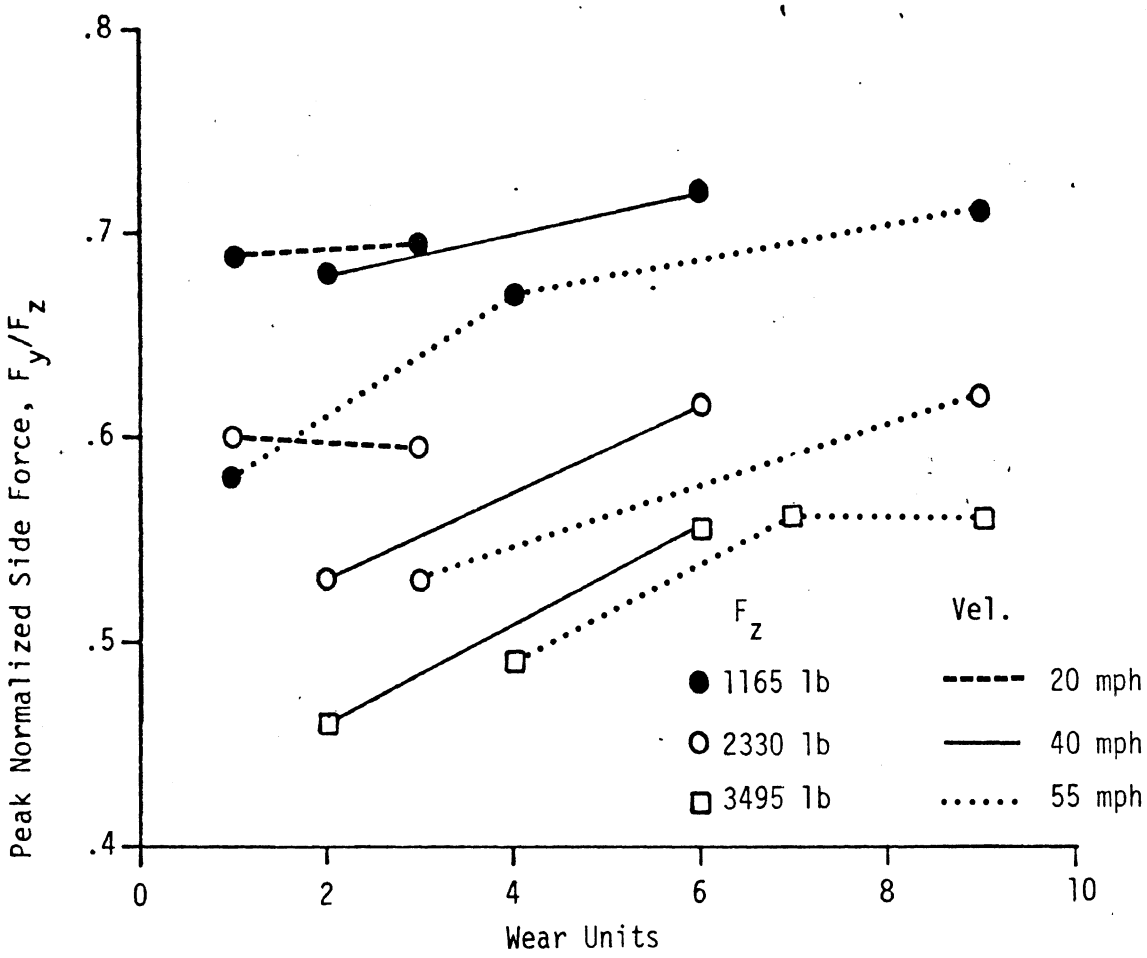

Figure 3.46. Peak lateral traction of the light truck tire.

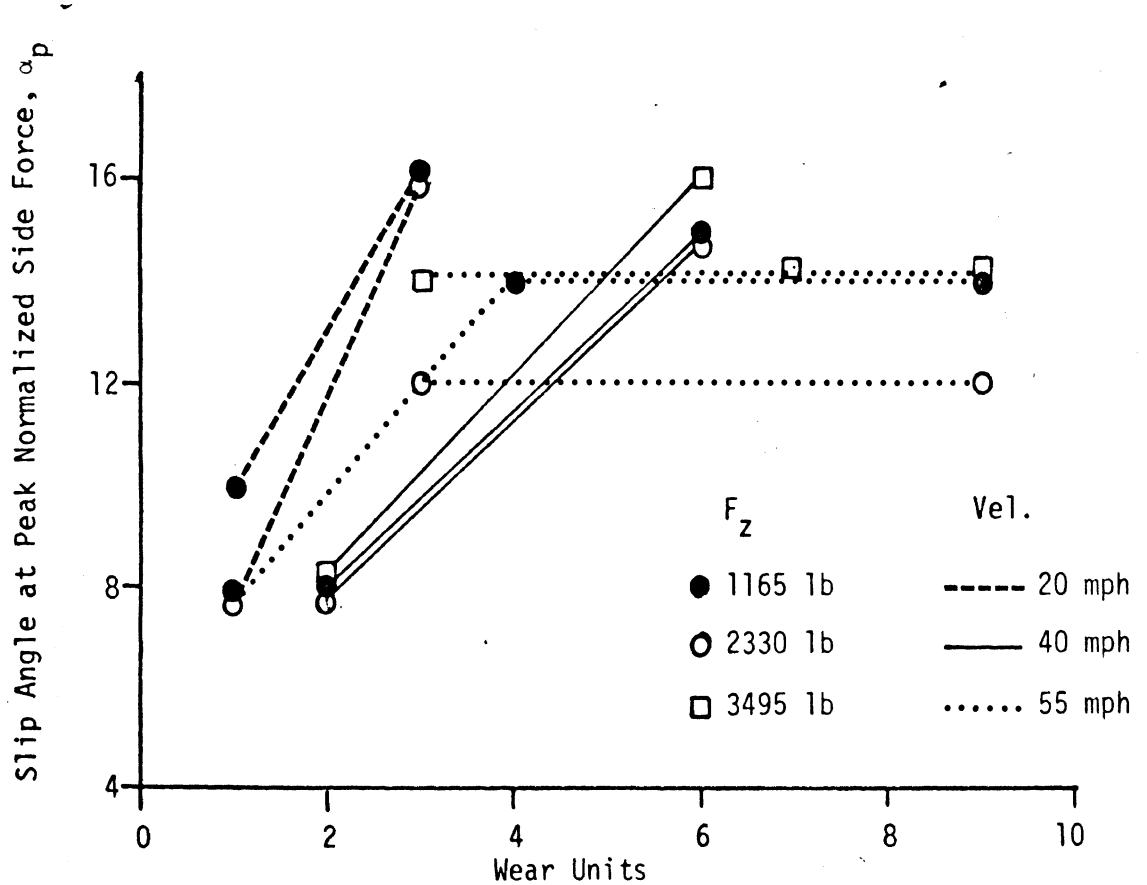

Figure 3.47. Steer angle at which peak lateral traction occurs for the light truck tire.

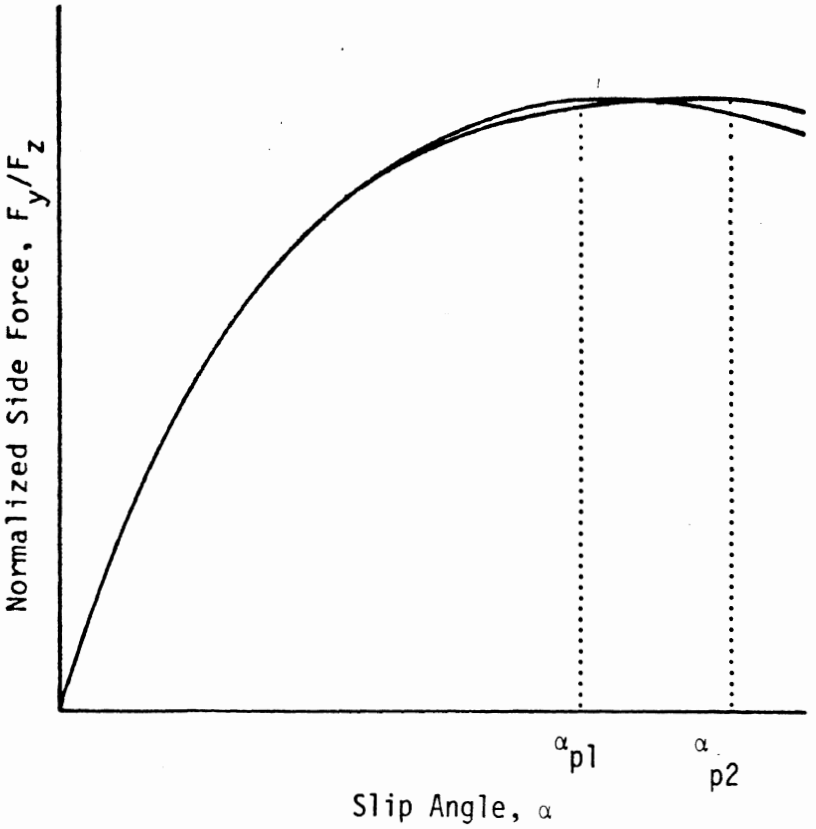

Figure 3.48. Normalized side force versus slip angle.

As for the heavy truck tire tested at TIRF, peak F_y/F_z data is displayed as a function of load, velocity, and wear in Figure 3.49. (Note that all the data points indicated in this figure occurred at a slip angle of 12°.) This figure would tend to confirm the findings of the mobile tire test program discussed earlier; namely, that while peak F_y/F_z of the lighter tires appeared to be sensitive to wear, the heavy truck tires did not display this tendency. The data also indicate the usual sensitivity to load (decreased peak F_y/F_z with increasing load) and little distinguishable sensitivity to velocity.

3.3.3 Combined Traction - TIRF Results. The light and heavy truck test tires were both subjected to a program of combined traction testing at TIRF. Each tire was tested at one load (2330 lb for the light tire and 4500 lb for the heavy tire) and three velocities (20, 40, and 55 mph). The light tire experienced full

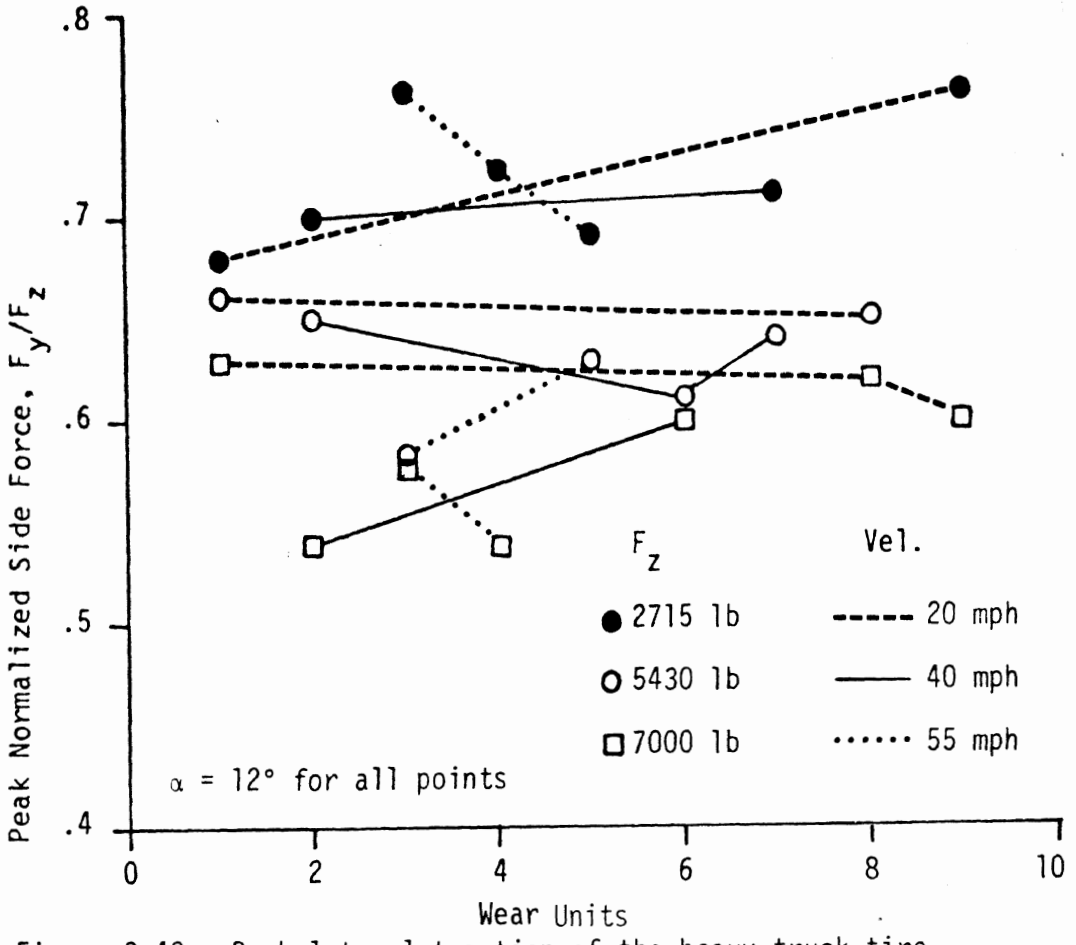

Figure 3.49. Peak lateral traction of the heavy truck tire.

longitudinal slip excursions (0-100%) while at slip angles of 4, 8, and 12 degrees. In a similar sequence, the heavy tire was tested at 2, 4, and 8 degrees. (Full details and results from combined slip testing appear in Appendix C.)

Figures 3.50 and 3.51 present sample results for the light and heavy tire, respectively. The finding of note in this data is the rapid drop-off of lateral force with increasing longitudinal slip. (This drop-off is perhaps twice as rapid as might be expected for a passenger car tire.) This finding is not altogether unexpected, inasmuch as it is consistent with the similarly early peaking of longitudinal shear force. This early peaking was noted in the discussion of TIRF longitudinal traction data, and it is apparent again in the data of Figures 3.50 and 3.51. However, as in the case of the longitudinal traction data, the finding is somewhat suspect, given that the longitudinal traction data do not project through the origin of the plot (as the definition of longitudinal slip requires).

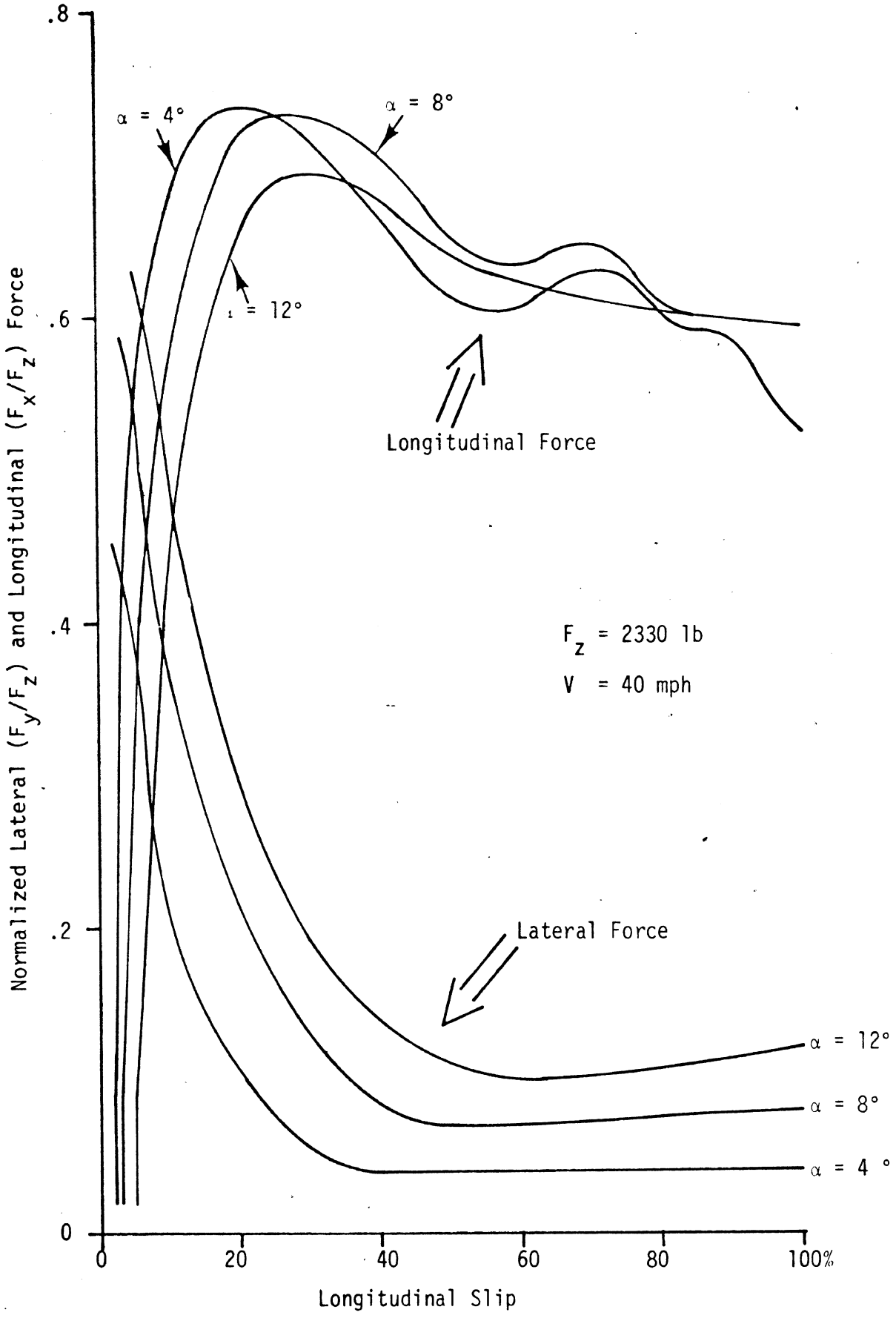

Figure 3.50. Combined traction performance of the light truck tire.

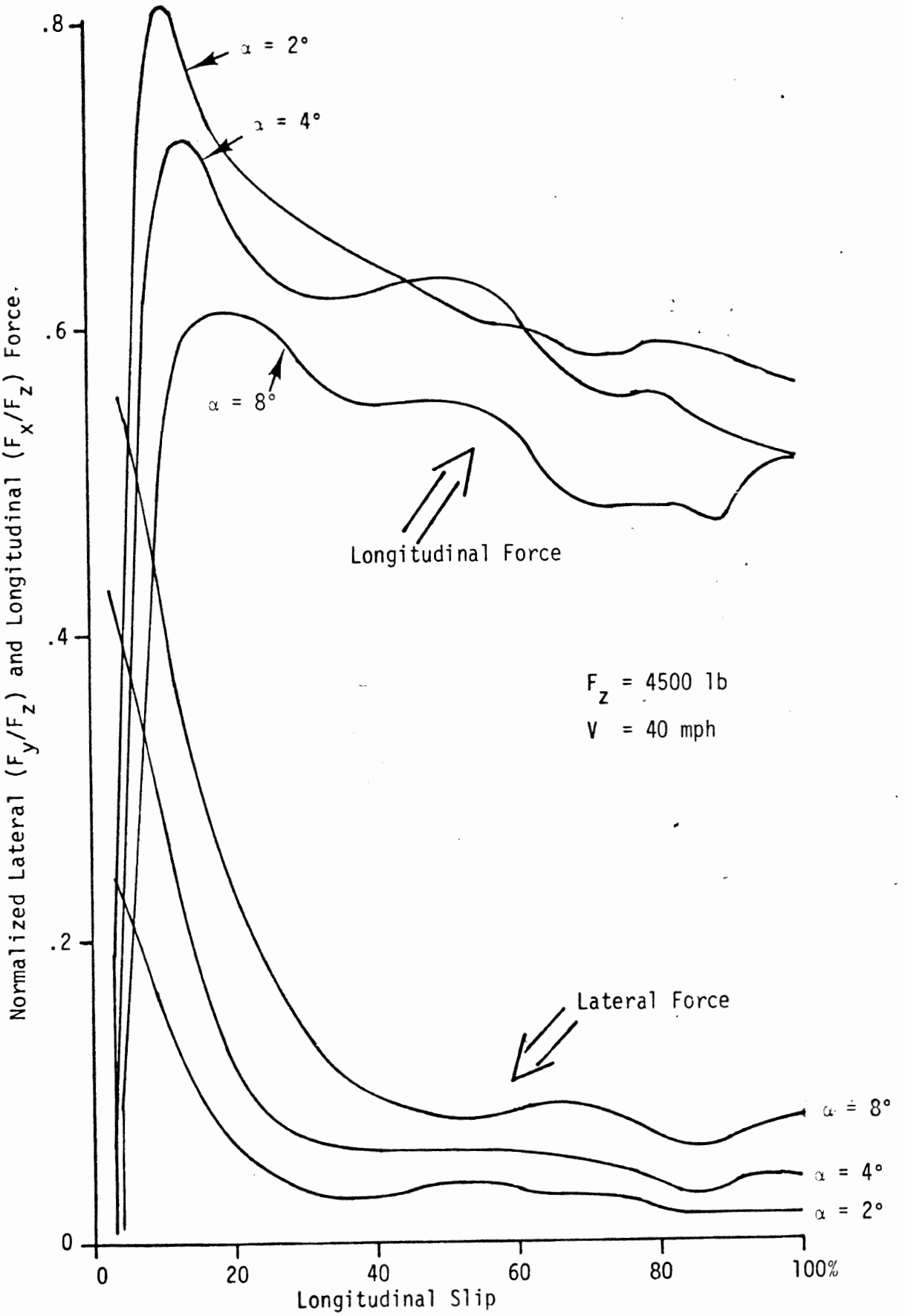

Figure 3.51. Combined traction performance of the heavy truck tire.

Inasmuch as the peak F_x/F_z condition prevails at approximately half of the value of longitudinal slip as has prevailed at the peak condition in all HSRI mobile experiments, the TIRF combined-slip results are presented here as preliminary measures. The reader is advised to seek confirming evidence of the rapid drop-off in the (F_y versus s) curves (Figures 3.50 and 3.51) before applying these results.

4.0 FINDINGS RELATING TIRE PROPERTIES TO VEHICLE MANEUVERING

In this section, the results of full-scale vehicle tests and simulations are summarized. Since many thousands of test and simulation runs were conducted, only generalized trends can be treated here. Accordingly, the reader with particular interests in specific maneuvering conditions is referred to appended data sections.

Results presented in this section reveal the influence which selected tire installations impose upon vehicle response characteristics. Since simulated "tire installations" were selected to represent the traction fields of actual individual tires, the results do not present an opportunity for clearly separating tire behavioral parameters. That is, specific tires were simulated, encompassing the full set of descriptive parameters associated with each selection. An exhaustive examination of the influence of a matrix of clearly differentiated traction parameters was thus beyond the scope of effort applied here.

Test data to be summarized in this section include measurements obtained on the two light vehicles and on the heavy truck. As stated earlier, planned tests for the fourth vehicle, the intercity bus, were eliminated from the study following the occurrence of the rollover event involving the heavy truck test vehicle. Associated with the observations deriving from the rollover, a special simulation study was designed and conducted. Results of this special study are included in the final portion of this section.

4.1 Findings Deriving from Full-Scale Tests

Individual plots of vehicle responses measured during full-scale tests are presented in Appendix E. In this section the salient findings deriving from these data are summarized. As

was described in Section 2.3, test procedures were designed so as to restrain maneuvering severity well below the rollover threshold.

Since variations in test tires were selected on the basis of lateral properties, the test maneuver providing the most discriminating performance measure was the trapezoidal steer test. Although the sinusoidal steer maneuver can be seen in the data of Appendix E to be somewhat sensitive to tire and load variations, each indicated severity is confirmed and significantly enhanced in the trapezoidal steer data. Accordingly, vehicle test data is summarized here in the form of trapezoidal steer results.

4.1.1 Results of Tests Conducted with Ford Econoline Van. Test data for the light van are shown in Figure 4.1. The plot illustrates peak values of lateral acceleration and yaw rate which were obtained at the indicated steer amplitudes at each of the two test velocities, 30 and 50 mph. The steering input levels employed in these tests were selected to yield equivalent steady turning levels of the linear OE vehicle system at both test velocities. Thus, the 50-mph data are registered at distinctly lower δ values than are the data from the 30-mph tests. Each set of data represents the nominal bands of response which were obtained by the van test vehicle in each of three conditions, namely:

1) unloaded, with the original equipment tire (code L-2, in Table 3.1) employed at all wheel locations

2) loaded, employing the OE tire

3) loaded, employing the extreme variation (E.V.) tire arrangement comprised of OE tires on the front axle and bias-ply snow tires (code L-11) on the rear.

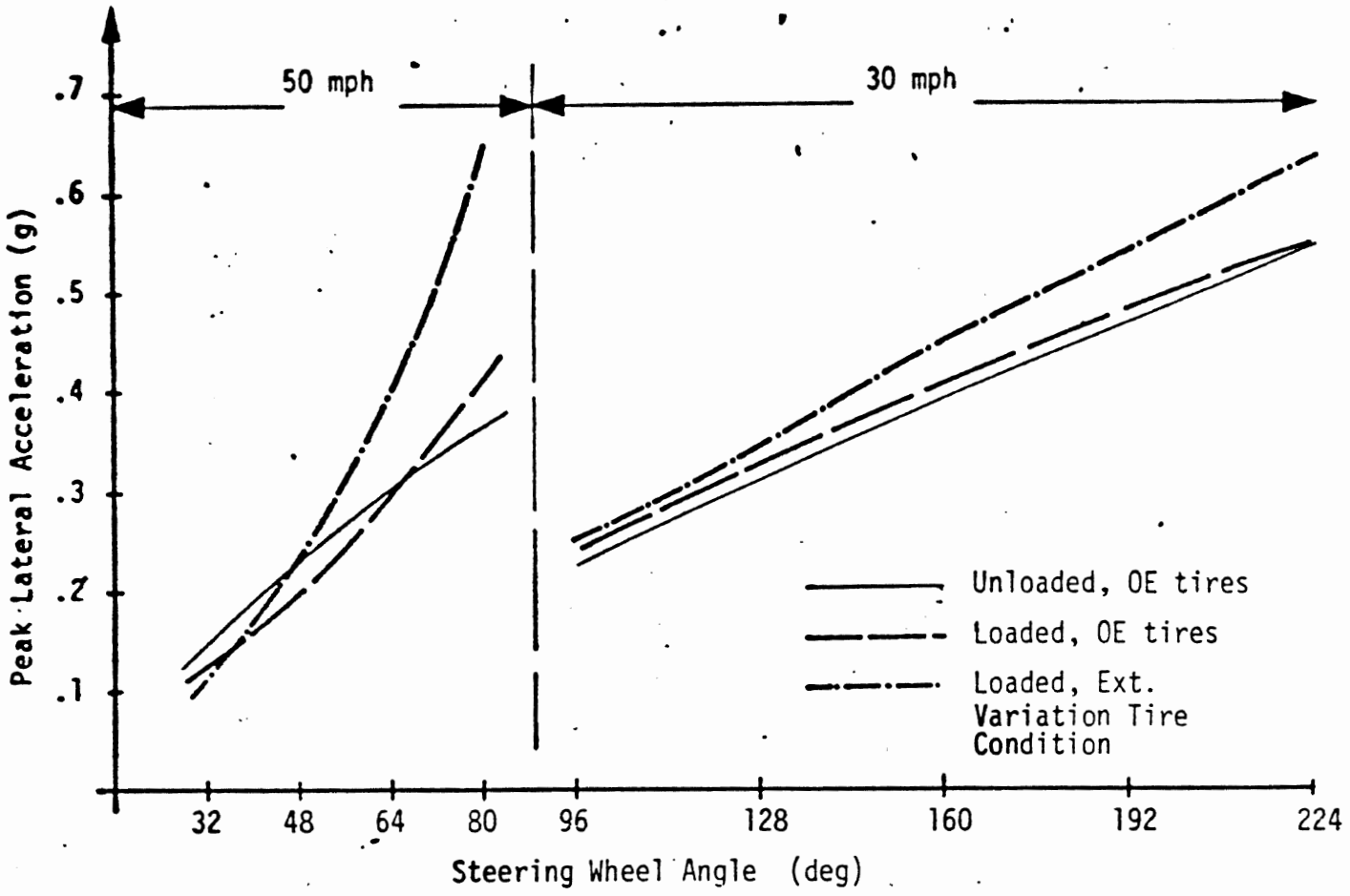

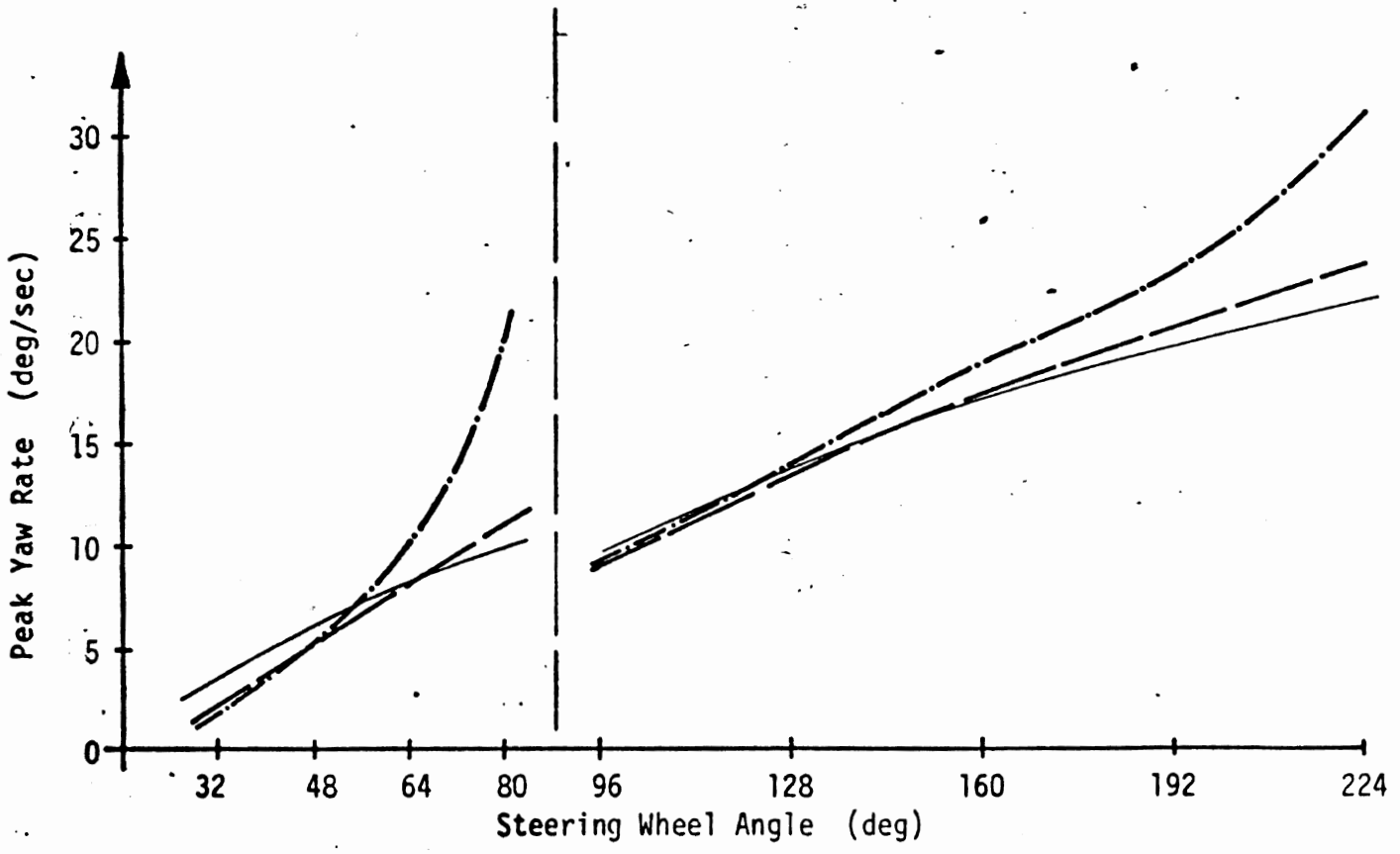

Figure 4.1. Trapezoidal steer responses (peak A_y & r) obtained in light van tests at 30 and 50 mph.

As can be seen in the 50-mph data, the range of lateral acceleration and yaw rate values can be markedly influenced by the installed tire arrangement. Indeed, at the 80° steering wheel input the lateral acceleration response is seen to extend from 0.3 g, in the OE tire condition, to 0.75 g with the EV tire arrangement. Thus the vehicle can exhibit a behavior that converts an otherwise normal level turning response into a spin-out response as a consequence of an unfavorable, but not uncommon, arrangement of tires.

Another interesting point of these data is that the vehicle is not affected to a major degree in its OE condition by the addition of the 2715-lb load, even though that loading serves to shift the mass center toward the rear by 3.7 inches. This result is apparently explained by noting a peculiar feature of the C_α versus F_Z plot for the OE tire, as shown in Figure 4.2. The load sensitivity of cornering stiffness indicated in this figure is reasonably approximated over the load range of interest by the linear relation:

$$C_\alpha = K F_Z$$

Thus the tires mounted on the front axle provide a total front cornering stiffness of:

$$C_{\alpha_1} = 2KW\left(\frac{b}{a+b}\right) \qquad (1)$$

and, likewise, the rear tires provide a total rear cornering stiffness of:

$$C_{\alpha_2} = 2KW\left(\frac{a}{a+b}\right) \qquad (2)$$

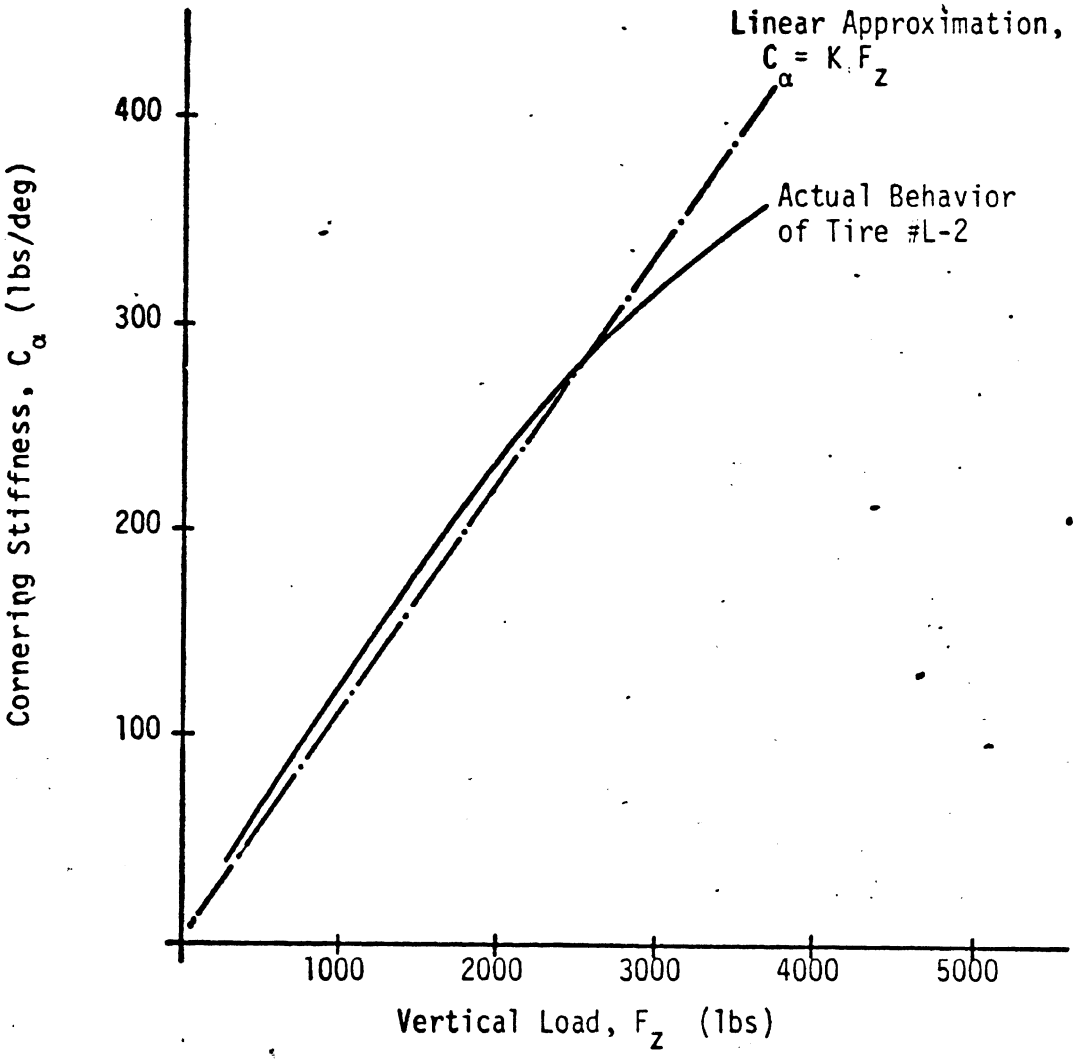

Figure 4.2. Linear approximation to the C_α/F_z behavior of tire #1-2, Goodyear Custom HiMiler 8.75 x 16.5/E.

We can relate the influence of these load sensitivities to the understeer coefficient, U, defined by the relation:

$$U = -\frac{W}{\ell}\left(\frac{a}{C_{\alpha_2}} - \frac{b}{C_{\alpha_1}}\right) \text{ rad/g} \qquad (3)$$

Upon substituting Equations (1) and (2) for the C_α terms in Equation (3), we find that the quantity in parentheses in Equation (3) is equal to zero for all loading configurations. Thus to the extent that tire cornering stiffness influences understeer, the vehicle is neutral steer under any load. While, in fact, certain mechanisms deriving from the kinematics and compliance of the steering and suspension system provide a net understeer behavior, the above illustration is nevertheless significant. Especially when one considers that the light commercial vehicle will experience very large increments in tire loading as a result of payload carriage, the contrast between the C_α/F_z behavior of light truck tires and car tires is indeed beneficial to the light truck.*

While tests were not run at varied levels of inflation pressure (tires were inflated per manufacturer's recommendation, 40 psi front, 60 psi rear), simulation results are presented in Section 4.2 indicating that certain features of the van test data may have derived from peculiarities in the pressure sensitivities of the selected tires.

4.1.2 Results of Tests Conducted with Ford F-250 Pickup Truck. A Ford F-250 pickup truck was tested at TTI in both its loaded and unloaded conditions, with a series of selected tire installations. The tire installations and loading conditions examined are listed below:

*Cases undoubtedly arise in which this generalization is not valid.

Condition	Load	Front Tires	Rear Tires
1	Unloaded	L1 (bias-rib)	L1 (bias-rib)
2	Unloaded	L13 (radial-rib)	L13 (radial-rib)
3	Unloaded	L16 (bias-rib)	L16 (bias-rib)
4	Unloaded	L1 (bias-rib)	L9 (bias-lug/snow)
5	GVW	L1	L1
6	GVW	L13	L13

Considering first the data taken in 30-mph trapezoidal steer, Figure 4.3, a remarkably narrow band of lateral acceleration responses was observed in the normal maneuvering range, below about 0.4 g. Even for the major changes in vehicle loading and tire distribution indicated, the vehicle exhibited a virtually constant behavior in this low level J-turn-type maneuver. The insensitivity to loading indicated here basically derives from the nearly linear relationship between C_α and F_z as was discussed in regard to the preceding data sets covering the van test vehicle.

The spreading range of response values at higher maneuver levels is clearly indicated in the 50-mph tests as shown in Figure 4.4. In this figure, the lateral acceleration responses begin to "string out" more emphatically in the vicinity of 0.4 g's and above. Clearly, in these data the nonlinear characteristics of the vehicle's behavior under the various tire and load conditions causes a greater discrimination among test conditions. It is somewhat surprising to see that the rib-front, snow tire-rear configuration yields relatively low lateral acceleration gain and an apparently front-tire-saturated yaw limit for the unloaded vehicle. Conversely, the vehicle outfitted with the four Michelin radial XCA tires yields the highest acceleration response levels for the unloaded vehicle. When the vehicle is loaded, a peculiar asymmetry in steering response to right- and left-hand inputs was observed. Further, the vehicle is clearly more destabilized at high maneuvering levels with the addition of load, yielding the more abrupt spinout-limited response with the OE bias-ply tire.

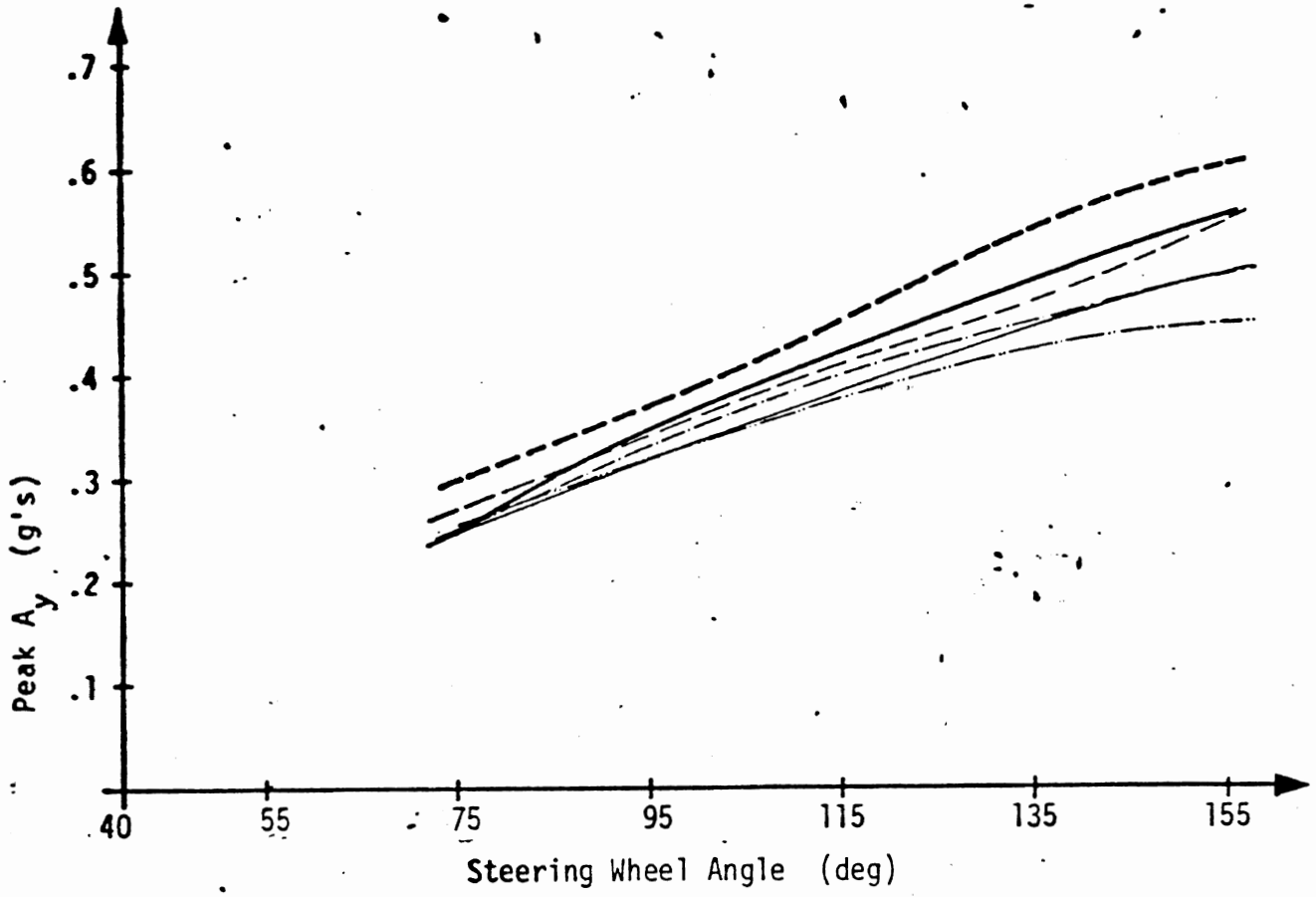

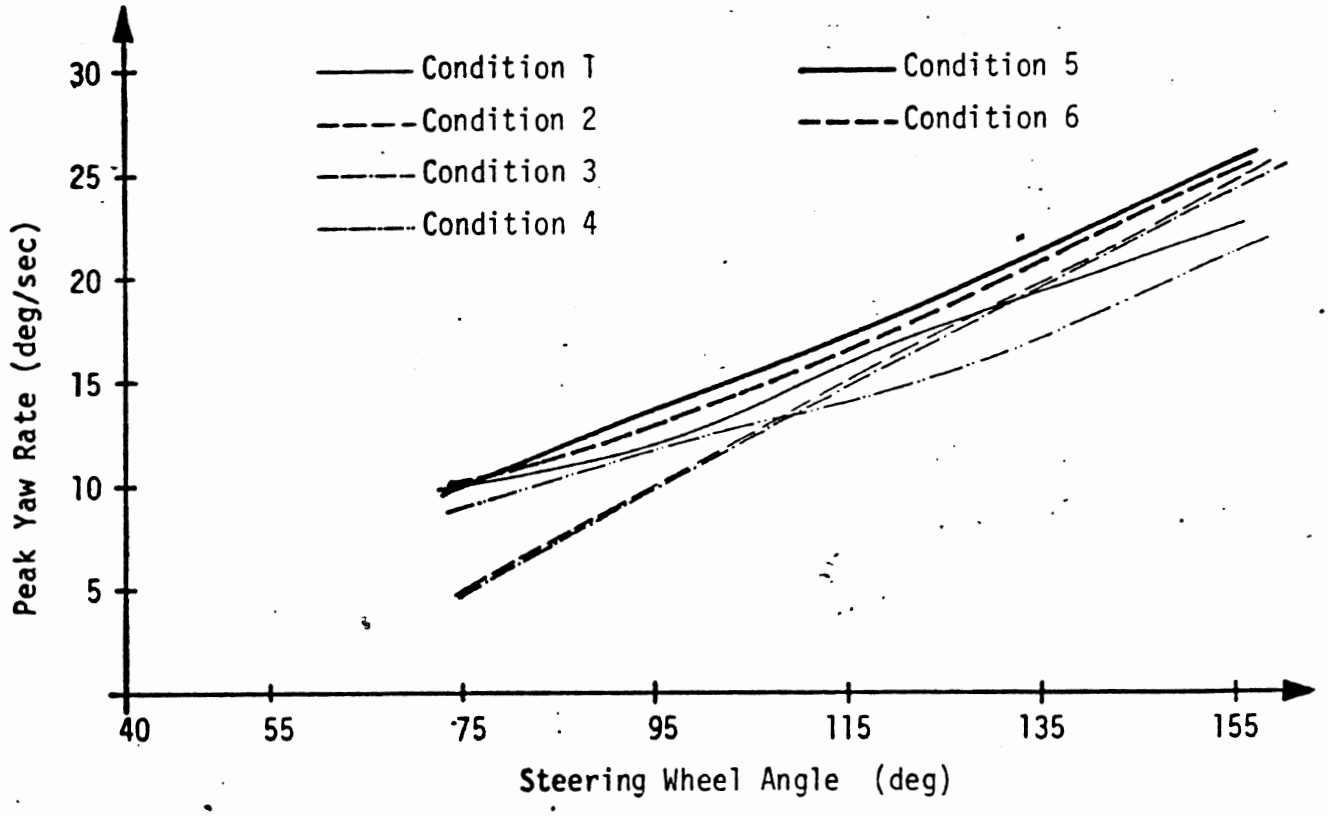

Figure 4.3. Trapezoidal steer responses obtained with pickup truck at 30 mph.

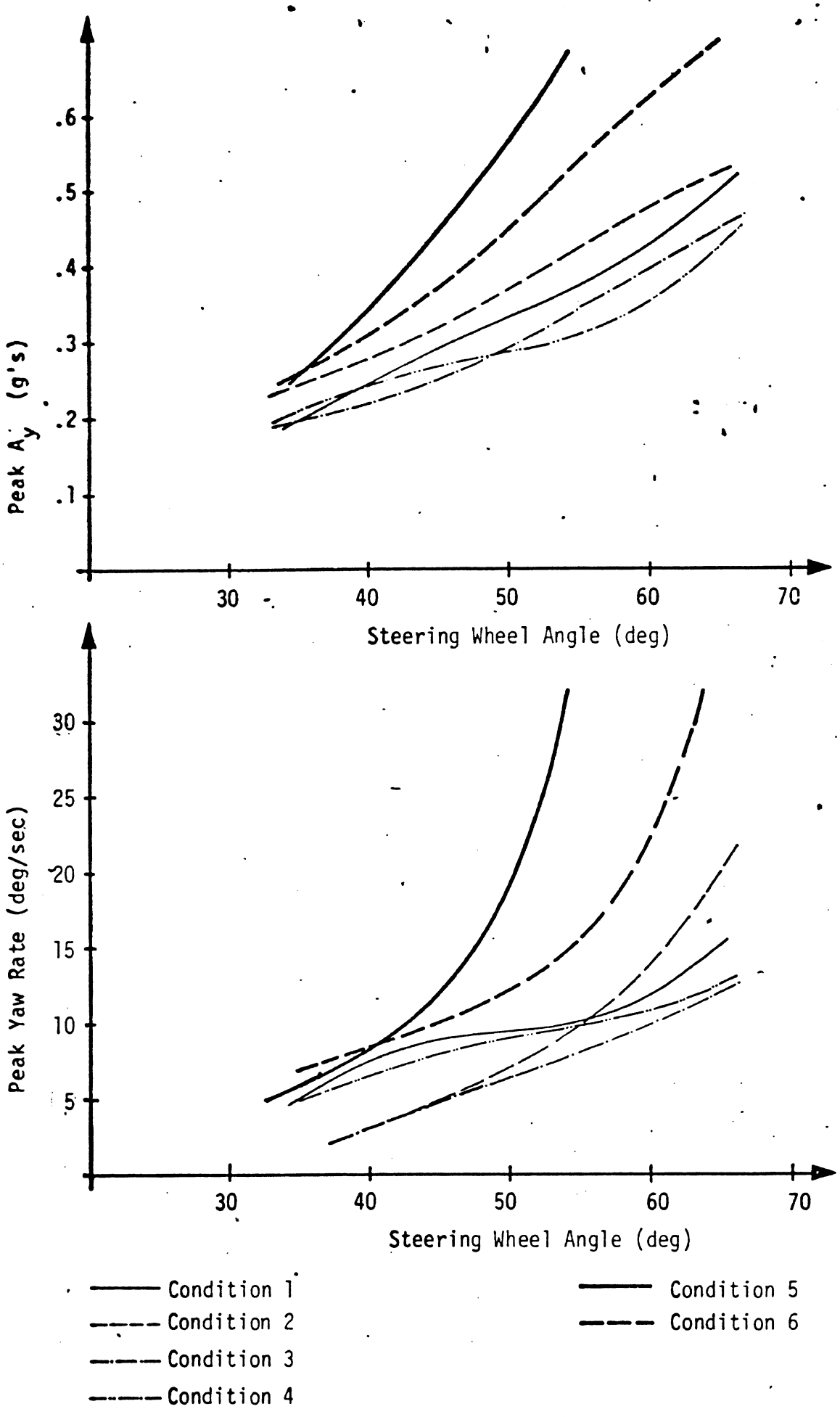

Figure 4.4. Trapezoidal steer responses obtained with pickup truck at 50 mph.

As a simplification of the test matrix, all tires were operated at a common inflation pressure value of 60 psi cold.

Test data on this vehicle tend to indicate, in general, that the normal maneuvering of a pickup truck will not be heavily influenced by the installed tires and loading conditions (barring grossly dissimilar tire mixes). On the other hand, significant changes in behavior in severe directional maneuvers may accompany changes in tire selection and, particularly, loading.

4.1.3 Results of Tests Conducted on White 4x2 Road Boss Truck. A limited set of vehicle tests were conducting using the heavy truck test vehicle. As mentioned earlier, testing of this vehicle was terminated by the inadvertent rollover and destruction of the truck. Prior to this occurrence, certain trapezoidal steer results, shown in Figure 4.5, had been obtained at 30 and 50 mph with the vehicle in its unloaded condition. Data points are plotted showing response to both ascending and descending sequences of steering amplitude. The ascent/descent variation was intended to discriminate any monotonic influence of test-induced wear which might have been evident during the experiments. The close agreement of the ascent/descent data points suggests (given the tire wear sensitivities discussed in Section 3.3.2) that the low severity test maneuvers were avoiding the accrual of traction-modifying wear.

The spread in data clustered about the high value of steer amplitude in Figure 4.5 derived from right- and left-turn repeat runs which clearly indicated a substantial steering asymmetry. While the single tire selection and the unloaded-only test condition provides no opportunity to assess vehicle response sensitivities, we do note that the subject configuration does yield a very linear response up to 0.4 g lateral acceleration.

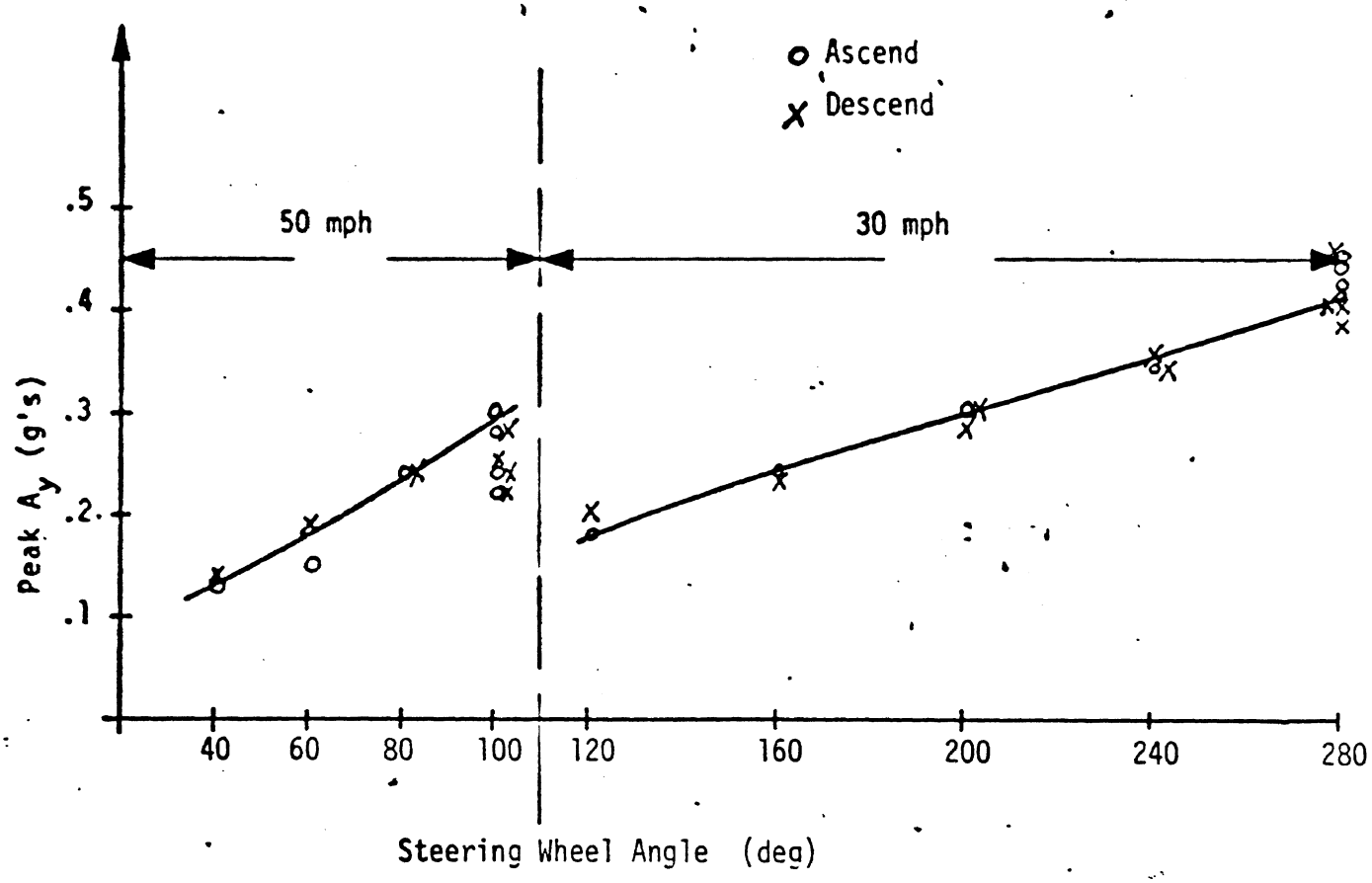

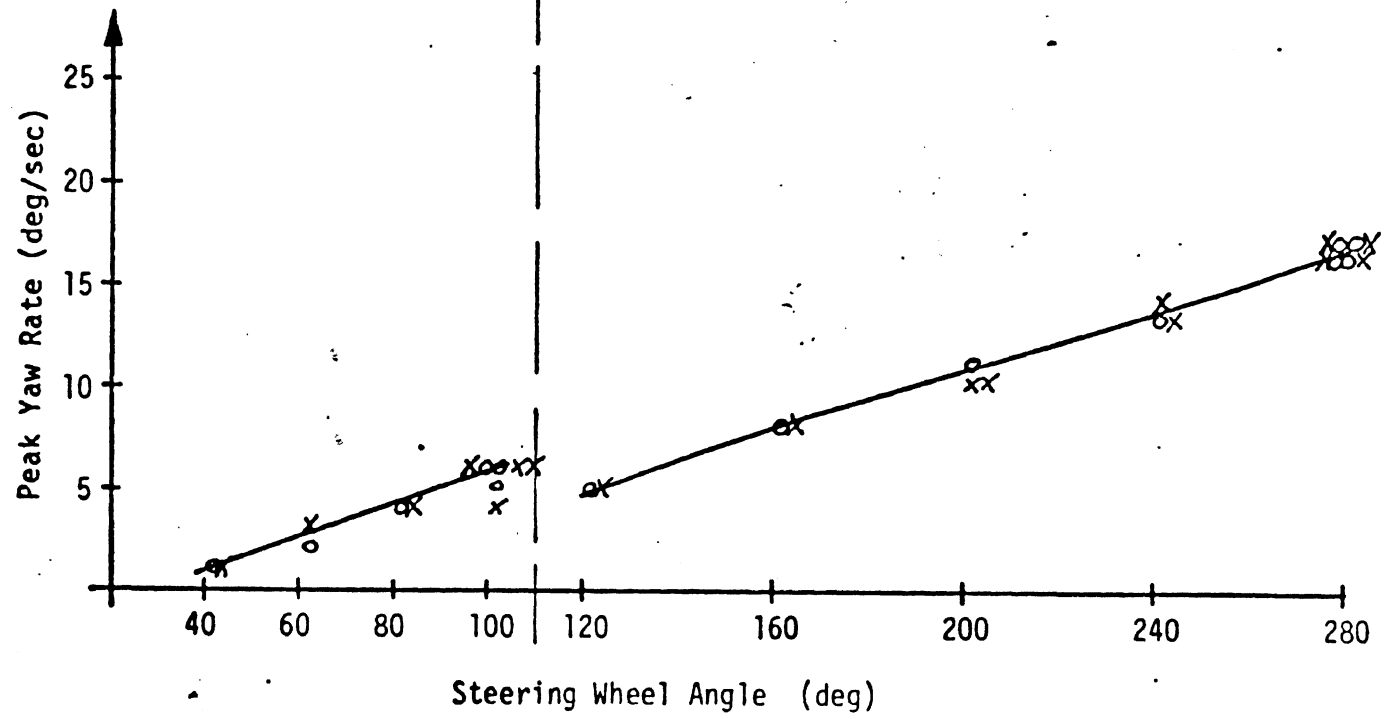

Figure 4.5. Trapezoidal steer responses obtained on heavy truck at 30 and 50 mph.

4.2 Findings Deriving from Simulations Conducted Using APL Model

Simulated responses on the light and heavy truck and bus vehicles were conducted on the hybrid computing facility at the Applied Physics Laboratory. Due to an absence of data describing the combined slip behavior of commercial vehicle tires, simulations were confined to steering maneuvers only. Results are summarized here by vehicle type, covering tire installations such as were selected to cover major elements of each respective tire market (i.e., light truck tires, heavy truck tires, intercity bus "mileage" tires).

4.2.1 Simulation Results Illustrating Vehicle Response Sensitivity to Tire Selections - Light Van. Simulations of the light van vehicle covered both the unloaded and loaded vehicle conditions at both 30 and 50 mph. Various tire installations were simulated, incorporating parametric data gathered on the HSRI flat-bed and mobile test devices. Although Appendix F includes computed results covering various maneuvering conditions, the influence of differing tire installations can be well defined by the results of trapezoidal steer maneuvers alone. Results obtained for the unloaded vehicle at 30 and 50 mph illustrated negligible discrimination between the tire configurations examined. The loaded vehicle, however, was found to be markedly sensitive to certain tire installations.

Portraying the distinctions in traction performance among tires included in these calculations, Figure 4.6 illustrates the F_y/F_z versus α behavior of each tire at its rated load. The tire sample for van simulations is seen to include both bias-ply and radial selections and, in the bias construction, both highway rib and lug (snow) type treads. The selection provided significant variations in both linear and friction-limited traction behavior such as were shown in Section 3 to characterize the light truck tire market.

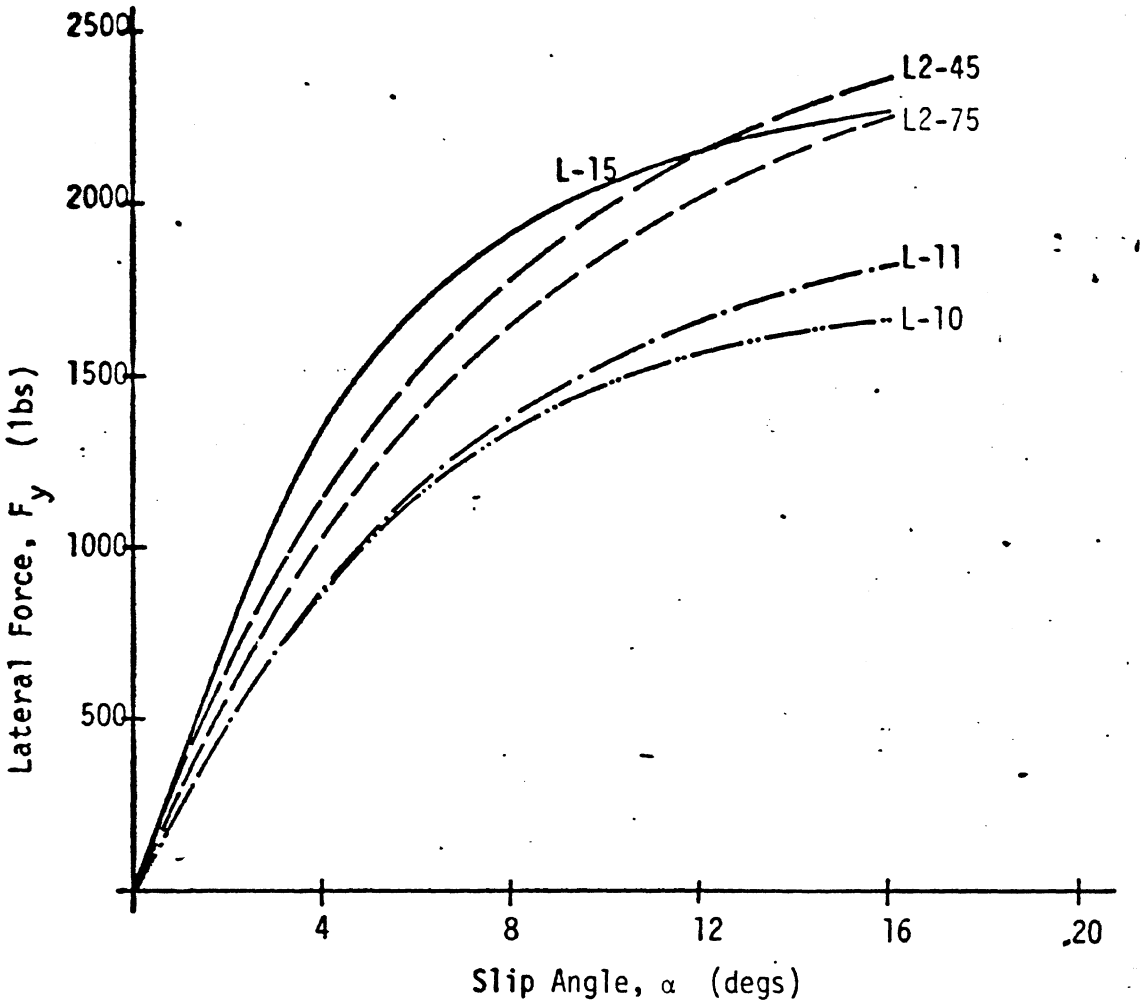

Figure 4.6 F_y versus α behavior of van tires at 2680 lbs. load.

As shown in Figure 4.7, we find that the placement of tires among the various wheel positions, as well as the distribution of inflation pressures, can significantly alter vehicle response. Consider, for example, the peak lateral acceleration responses at 30 mph which were obtained in tire configuration E_4 employing the "OE" tire in the front (Goodyear Custom Hi Miler 8.75 x 16.5/E) and a mud and snow tire on the rear (Firestone Town & Country 8.75 x 16.5/E). These calculations show that the vehicle with this mix of rib and lug treads becomes directionally unstable at a steering input of $\delta_{sw} = 140°$ while all other tire configurations yield a stable response of about $A_y = 0.5$ g at that steering level.

The most "favorable" tire selection which was examined would appear to be the E_2 configuration, employing commonly-inflated Michelin XCA 8.75R16.5/D radials at all four wheel positions. In this configuration, the vehicle yielded the smallest sideslip response while exhibiting smooth A_y and r increases over the range of steer inputs.

It is also instructive to compare results obtained in configurations E_0 and E_3 in which the OE tire was employed with a common inflation pressure, 70 psi, at all four wheels (E_0) and then with 45 psi front and 70 psi rear (E_3) (inflation pressure levels approximating those recommended by the manufacturer of the baseline vehicle and for which tire data were available). The curiously increased A_y and r gains in the E_3 case illustrate the significance of the classically "backwards" inflation pressure sensitivity of the OE tire.

This result is further emphasized in Figure 4.8 in which the 50-mph trapezoidal steer responses are summarized. At the steer input condition, $\delta = 70°$, the biased-inflation configuration, E_3, yields a rapidly destabilizing response compared to the reference E_0 configuration. Also, of course, we see the rib tire/snow tire mix (E_4) to render a dramatically destabilized response in the vicinity of $\delta = 50°$.

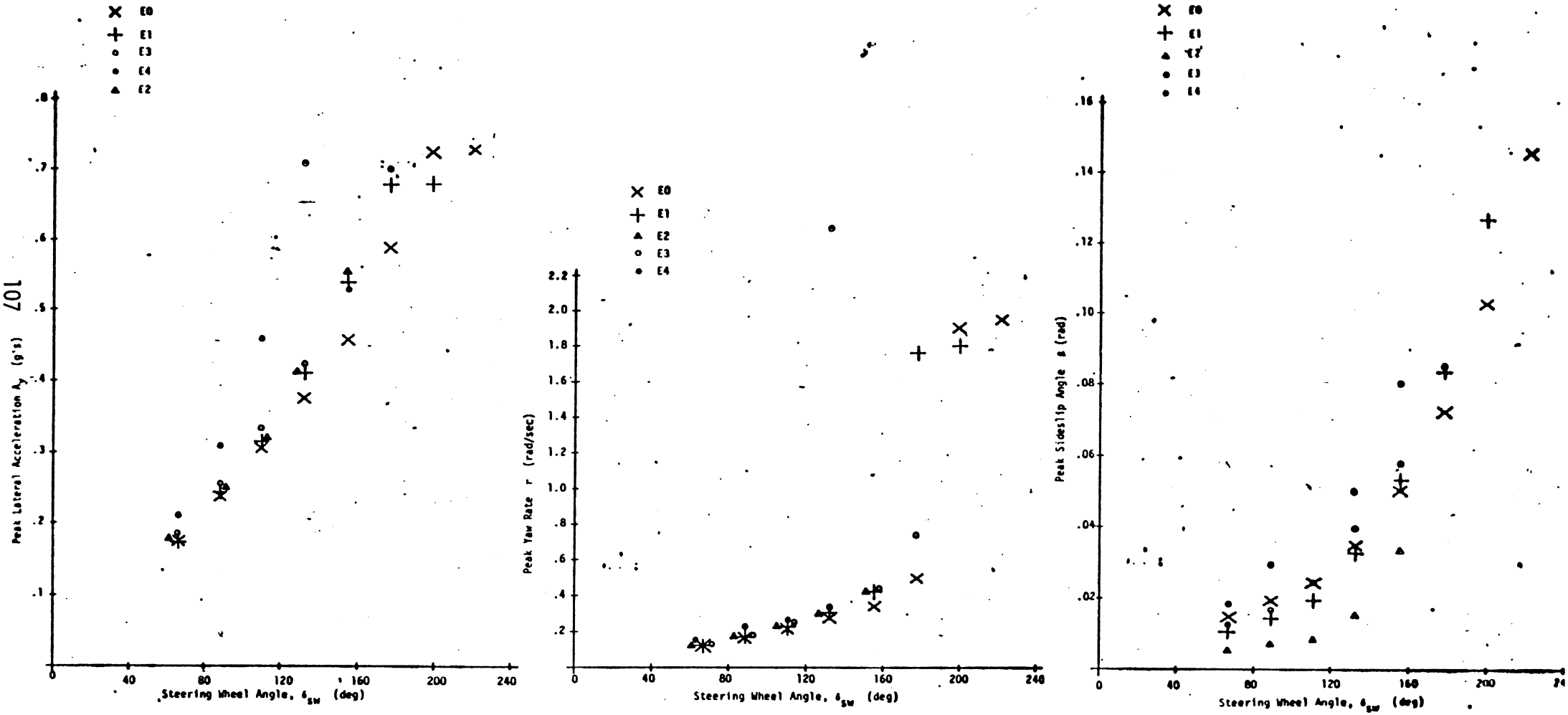

Figure 4.7 Simulated response of the Econoline van to a sequence of trapezoidal steer inputs at 30 mph, in the loaded condition.

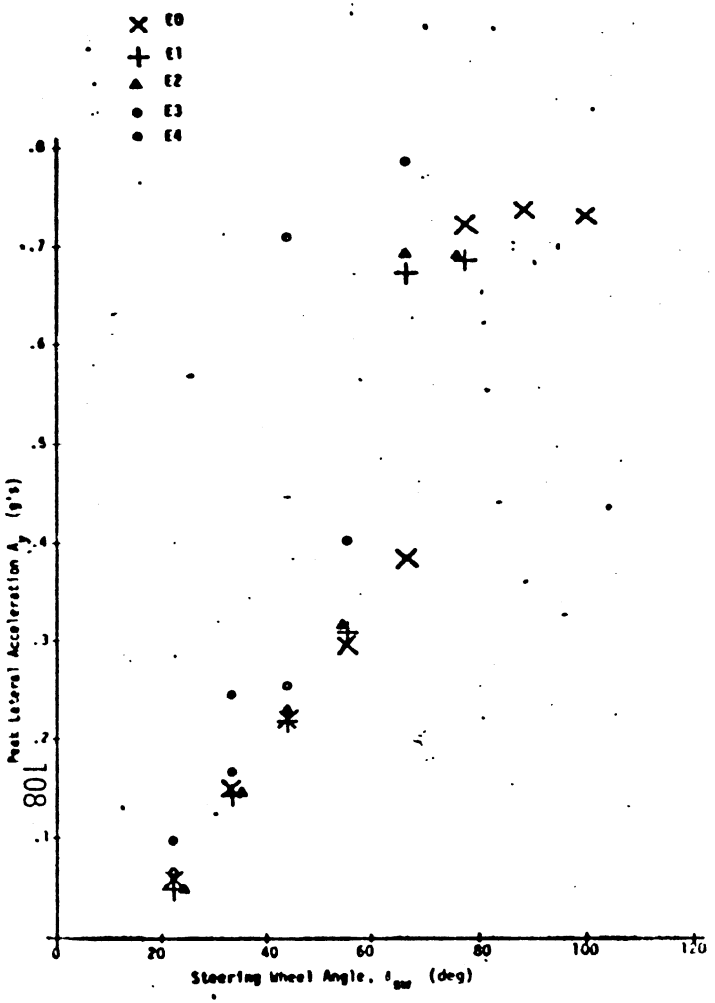

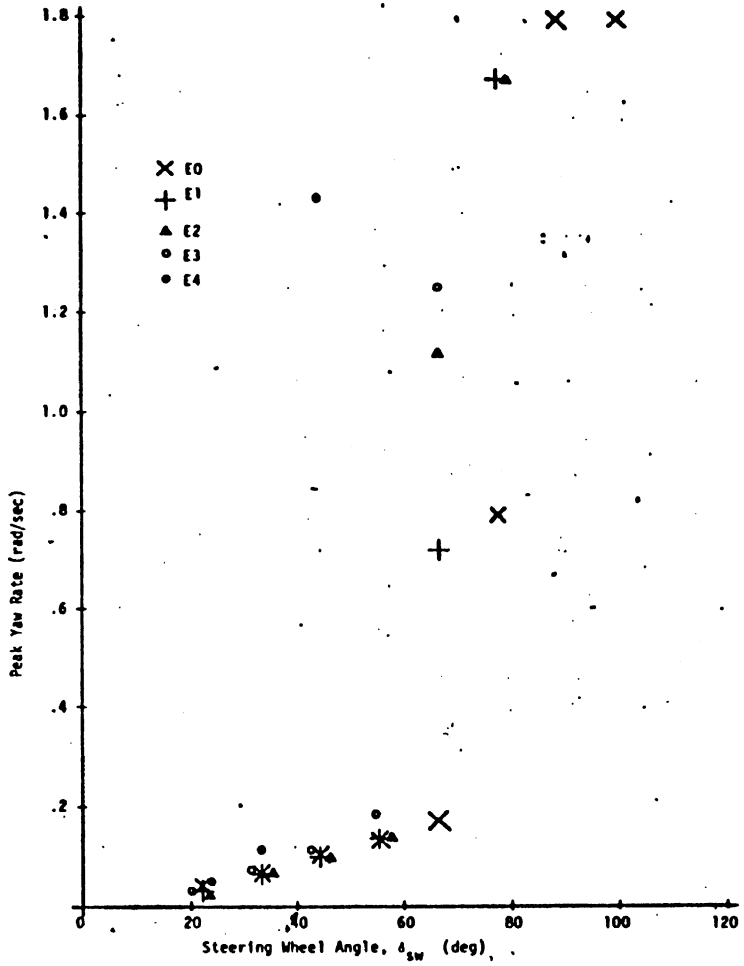

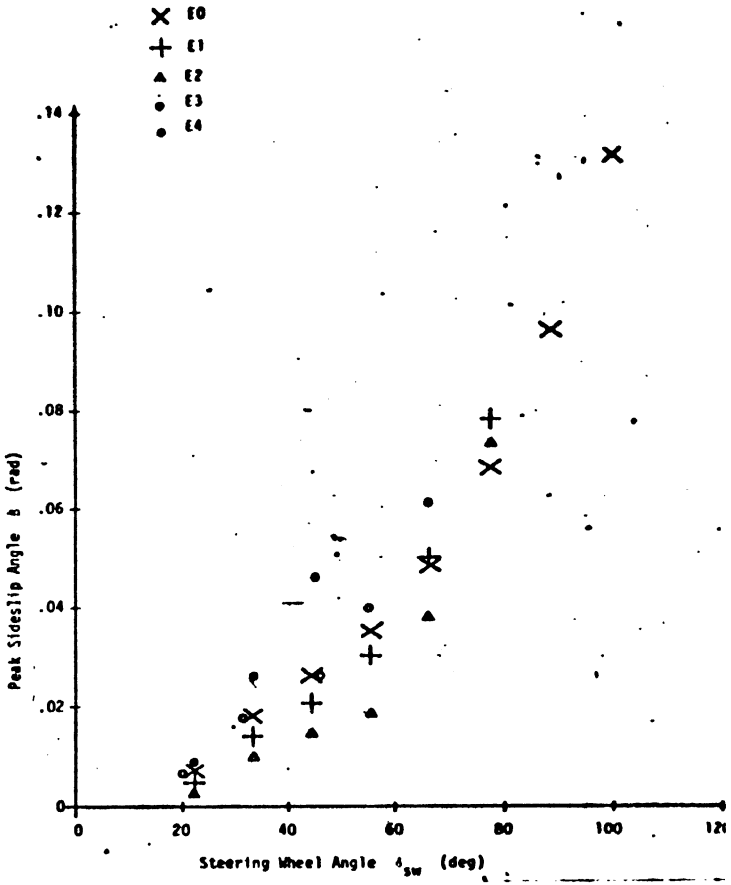

Figure 4.8 Simulated response of the Econoline van to a sequence of trapezoidal steer inputs at 50 mph, in the loaded condition.

Overall, the van results indicate that the installation of four tires of the same type and at the same inflation pressure yields a reasonable directional behavior over the entire performance range regardless of the specific shear force behavior of the various types examined. In contrast, any fore/aft bias in tire distribution which places the lower lateral traction capability in the rear will result in the classical reduction in directional stability.

Particularly significant is the calculation of reduced yaw stability for the case of the OE tire installed with its recommended inflation pressure bias. Insofar as light truck tires may or may not indicate the classical polarity of slope in their lateral traction sensitivity to inflation pressure, it would appear that recommendations of a biased distribution of inflation pressure are open to question.

4.2.2 Simulation Results Illustrating Vehicle Response Sensitivity to Tire Selections - Pickup Truck. Design parameters measured on the pickup truck test vehicle were applied in a sequence of simulations examining the influence of "pickup truck tires" on the yaw behavior of the subject vehicle. In these calculations the selected tires covered F_y/F_z versus α characteristics as shown in Figure 4.9. As was shown in the case of the tires selected for the van simulations, the range of properties spans linear range variations as well as variations in the high slip behavior. Note, also, that the traction properties employed in these simulations represent actual tires rather than artificially-generated descriptions.

Three tire configurations were examined with the vehicle in its unloaded condition. As shown in Figure 4.10, calculations of response to trapezoidal steer at 30 mph illustrate virtually zero sensitivity to the differing tires installed uniformly at all four wheel positions. Note that although the sideslip response of the E_0 data indicates a large departure from the other configurations, the expanded β scale tends to exaggerate an otherwise insignificant distinction.

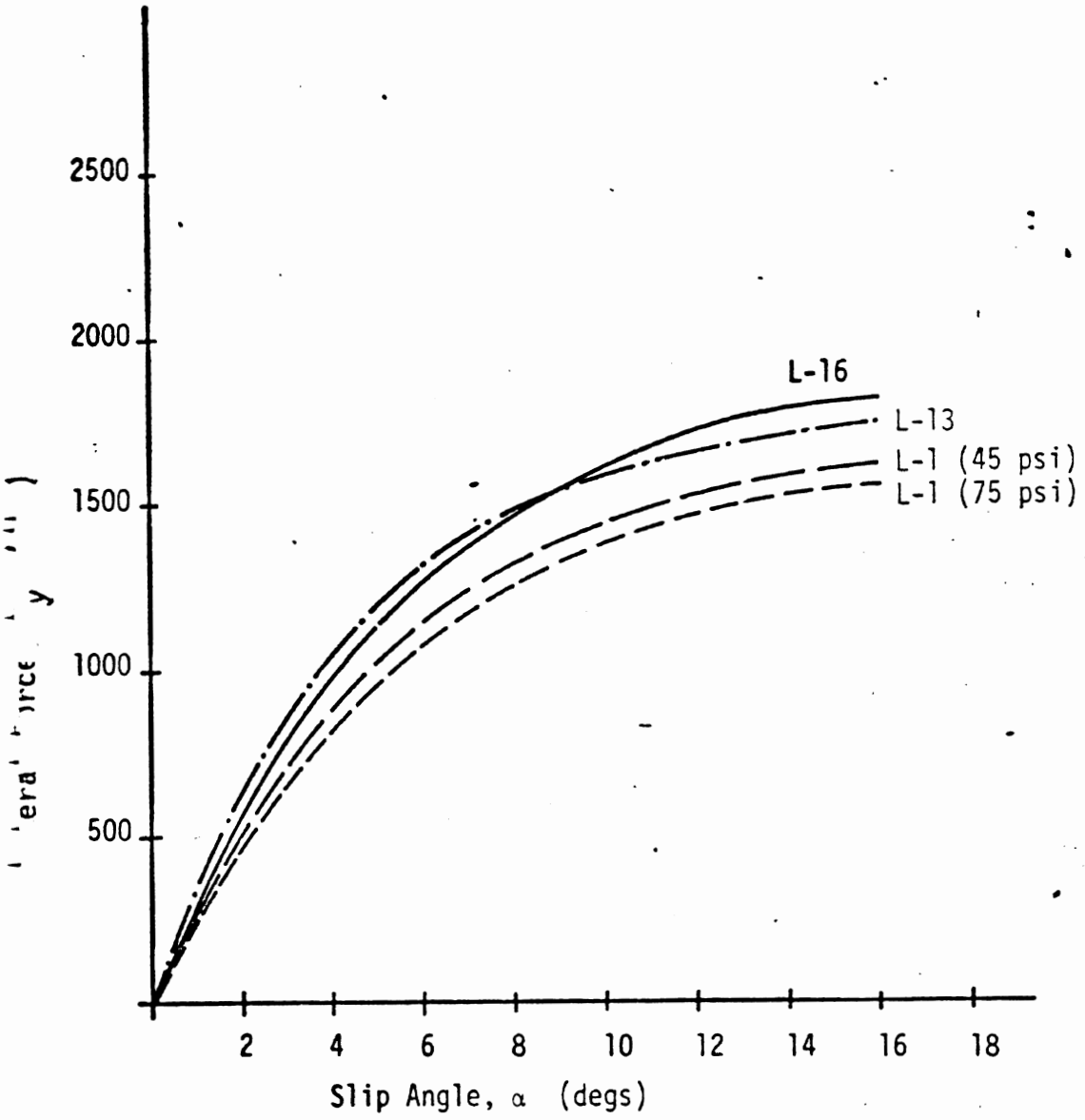

Figure 4.9. F_y versus α behavior of pickup truck tires at 2050 lbs. load.

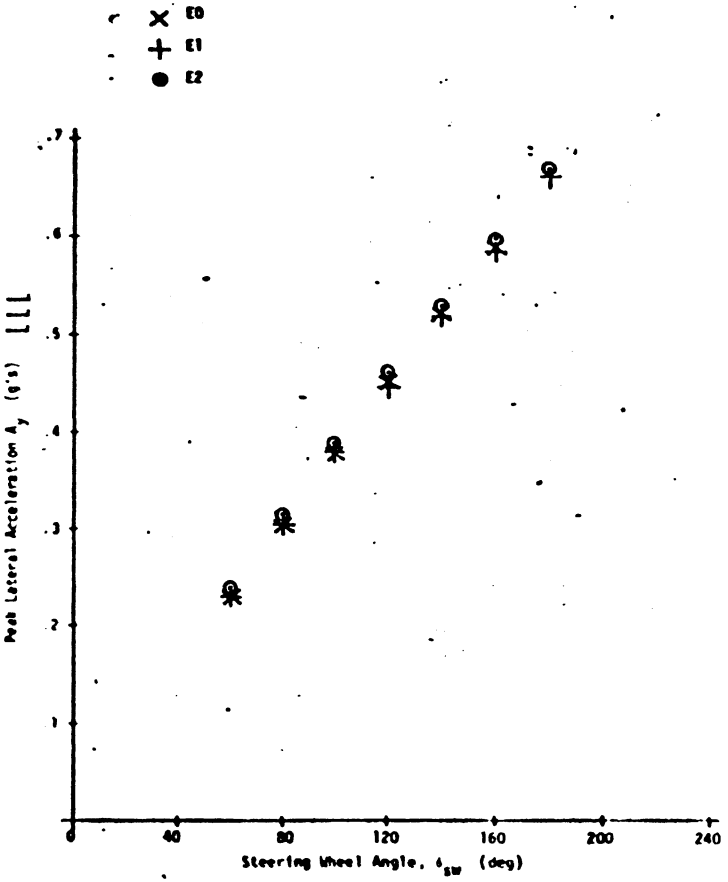

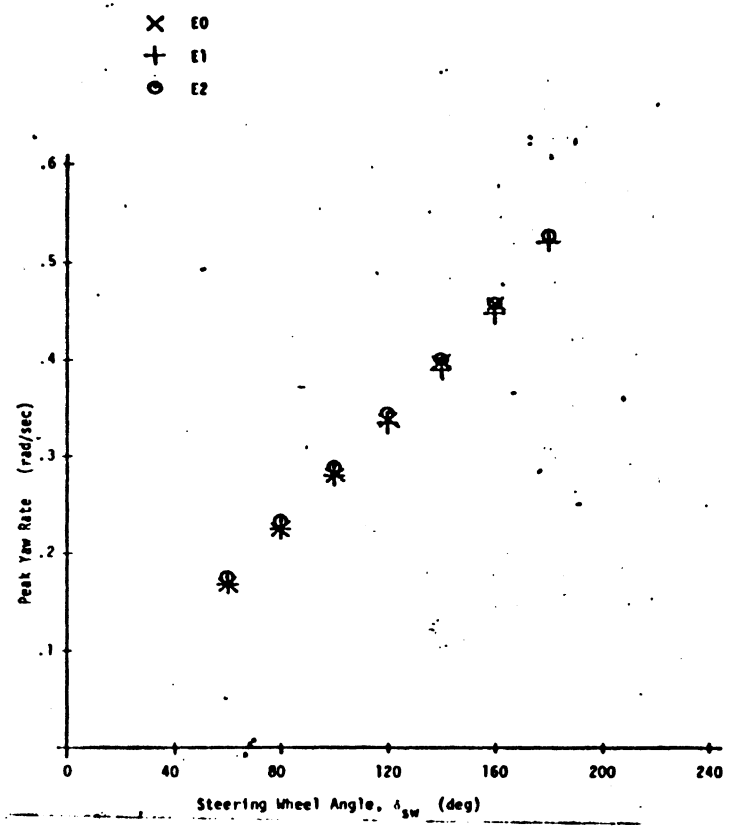

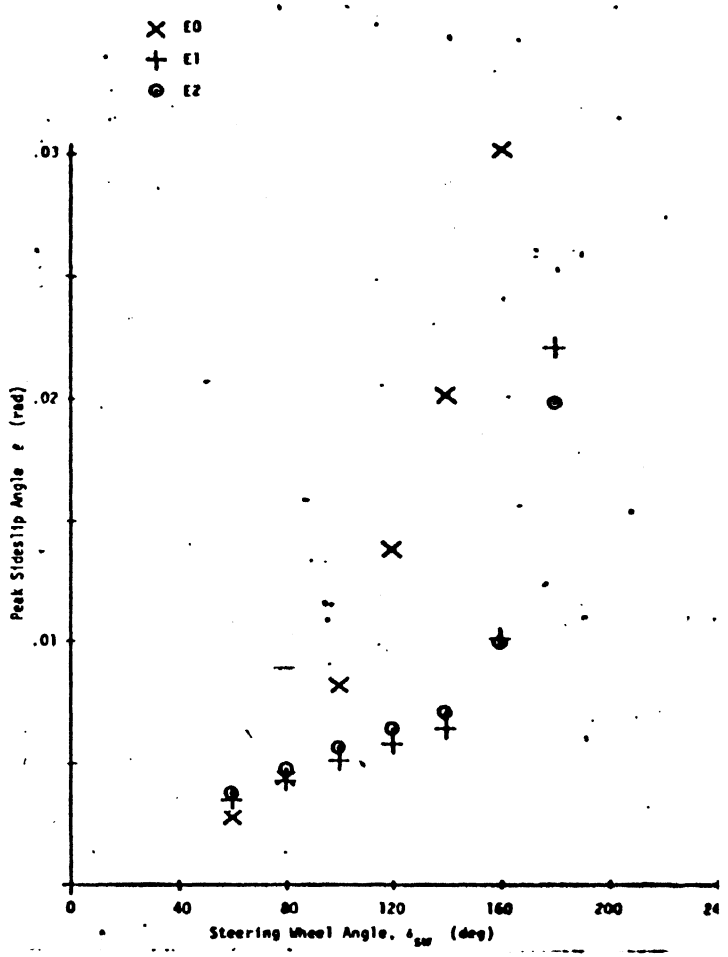

Figure 4.10 Simulated response of the F-250 pickup truck to a sequence of trapezoidal steer inputs at 30 mph in the unloaded condition.

Figure 4.11 illustrates results obtained at 50 mph, again revealing negligible separations in performance among the three configurations. The consistently higher β values for the E_0 tire condition, together with indistinguishable A_y and r differences, reflects the fact that the (E_0) rear tires are sufficiently lower in cornering stiffness at the prevailing rear axle loads that the truck must operate at higher steady-state values of β to achieve a yaw moment balance.

Considering the pickup in its fully loaded condition, we find from the 30 and 50 mph results shown in Figures 4.12 and 4.13 that a powerful discrimination of tire sensitivity can be obtained when the recommended inflation pressure bias is considered. As in the case of the van simulations, the rear-75 psi, front-45 psi conditions (E_3) has the effect of increasing the yaw rate gain while destabilizing the limit response. In contrast to the other uniformly-distributed tire configurations, the E_3 arrangement clearly provides the most significant variation in performance.

The E_3 condition tends to destabilize the system because the more highly inflated (rear-mounted) tire yields the lower side force responses. As with the van, this obviously less advantageous arrangement was considered only because it represents the nominal inflation pressure bias recommended by the manufacturer. Again, the uniformly-distributed radial, E_2, serves to provide the lowest gain A_y and r responses as well as the minimum values of peak sideslip angle.

4.2.4 Simulation Results - Heavy Truck. Heavy truck simulations were conducted using the model and the computer facilities at APL as well as the model and facilities at HSRI. APL results are presented here while HSRI's results deriving from a pointed study of truck yaw divergencies are presented in the next section.

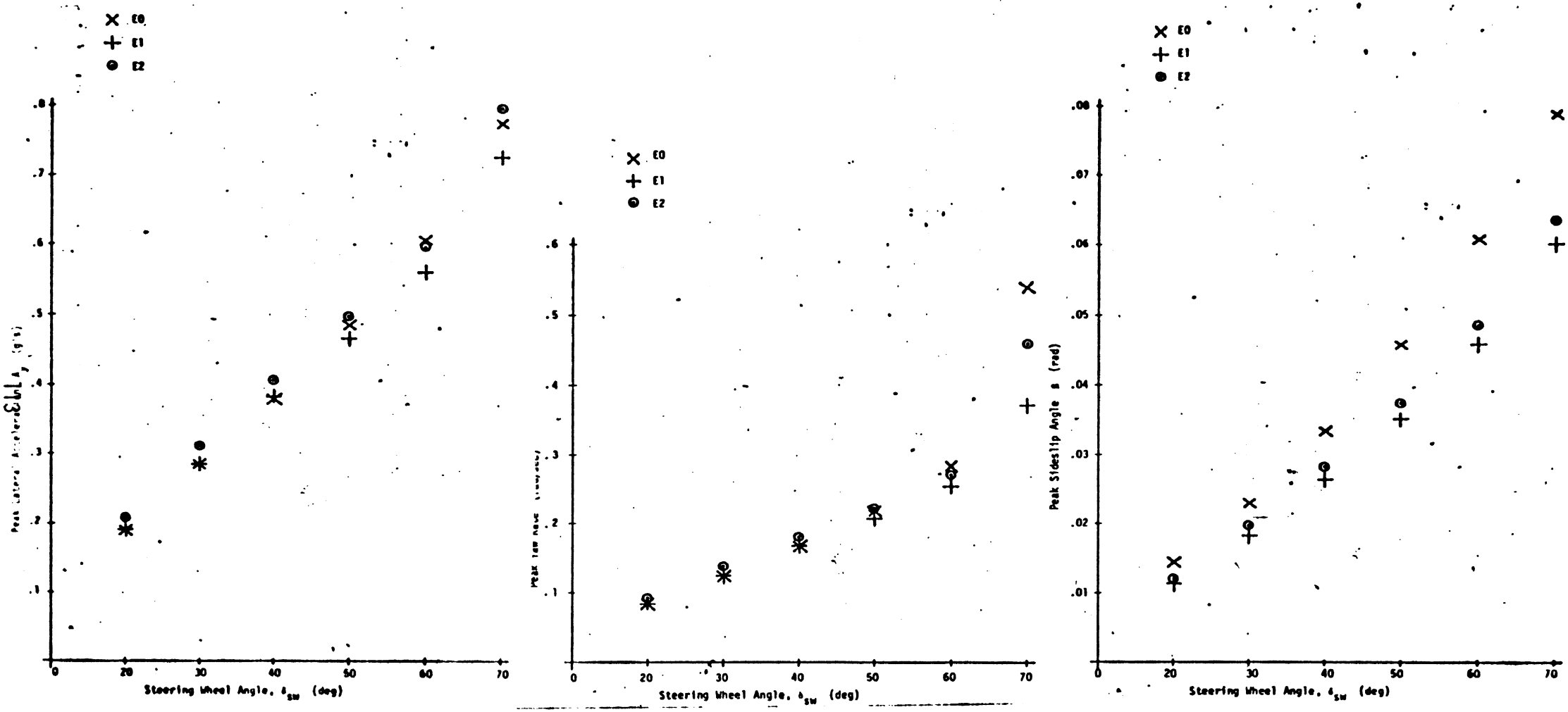

Figure 4.11 Simulated response of the F-250 pickup truck to a sequence of trapezoidal steer inputs at 50 mph in the unloaded condition.

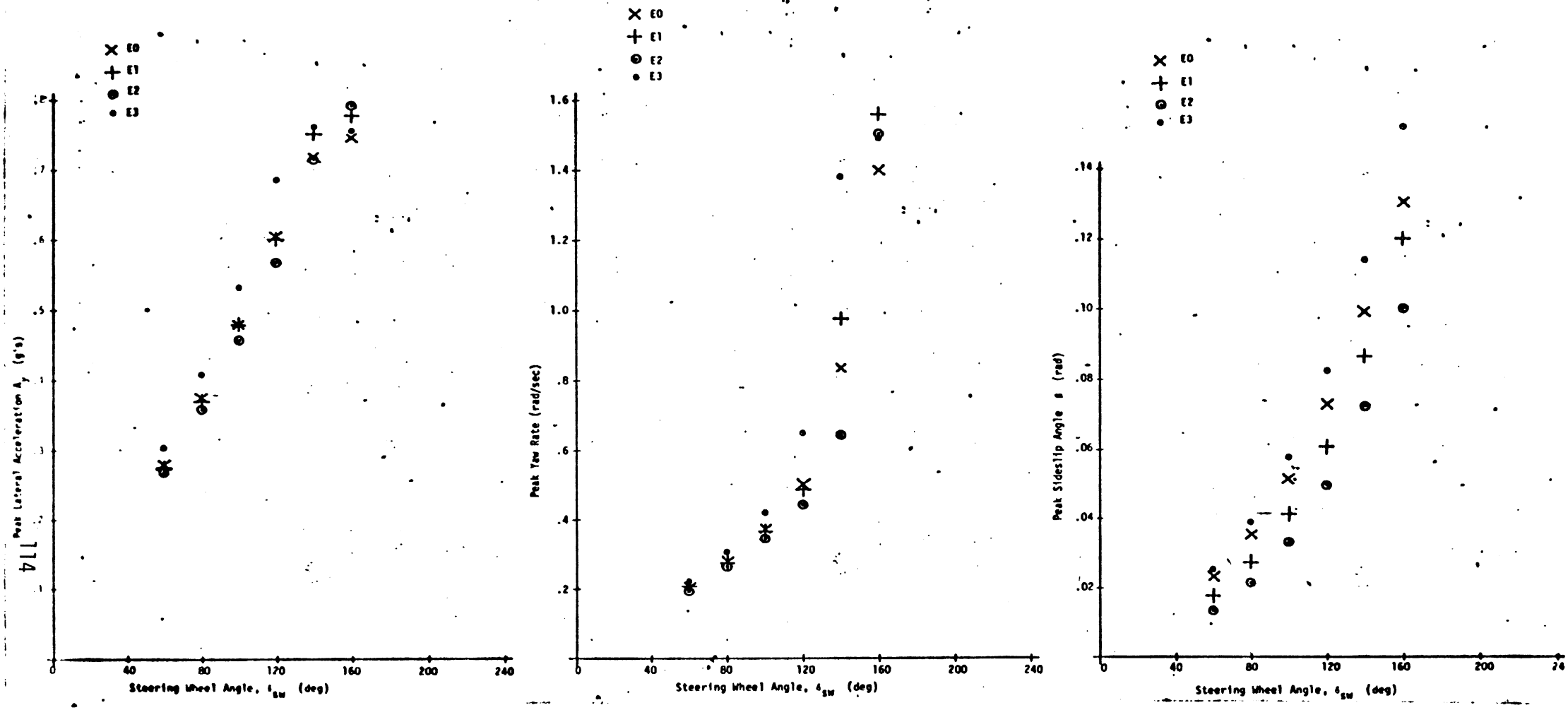

Figure 4.12 Simulated response of the F-250 pickup truck to a sequence of trapezoidal steer inputs at 30 mph in the loaded condition.

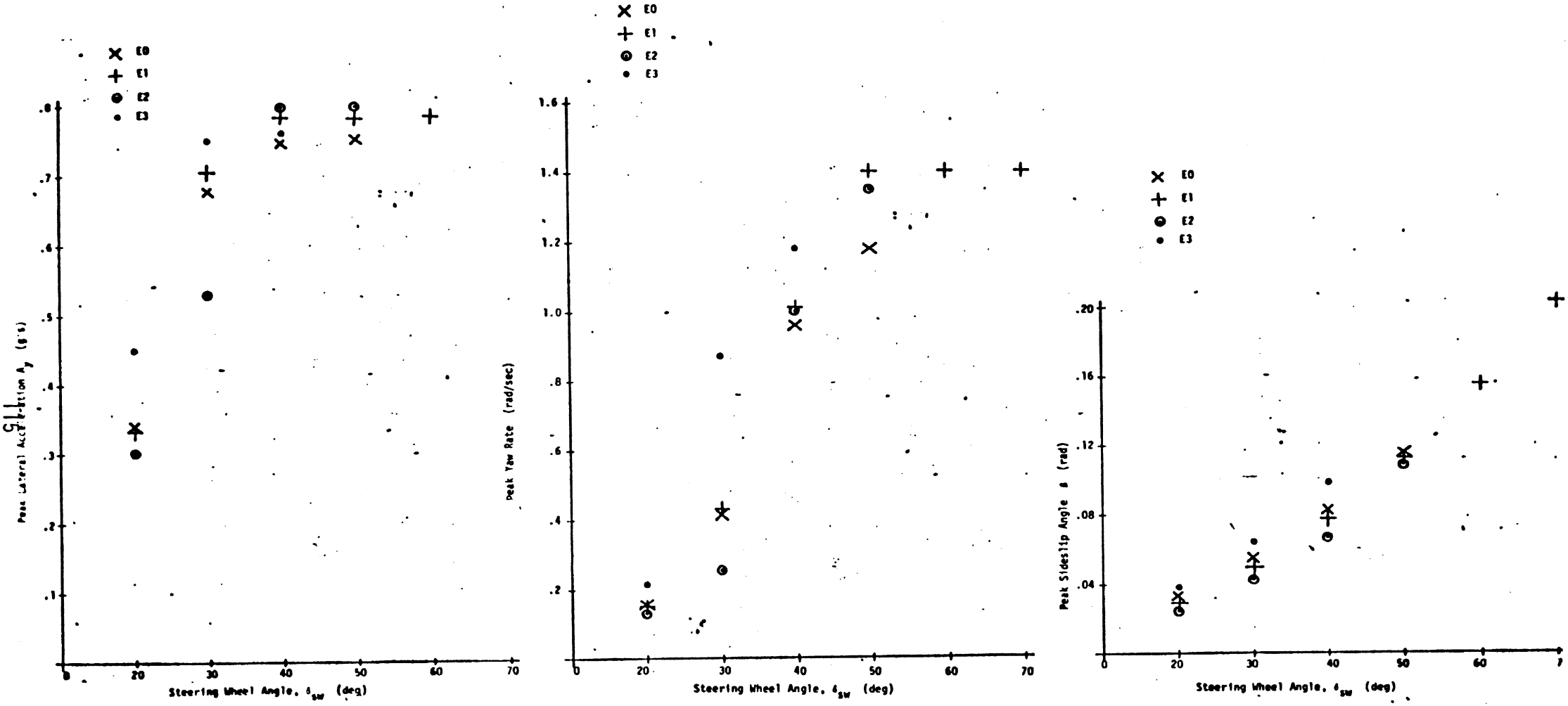

Figure 4.13 Simulated response of the F-250 pickup truck to a sequence of trapezoidal steer inputs at 50 mph in the loaded condition.

Calculations at APL covered the behavior of the unloaded and loaded White Road Boss truck as outfitted, in turn, with each of three tire selections listed below:

H-1 - The OE-bias/rib tire (see Table 3.1 for tire codes).

H-4 - A radial rib providing highest values of C_α (for a non-wide base tire) over the entire load range.

H-6 - A radial rib exhibiting the most unconventional C_α/F_z relationship.

The C_α/F_z behavior for each tire is shown in Figure 4.14, contrasting these selections with the remainder of the sample of heavy truck tires. Shown in Figures 4.15 and 4.16 are the trapezoidal steer numerics for the 30-mph and 50-mph simulation runs. As can be seen, the higher C_α tire yields the higher magnitude response at any value of steer level within the range of about 0.4 g, A_y. As the maneuver severity approaches the vehicle rollover limit (near A_y = .55 for the loaded truck), a change in relative responses is observed—indicating a vehicle behavior which is independent of the C_α property of each tire and derives from the sensitive balance of tire side forces at front and rear axles.

Interestingly, the tire selection, H6, illustrates an intermediate set of response amplitudes for the unloaded vehicle but a distinctly lowest set of A_y and r values for the loaded vehicle. Since the varying response amplitudes observed among the various tire selections clearly indicate varying relationships between front and rear tire slip angles on the simulated vehicle, a generalized explanation of these calculations (involving common tire installations at all wheel positions) is very difficult. Nevertheless, it is interesting to note that the H6 tire exhibited a relatively high value of C_α at low loads and a relatively low value at high loads. Correspondingly, Figures 4.15 and 4.16 indicate a significant drop in the relative position of the H6 responses between the unloaded and loaded vehicle calculations.

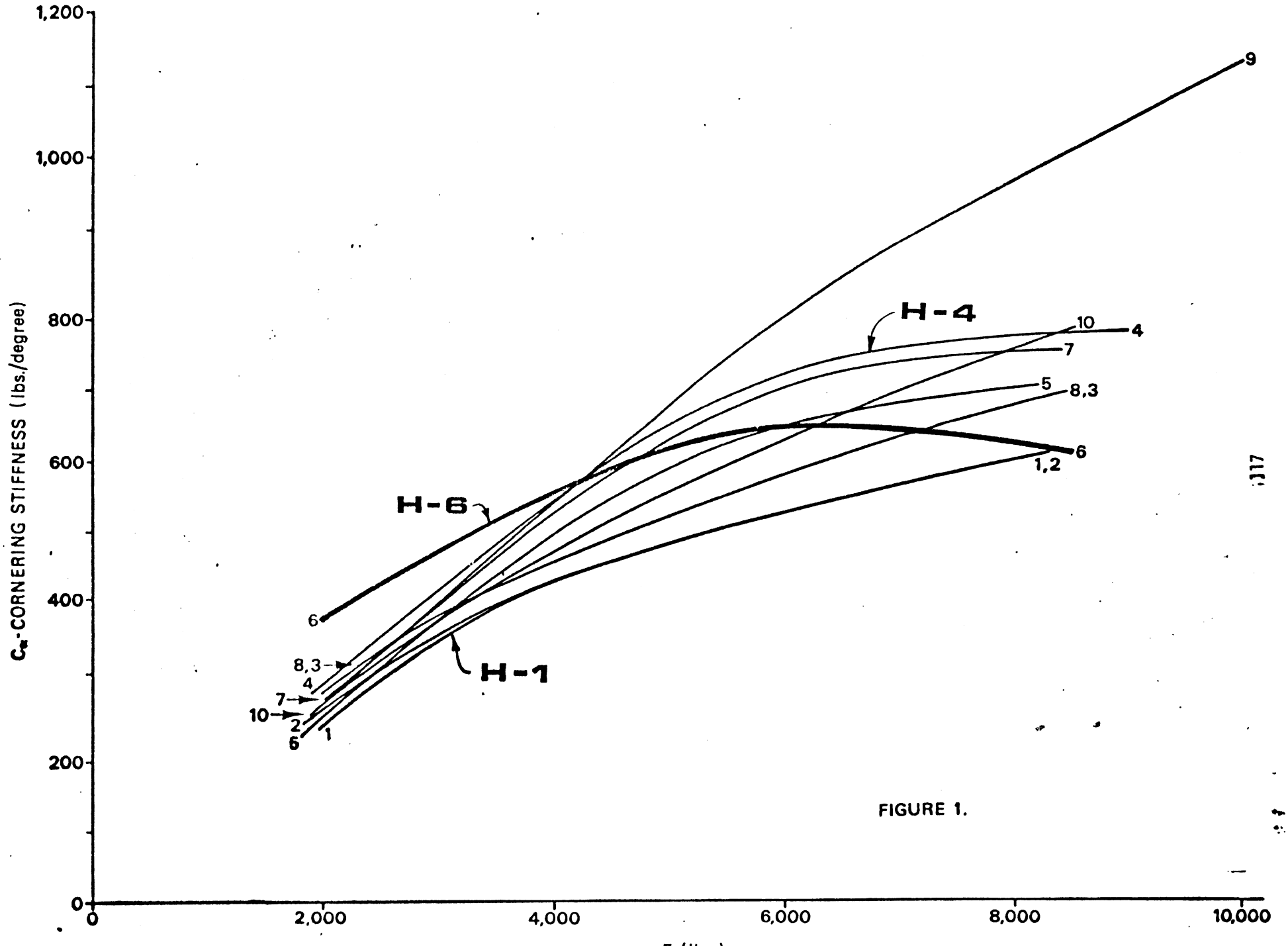

FIGURE 1.

Figure 4.14. Load sensitivity of the cornering stiffness parameter for the three tires, H1, H4, and H6, employed in heavy truck simulations (compared to the remainder of the heavy truck tire sample).

Heavy Truck 30 mph

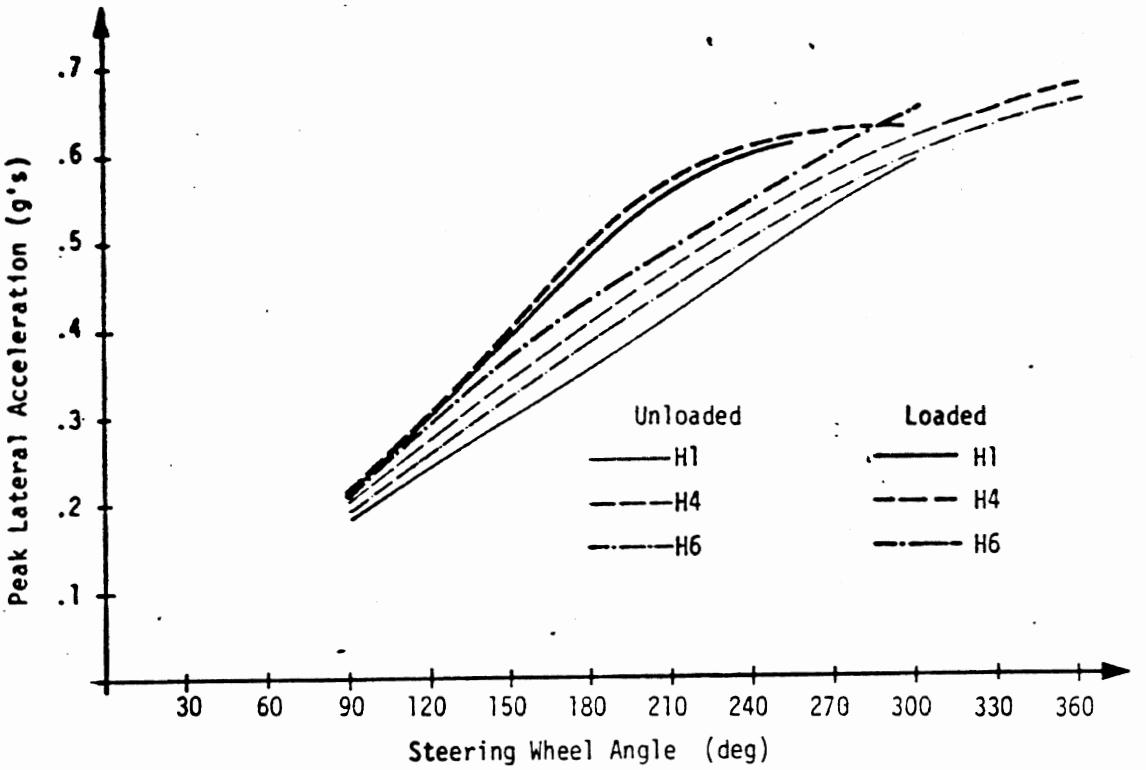

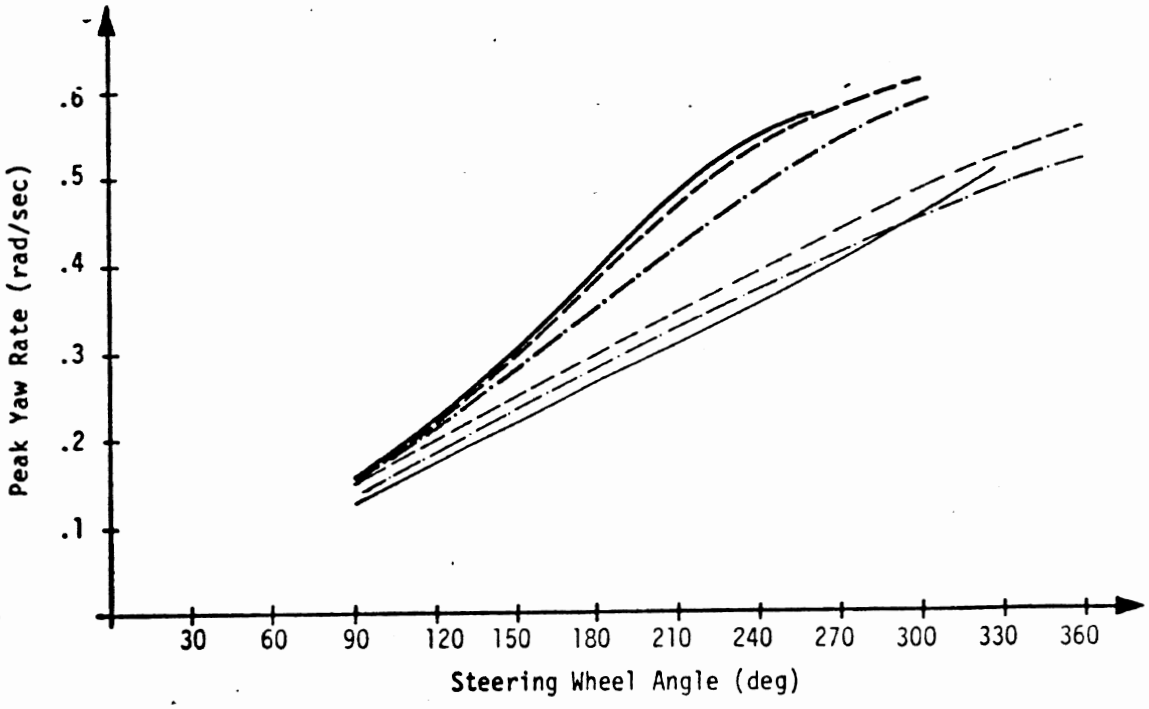

Figure 4.15. Simulated response of the White Road Boss to a sequence of trapezoidal steer inputs at 30 mph (loaded and unloaded).

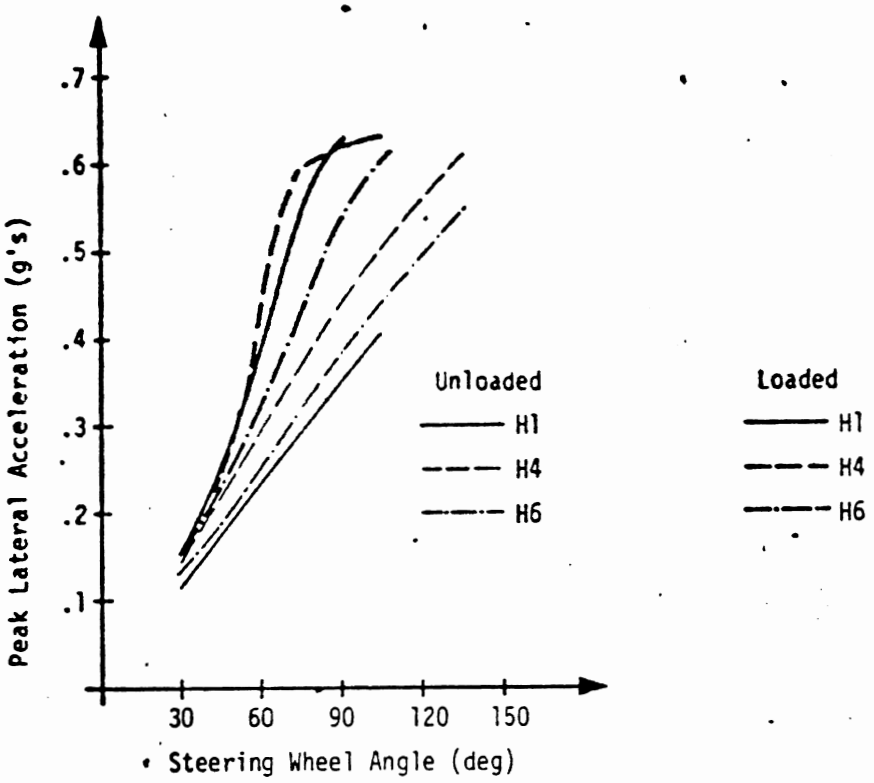

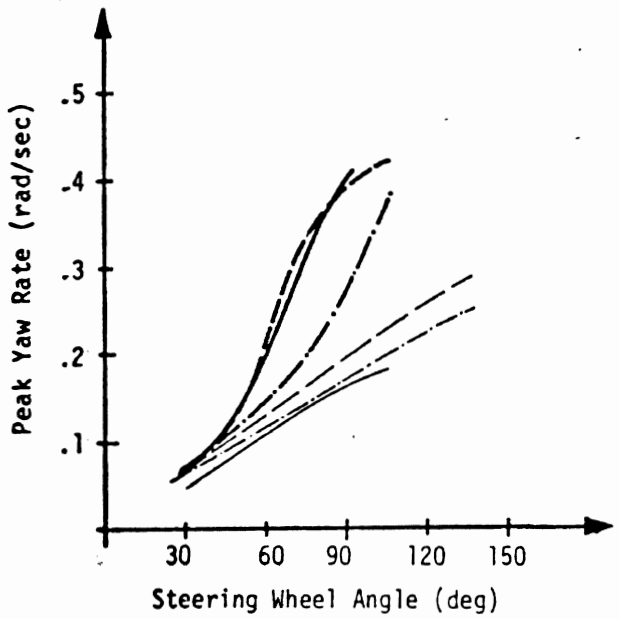

Figure 4.16. Simulated response of the White Road Boss to a sequence of trapezoidal steer inputs at 50 mph (loaded and unloaded).

Both the 30-mph and 50-mph responses serve to confirm the often-repeated finding, here, that the differences in vehicle response gain deriving from the common installation of alternative tire selections at all wheel positions (no tire mix) are generally small. Thus, for example, we see a rather small distinction between results obtained with the bias-ply tire, H1, and the stiff radial, H4. A somewhat more significant departure derives, however, in the case of the anomalous characteristics (in terms of C_α/F_z, at least) afforded by the radial sample, H6.

4.2.5 Simulation Results - Heavy Bus. The GMC intercity coach was simulated on the APL hybrid computer with three sets of tires and in both the loaded and empty conditions. An expected, but nonetheless, important feature of the results of these calculations is that the unloaded vehicle exhibits decidedly less understeer than does the loaded vehicle. This result is explained by noting that the empty vehicle has a rearward biased load center, with its engine cantilevered well aft of the rear axle. As the bus becomes loaded, with its passenger and cargo areas located forward of the empty vehicle's mass center, the total vehicle c.g. is translated forward considerably. Since both the bias- and radial-ply bus tires exhibited a significant curvature of their C_α/F_z relationship, the forward translation of the mass center is inadequately compensated by the upward increment in front tire cornering stiffness. Accordingly, the expression

$$\left(\frac{a}{C_{\alpha_2}} - \frac{b}{C_{\alpha_1}}\right)$$

becomes increasingly positive (more understeer) as the bus is loaded.

In Figures 4.17 and 4.18, the trapezoidal steer response of the bus is shown for simulations at 30 and 50 mph and for the loaded and unloaded vehicle configurations. Differences in

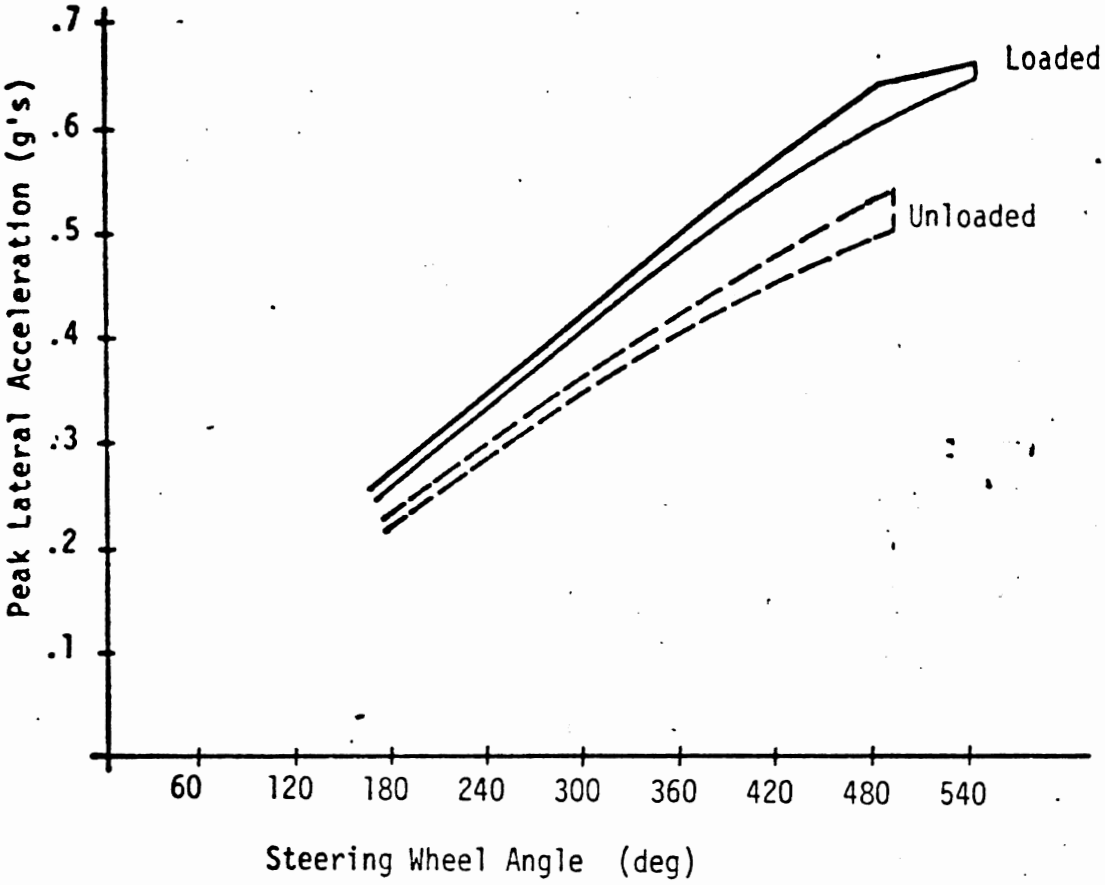

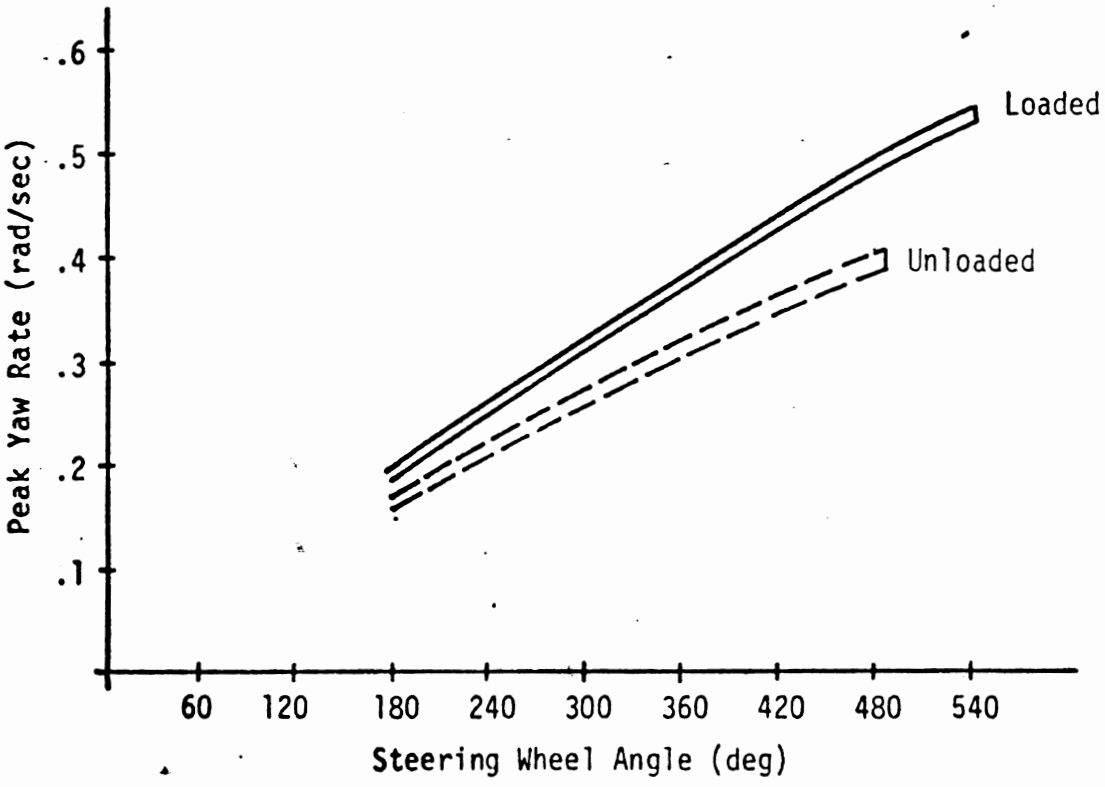

Figure 4.17. Envelopes of all simulated responses obtained for the GMC intercity coach at 30 mph (loaded and unloaded).

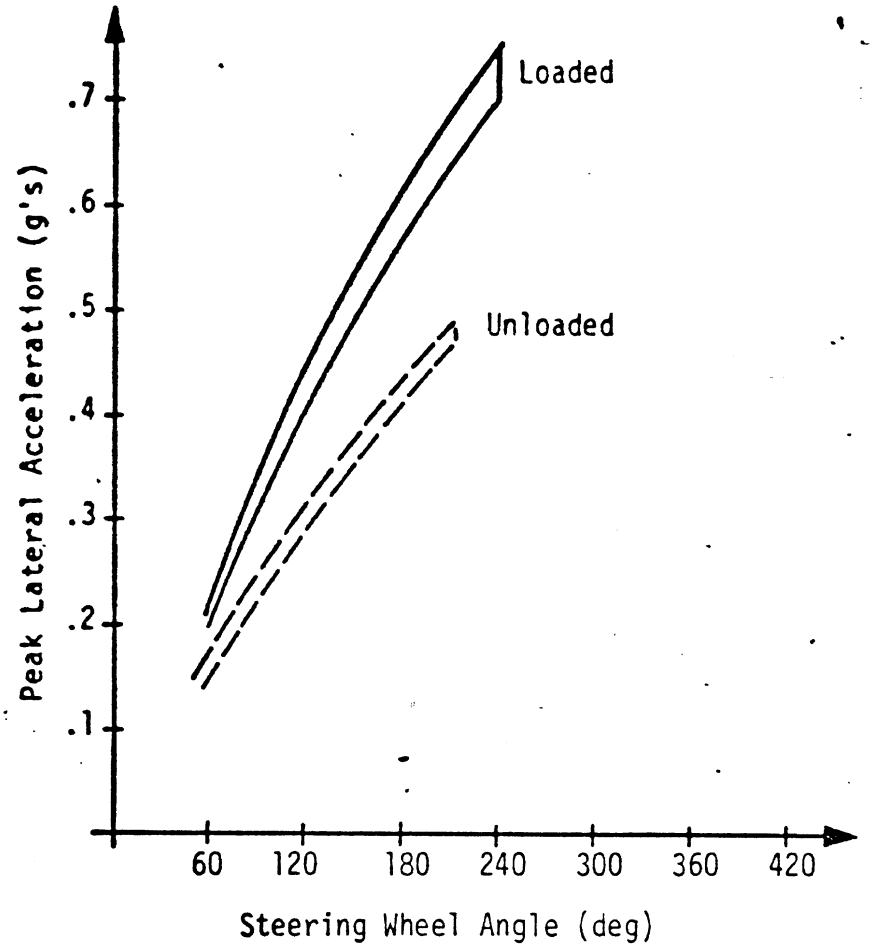

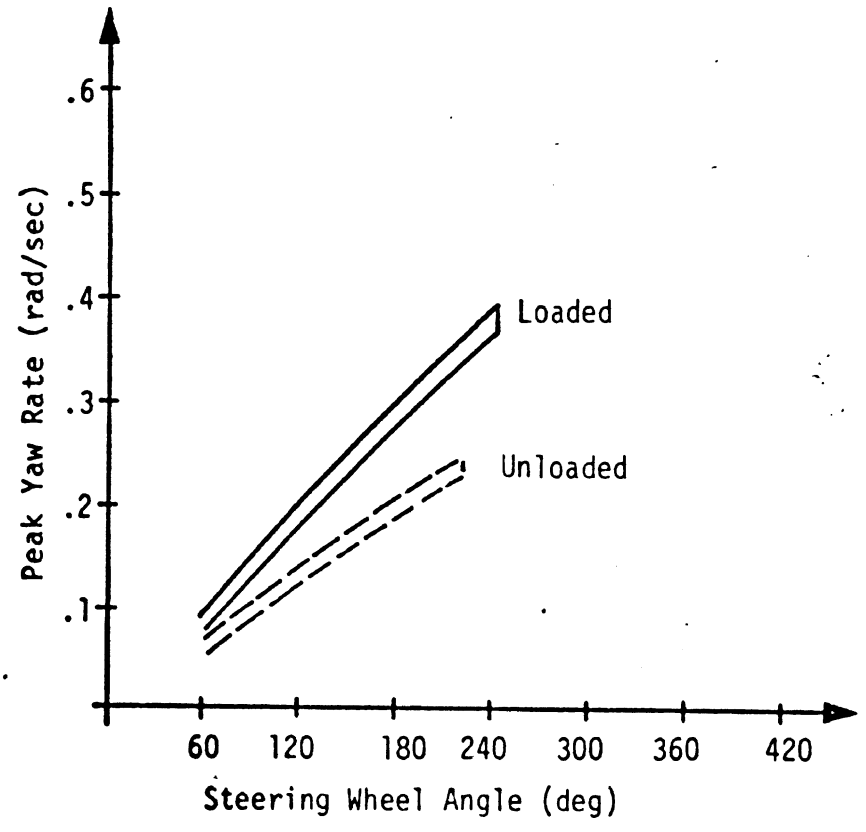

Figure 4.18. Envelopes of all simulated responses obtained for the GMC intercity coach at 50 mph (loaded and unloaded).

vehicle behavior resulting from the various tire installations were found to be so small as to be contained within the narrow envelopes indicated. The low velocity data, of course, illustrates the reduced yaw velocity gain and is expressed in this unnormalized fashion to give good data separation. As indicated, the loaded vehicle data falls below the empty vehicle responses in each case.

Three tire selections, whose C_α/F_z curves are shown in Figure 4.19, are represented in these calculations; the bias-ply, tube-type baseline tire (Firestone Commercial Mileage 12.5 x 22.5), a tube-type radial (Michelin XZA 11R20/H), and a tubeless radial (Michelin XZA 11R22.5/H). Since tire construction mixes are scrupulously avoided in the operation of intercity bus fleets, the question of a fore/aft mix in carcass construction types was not addressed. Further, since the intercity coach is not characteristically operated with lug-type tires on driving axles (in contrast to the line-haul tractor), the fore/aft mix of tread types is, likewise, a moot issue.

Although the trapezoidal steer response data were selected here to illustrate the positive loading effect and negligible tire effects, detailed results illustrating other less discriminating maneuvers are presented in Appendix F.

4.2.6 Simulation Results Specifically Addressing Heavy Truck Yaw Divergencies. A limited series of computations were performed using HSRI's digital simulation [4] to examine the generality of the divergent yaw response which was observed during full-scale testing of a heavy truck. The findings presented in this section serve to address the sensitivity of heavy truck spin-out to various vehicle configuration parameters, thereby expanding upon the test results and computations presented in Appendix G (which directly explained the spinout/rollover incident occurring in this study).

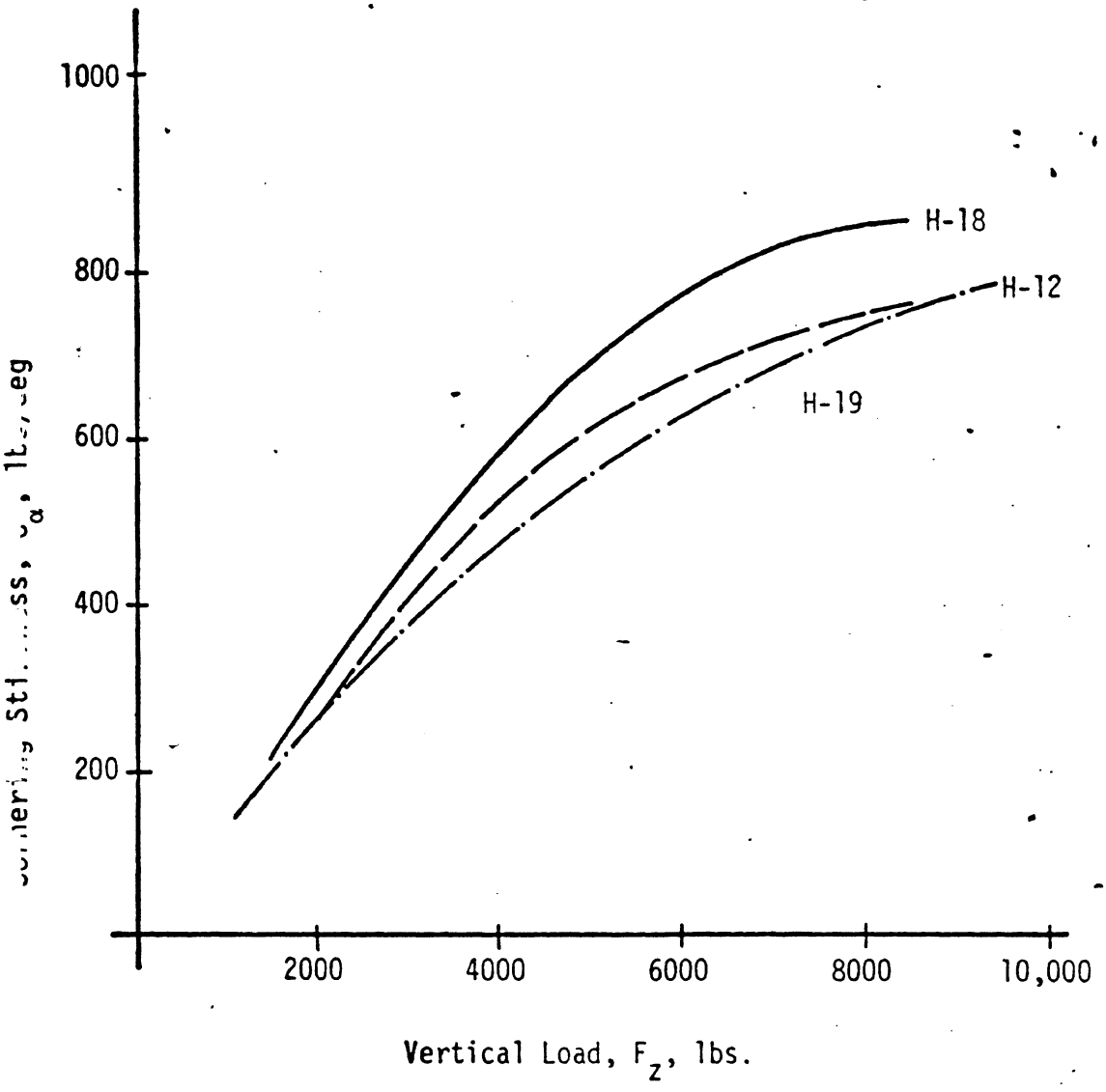

Figure 4.19. Load sensitivity of the cornering stiffness parameter for the three tires employed in intercity bus simulations.

The sensitivity examination was confined to reasonable perturbations in vehicle layout and payload placement, considering the White two-axle Road Boss as a baseline configuration. The baseline vehicle, while described by the parameters listed in Appendix A, can further be characterized, through linear analysis of the non-rolling vehicle, by an understeer factor of

$$U = 2.6°/g$$

where U was defined earlier by the relation:

$$U = -\frac{W}{\ell}\left(\frac{a}{C_{\alpha_2}} - \frac{b}{C_{\alpha_1}}\right)$$

Although, according to this simplified calculation, this vehicle is understeer by a rather narrow margin, one would not expect that any anomalous yaw behavior would derive in the sub-limit maneuvering range. Nevertheless, the simulation results shown in Figure 4.20 indicate that the baseline (loaded) truck begins to exhibit a slowly-growing divergency for turning maneuvers which, at 50 mph, exceed .45 g lateral acceleration. This response is first observed at a steering level of about 3° front wheel angle and involves a large enough positive exponential at steering levels of 3.5° and higher, that a wheel lift-off condition is calculated to occur within the simulated interval of 4.5 seconds. It should be noted that the fidelity of the simulation breaks down at very high roll angles and thus should be used for prediction of behavior only up to the wheel lift-off condition, in the vicinity of $\phi = 10°$.

Going beyond this basic finding (namely, that a heavy truck can exhibit yaw instability even in the vicinity of $A_y = .45$ g, that is, while its tires have not yet reached shear force

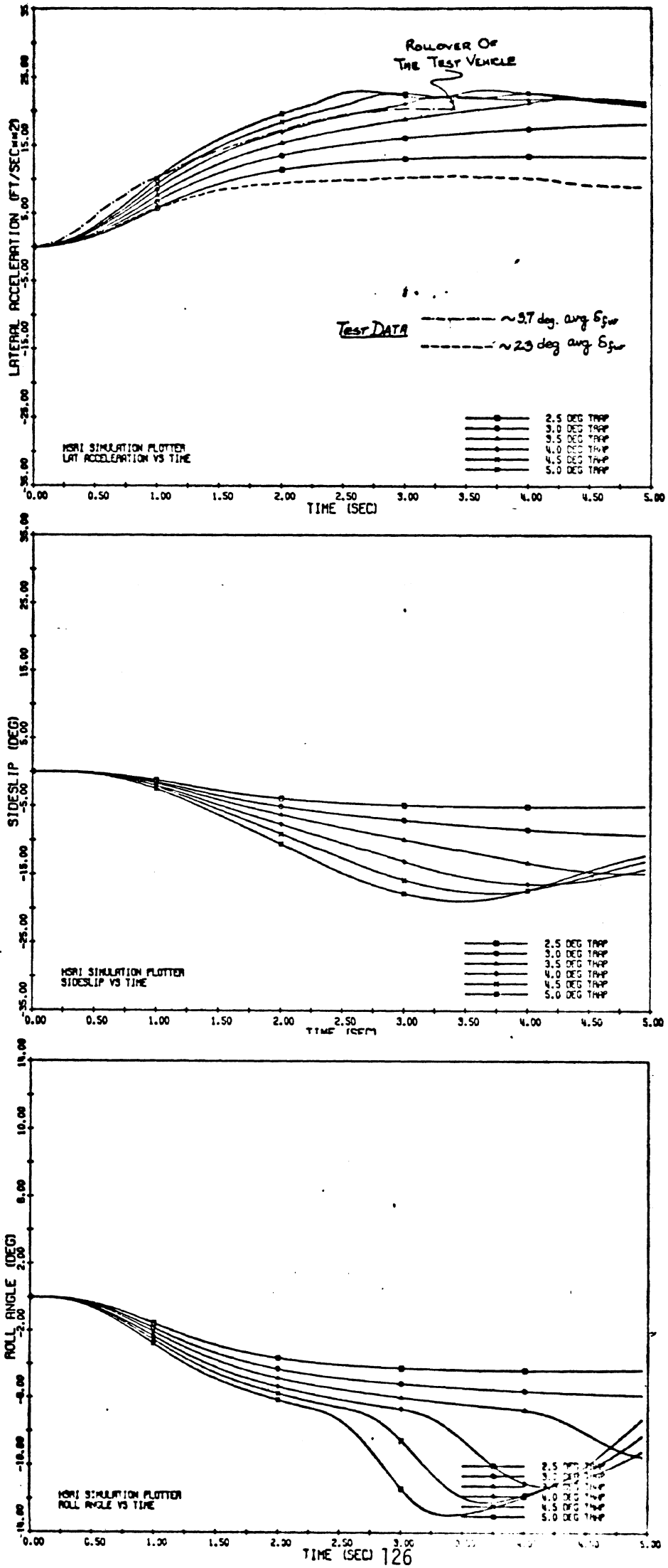

Figure 4.20 Simulated time history responses of the White Road Boss to trapezoidal steer inputs—the baseline loaded truck comparing both simulated and measured A_y responses.

saturation), computations were made in an attempt to identify the principal causes for the divergent behavior.*

Firstly, the importance of certain traction characteristics were examined to determine if properties peculiar to the lateral shear force behavior of truck tires would be implicated as heavily involved in the loss of yaw stability. The trapezoidal steer response of the baseline truck was simulated using an artificially simplified representation of the tire. The "simplified tire" was modeled so as to render both C_α and μ as constants, independent of vertical load. Such a simplification accounts for the principal mechanical features by which the typical truck tire significantly differs from the passenger car tire. Comparing Figures 4.21a-c with the response of the baseline vehicle (Figures 4.20a-c), we find that the simplified tire does not significantly alter the mechanisms which determine either the nature of the divergency or the A_y threshold beyond which it occurs. Thus it can be concluded that the spinout behavior of the baseline vehicle does not derive directly from a traction characteristic peculiar to truck tires.

The second feature suspected of playing a significant role was the rear-biased distribution of roll stiffness on the baseline truck. Indeed, the 4.5 to 1 ratio of rear-to-front roll stiffness (or, 2.25 to 1 ratio of roll stiffness, front-to-rear, per tire, thereby accounting for single tires on the front axle and duals in the rear) is not only immensely larger than would be found typically on a passenger car, but it is of a polarity which is classically recognized as destabilizing. Accordingly, when the truck is simulated with equal values of front and rear roll stiffness (with total roll stiffness equal to that of the original vehicle), we find a response which is directionally stable even at the highest steer inputs examined. As shown in Figure 4.22, the vehicle with equal front and rear roll stiffness (identified

*Please note that these calculations were designed to provide an understanding of the mechanisms involved and not to examine practical alternatives in motor truck design.

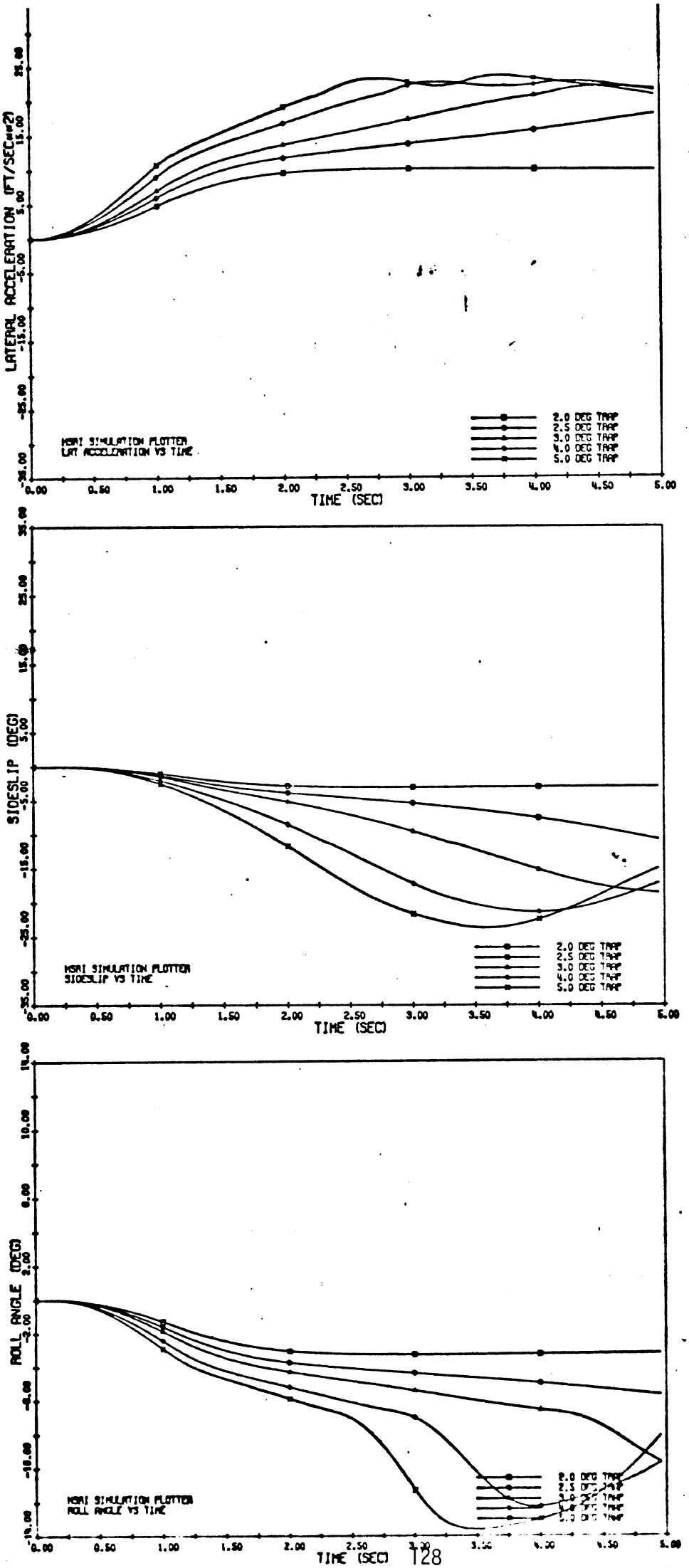

Figure 4.21 Simulated time history responses of the White Road Boss to trapezoidal steer inputs—loaded truck with simplified tire model, holding C_α and μ constant (i.e., independent of vertical load.)

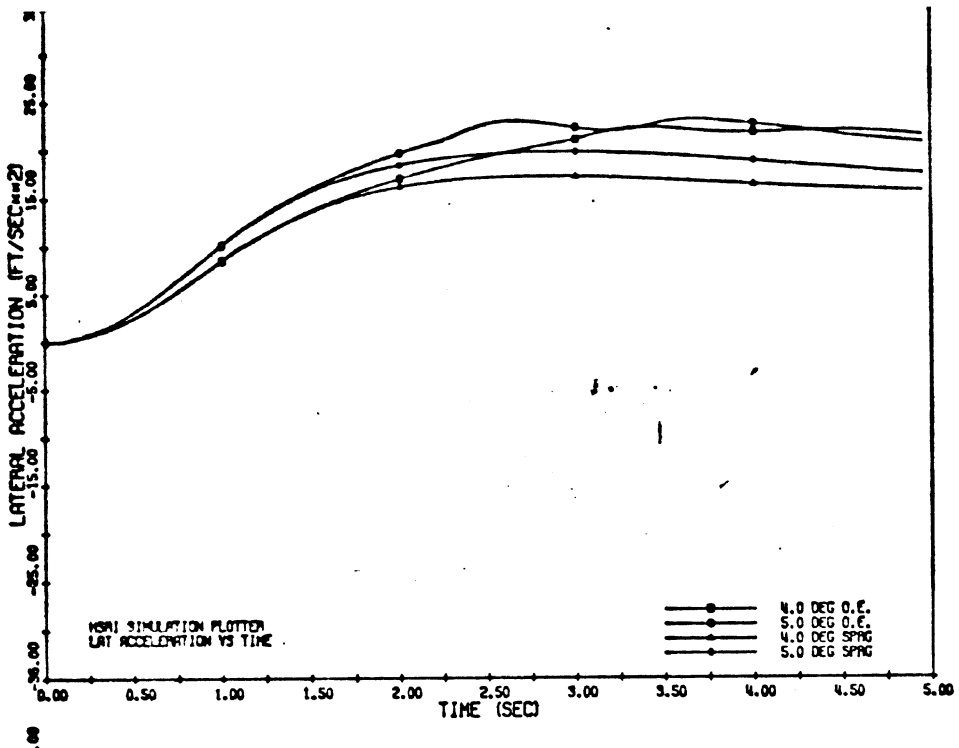

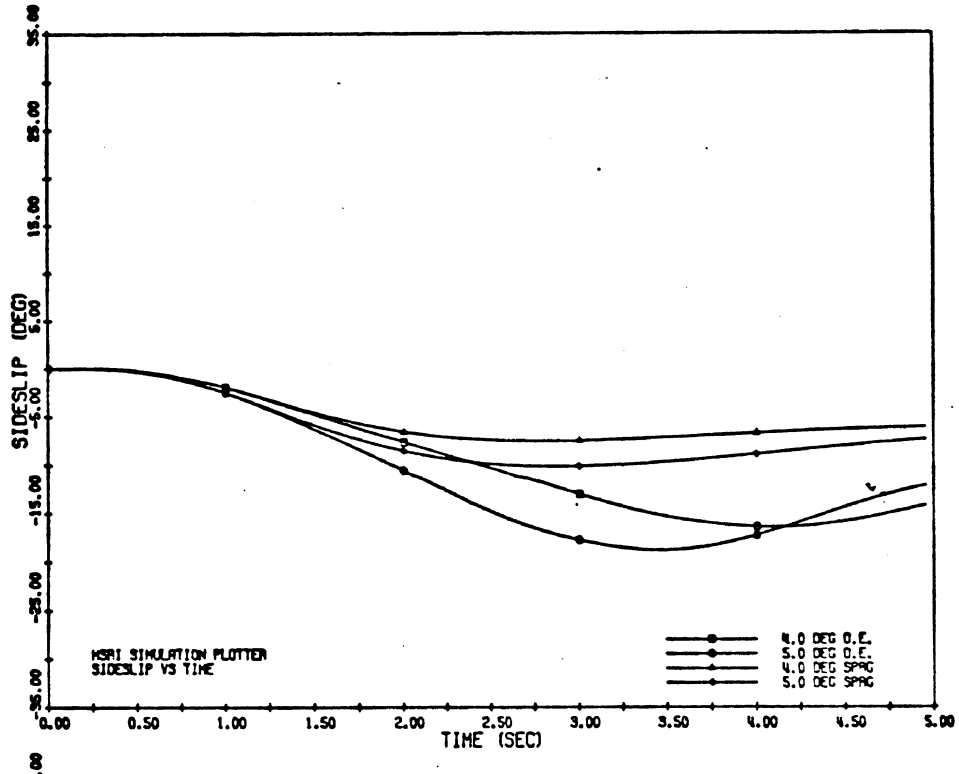

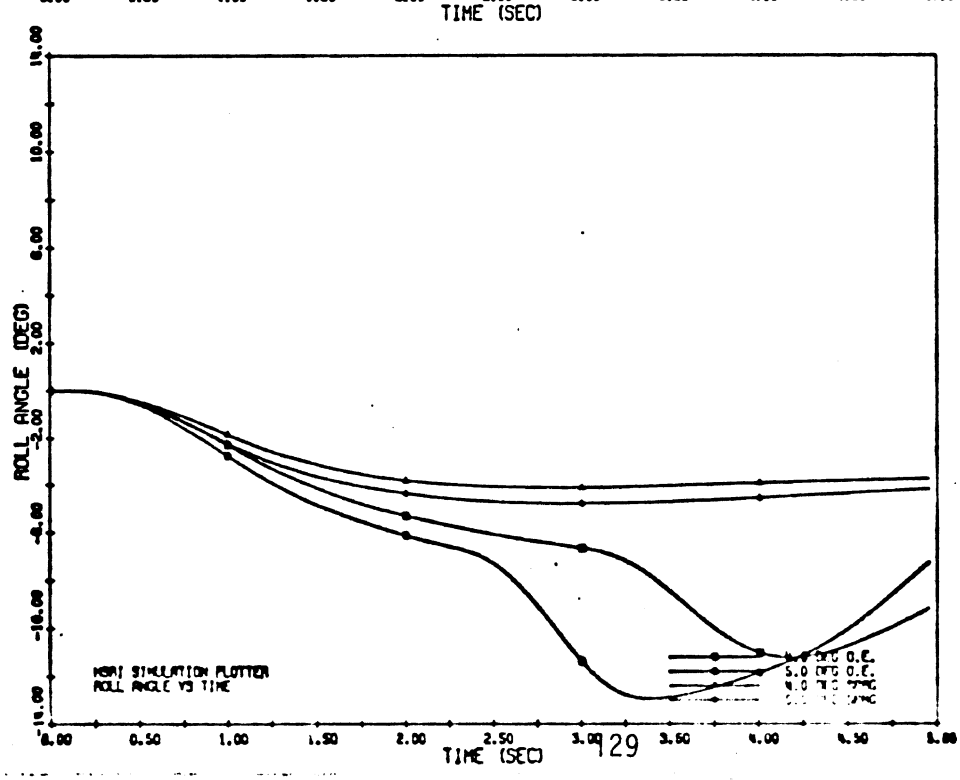

Figure 4.22 Simulated time history responses of the White Road Boss to trapezoidal steer inputs—loaded truck with equal values of front and rear roll stiffness.

as "SPRG") is clearly distinguishable from the vehicle in its OE configuration.

The influence of distributed roll stiffness on yaw stability can be understood by considering the tire's side force response to vertical load such as becomes exercised by the lateral transfer of load which prevails at front and rear axles during turning. The principal mechanism to consider involves the net loss in side force which accrues on any axle when one tire increases in load, by z pounds, while the load on the opposite tire decreases by z pounds. For the axle whose "z" increment in tire loads is greater, a correspondingly larger decrement in side force will be suffered. Additionally, as will be shown, an axle configured with dual tire sets (and which is reacting twice the roll moment) will suffer an even larger decrement in side force than a reference axle equipped with the same tires as singles.

As an example of these mechanisms, consider the baseline truck in a turning maneuver for which both front and rear tires are operating at $\alpha = 4°$*, but in which one of two cases applies, namely,

Case a) all tires retain their static load values, or

Case b) all tires assume the load values which, in fact, follow from the designed roll stiffness distribution and the needed equilibrium roll moment.

Referring to the F_y versus F_z plot for the White truck's "OE" tire, in Figure 4.23, we see that the front tires in case (a) generate a total F_y = 3700 lbs, while the (4) rear tires generate a total F_y = 7000 lbs. For case (b), the front tires have each experienced a 1600-lb increment in load, yielding a new total F_y = 3500 lbs (i.e., down 5% from the non-load-transferred case). Load transfer at the rear axle causes a nominal ±2470-lb load change on each tire with the tires in a dual pair further spread by ±380 lbs from that nominal value. Accordingly, the total side

*The $\alpha = 4°$ condition at all four tires is approximately representative of the tire slip accrued in the trapezoidal steer response at 50 mph, with $\delta_{fw} = 3.0°$.

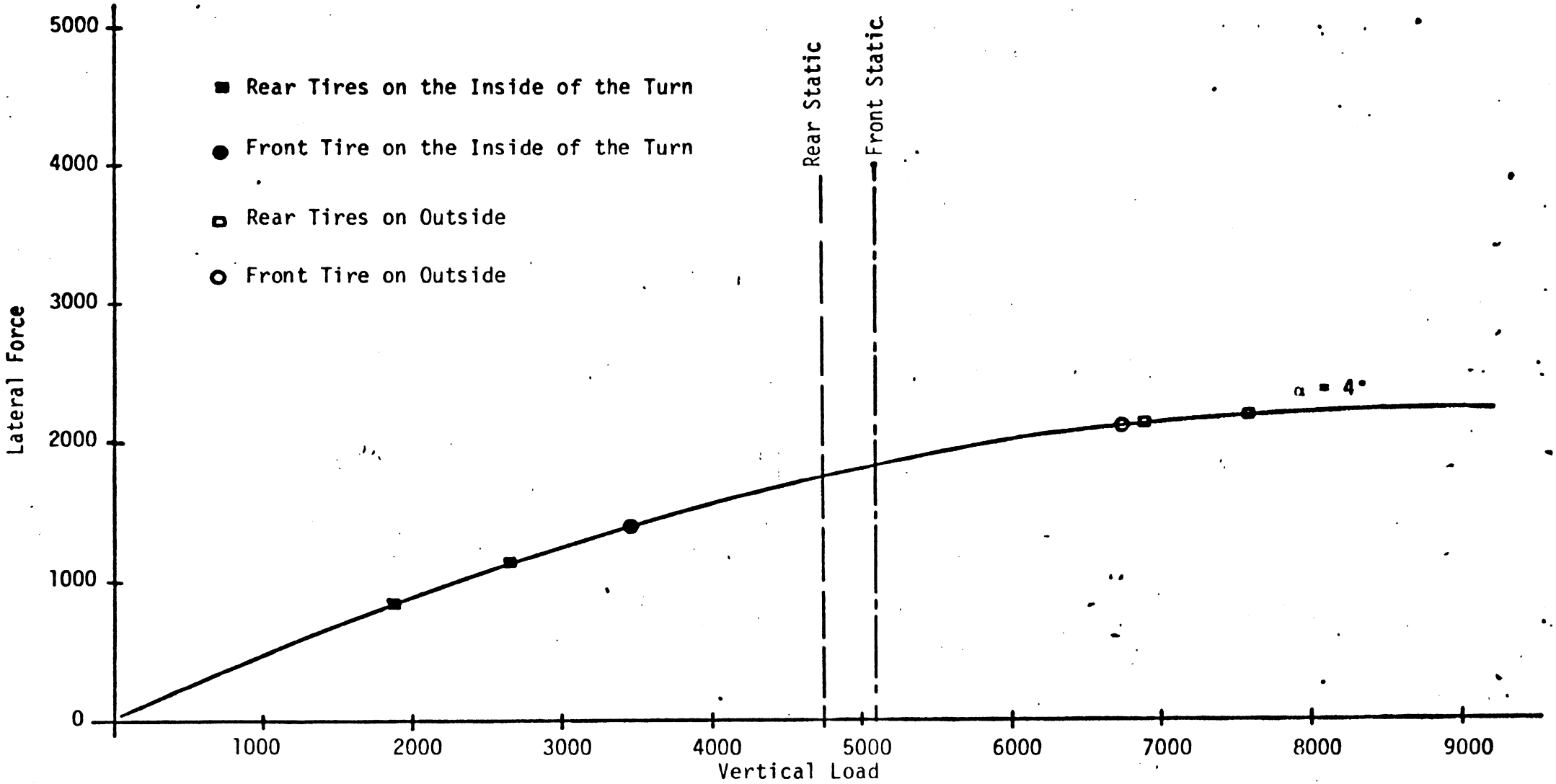

Figure 4.23. Lateral force changes at $\alpha = 4°$ which derive from changing loads on left and right side tires as White Road Boss responds to a trapezoidal steer input of $\delta_{fw} = 3°$.

force provided by all four rear tires is F_y = 6230 lbs (i.e., down 11% from the value obtained in the absence of load transfer). Thus the net loss in rear tire side force is greater than that experienced at the front simply as a result of the pneumatic tire's fundamentally nonlinear F_y response to vertical load.

For a vehicle system which is marginally understeer in the "curb" condition, the influence of an unfavorable roll stiffness bias is thus seen as a quite ample means of disturbing the yaw moment balance and converting the system to an unstable behavior at relatively low levels of lateral acceleration. From a vehicle design point of view, one can easily appreciate that rear-placed payloads require the installation of a stiff rear suspension assembly. Additionally, since the frame is such a compliant coupling between payload-induced roll moments and the front suspension, the achievement of a substantial front roll couple reaction is virtually impossible. Accordingly, the modern motor truck and tractor exhibits a heavily rear-biased distribution in roll stiffness as a result of certain design fundamentals which are inherently linked to the vehicle's geometric layout, its mission of freight transport, and its parallel rail frame construction.

Another major determinant of the stability of the baseline truck is the location of the mass center of its payload. The baseline position for the payload was, generally speaking, rather conservative, being 22 inches forward of the rear axle and 63.5 inches above the ground. Examining the significance of the longitudinal placement of payload, Figure 4.24 illustrates the marked influence which this variable has on yaw gain as well as yaw stability. All four runs shown in Figure 4.24 represent the vehicle's response to 3.0 degree steer input to the front wheels at 50 mph. Payload locations are identified with respect to the baseline (PX=22) location and are represented as shifts wither forward (as in PX=33) or rearward (as in PX=11) from the baseline. A shift of the payload mass center to the "00" position (that is, directly over the rear axle center) results in a marked

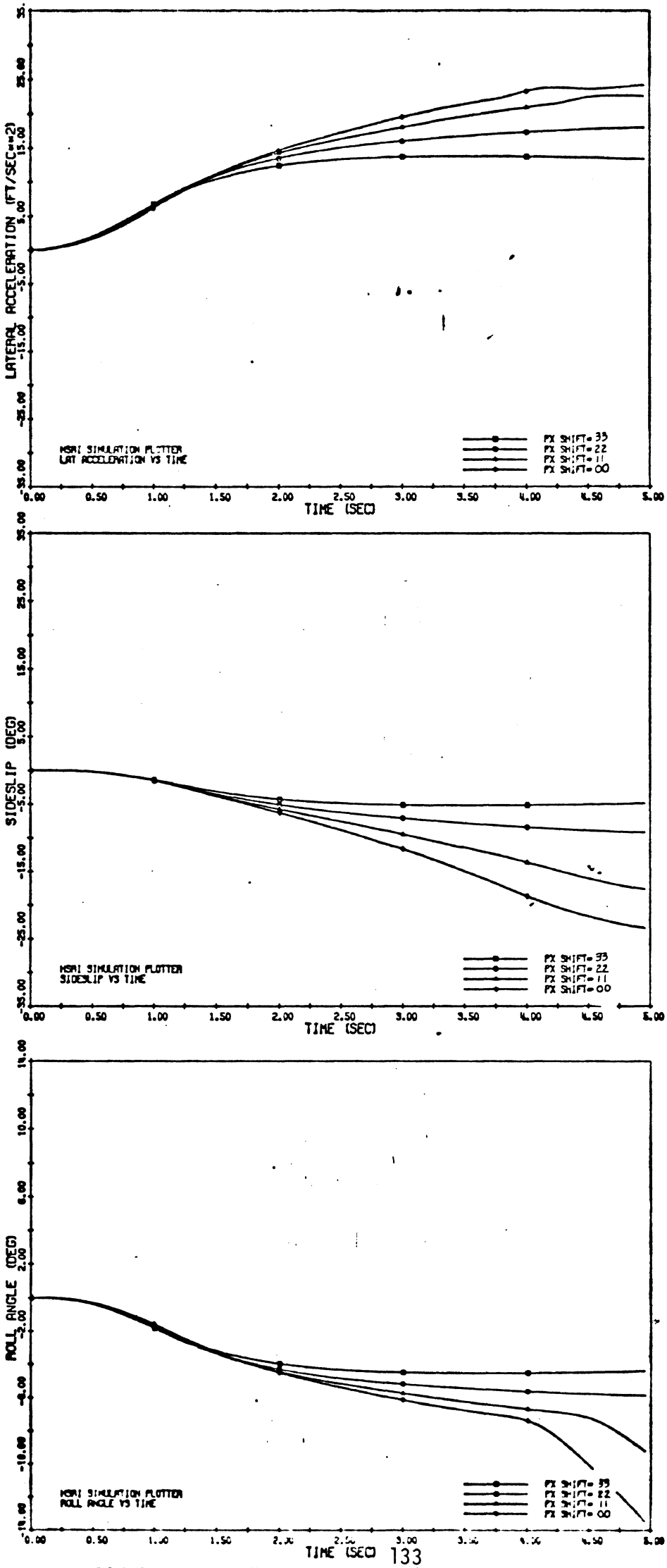

Figure 4.24 Simulated time history responses of the White Road Boss to trapezoidal steer inputs—loaded truck with the payload mass center placed at a longitudinal position of "PX" inches forward of the rear axle center—all runs represent response to a 3.0° steer input.

reduction in stability, and is significant insofar as it represents a not uncommon location of a fifth wheel trailer coupling such as was employed in a combination vehicle simulation to be discussed later. In general, variations in placement of payload on a straight truck are comparable in significance to variations in fifth wheel kingpin placement on a tractor loaded equivalently by a trailer, as will be shown.

In an examination of the sensitivity of the unstable behavior to various changes in the basic vehicle configuration, computations were performed covering the following conditions:

1) The baseline vehicle outfitted with typical bias-ply lug tires in the rear (with low value of C_α) and a high C_α bias-ply rib tire in the front.

2) The baseline vehicle outfitted with a tandem rear suspension whose tandem center coincides with the original single rear axle position, and loaded proportionately to the higher three-axle gvw.

3) The baseline vehicle employed not as a straight truck but as a tractor with its trailer kingpin located just ahead of the rear axle center (as is commonly practiced) and which tractor is pulling a 37-foot loaded van-type trailer.

4) The same case as #3 but with a tandem suspension-equipped tractor.

As shown in Figure 4.25, the mixed lug and rib tire arrangement is decidedly unfavorable from a yaw stability point of view. Indeed, the vehicle incorporating the rib/lug mix is of grossly reduced stability even at the 2.0° steer level. This rather expected result is notable considering the dramatic reduction in the range of stable steering levels which results and considering the wide popularity of lug tires on driving (rear) axles. As was recently documented in Reference [9], the rib-front, lug-rear mix

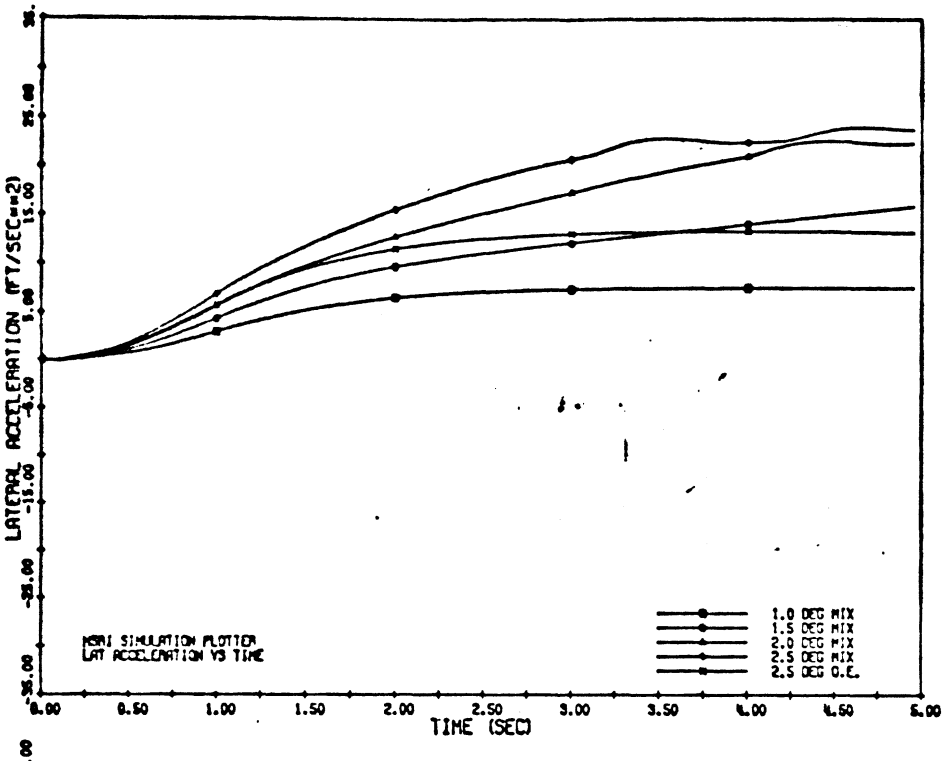

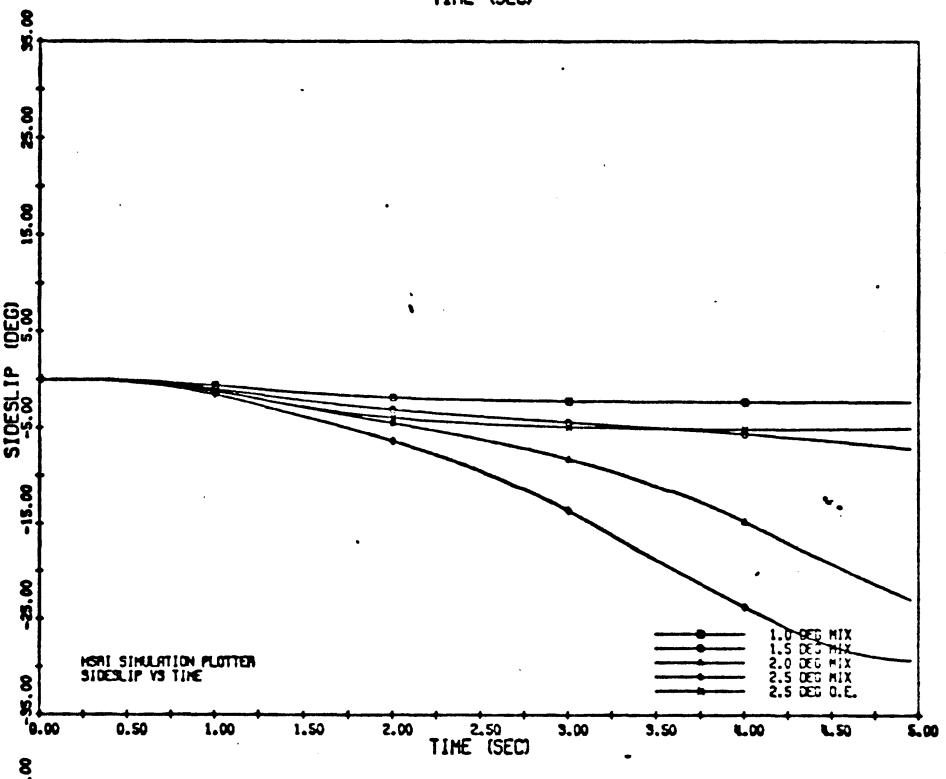

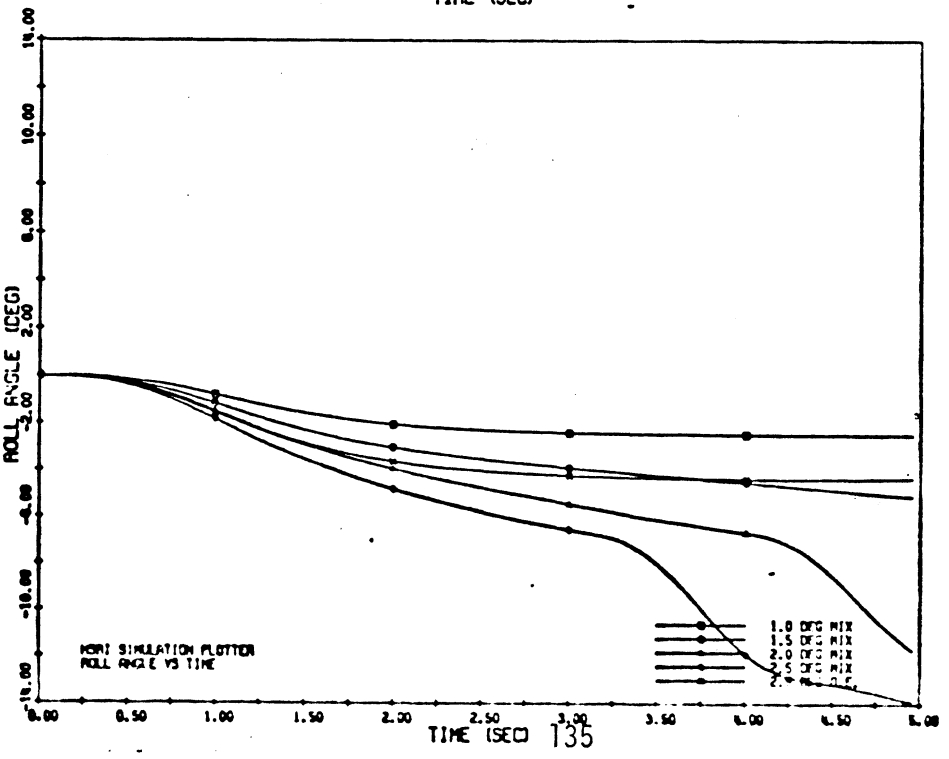

Figure 4.25 Simulated time history responses of the White Road Boss to trapezoidal steer inputs—loaded truck outfitted with a tire mix (bias-ply rib tread tires front and bias-ply lug tread tires rear)—at various steer input levels, compared to the baseline vehicle response at a 2.5° steer input.

also implies a reduction, on the order of 2°/g, in the nominal understeer factor of a two-axle truck.

The second variation, employing a tandem axle on the baseline truck, results in a major improvement in the range of stable behavior. Computed responses shown in Figure 4.26 indicate that the three-axle truck will not become directionally unstable prior to reaching its rollover limit. The principal mechanism by which the tandem-equipped truck provides enhanced yaw stability is by means of an additional (understeering) moment which derives from the resistance of the two fixed axles to being yawed. The "yaw resistance" of the tandem set as a whole is further augmented by the yaw resistive moments provided by two more sets of dual tires—each of which contributes a moment in response to yaw velocity, although this moment is generally insignificant at highway velocities.

Combining the tandem axle influence with considerations of longitudinal placement of payload, Figure 4.27 illustrates both two- and three-axle trucks with payloads placed at the baseline location (PX - 22) and at the location of the rear axle center (PX - 00). Additionally, the three-axle vehicle is represented as carrying the payload employed on the two-axle truck (PLD - OE) as well as a double-size payload (PLD - DBL) scaled to the higher gvw afforded by the tandem. It is interesting to note that the three-axle truck elicits virtually identical A_y responses at both the (OE-22) and (DBL-22) payload levels even though it achieves the expected double roll angle value at the higher load.

Thus, the tandem-equipped vehicle is virtually insensitive to load application as long as that load is installed with a comfortably-forward mass center position. In contrast, the tandem-axle truck is markedly sensitive to the load level when the load is placed over the tandem center (PX=00) as shown in runs labeled OE-00 and DBL-00. Although in each corresponding case the tandem-equipped truck provides a considerably more stable

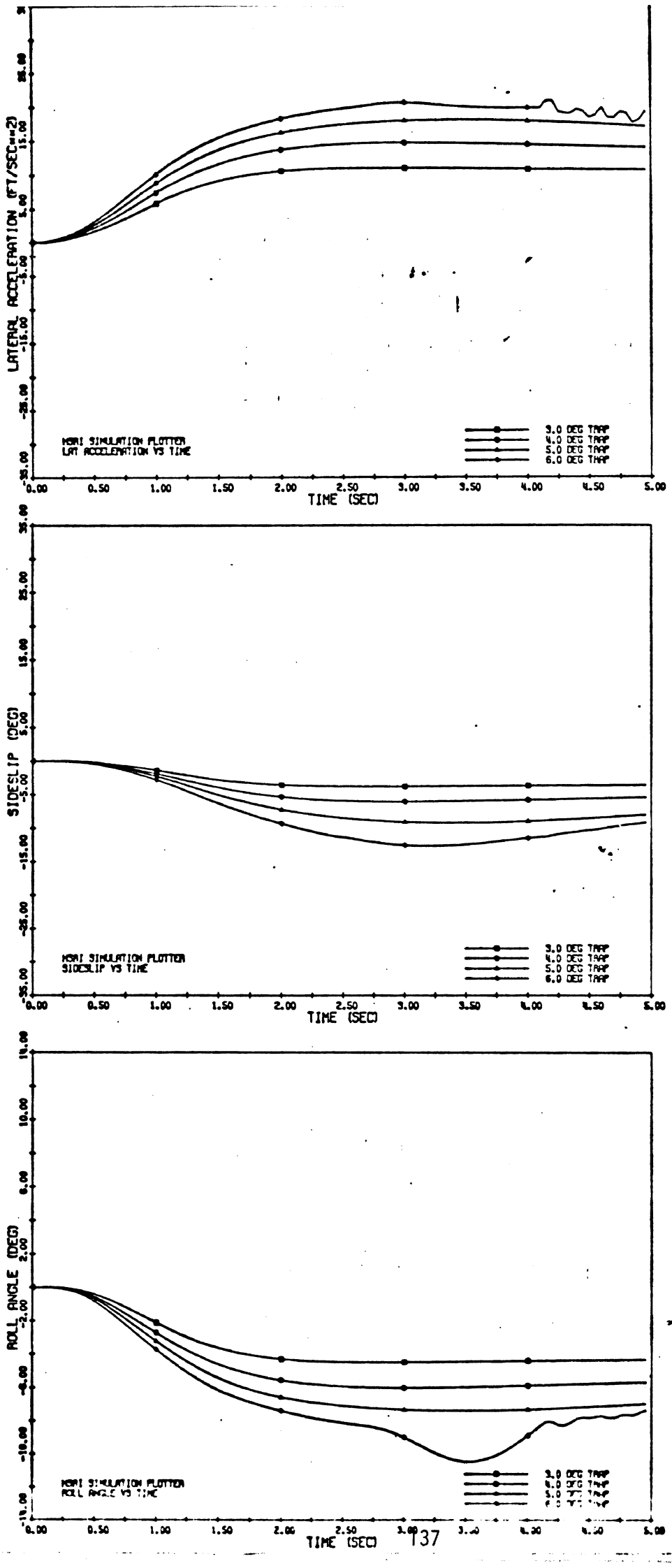

Figure 4.26 Simulated time history responses of a tandem-equipped White Road Boss over a range of trapezoidal steer input levels which had resulted in a yaw divergency of the baseline, two-axle truck.

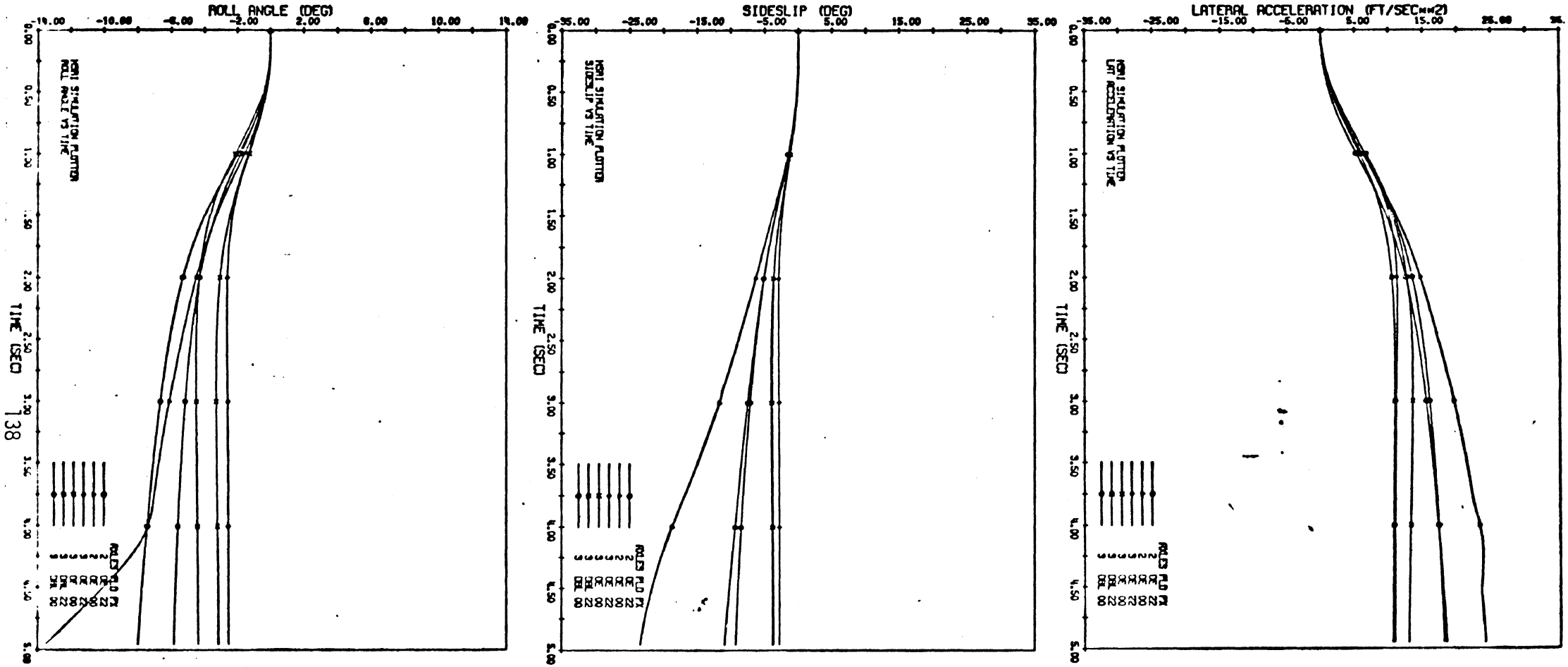

Figure 4.27 Simulated time history responses of two- and three-axle White Road Boss trucks as loaded with either the baseline (BF) or double-sized (DBL) payload. Load is placed at a longitudinal distance of (PX) inches forward of rear axle center.

response than the two-axle vehicle, an increasingly rearward payload placement provides the classical reduction in yaw stability.

In the third arrangement, with the two-axle baseline vehicle employed as a tractor coupled to a loaded trailer, it was found that the combination vehicle jackknifes and rolls over at less than a 2.5° steer angle. Thus, the tractor-trailer is less stable with its typically-placed kingpin loading than is the baseline truck. This result is explained by noting that:

a) The longitudinal position at which trailer side forces are applied to the tractor can, indeed, be far aft—at the kingpin location, which is often very near to the rear axle position.

b) Trailer c.g. heights are commonly higher than the payload location employed on the truck which was tested. The sprung mass center of the simulated trailer was at a height of 68.6 in., while the corresponding height of the mass center of the payload on the straight truck was 63.5 in.

c) The trailer coupling at the fifth wheel is a rather roll-rigid connection, permitting, in the case of a low roll-stiffness suspension at the rear trailer axles, a further aggravation in the sharing of load transfer between tractor front and rear axles.

In the case of the tandem tractor with trailer, a result similar to that of the tandem-equipped straight truck is calculated, namely, an improvement in yaw stability is obtained over the two-axle reference. Again, however, the typically-rearward kingpin placement on the two- or three-axle tractor makes the combination vehicle less stable than a truck whose payload is more advantageously placed, as in the baseline vehicle considered here.

A final examination concerned the directional stability of a three-axle straight truck such as was employed by Systems Technology, Inc., in the preceding NHTSA-sponsored study entitled "Truck and Bus Handling" [1]. Since STI had not discovered a spinout instability in its testing, there was interest in comparing the HSRI finding with STI's experience. The computed time histories in Figure 4.28 show the STI truck, a very long wheelbase tanker, to be directionally stable right up to its rollover limit.

Thus, despite its relatively disadvantageous payload location (higher and more rearward than on HSRI's rolled-over test vehicle), the "STI truck" apparently accrued the improved yaw stability which is afforded by a tandem axle configuration. Additionally, the higher c.g. on the STI vehicle causes the roll stability limit to occur at about 0.5 g lateral acceleration, thus serving to put aside any questions about directional limits (which could never be reached by that vehicle on a high friction surface). In contrast, the two-axle test truck employed by HSRI set the scene for discovering a yaw stability limit by initiating a spinout from 0.45 g and then finally rolling over at about 0.62 g.

A cautionary note which applies to all of the findings indicated in this section concerns the unaddressed and unsimulated influences of truck and trailer frame flexibility. Although it was seen that roll stiffness distribution is an elementary determinant of stability limits, it must be recognized that the torsional compliance of the structure existing between front and rear suspension assemblies is also significant since it acts to transmit the suspension reaction moments to the rolling masses. While the passenger car, in the context of such discussions, can be assumed to be a rigid body, the conventionally frame-rail-constructed truck cannot. Rather, the truck (or tractor, or trailer) is comprised of distributed stiffnesses and masses. In

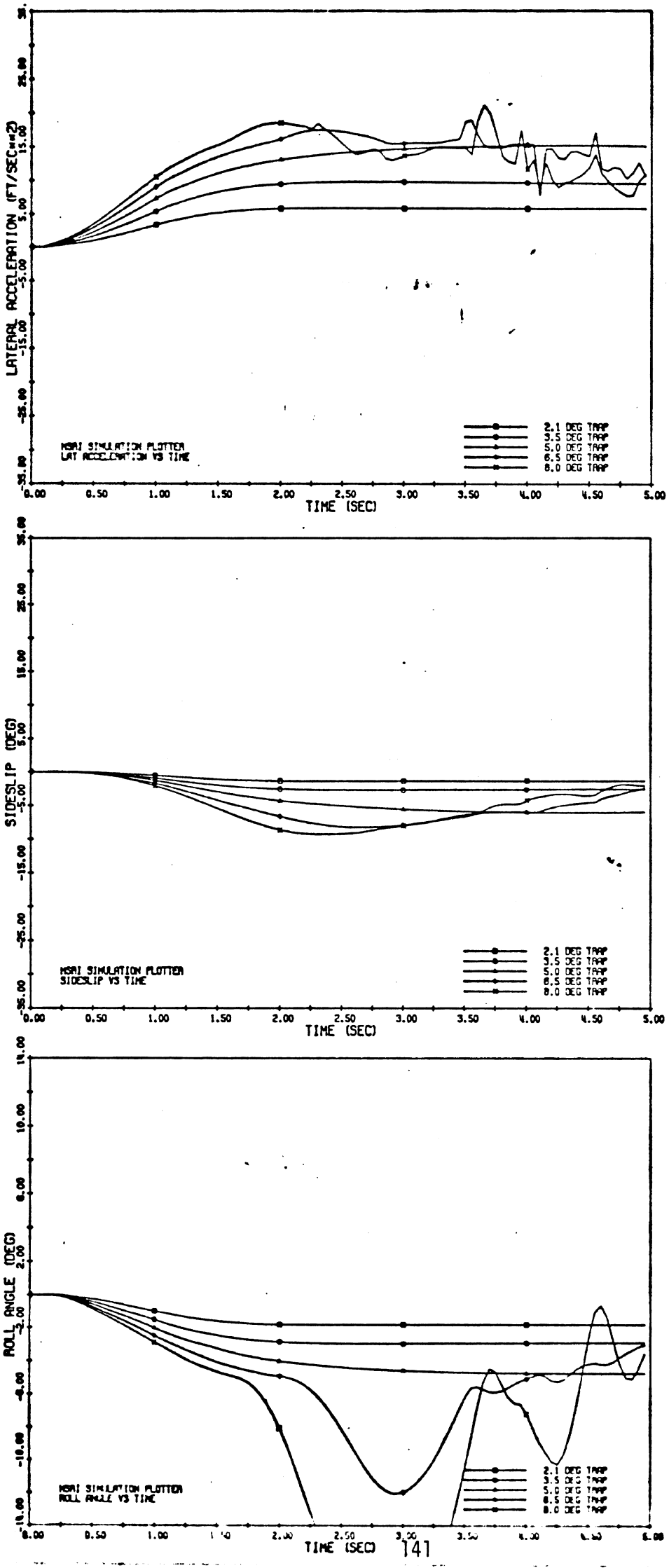

Figure 4.28 Simulated trapezoidal steer response histories of three-axle tanker truck employed in Reference [1] study.

a simplified view of the problem, the distances between the primary mass elements and the front and rear suspension centers is the key item. For example, referring to the simplified (concentrated mass) vehicle system diagrammed in Figure 4.29, with a uniformly-distributed frame stiffness, K, we find that the ratio of rear/front roll stiffness is defined by the relationship:

$$\frac{\text{Rear Roll Stiffness}}{\text{Front Roll Stiffness}} = \frac{K_R(\ell_1 K_F + K)}{K_F(\ell_2 K_R + K)}$$

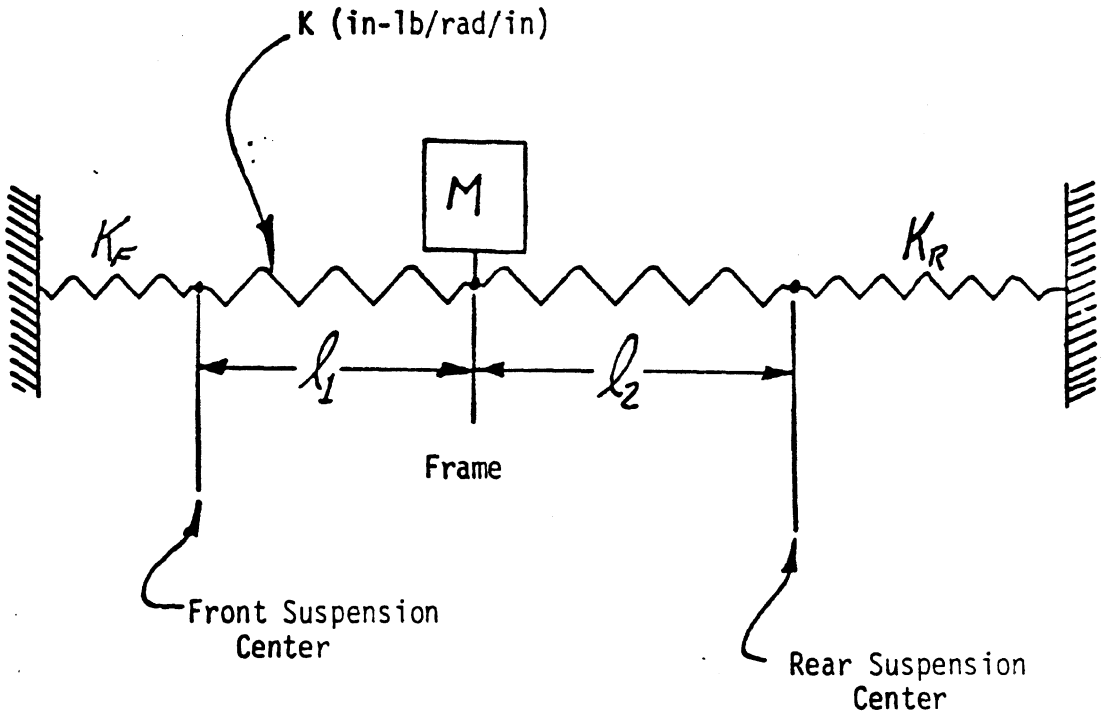

Figure 4.29. Diagram of simplified frame and suspension torsional compliances.

Considering a special case of this system, the reaction of roll moment at front and rear suspensions will be identical to that of a rigid frame vehicle when the mass, M, is placed so that:

$$\frac{\ell_1}{\ell_2} = \frac{K_R}{K_F} \qquad (2)$$

Although actual vehicles are comprised of numerous mass elements, we can consider the payload to be the mass which is of primary importance in the critical loaded vehicle condition. We can then crudely evaluate the validity of the results obtained with the (rigid frame) truck simulation by considering the applicability of Equation (2) to the vehicle configurations which were examined. The baseline vehicle with its 4.5-to-1 rearward bias in roll stiffness was, in fact, loaded to produce an ℓ_1/ℓ_2 of 5.4. Thus, the flexible frame vehicle would actually provide a less favorable (more rearward) distribution of effective roll stiffness than was simulated. Accordingly, the actual baseline vehicle would tend to exhibit a narrower range of stable yaw behavior than was calculated. Likewise, all computations reported previously, with payloads at the baseline location, or further aft (including the trailer fifth wheel attachments just ahead of the rear axle position) can be presumed to reflect more stability, if anything, than the corresponding actual vehicles. Since the trailer which was simulated was of the torsionally-rigid van-type construction, no confounding flexibility effects need to be considered.

Thus, although a rigorous treatment of frame compliance has not been included in state-of-the-art motor vehicle simulations, a simplified view of the problem indicates that results presented here are useful as estimates of the maximum level of control inputs within which stable operation can be expected.

5.0 CONCLUSIONS AND RECOMMENDATIONS

This study has endeavored to apply the principles of engineering mechanics in a concentrated examination of the heavy truck and bus tire and its influence on the control behavior of commercial vehicles. A primary output of this study has been the expansion of the data base defining the traction properties of the commercial vehicle tire. An equally important output, however, is the extension of the state of knowledge concerning the mechanical properties of commercial vehicles themselves—with this extension putting into focus numerous features for which an analogy with the passenger car fails. The failure of various "rules of thumb" concerning control relationships based upon passenger car experience and technology appears to be a significant general finding. Insofar as the great preponderance of literature treating the mechanics of motor vehicles is based upon passenger cars and upon tires suited to passenger cars, it is relevant to be concerned about the validity of applying the state of the art in passenger vehicle dynamics to trucks. Although there should be no "surprises" in applying the basics of passenger car analysis to trucks, the application appears to become increasingly tenuous as one endeavors to simplify a commercial tire-vehicle system according to generalizations that arise out of passenger car experience.

A number of specific findings and observations have derived from this study in support of the foregoing general conclusion. Although certain of these findings are believed to constitute new discoveries, others have been cited in the text as confirming previously published results. The following conclusions summarize specific observations of the study and serve to elucidate the mechanical behavior of commercial vehicles and their tires.

5.1 Conclusions—Concerning the (dry) longitudinal traction properties of commercial tires:

1) The commercial vehicle tire exhibits a large falloff in longitudinal shear force capability at values of longitudinal slip beyond which peak traction prevails. This behavior contrasts markedly with passenger car tires which typically yield a small falloff, if any, on dry pavements.

2) The various tread and carcass constructions currently used in commercial vehicle tires exhibit a broad range of longitudinal stiffness (namely, longitudinal force per unit slip in the domain of normal braking).

3) Peak braking traction afforded by commercial vehicle tires is comparable to that obtained with passenger cars, although "slide" values are markedly lower.

4) Both peak and slide values of the braking traction of commercial tires normalized with respect to the vertical load are significantly sensitive to the imposed value of vertical load, invariably reducing their traction potential as load increases.

5) Slide values of braking traction reduce markedly with vehicle velocity, especially in the range from 0 to 30 mph, whereas peak traction is only slightly influenced by velocity.

6) The lug or cross-bar type truck tire typically exhibits lower levels of braking traction than tires configured with the rib-type tread pattern. This characteristic of lug tires particularly influences the braking performance of heavy trucks and tractors because of the widespread, year-around use of these tires on the drive axles of these vehicles.

7) The braking traction of tires employed on heavy commercial vehicles is observed to be remarkably stable throughout extended test sequences whereas limited measurements have shown light truck tires to be rather sensitive to test-induced wear.

Concerning (dry) lateral traction properties:

8) A large range in values of cornering stiffness, C_α, is available among the various tread and carcass constructions represented in the commercial tire market.

9) The C_α sensitivity to vertical load is perhaps the most significant lateral traction characteristic distinguishing the truck tire from the passenger car tire. In particular, the truck tire exhibits a steep slope in its C_α versus F_z relationship in the vicinity of rated load thereby providing a significant first-order adjustment in cornering stiffness to compensate for the placement of payload. Some light truck tires were found to be so nearly linear in their C_α versus F_z behavior (over the operating range) that the linear directional properties of light trucks outfitted with common tires on all wheels would be virtually insensitive to changes in payload.

10) Normalized lateral forces (F_y/F_z) generated at high slip angles (above $\alpha = 8°$) decrease significantly with increased vertical load.

11) The sensitivity of lateral traction to velocity has been observed to be virtually insignificant for all tires examined in this program.

12) Lateral force saturation of commercial tires has been observed to occur at normalized traction levels comparable to that obtained with passenger car tires. Since most heavy trucks and buses will roll over prior to tire side force saturation, however, this property is of little general significance.

13) The basic features distinguishing the lateral traction properties of radial versus bias and rib versus lug constructions are, in general, common to both truck and car tires. For example, characteristics typifying radial tires used on motor cars are also generally seen in lateral traction measurements of heavy truck radials. The relatively lower values of cornering stiffness possessed by lug-type tires is, probably, of greater significance to the heavy truck because of the tendency to use them almost exclusively on driving (rear) axles.

14) Test-induced shoulder wear significantly influences the lateral traction generated by commercial tires and thus poses a significant confounding influence in the interpretation of experimental data.

15) The dependency of cornering stiffness on inflation pressure is a property distinguishing commercial tires from passenger car tires. Whereas decreased inflation pressure typically reduces the cornering stiffness of the passenger car tire, the commercial tire (most significantly, the light truck tire) does not exhibit a comparable systematic behavior. Thus, manufacturer's recommendations for inflation pressure differentials between axles hold the potential for randomly influencing vehicle directional properties depending upon the polarity and the strength of the sensitivity of installed-tire cornering stiffness to changes in inflation pressure.

Concerning the mechanics of commercial vehicles:

16) The "typical" heavy truck has been found to be capable of eliciting a yaw instability while initiating a turn whose severity is much lower than that

needed to achieve limit response of passenger cars. Further, it is significant that a marked degradation in directional controllability can accrue well in advance of the maneuver severity required for commercial vehicle rollover. A corollary to these observations is that truck yaw instability can be precipitated while tires are operating at relatively low slip angles. In contrast, passenger cars (which are spinout-limited) generally destabilize as a consequence of side force saturation (large slip angles) occurring at the rear tires.

17) A primary mechanism serving to aggravate truck yaw stability is the rear-biased distribution of suspension roll stiffness. Further, typical truck and tractor frames are quite compliant in their transmission of roll moments. Thus, the high roll stiffness incorporated into rear suspensions is seen as a design necessity given the need to react the rear-biased roll moments imposed by straight-truck payloads and by semitrailers.

18) The use of tandem rear axles tends to markedly improve the directional stability of fully-loaded trucks and tractors.

19) The installation of differing tire constructions at front and rear axles has been seen to provide a powerful mechanism for influencing the directional behavior of light and heavy trucks. The classically-degrading mixes (radial front/bias rear, and/or rib-tread front/lug rear) can serve to destabilize vehicles which, by dint of unfavorable payload placement and roll stiffness distribution, tend to be otherwise marginally stable in the small disturbance regime. This (perhaps unsurprising) finding is particularly noteworthy since it is the practice of heavy truck manufacturers to

provide vehicles with a great variety of tire combinations as requested by the purchaser.

20) The directional behavior of heavy trucks and tractors is markedly sensitive to the longitudinal as well as vertical placement of payload (or fifth wheel kingpin). Insofar as many road tractors are outfitted with so-called "slider" (movable) fifth wheels, the significance of kingpin location to tractor yaw stability deserves special consideration.

21) The addition of payload to an intercity bus, although clearly more constrained in placement than truck payloads, generally increases the understeer of the bus because of the typically rearward mass center location of an unloaded bus with its engine located at the rear.

Overall, the commercial tire by dint of its tread compounding, carcass construction, unit loading, and operating load range has been found to exhibit a number of unique characteristics which impact directly upon truck and bus control behavior. The commercial vehicle, and most notably, the heavy truck and tractor, have been found to exhibit certain unusual control characteristics which derive, in large part, from various features unique to the construction and usage of such vehicles.

5.2 Recommendations

It would appear that the first item of follow-up to this study should be an investigation of the significance of the finding concerning the marginal yaw stability of heavy trucks and tractor-trailers. Significance should be evaluated along two fronts, one scientific—utilizing the engineering and psychophysical disciplines to study the vehicle control problem directly—and the other empirical—studying the evidence afforded by the accident record. Primary questions to be asked in the scientific pursuit are:

a) To what extent can the professional truck driver control a directionally unstable truck or tractor-trailer, given that the positive exponentials defining the divergencies are likely to be rather small?

b) Are there specific maneuvering conditions, such as encountering circular freeway exit ramps at elevated velocities, which render the driver's stabilization task virtually insurmountable?

c) What level of improvement in the directional stability of trucks will be significant with respect to driver ability to control vehicle motions?

An empirical study of truck accident data may well prove unenlightening until such time as accident evidence can be gathered to include the relevant information. In particular, since loss of control in a yaw divergency implies vehicle rollover in the case of a straight truck, and jackknife, possibly followed by rollover, in the case of a tractor-trailer, the divergency incident may well be masked by the distracting evidence associated with the rollover of a heavy vehicle. Further, since heavy vehicle spinout can be precipitated without tires encountering high values of lateral slip, tire marks may not be evident or visible.

It would seem that the accident investigation community would be well advised, nevertheless, to begin considering truck and tractor-trailer loss of control accidents with the recognition that yaw divergency can, indeed, precede rollover. It should be further emphasized that the traditional notion that jackknifing accrues only during heavy braking is not a comprehensive rule. From a causality point of view, it should be made clear that a heavy vehicle operator may have encountered the challenge of yaw stabilization prior to any variety of final impact, rollover, or ran-off-road consequences.

Going beyond the matter of further yaw stability investigations, it appears that much remains to be learned about the mechanics of motor trucks. A broad study of the implications of frame compliance would serve to establish the extent to which rigid body models of heavy vehicles may be inadequate. There also remain numerous kinematic and compliance properties of truck steering and suspension systems which have not been adequately examined. In addition, the inertial properties associated with many of the common truck body configurations have not been formally evaluated. Overall, there is a need to obtain, for heavy trucks, a level of understanding of common control properties such as obtains for passenger cars, thereby providing a solid and comprehensive basis upon which to found investigations of specific interest.

With regard to articulated vehicles, one specific item seems relevant to the foregoing discussions. By way of extension to the recommended study of frame compliance effects, the torsional compliance of semi-trailers is a similarly crucial item insofar as it determines the distribution of trailer roll moment reaction between tractor suspensions and trailer suspensions (and thus between the respective tire sets). An associated inventory of roll stiffnesses afforded by common trailer suspensions should accompany any study of the effects of trailer frame compliance. Additionally, the articulated commercial vehicle is seen as a configuration tending, in general, to further exacerbate whatever control anomalies exist in straight trucks. Accordingly, studies of articulated vehicle control behavior are recommended as logical extensions to research programs which have effectively addressed and resolved the mysteries of the unit truck.

In the specific area of tire mechanics, the most significant unresolved item involves the combined slip behavior of commercial vehicle tires. This complex regime of traction behavior remains virtually unexplored. In the authors' view, no serious analyses and predictions of braking-in-a-turn response of commercial vehicles can be entertained until these data are available.

Additionally, there is a need to expand the dry surface measures of longitudinal and lateral traction of commercial tires to include measurements on wetted and snow-covered pavements. Although some limited measurements of heavy truck tires have been made on wet pavements [10], these experiments should be extended to constitute a general inventory of wet traction produced by commercial tires employed in the U.S.

Also, the prevalent usage of wheel slip control systems on heavy trucks since promulgation of FMVSS 121 suggests a need to examine the influence of dynamically varying longitudinal slip on traction behavior. While such investigation might concentrate initially upon the relationship between slip dynamics and longitudinal traction, the influence of slip dynamics on traction response in combined braking and cornering seems also pertinent for study.

Observations of the non-classical sensitivity of cornering stiffness to inflation pressure on many light and heavy truck tires suggests that follow-up investigations are in order to evaluate the control significance of manufacturer recommendations for an inflation pressure bias. While current recommendations of inflation pressure bias may be prompted by considerations of load-carrying capacity rather than vehicle directional response to steering, the destabilizing effect of commonly recommended biases suggests that the recommended practices deserve serious scrutiny.

With respect to the test practices which may be employed in future full-scale experiments conducted with commercial vehicles, certain recommendations are prompted by the experience obtained in this study. Firstly, it would appear wise that no full-scale test of a heavy vehicle proceed without adequate roll-protective structures deployed. Further, in tests conducted to examine directional behavior at lateral acceleration levels which even slightly exceed the normal maneuvering range, it is recommended that experiments be conducted either in an unmanned (remotely controlled) mode or in a manual mode with a human operator who

is suitably protected using rollover preventing hardware. Reflecting upon passenger car experience, the anti-rollover outrigger is an indispensible component in severe maneuvering studies—but only when the outrigger design can be confidently demonstrated to provide a conservative level of protection. While such devices have been reported in studies investigating the dynamics of heavy trucks [11], the adequate fastening of such hardware to heavy truck frame rails is not altogether straightforward.

An overall assessment of the technology of truck dynamic prediction would suggest that full-scale testing should proceed cautiously when tests are in order at all. The general familiarization of the researcher with a new regime or mode of maneuvering, however, should be initiated (before testing) using computerized simulation and laboratory measurement of mechanical parameters.

A truly general view of the foregoing study's potential for impacting programs in truck and bus safety suggests that we recognize the user-dominated character of the commercial vehicle system. To the extent that heavy vehicles, especially trucks and tractors, are largely specified by their purchaser, it would appear that certain safety advisory information must ultimately be directed at "the trucker." Accordingly, recommended practices concerning tire installation, payload placement, fifth wheel location, etc., must be effectively presented to the professional driving community and to the associated fleet owners. Correspondingly, it would appear that the results of broadened research into the mechanical behavior of trucks as derives from vehicle design features (i.e., suspensions, frames, steering systems, etc.) should be effectively disseminated to the truck engineering community. The truck manufacturer could then be expected to rationally constrain the availability of those assembly options (or combinations of options) which are found to yield undesirable control quality.

While rulemaking in the area of commercial vehicle handling may be a facet of NHTSA's overall charter, it is recommended that near-term improvements in heavy vehicle safety may well be effected through information initiatives that build upon recent research findings such as those developed in this particular study.

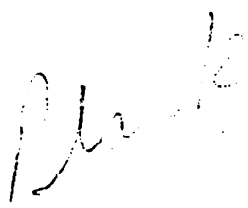

6.0 REFERENCES

1. Weir, D.H., et al., Analysis of Truck and Bus Handling, Final Report, Contract DOT-HS-242-2-421, June, 1974.

2. Roland, R.D., Rice, R.S., and Dell'Amico, F., The Influence of Tire Properties on Passenger Vehicle Handling, Final Report, Contract DOT-HS-053-3-727, June, 1974.

3. Murphy, R.W., Bernard, J.E., and Winkler, C.B., A Computer Based Mathematical Method for Predicting the Braking Performance of Trucks and Tractor-Trailers, Phase I Report, Motor Truck Braking and Handling Performance Study, Highway Safety Research Institute, Univ. of Michigan, September 15, 1972.

4. Bernard, J.E., Winkler, C.B., and Fancher, P.S., A Computer Based Mathematical Method for Predicting the Directional Response of Trucks and Tractor-Trailers, Phase II Technical Report, Motor Truck Braking and Handling Performance Study, Highway Safety Research Institute, Univ. of Michigan, June 1, 1973.

5. Ervin, R.D., Grote, P., Fancher, P.S., MacAdam, C.C., and Segel, L., Vehicle Handling Performance, Final Report, Contract DOT-HS-031-1-159, November 1972.

6. Bohn, P.F. and Keenan, R.J., "NHTSA/APL Hybrid Computer Vehicle Handling Program," Proceedings of a Symposium on Commercial Vehicle Braking and Handling, Univ. of Michigan, May 5-7, 1975, pp. 221-244.

7. Bernard, J.E., Fancher, P.S., Gupta, R., Moncarz, H., and Segel, L., Vehicle In Use Limit Performance and Tire Factors - The Tire In Use, Final Report, Contract DOT-HS-031-3-693, March 1975.

8. Ervin, R.D., MacAdam, C.C., and Fancher, P.S., The Longitudinal Traction Characteristics of Truck Tires as Measured on Dry Pavements, Report #UM-HSRI-PF-75-3, Highway Safety Research Inst., Univ. of Michigan, February 1975.

9. Ervin, R.D. and Wild, R.E., The Noise and Traction Characteristics of Bias-Ply Truck Tires, Report # UM-HSRI-PF-76-2-1, Highway Safety Research Institute, Univ. of Michigan, January 1976.

10. Dijks, A., "Wet Skid Resistance of Car and Truck Tires," Tire Science & Technology, TSTCA, Vol. 2, No. 2, May 1974, pp. 102-116.

11. Strandberg, L., Nordström, O., and Nordmark, S., "Safety Problems in Commercial Vehicle Handling," Proceedings of a Symposium on Commercial Vehicle Braking and Handling, Univ. of Michigan, May 5-7, 1975, pp. 463-528.

APPENDIX A

PARAMETERS DESCRIBING TEST VEHICLES

A.1 INTRODUCTION

A wide range of parameters are required to characterize the vehicle in a manner suitable for computerized simulation. These parameters can be divided into five main categories:

1. Vehicle Layout Geometry
2. Steering System Kinematics and Compliance
3. Suspension Kinematics and Compliance
4. Inertial Properties
5. Tire Shear Force and Moment Properties

This appendix describes the procedures employed to measure vehicle parameters and also presents complete parametric descriptions of four test vehicles used in this study. Tire properties are described in detail in Appendix C and are not considered here. The four vehicles tested were:

a) 1974 Ford F-250 Pickup (LT)

b) 1969 Ford Econoline Van (LV)

c) 1974 White Road Boss (4x2) Heavy Truck (HT)

d) 1966 GMC-PD 4107 Intercity Bus (HB)

Complete parameter measurements were performed by HSRI on the Ford pickup and the Ford van. For the White truck certain parameters were obtained from Reference (A-1) while certain bus parameters were obtained from Reference (A-2).

A brief description of the test vehicles is given in Table A-1.

TABLE A-1. TEST VEHICLES DESCRIPTION

	Pickup (LT)	Van (LV)	Truck (HT)	Bus (HB)
General	3/4 ton (F-250)	Club Wagon	Road Boss 4x2	Intercity
	6900 lb GVWR	8100 lb GVWR	29790 lb GVWR	38 Passengers
	133" WB	124" WB	156" WB	7000 lb Passenger & Cargo Load
				260" WB
Suspension				
Front	Twin I-Beam	Twin I-Beam	Solid	Solid
	Coil Springs	Coil Springs	Leaf Springs	2 Air Springs
	2600 lb GAWR	3300 Lb GAWR	10750 lb GAWR	
Rear	Solid	Solid	Solid	Solid
	Leaf Springs	Leaf Springs	Leaf Springs	4 Air Springs
	4300 lb GAWR	4800 lb GAWR	19040 lb GAWR	Auxiliary Roll Bar
Brakes				
	Hydraulic	Hydraulic	Duals Full Air	Duals Full Air
	Disk Front Drum Rear	Drum Front and Rear	Drum Brakes	Drum Brakes
OE Tires				
	Firestone Transport 500 8.00x16.5/D	Goodyear Custom Hi Miler 8.75x16.5/E	Uniroyal Triple Tread 10.00x20/F	Firestone Comm. Mileage 12.5x22.5/G

In the following sections of this appendix a set of laboratory measurement methods employed on these vehicles will be presented using the Ford F250 pickup as an example for illustrating results format. Parameter values for all vehicles in the sample were obtained in the unloaded condition. The associated loaded-vehicle parameters were estimated. A complete list of parameters covering each test vehicle is presented in Section A.6.

A.2 VEHICLE GEOMETRY

Vehicle geometry includes all parameters that are dimensional in nature such as wheelbase, track, separation between suspension springs, axle height above ground, etc. The results of the measurements obtained for the test vehicle are presented below.

Parameter (Units)	Measurements for Ford F250 Pickup
a) Wheelbase (in)	133
b) Front Track (in)	66
c) Rear Track (in)	64.5
d) Separation Between Dual Tires (in)	x
e) Separation Between Front Springs (in)	50.0
f) Separation Between Rear Springs (in)	44.75
g) Wheel Center Above Ground - Front (in)	15.375
Rear (in)	15.375

A.3. STEERING KINEMATICS AND COMPLIANCE

A.3.1 Steering Gear Ratio Test

The objective of this test is to obtain a direct functional relation between the steering wheel angle and the wheel angles for the left and right front wheels.

The test is conducted by resting the front wheels on a calibrated slide-and-turn table with the car horizontally leveled. In the straight-ahead-steering wheel lock position the turntable calibrations are set to zero angular displacement. The steering wheel angle is read on a protractor on the steering wheel, and the corresponding wheel angles are read on the turn-table calibrations.

The results of this test include the effects of variable gear ratio, steering linkage ratio, Ackerman geometry, and the steering system play. A typical set of data obtained for the light pickup is shown in Figure A.1. The results for the test vehicle, as deduced from Figure A.1, are given below.

Parameter	Test Results
Steering System Ratio	22.5
Steering System Play (deg)	15°

A.3.2 STEERING SYSTEM COMPLIANCE MEASUREMENT

The objective of this test is to obtain the steering column and the steering linkage stiffnesses.

The test is conducted using a laboratory set-up designed at HSRI. The design permits a pure torque to be applied to one front wheel on the vehicle, with the steering wheel held fixed, and the other wheel free to rotate about its kingpin axis. The

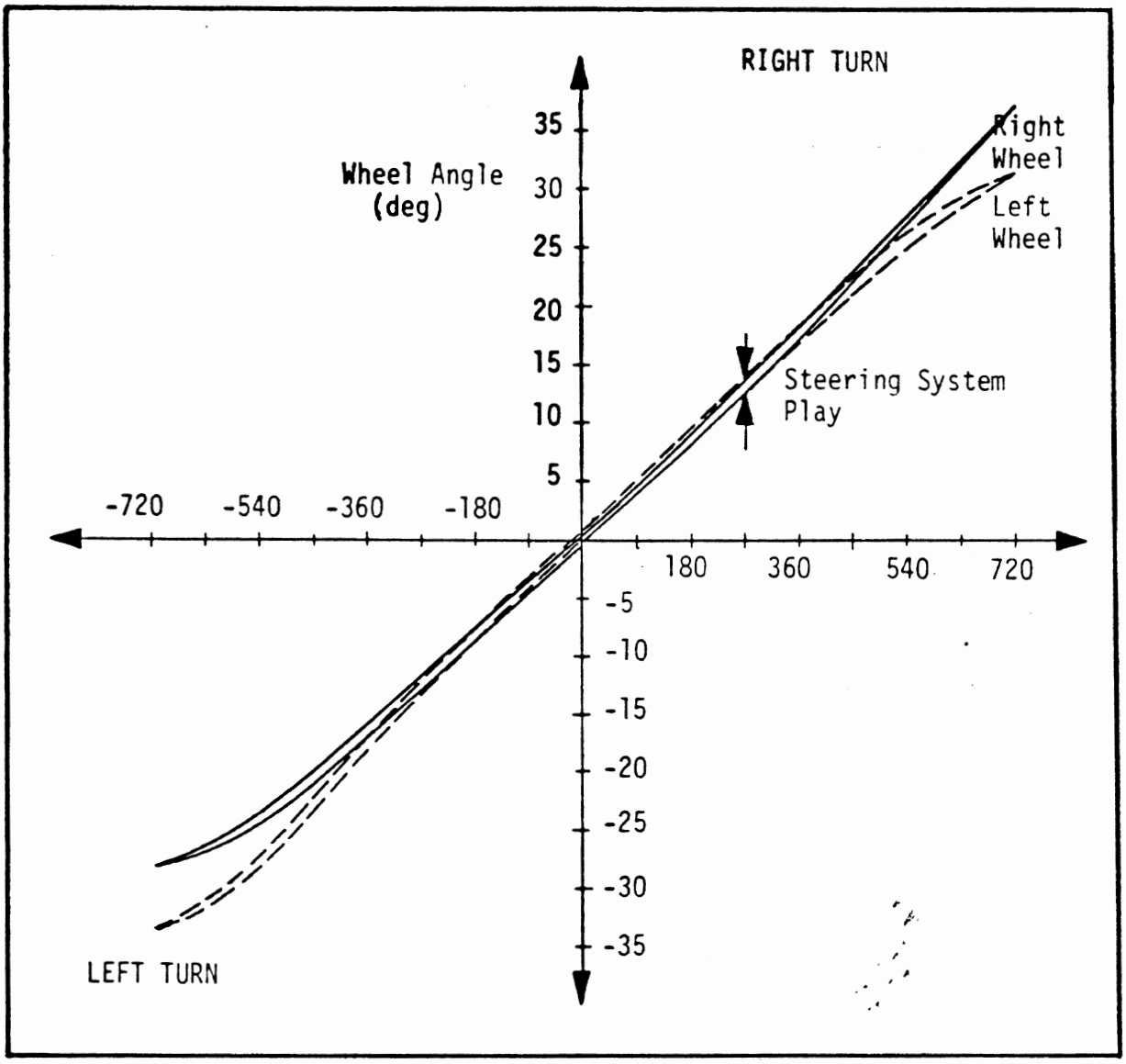

Figure A.1. Test results of the steering gear ratio test for the light pickup.

front wheels rest on a turn-table exerting normal static vertical load. A turnbuckle is used to increase or decrease the tension in the cable thereby increasing or decreasing the torque applied to the wheel. (The internal friction of the turn-table requires about 8 ft-lbs torque to rotate under a load of 800 lbs.) Cable tension is measured with the load cell and the wheel angles by using slip gauges. By measuring the wheel angles as a function of the applied torque, the steering column and steering linkage compliances can be calculated, provided the steering gear ratio and the linkage ratio are known.

A typical set of data obtained for the light pickup is shown in Figure A.2.

The steering column and steering linkage compliances computed from the data in Figure A.2 were:

Parameter (Units)	Results for Ford F-250 Pickup
Steering Linkage Compliance (in-lb/rad)	400000.
Steering Column Compliance (in-lb/rad)	395.

A.4 SUSPENSION STIFFNESS TESTS

The objectives of these tests are to obtain the functional relation between the spring force and spring displacement, and the wheel position changes as related to vertical spring deflection.

To obtain suspension characteristics, the sprung mass is held in place, while the axle is free to move between the rebound and bump stops.

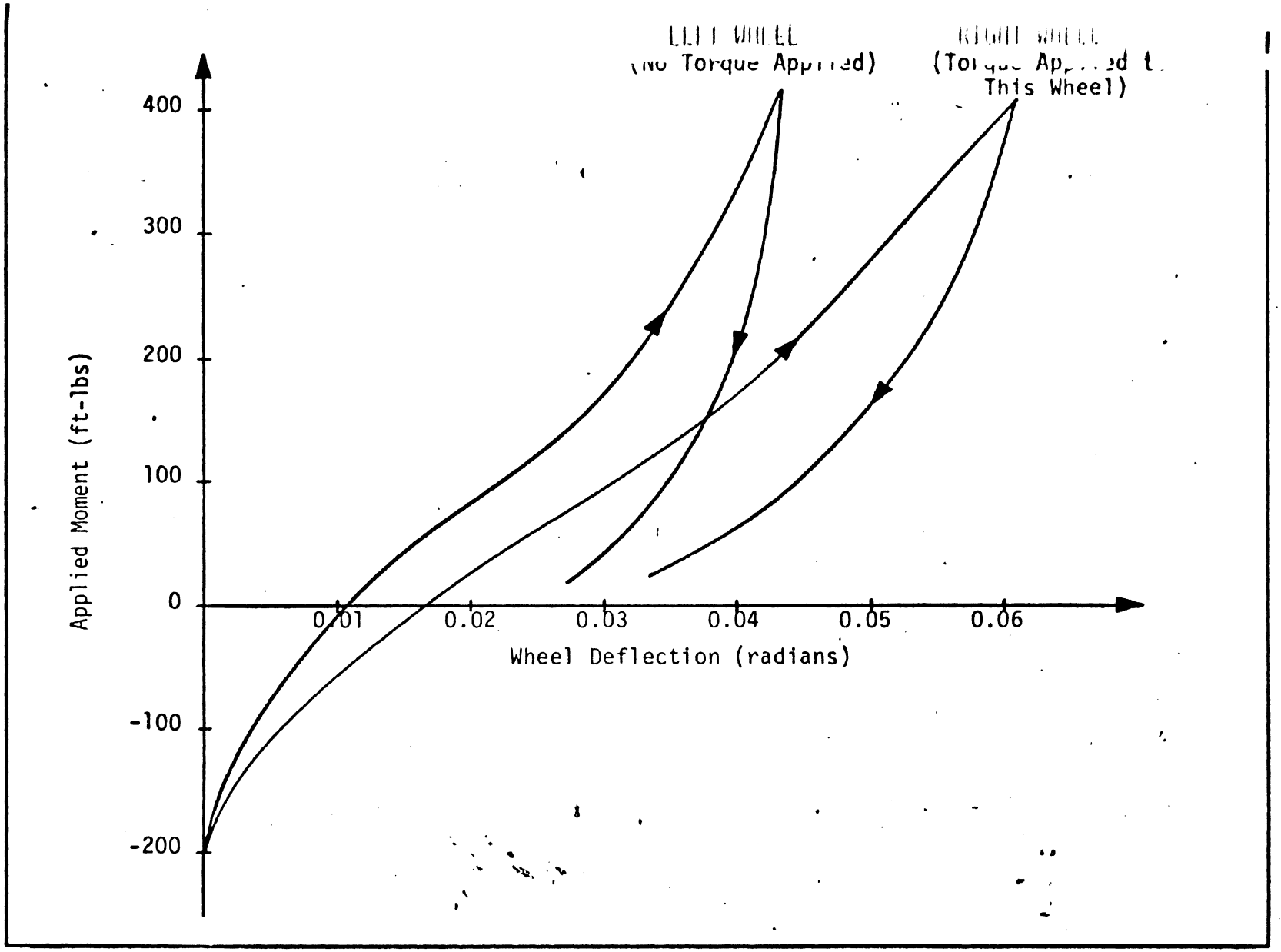

Figure A.2. Result of steering compliance test for light pickup.

For the front suspension, the right wheel is held at the rebound stop, while the left wheel is free to move. The hydraulic jack and the load cell adapter assembly rest on a slide and turn-table so as to insure vertical orientation for the jack. Vertical load is read on the digital readout for the load cell, and vertical displacement read from the calibrations on the jack. Experimental set-up for this test is shown in Figure A.3.

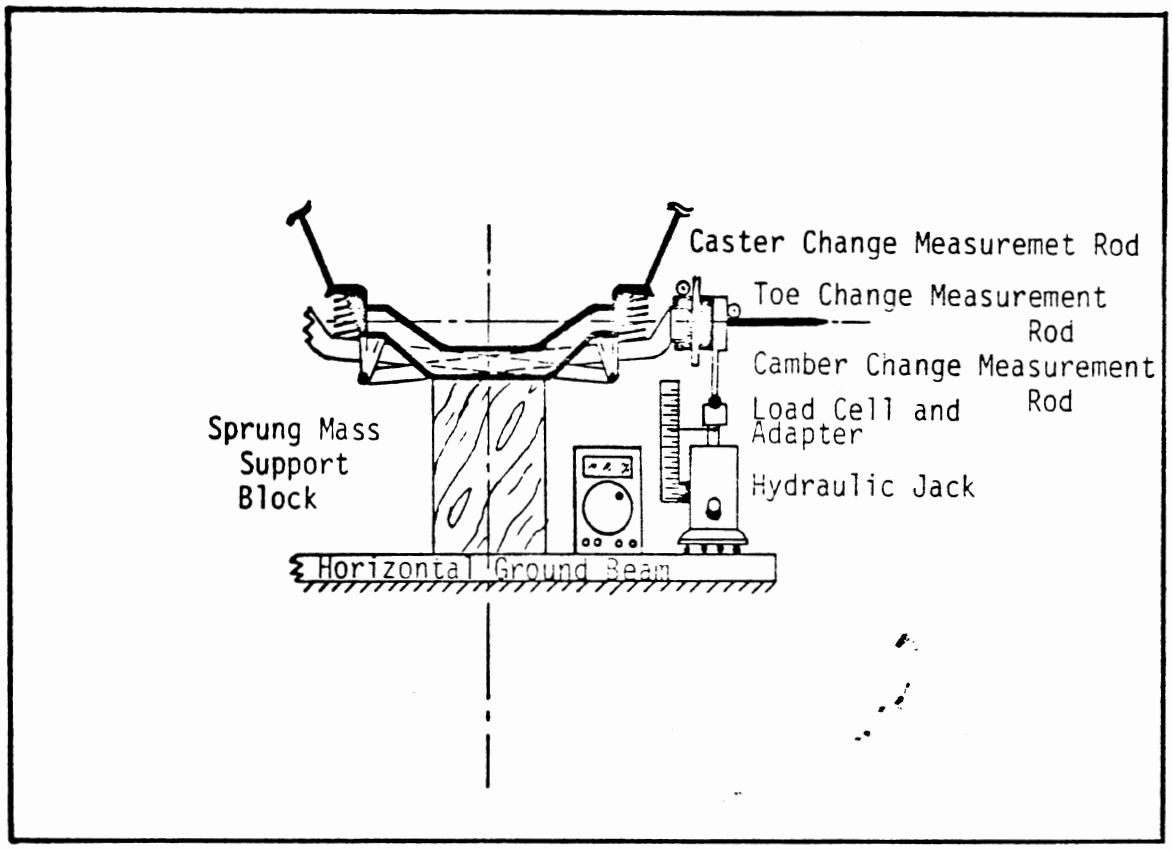

Figure A.3. Experimental set-up for twin I-beam front suspension measurement.

It should be noted that these are wheel load versus wheel deflection curves, and the spring stiffness obtained is for an equivalent spring translated to the wheel plane. Results of the test for the Ford pickup are shown in Figure A.4.

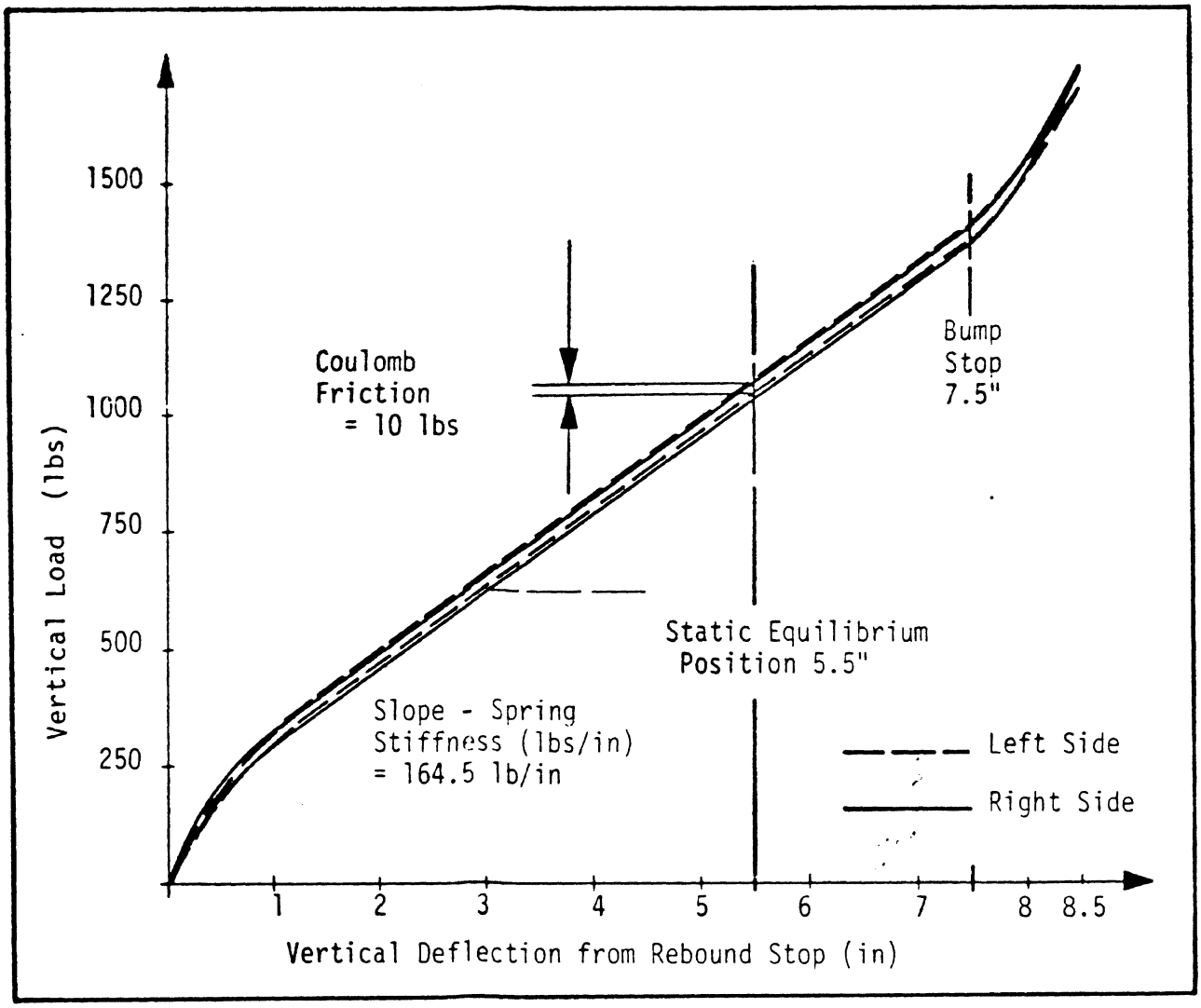

Figure A.4. Front spring stiffness test results for Ford F-250 pickup.

Angular changes in toe-in, camber, and caster for vertical deflection of the front wheel are also measured using slip gauges. The results obtained for the Ford pickup are shown in Figures A.5, A.6, and A.7. Knowing the static wheel alignment specifications, curves for absolute changes in toe-in, camber angle, and caster angle can be computed for each front suspension.

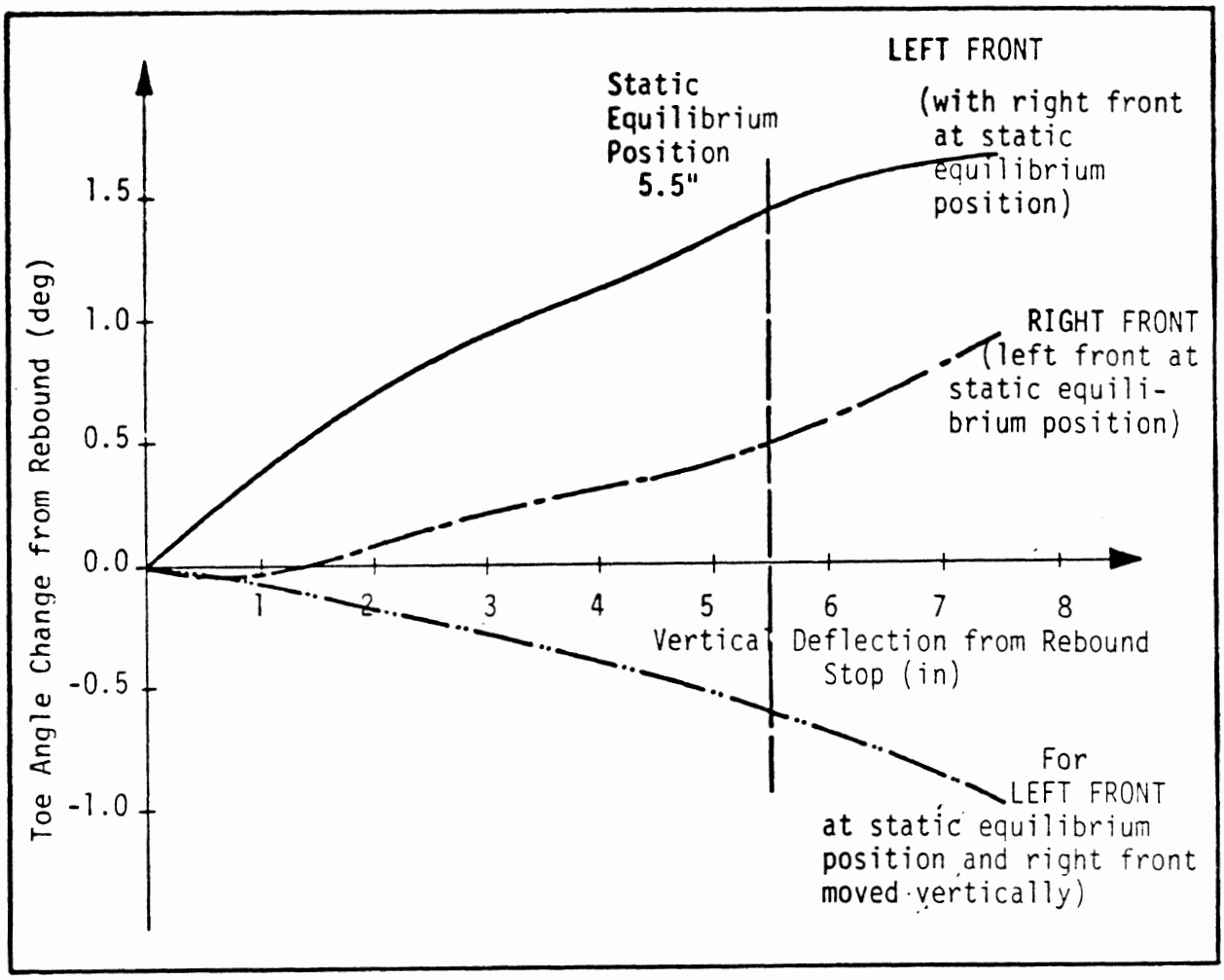

Figure A.5. Toe angle measurement results for Ford F-250 pickup.

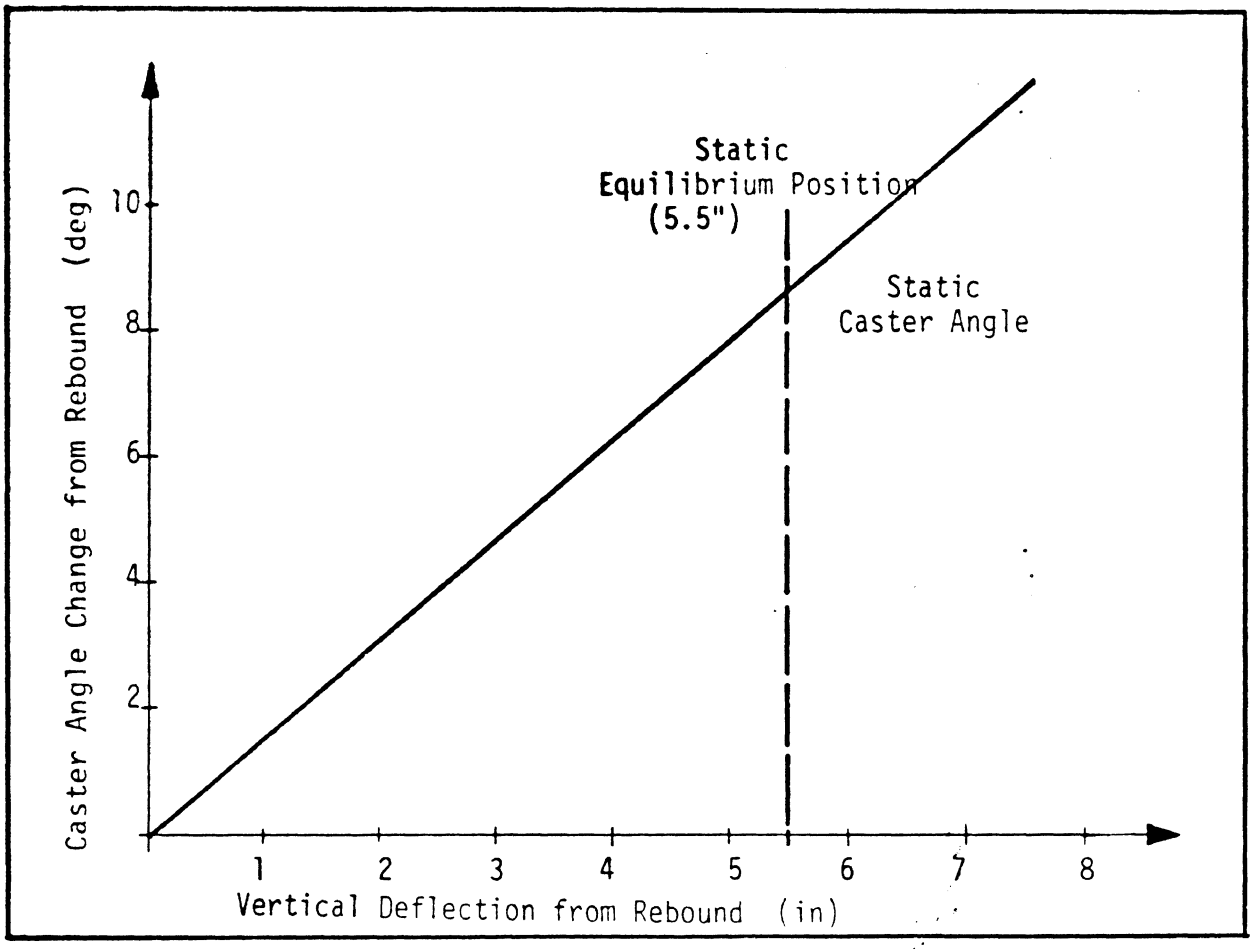

Figure A.6. Caster angle measurements for Ford F-250 pickup.

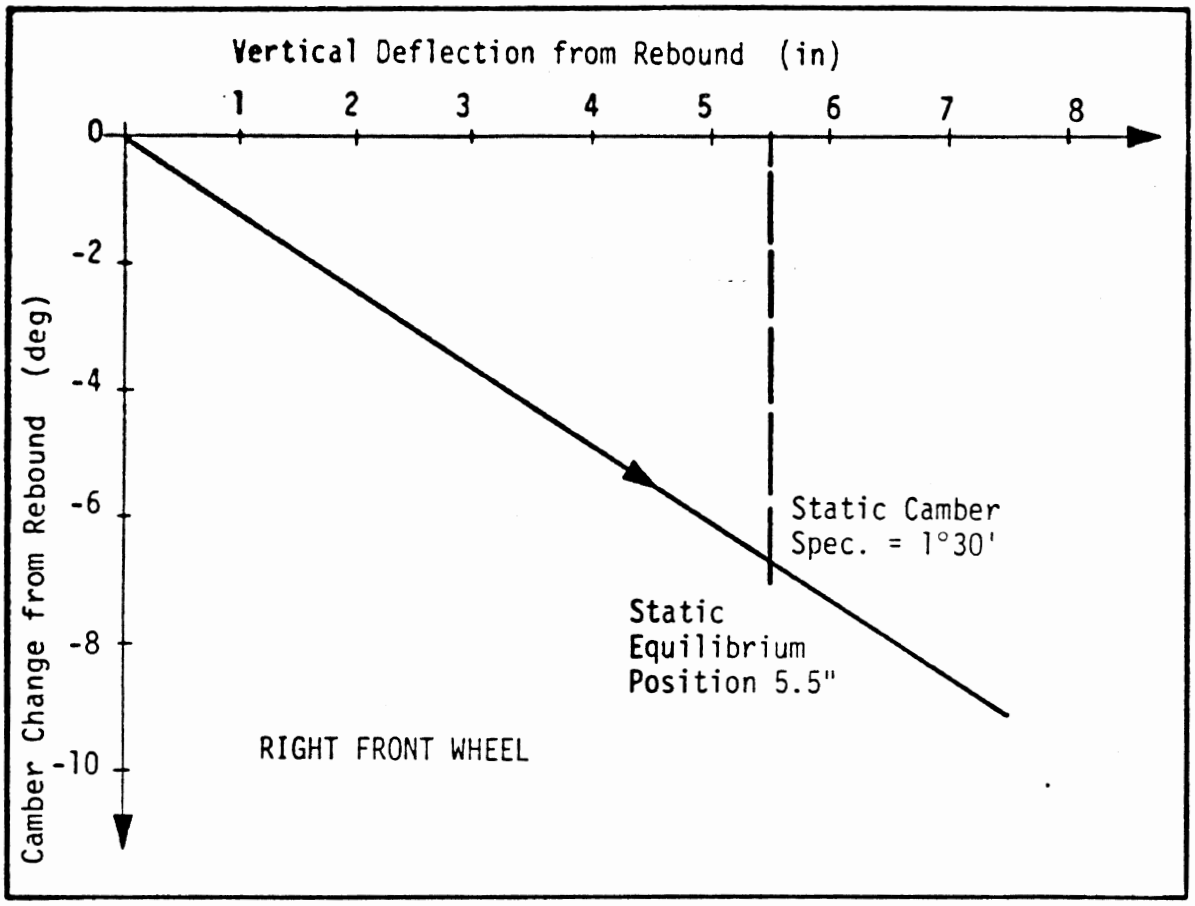

Figure A.7. Camber angle measurement for light pickup.

For the solid rear suspension, a special fork-like support is attached to facilitate load application on the axle. Load deflection curves are used to obtain the spring stiffness. It should be noted that the spring stiffness is for both the rear springs, effective at the spring position. Longitudinal axle displacement is also recorded to compute the roll-steer coefficient. Figures A.8 and A.9 show the results obtained for the test.

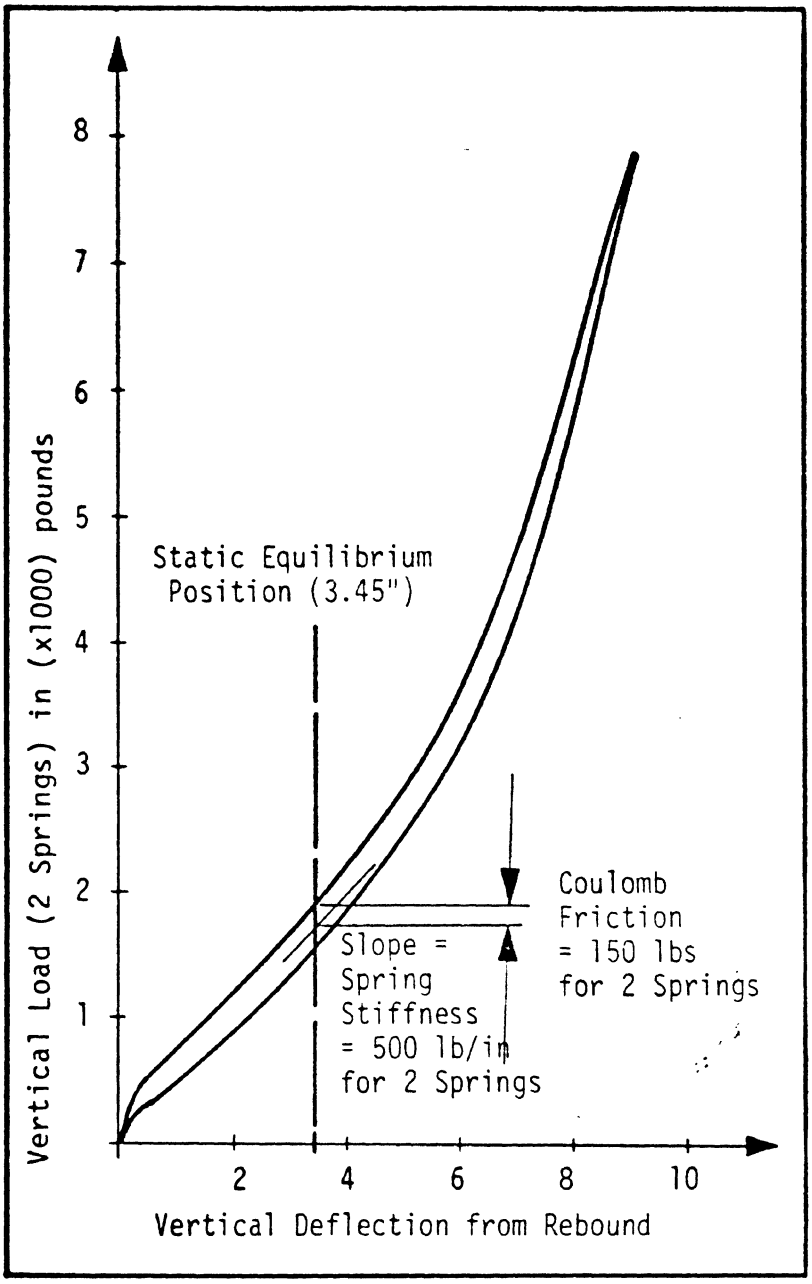

Figure A.8. Rear spring stiffness test results for the light pickup.

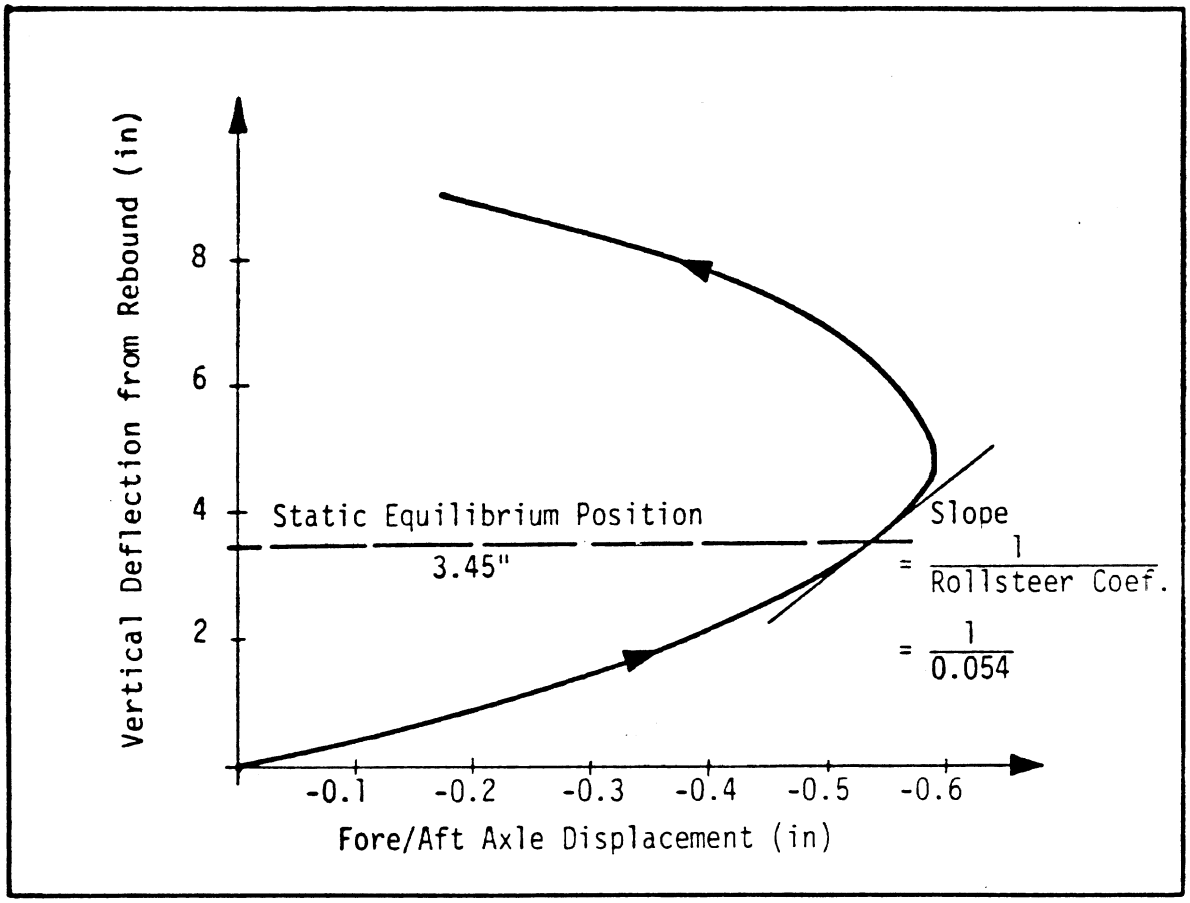

Figure A.9. Rear axle displacement for the light pickup.

For the intercity bus, the air suspension stiffness was obtained from the load-deflection characteristics provided by the air spring manufacturer (A-3). Figure A.10 shows the load deflection characteristics for the air spring.

A.5. CENTER OF GRAVITY AND INERTIAL PROPERTIES MEASUREMENT

The objective of these tests is to obtain the exact location of the center of gravity and the pitch, roll, and yaw moments of inertia for the sprung mass.

The computer simulation model requires as input data:

a) Fore/aft location of sprung mass c.g.

b) Vertical location of sprung mass c.g.

c) Pitch moment of inertia of sprung mass

d) Roll moment of inertia of sprung mass

e) Yaw moment of inertia of sprung mass

f) Roll moment of inertia of sprung mass

The HSRI c.g. and pitch inertia measurement swing was used for this test, as shown in Figure A.11. C.g. and pitch moment of inertia were measured for the vehicle, and the sprung mass properties were computed knowing the properties of the unsprung mass.

A.5.1 Center of Gravity Test

The fore/aft location of c.g. is obtained by placing knife edges, laterally to the vehicle, at the point of balance.

Vertical c.g. location requires measurement of the tilt angle (A-4). With the knife edges slightly shifted from the fore/aft c.g. position, the vehicle tilt angle is measured using an accurate inclinometer. Known torques are applied to the swing and corresponding tilt angles recorded. Figure A.12 shows the terminology used in the experimental set-up. Given the weight, fore/aft

GYRL-900

Ass'y. Part No. 566-18-2-015

DYNAMIC CHARACTERISTICS	
Nominal Design Height	10 in
Air Pressure	100 psig
Load	3600 lbs
Effective Area	36 sq in
Spring Rate	550 lbs/in
Natural Frequency	74 cpm

Assembly Weight—8.0 lbs (ref.)

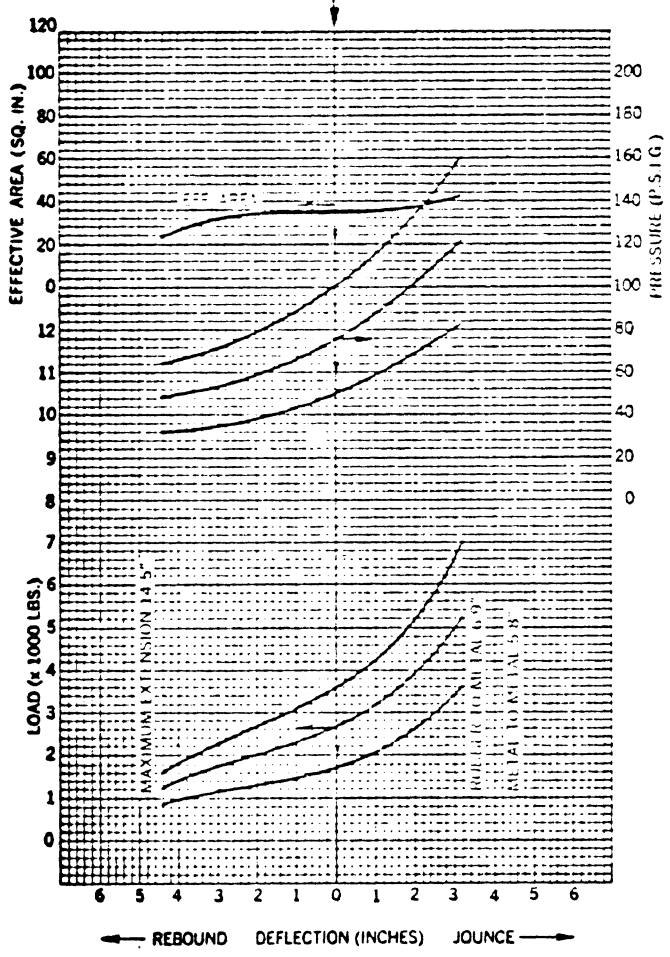

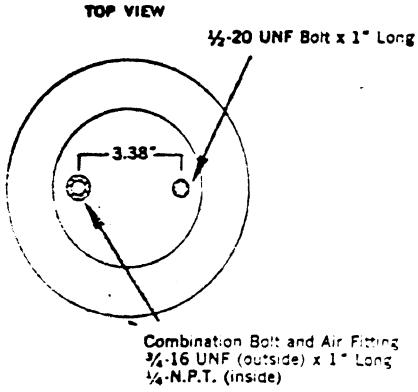

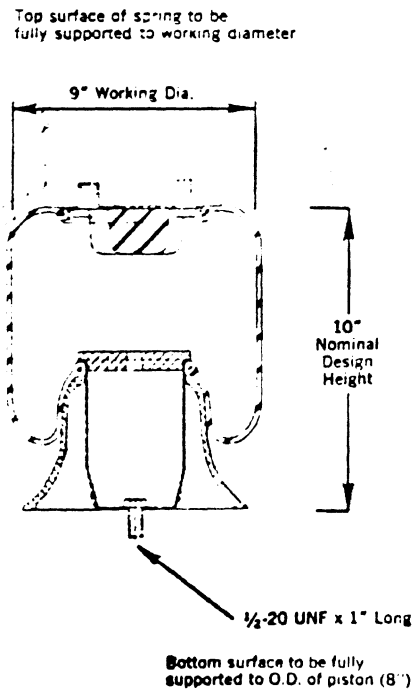

GOODYEAR

Figure A.10. Intercity bus air spring characteristics.

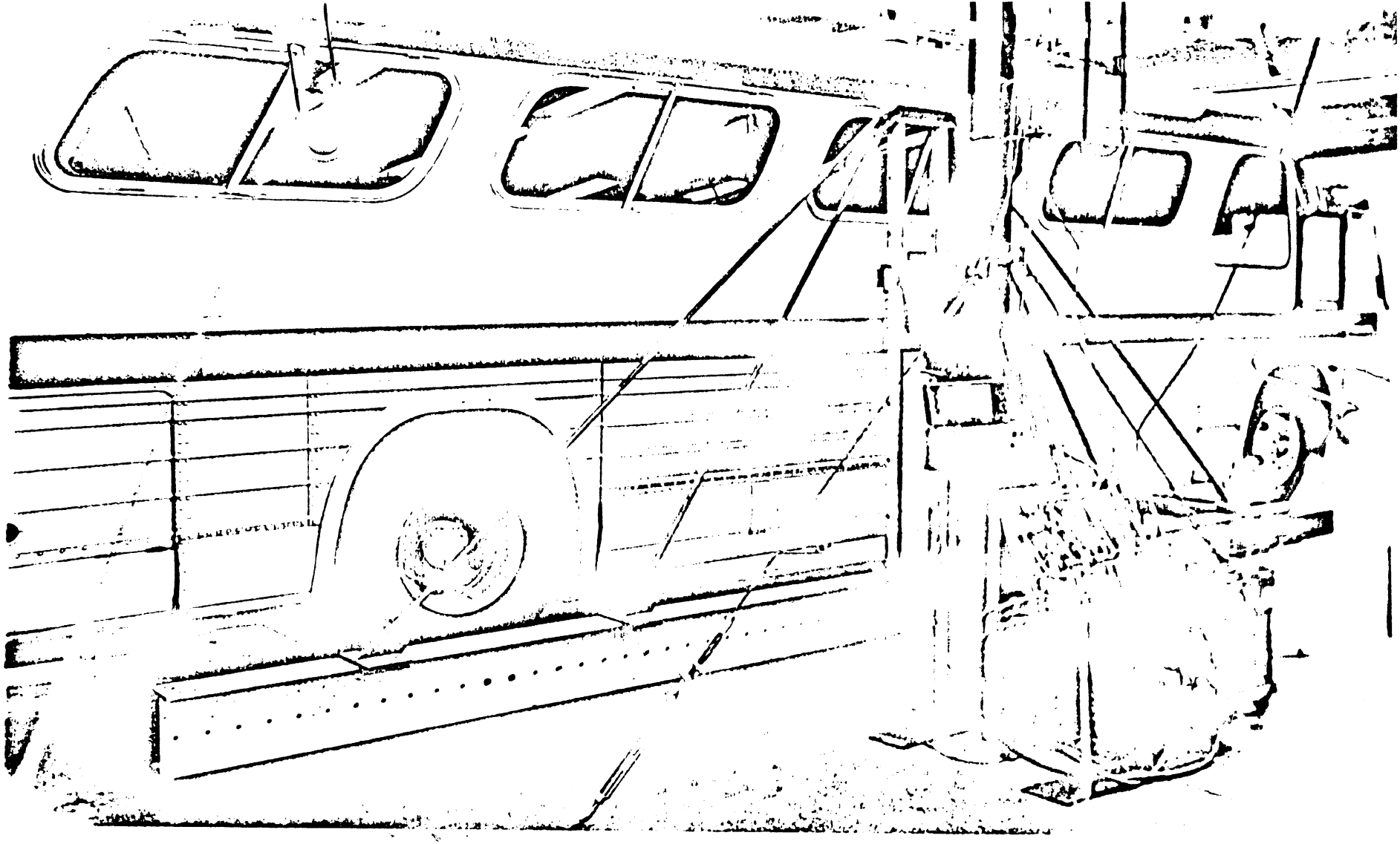

Figure A.11. HSRI center of gravity and pitch inertia measurement swing.

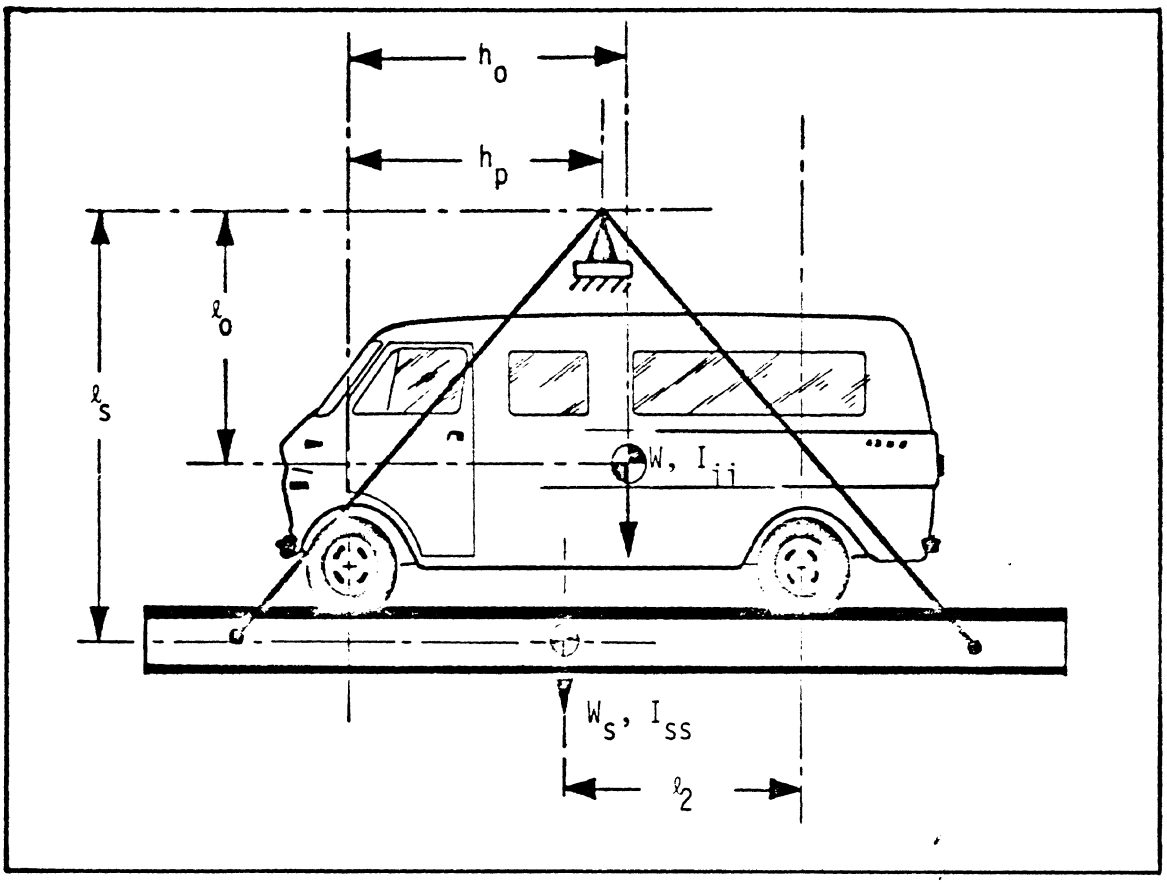

Figure A.12. Schematic of the terminology used for c.g. and inertia measurement.

c.g. location, tilt angles, and the torques, the vertical c.g. location above ground plane can be calculated, using the equation:

$$\ell_o = \frac{1}{W}\left(\left(\frac{\tau_i}{\sin\theta_i - \cos\theta_i \tan\theta_o}\right) - W_s \ell_s\right)$$

$$h_o = h_p + \left(\frac{W_s \ell_s + W \ell_o}{W_s + W}\right)\tan\theta_o$$

where

h_o = fore/aft location of vehicle c.g.

h_p = front axle to pivot point distance

ℓ_o = vehicle c.g. from pivot points

ℓ_s = swing c.g. from pivot point

W = vehicle total weight (lbs)

W_s = weight of swing (lbs)

θ_o = initial balance angle (deg) for i^{th} sample

θ_i = resulting tilt angles (deg) for i^{th} sample

τ_i = applied torque (in-lbs) for i^{th} sample

From the vehicle c.g. position, the c.g. for the sprung mass can be computed knowing the unsprung mass. For direct measurements of unsprung mass, the suspension components of interest must be removed and weighed. However, reasonable formulas for estimating the unsprung weights for standard front engine, rear axle drive passenger cars have been documented in the literature (A-5). These formulas are

$$W_{uf} = 0.04\, W_t + 60$$

$$W_{ur} = 0.067\, W_t + 90$$

where

W_{uf} = unsprung weight in front (lbs)

W_{ur} = unsprung weight in rear (lbs)

W_t = total vehicle weight (lbs)

For the Ford F-250 pickup the results obtained were:

Weight of the vehicle (lbs)	= 4459
c.g. position aft of front axle (in)	= 55.77
c.g. position above ground (in)	= 29.32
Front unsprung weight (lbs)	= 272
Rear unsprung weight (lbs)	= 338

Assuming unsprung c.g. lies on the axle centerline, the sprung mass and its c.g. can be computed for the simulation.

A.5.2 Moment of Inertia Measurement

A.5.2.1 Pitch and Roll Moment of Inertia. The classical compound pendulum technique was applied to determine the pitch and roll moments of inertia. The HSRI center of gravity and inertia measurement swing, shown in Figure A.11, was used for pitch inertia measurement. In addition to the measurements for the c.g. location, periods for oscillations with and without the vehicle are recorded for the swing. Using the terminology of Figure A.12, the pitch and roll moments of inertia for the vehicle can be calculated using the formula:

$$I_{ii} = W \ell_o \left[\frac{t^2}{4\pi^2} - \frac{\ell_o}{g}\right] + \left[\frac{W_s \ell_s}{4\pi^2} t^2 - t_s^2\right]$$

where

i = x (for roll moment) or y (for pitch moment)

t = period of oscillation for swing with the vehicle (sec)

t_s = period of oscillation for swing alone (sec)

W = vehicle weight (lbs)

W_s = swing weight (lbs)

Knowing the vehicle inertias, the sprung mass inertia values can be obtained using the parallel axis theorem.

A.5.2.2 Yaw Moment of Inertia Measurement. Compound pendulum principles are used to obtain the vehicle yaw moment of inertia. The vehicle is suspended by cables arranged symmetrically about the vehicle c.g. Small yawing oscillations are introduced and the period of oscillations determined. Using the notation of Figure A.13, the yaw moment of inertia for the vehicle can be calculated using the formula:

$$I_{zz} = \frac{Wr^2t^2}{4\pi^2 \ell} + \frac{W_s r^2}{4\pi^2 \ell}\left[t^2 - t_s^2\right]$$

where

ℓ = length of cables (in)

t = period of oscillation for swing and vehicle (sec)

t_s = period of oscillation for swing alone (sec)

The above equation is based on small angle approximations; and the accuracy of results can be improved by maintaining small oscillations and long cables. A sensitivity analysis of the equation shows that large value of ℓ and small values of r and W_s are desirable. Knowing the total vehicle yaw moment of inertia, the sprung mass yaw inertia value can be computed. Results obtained

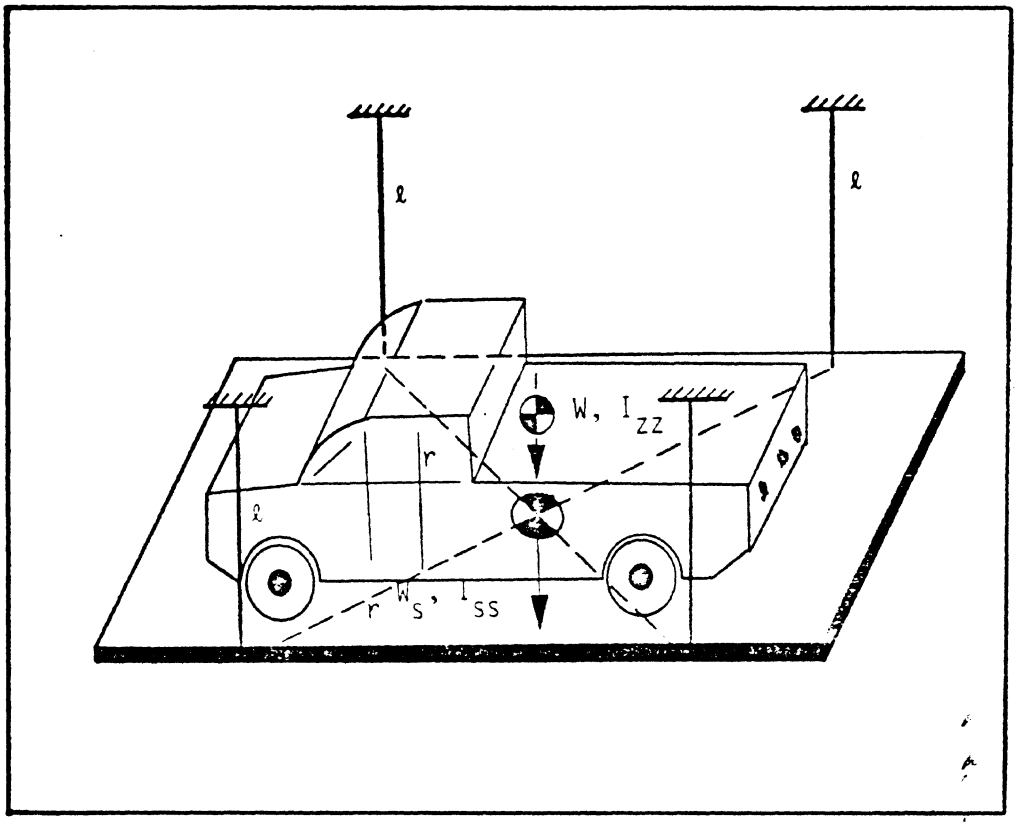

Figure A. 13. Schematic of yaw inertia measurement set-up.

for the Ford F-250 pickup on the inertia swings were:

Vehicle pitch moment of inertia ($in\text{-}lb\text{-}sec^2$)	= 51197
Vehicle roll moment of inertia ($in\text{-}lb\text{-}sec^2$)	= 8918
Vehicle yaw moment of inertia ($in\text{-}lb\text{-}sec^2$)	= 48778

Knowing the unsprung mass, unsprung moments of inertia, the sprung mass inertia values can be computed using the Parallel Axis Theorem.

A.6. SUMMARY OF VEHICLE PARAMETERS USED IN SIMULATION

A sample set of vehicle parameter data for the four test vehicles in the unloaded and loaded OE conditions is listed in Tables A-2 through A-9. Table A-10 defines each symbol according to the format required by the computer simulation model at the Applied Physics Laboratory of Johns Hopkins University (A-6).

PARAMETER VALUES - N C MICL JDFL ISRI RD OLIT NLC

1	MS= 12.600	2	MUF= 0.70400	3	MUR= 0.87500	4	ZF= 1[illegible].000	5	[illegible]= 18.[illegible]
6	A= 56.820	7	B= 67.180	8	TF= 66.000	9	TR= 68.000	10	TSR= 50.000
11	IX= 8996.0	12	IY= 39118.	13	IZ= 37366.	14	IXZ= 0.0	15	IR= 600.00
16	CF= 0.0	17	RF= 0.0	18	CFPR= 30.000	19	KF= 185.00	20	LAMF= -1.0000
21	OMFC= 2.9800	22	OMFT= 4.1000	23	CR= 0.0	24	RR= 0.0	25	CRPR= 150.00
26	KR= 293.75	27	LAMR= 0.0	28	OMRC= 5.0750	29	OMRT= 4.3000	30	KRS= 0.45000E-01
31	RW= 16.125	32	SFSF= 0.40000E-01	33	FOT= 0.24250	34	A0= -374.17	35	A1= 8.2500
36	A2= 14845.	37	A3= 0.0	38	A4= 1.0000	39	TIR = 0.0	40	TOR = 0.0
41	KSC= 2400.0	42	NG= 21.500	43	LAFC= 4.0000	44	LAFT= 10.000	45	LARC= 2.8000
46	LART= 10.000	47	IFW= 11.000	48	IF = 0.0	49	IWF= 17.000	50	IWR= 17.000
51	IDR= 0.60000	52	ARR= 3.2500	53	TSF = 0.0	54	KFS = 0.0	55	PT= 0.0
56	YSA1= 4.2200	57	YSA2= -4.2200	58	PHS1=-0.26180E-01	59	PHS2= 0.26180E-01	60	CTSW= 1.0000
61	IDF= 0.0	62	ARF= 0.0	63	P-IN= 0.0	64	Q-IN= 0.0	65	R-IN= 0.0
66	U-IN= 30.000	67	V-IN= 0.0	68	W-IN= 0.0	69	X-IN= 0.0	70	Y-IN= 0.0
71	Z-IN= -33.347	72	THIN=-0.44475E-01	73	PHIN= 0.0	74	PSIN= 0.0	75	DT= 0.10000E-01
76	TN= 5.0000	77	KT1= 1770.0	78	KT2= 1770.0	79	KT3= 1770.0	80	KT4= 1770.0
81	RPS1= 0.0	82	RPS2= 0.0	83	RPS3= 0.0	84	RPS4= 0.0	85	B1=-0.21300E-04
86	B2= 0.0	87	B3= 0.90700	88	B4= 0.0	89	D1DT= 0.0	90	D2DT= 0.0
91	D3DT= 0.0	92	DFLF= 0.0	93	DFLR= 0.0	94	DFL3= 0.0	95	PHDT= 0.0
96	PHIR= 0.0	97	DFW1= 0.0	98	DFW2= 0.0	99	U1PR= 0.0	100	U2PR= 0.0
101	U3PR= 0.0	102	U4PR= 0.0	103	S1PR= 0.0	104	S2PR= 0.0	105	S3PR= 0.0
106	S4PR= 0.0	107	PPRT= 1.0000	108	FRFQ= 0.40000	109	RWSF= 20.000	110	TQMX= 4428.0
111	KTQ= 738.00	112	VC= 0.0	113	MTSW= 0.0	114	DSWM= 62.000	115	TST= 1.0000
116	DSLP= 1.0000	117	CGAM= 3.0000	118	CS= 3.0000	119	TQR= 0.0	120	TQF= 0.0
121	PFL= 300.00	122	T1= 0.0	123	DSW= 0.0	124	= 0.0	125	ISW5= 0.0
126	SW15= 0.0	127	PQSW= 0.0	128	VTPS= 3.0000	129	VHTP= 0.0	130	AMCR= 0.85000E-01
131	FSP= 0.0	132	KSL1= 0.25000E 06	133	KSL2= 0.25000E 06	134	AA1= 7.0000	135	AA2= 7.0000
136	CCR= 0.0	137	CFCR= 0.0	138	AP= 5.6000	139	EP1= 0.0	140	EP2= 0.0
141	AERO= 0.0	142	VYW = 0.0	143	OMXW= 0.0	144	OMZW= 0.0	145	RHOA= 7.5000
146	CYP = 0.0	147	CYR = 0.0	148	CZAL= 0.0	149	CZQ = 0.0	150	CLP = 0.0
151	CLR = 0.0	152	CMAL= 0.0	153	CMQ = 0.0	154	CNP = 0.0	155	CNR = 0.0
156	SF = 0.0	157	VLEN= 0.0	158	REWV= 0.0	159	= 0.0	160	= 0.0
161	= 0.0	162	= 0.0	163	= 0.0	164	= 0.0	165	= 0.0
166	= 0.0	167	= 0.0	168	= 0.0	169	SNT= 72.000	170	SNSO= 72.000
171	SNS1= 72.000	172	SNSW= 2.0000	173	DIST= 0.0	174	PL = 0.0	175	TSCP= 0.25000
176	= 0.0	177	= 0.0	178	= 0.0	179	= 1.0000	180	PASS= 4.0000
181	= 1.0000	182	SI1= 0.20000	183	SI2= 0.20000	184	SI3= 0.20000	185	SI4= 0.20000
186	= 0.0	187	= 0.0	188	= 0.0	189	= 0.0	190	= 0.0
191	= 0.0	192	MTQB= 1.0000	193	DCSW= 0.0	194	LDF= 0.0	195	LDRF= 0.0
196	EK1=-0.25000	197	EK2= 0.25000	198	BMPL= 0.0	199	BMPS= 0.0	200	BMPH= 1.5000
201	XB= 0.0	202	APF1= 1.0700	203	APF2=-0.66700E-04	204	APR1= 1.0700	205	APR2=-0.66700E-04
206	MUSF= 0.75000	207	MUSR= 0.75000	208	BCON= 0.30000E-01	209	= 1.0000	210	= 0.0
211	= 0.0	212	= 0.0	213	= 0.0	214	= 0.0	215	= 0.0
216	= 0.0	217	= 0.0	218	= 0.0	219	FEE1= 0.55000	220	FEE2=-0.55000
221	THE1= 3.5000	222	THE2= 3.5000	223	= 0.0	224	= 0.0	225	= 0.0
226	= 0.0	227	= 0.0	228	= 0.0	229	= 0.0	230	= 0.0
231	H1= 300.00	232	H2= 300.00	233	LAMD= 0.0	234	AKF1= 185.00	235	AKF2= 185.00
236	AKF3= 293.75	237	AKF4= 293.75	238	BR1= 1.0000	239	BR2= 1.0000	240	BR3= 1.0000
241	BR4= 1.0000	242	KCF=-0.20000E-04	243	KCR=-0.20000E-04	244	KSR= 0.15000E-05	245	RH1=-0.21300E-04
246	RH2= 0.0	247	RH3= 0.90700	248	RH4= 0.0	249	AFK1=-0.48000E-03	250	AFK2= 0.38760E-03
251	AFK3= 0.0	252	ARK1=-0.48000E-03	253	ARK2= 0.38760E-03	254	ARK3= 0.0	255	OFC0= 0.0
256	OFC1= 0.0	257	OFC2= 0.0	258	OFC3= 0.0	259	ORC0= 0.0	260	ORC1= 0.0
261	ORC2= 0.0	262	ORC3= 0.0	263	CP0F= 0.0	264	CP1F= 0.0	265	CP2F= 0.0
266	CP0R= 0.0	267	CP1R= 0.0	268	CP2R= 0.0	269	CR0F= 0.0	270	CR1F= 0.0
271	CR2F= 0.0	272	CR0R= 0.0	273	CR1R= 0.0	274	CR2R= 0.0	275	= 0.0
276	= 0.0	277	RMPN= 0.0	278	TQB0= 0.0	279	TQB1= 0.0	280	= 0.0
281	= 1.0000	282	= 1.0000	283	= 0.0	284	HFC= 8.0500	285	HRC= 0.0
286	DRSW= 0.0	287	AXLE= 1.0000	288	DUAL= 0.0	289	WEEL= 4.0000	290	ROT = 0.24250
291	RA0 = -374.17	292	RA1 = 8.2500	293	RA2 = 14845.	294	RA3 = 0.0	295	RA4 = 1.0000

PARAMETER VALUES - MODEL C - VEHICLE MODEL * HSRI: FORD ECONOLINE (LOADED)

1	MS=	16.700	2	MUF=	0.70400	3	MUR=	0.67500	4	ZF=	20.400	5	ZR=	20.400	
6	A=	80.000	7	B=	44.000	8	TF=	60.000	9	TR=	60.000	10	TSP=	50.000	
11	IX=	11400.	12	IY=	54000.	13	IZ=	51000.	14	IXZ=	0.0	15	IR=	600.00	
16	CF=	0.0	17	RF=	0.0	18	CFPR=	30.000	19	KF=	185.00	20	LAMF=	1.0000	
21	OMFC=	2.9800	22	OMFT=	4.1000	23	CR=	0.0	24	RR=	0.0	25	CRPR=	150.00	
26	KR=	277.00	27	LAMR=	0.0	28	OMRC=	5.0750	29	OMRT=	4.3000	30	KRS=	0.18000	
31	RW=	16.125	32	SFSF=	0.40000E-01	33	FOT=	0.24250	34	A0=	-374.17	35	A1=	8.2500	
36	A2=	14845.	37	A3=	0.0	38	A4=	1.0000	39	TIR=	0.0	40	TOR=	0.0	
41	KSC=	2400.0	42	NG=	21.500	43	LAFC=	4.0000	44	LAFT=	10.000	45	LARC=	2.8000	
46	LART=	10.000	47	IFW=	11.000	48	IF=	0.0	49	IWF=	17.000	50	IWR=	17.000	
51	IDR=	0.60000	52	ARR=	3.2500	53	TSF=	0.0	54	KFS=	0.0	55	PI=	0.0	
56	YSA1=	4.2200	57	YSA2=	-4.2200	58	PHS1=	-0.26180E-01	59	PHS2=	0.26180E-01	60	CTSW=	1.0000	
61	IDF=	0.0	62	ARF=	0.0	63	P-IN=	0.0	64	Q-IN=	0.0	65	R-IN=	0.0	
66	U-IN=	30.000	67	V-IN=	0.0	68	W-IN=	0.0	69	X-IN=	0.0	70	Y-IN=	0.0	
71	Z-IN=	-35.729	72	THIN=	0.28244	73	PHIN=	0.0	74	PSIN=	0.0	75	DT=	0.10000E-01	
76	TN=	5.0000	77	KT1=	1770.0	78	KT2=	1770.0	79	KT3=	1770.0	80	KT4=	1770.0	
81	RPS1=	0.0	82	RPS2=	0.0	83	RPS3=	0.0	84	RPS4=	0.0	85	B1=	-0.21300E-04	
86	B2=	0.0	87	B3=	0.90700	88	B4=	0.0	89	D1DT=	0.0	90	D2DT=	0.0	
91	D3DT=	0.0	92	DELF=	-2.7800	93	DELR=	-3.1800	94	DEL3=	0.0	95	PHDT=	0.0	
96	PHIR=	0.0	97	DFW1=	0.0	98	DFW2=	0.0	99	U1PR=	0.0	100	U2PR=	0.0	
101	U3PR=	0.0	102	U4PR=	0.0	103	S1PR=	0.0	104	S2PR=	0.0	105	S3PR=	0.0	
106	S4PR=	0.0	107	PPRT=	1.0000	108	FREQ=	0.40000	109	RWSF=	20.000	110	TQMX=	4428.0	
111	KTQ=	738.00	112	VC=	0.0	113	MTSW=	0.0	114	DSWM=	52.000	115	TST=	1.0000	
116	DSLP=	1.0000	117	CGAM=	3.0000	118	CS=	3.0000	119	TQR=	0.0	120	TQF=	0.0	
121	PFL=	300.00	122	T1=	0.0	123	DSW=	0.0	124	=	0.0	125	ISW5=	0.0	
126	SW15=	0.0	127	PQSW=	0.0	128	VTPS=	3.0000	129	VHTP=	0.0	130	AMCR=	0.85000E-01	
131	ESP=	0.40000	132	KSL1=	0.25000E 06	133	KSL2=	0.25000E 06	134	AA1=	7.0000	135	AA2=	7.0000	
136	CCR=	0.0	137	CFCR=	0.0	138	AP=	5.6000	139	EP1=	0.0	140	EP2=	0.0	
141	AERO=	0.0	142	VYW =	0.0	143	OMXW=	0.0	144	OMZW=	0.0	145	RHOA=	7.5000	
146	CYP =	0.0	147	CYR =	0.0	148	CZAL=	0.0	149	CZQ =	0.0	150	CLP =	0.0	
151	CLR =	0.0	152	CMAL=	0.0	153	CMQ =	0.0	154	CNP =	0.0	155	CNR =	0.0	
156	SF =	0.0	157	VLEN=	0.0	158	REWV=	0.0	159	=	0.0	160	=	0.0	
161	=	0.0	162	=	0.0	163	=	0.0	164	=	0.0	165	=	0.0	
166	=	0.0	167	=	0.0	168	=	0.0	169	SNT=	72.000	170	SNSO=	72.000	
171	SNS1=	72.000	172	SNSW=	2.0000	173	DIST=	0.0	174	PL =	0.0	175	TSCP=	0.25000	
176	=	0.0	177	=	0.0	178	=	0.0	179	=	1.0000	180	PASS=	4.0000	
181	=	1.0000	182	SI1=	0.20000	183	SI2=	0.20000	184	SI3=	0.20000	185	SI4=	0.20000	
186	=	0.0	187	=	0.0	188	=	0.0	189	=	0.0	190	=	0.0	
191	=	0.0	192	MTQB=	1.0000	193	DCSW=	0.0	194	LDF=	0.0	195	LDRF=	0.0	
196	EK1=	-0.25000	197	EK2=	0.25000	198	BMPL=	0.0	199	BMPS=	0.0	200	BMPH=	1.5000	
201	XB=	0.0	202	APF1=	1.0700	203	APF2=	-0.66700E-04	204	APR1=	1.0700	205	APR2=	-0.66700E-04	
206	MUSF=	0.75000	207	MUSR=	0.75000	208	RCON=	0.30000E-01	209	=	1.0000	210	=	0.0	
211	=	0.0	212	=	0.0	213	=	0.0	214	=	0.0	215	=	0.0	
216	=	0.0	217	=	0.0	218	=	0.0	219	FEE1=	0.55000	220	FEE2=	-0.55000	
221	THE1=	3.5000	222	THE2=	3.5000	223	=	0.0	224	=	0.0	225	=	0.0	
226	=	0.0	227	=	0.0	228	=	0.0	229	=	0.0	230	=	0.0	
231	H1=	300.00	232	H2=	300.00	233	LAMO=	0.0	234	AKF1=	185.00	235	AKF2=	185.00	
236	AKF3=	293.75	237	AKF4=	293.75	238	BR1=	1.0000	239	BR2=	1.0000	240	BR3=	1.0000	
241	BR4=	1.0000	242	KCF=	-0.20000E-04	243	KCR=	-0.20000E-04	244	KSR=	0.15000E-05	245	RB1=	-0.21300E-04	
246	RB2=	0.0	247	RB3=	0.90700	248	RB4=	0.0	249	AFK1=	-0.54000E-03	250	AFK2=	0.62000E-03	
251	AFK3=	0.0	252	ARK1=	-0.54000E-03	253	ARK2=	0.62000E-03	254	ARK3=	0.0	255	OFC0=	0.0	
256	OFC1=	0.0	257	OFC2=	0.0	258	OFC3=	0.0	259	ORC0=	0.0	260	ORC1=	0.0	
261	ORC2=	0.0	262	ORC3=	0.0	263	CP0F=	0.0	264	CP1F=	0.0	265	CP2F=	0.0	
266	CP0R=	0.0	267	CP1R=	0.0	268	CP2R=	0.0	269	CR0F=	0.0	270	CR1F=	0.0	
271	CR2F=	0.0	272	CR0R=	0.0	273	CR1R=	0.0	274	CR2R=	0.0	275	=	0.0	
276	=	0.0	277	BMPN=	0.0	278	TQB0=	0.0	279	TQB1=	0.0	280	=	0.0	
281	=	1.0000	282	=	1.0000	283	=	0.0	284	HFC=	8.0500	285	HRC=	0.0	
286	DRSW=	0.0	287	AXLE=	1.0000	288	DUAL=	0.0	289	WEEL=	4.0000	290	ROT =	0.24250	
291	RA0 =	-374.17	292	RA1 =	8.2500	293	RA2 =	14845.	294	RA3 =	0.0	295	RA4 =	1.0000	

PARAMETER VALUES - MODEL C - VEHICLE MODEL * HSRT: FORD PICKUP (UNLOADED)

1	MS= 11.215	2	MUF= 0.70400	3	MUR= 0.87500	4	ZF= 16.054	5	ZR= 15.804
6	A= 54.740	7	B= 78.260	8	TF= 66.000	9	TR= 64.500	10	TSR= 44.750
11	IX= 7866.0	12	IY= 43501.	13	IZ= 40214.	14	IXZ= 0.0	15	IP= 600.00
16	CF= 0.0	17	RF= 0.0	18	CFPP= 3[illegible]	19	KF= 164.50	20	LAMF= 1.0000
21	OMFC= -1.2500	22	OMFT= 6.2500	23	CR= 0.0	24	RR= 0.0	25	CRPR= 150.00
26	KR= 298.00	27	LAMR= 1.0000	28	OMRC= -5.5000	29	OMRT= 4.0000	30	KRS= 0.54000E-01
31	RW= 15.375	32	SFSF= 0.40000E-01	33	ROT= 0.28400	34	A0= 202.42	35	A1= 10.313
36	A2= 7376.0	37	A3= 0.21540	38	A4= -1200.0	39	TIR = 0.0	40	TOR = 0.0
41	KSC= 4740.0	42	NG= 19.000	43	LAFC= 2.0000	44	LAFT= 10.000	45	LARC= 2.0000
46	LART= 10.000	47	IFW= 17.000	48	IF = 0.0	49	IWF= 17.000	50	IWR= 17.000
51	IDR= 0.60000	52	ARR= 3.2500	53	TSF = 5.5	54	KFS = 0.0	55	PI= 0.90000
56	YSA1= 4.2500	57	YSA2= -4.2500	58	PHS1=-0.26000E-01	59	PHS2= 0.26000E-01	60	CTSW= 1.0000
61	IDF= 0.0	62	ARF= 0.0	63	P-IN= 0.0	64	Q-IN= 0.0	65	R-IN= 0.0
66	U-IN= 40.000	67	V-IN= 0.0	68	W-IN= 0.0	69	X-IN= 0.0	70	Y-IN= 0.0
71	Z-IN= -30.857	72	THIN= 0.51828E-01	73	PHIN= 0.0	74	PSIN= 0.0	75	DT= 0.50000E-02
76	TN= 5.0000	77	KT1= 2700.0	78	KT2= 2700.0	79	KT3= 2700.0	80	KT4= 2700.0
81	RPS1= 0.0	82	RPS2= 0.0	83	RPS3= 0.0	84	RPS4= 0.0	85	B1=-0.32100E-04
86	B2=-0.20000E-02	87	B3= 0.91700	88	B4=-0.19191E-07	89	D1DT= 0.0	90	D2DT= 0.0
91	D3DT= 0.0	92	DELF= 0.0	93	DELR= 0.0	94	DEL3= 0.0	95	PHDT= 0.0
96	PHIR= 0.0	97	DFW1= 0.0	98	DFW2= 0.0	99	U1PR= 0.0	100	U2PR= 0.0
101	U3PR= 0.0	102	U4PR= 0.0	103	S1PR= 0.0	104	S2PR= 0.0	105	S3PR= 0.0
106	S4PR= 0.0	107	PPRT= 1.0000	108	FFF0= 0.40000	109	RWSF= 20.000	110	TQMX= 0.0
111	KTQ= 0.0	112	VC= 0.0	113	MTSW= 0.0	114	DSWM= 62.000	115	TST= 1.0000
116	FSLP= 1.0000	117	CGAM= 3.0000	118	CS= 3.0000	119	TQR= 0.0	120	TQF= 0.0
121	PFL= 300.00	122	T1= 0.0	123	DSW= 0.0	124	= 0.0	125	ISWS= 0.0
126	SW15= 0.0	127	PQSW= 0.0	128	VTPS= 3.0000	129	VHTP= 0.0	130	AMCR= 0.85000E-01
131	FSP= 0.0	132	KSL1= 0.40000E 06	133	KSL2= 0.40000E 06	134	AA1= 7.0000	135	AA2= 7.0000
136	CCR= 0.0	137	CFCR= 0.0	138	AP= 5.6000	139	EPI= 0.0	140	EP2= 0.0
141	AERO= 0.0	142	VYW = 0.0	143	OMXW= 0.0	144	OMZW= 0.0	145	RHOA= 0.0
146	CYP = 0.0	147	CYR = 0.0	148	CZAL= 0.0	149	CZQ = 0.0	150	CLP = 0.0
151	CLR = 0.0	152	CMAL= 0.0	153	CMQ = 0.0	154	CNP = 0.0	155	CNR = 0.0
156	SF = 0.0	157	VLEN= 0.0	158	REWV= 0.0	159	= 0.0	160	= 0.0
161	= 0.0	162	= 0.0	163	= 0.0	164	= 0.0	165	= 0.0
166	= 0.0	167	= 0.0	168	= 0.0	169	SNT= 72.000	170	SNSO= 72.000
171	SNS1= 72.000	172	SNSW= 2.0000	173	DIST= 0.0	174	PL = 0.0	175	TSCP= 0.25000
176	= 0.0	177	= 0.0	178	= 0.0	179	= 1.0000	180	PASS= 4.0000
181	= 1.0000	182	SI1= 0.20000	183	SI2= 0.20000	184	SI3= 0.20000	185	SI4= 0.20000
186	= 0.0	187	= 0.0	188	= 0.0	189	= 0.0	190	= 0.0
191	= 0.0	192	MTQR= 1.0000	193	DCSW= 0.0	194	LDF= 0.0	195	LDRF= 0.0
196	EK1=-0.25000	197	EK2= 0.25000	198	BMPL= 0.0	199	BMPS= 0.0	200	BMPH= 1.5000
201	XB= 0.0	202	APF1= 1.0000	203	APF2= 0.0	204	APR1= 1.0000	205	APR2= 0.0
206	MUSF= 0.75000	207	MUSR= 0.75000	208	BCON= 0.30000E-01	209	= 1.0000	210	= 0.0
211	= 0.0	212	= 0.0	213	= 0.0	214	= 0.0	215	= 0.0
216	= 0.0	217	= 0.0	218	= 0.0	219	FFF1= 0.55000	220	FFF2=-0.55000
221	THF1= 3.5000	222	THF2= 3.5000	223	= 0.0	224	= 0.0	225	= 0.0
226	= 0.0	227	= 0.0	228	= 0.0	229	= 0.0	230	= 0.0
231	H1= 2160.0	232	H2= 2160.0	233	LAMD= 0.0	234	AKF1= 164.50	235	AKF2= 164.50
236	AKF3= 298.00	237	AKF4= 298.00	238	BR1= 1.0000	239	BR2= 1.0000	240	BR3= 1.0000
241	BR4= 1.0000	242	KCF= 0.0	243	KCR= 0.0	244	KSR= 0.0	245	RB1=-0.32100E-04
246	RB2=-0.20000E-02	247	RB3= 0.91700	248	RB4=-0.19191E-07	249	AFK1=-0.48000E-03	250	AFK2= 0.48000E-03
251	AFK3= 0.0	252	ARK1=-0.48000E-03	253	ARK2= 0.48000E-03	254	ARK3= 0.0	255	OFC1= 0.0
256	OFC1= 0.0	257	OFC2= 0.0	258	OFC3= 0.0	259	ORCC= 0.0	260	ORC1= 0.0
261	ORC2= 0.0	262	ORC3= 0.0	263	CP1F= 0.0	264	CP1F= 0.0	265	CP2F= 0.0
266	CPOR= 0.0	267	CP1R= 0.0	268	CP2R= 0.0	269	CROF= 0.0	270	CP1F= 0.0
271	CR2F= 0.0	272	CROR= 0.0	273	CR1R= 0.0	274	CR2R= 0.0	275	= 0.0
276	= 0.0	277	BMPN= 0.0	278	TWE0= 0.0	279	TQB1= 0.0	280	= 0.0
281	= 1.0000	282	= 1.0000	283	= 0.0	284	HFC= 8.0500	285	HRC= 0.0
286	DRSW= 0.0	287	AXLE= 1.0000	288	DUAL= 0.0	289	WFFL= 4.0000	290	ROT = 0.28400
291	RA0 = 202.42	292	RA1 = 10.313	293	RA2 = 7376.0	294	RA3 = 0.21540	295	RA4 = -1200.0

PARAMETER VALUES - MODEL C - VEHICLE MODEL * HSR1: FORD PICKUP (LOADED)

1	MS= 16.348	2	MUF= 0.70400	3	MUR= 0.28750	4	ZF= 16.340	5	ZR= 16.090
6	A= 78.250	7	B= 54.750	8	IF= 60.000	9	IR= 64.500	10	TSR= 44.750
11	IX= 9024.0	12	IY= 66162.	13	IZ= 64.34.	14	IXZ= 0.0	15	IR= 600.00
16	CF= 0.0	17	KF= 0.0	18	CFPR= 20.000	19	KF= 164.50	20	LAMF= 1.0000
21	UMFC=-0.75000	22	UMFI= 6.7500	23	CR= 0.0	24	RR= 0.0	25	CRPR= 150.00
26	KR= 400.00	27	LAMR= 1.0000	28	UMRC= -3.0000	29	UMRI= 6.5000	30	KRS=-0.60000E-01
31	RW= 15.375	32	SFSF= 0.40000E-01	33	FBT= 0.28400	34	A0= 202.42	35	A1= 10.313
36	A2= 7376.0	37	A3= 0.21540	38	A4= -1200.0	39	TIR = 0.0	40	TOR = 0.0
41	KSC= 4740.0	42	NG= 18.000	43	LAMC= 2.0000	44	LAMI= 10.000	45	LAMC= 2.0000
46	LAMT= 10.000	47	IFW= 17.000	48	IR = 0.0	49	IWF= 17.000	50	IWR= 17.000
51	IDR= 0.60000	52	ARR= 3.2500	53	TSF = 0.0	54	KFS = 0.0	55	PI= 3.14000
56	YSA1= 4.2500	57	YSA2= -4.2500	58	PHS1=-0.26000E-01	59	PHS2= 0.26000E-01	60	CTSW= 1.0000
61	IDF= 0.0	62	ARF= 0.0	63	P-IN= 0.0	64	Q-IN= 0.0	65	R-IN= 0.0
66	U-IN= 40.000	67	V-IN= 0.0	68	W-IN= 0.0	69	X-IN= 0.0	70	Y-IN= 0.0
71	Z-IN= -30.907	72	THIN= 0.20201	73	PHIN= 0.0	74	PSIN= 0.0	75	D1= 0.50000E-02
76	TN= 5.0000	77	KT1= 2700.0	78	KT2= 2700.0	79	KT3= 2700.0	80	KT4= 2700.0
81	RPS1= 0.0	82	RPS2= 0.0	83	RPS3= 0.0	84	RPS4= 0.0	85	B1=-0.32100E-04
86	B2=-0.20000E-02	87	B3= 0.91700	88	B4=-0.19191E-07	89	D1D1= 0.0	90	D2D1= 0.0
91	D3D1= 0.0	92	DELF= 0.0	93	DELR= 0.0	94	DEL3= 0.0	95	PHD1= 0.0
96	PHIR= 0.0	97	DFW1= 0.0	98	DFW2= 0.0	99	U1PR= 0.0	100	U2PR= 0.0
101	U3PR= 0.0	102	U4PR= 0.0	103	S1PR= 0.0	104	S2PR= 0.0	105	S3PR= 0.0
106	S4PR= 0.0	107	PPRT= 1.0000	108	FREQ= 0.40000	109	RWSE= 20.000	110	TGMX= 0.0
111	KTG= 0.0	112	VG= 0.0	113	MTSW= 0.0	114	DSWM= 62.000	115	TS1= 1.0000
116	DSLP= 1.0000	117	CGAM= 3.0000	118	CS= 3.0000	119	TGR= 0.0	120	TGF= 0.0
121	PFL= 300.00	122	T1= 0.0	123	DSW= 0.0	124	= 0.0	125	ISWS= 0.0
126	SW15= 0.0	127	PQSW= 0.0	128	VTPS= 3.0000	129	VHTP= 0.0	130	AMCR= 0.85000E-01
131	ESP= 0.0	132	KSL1= 0.40000E 06	133	KSL2= 0.40000E 06	134	AA1= 7.0000	135	AA2= 7.0000
136	CCR= 0.0	137	CFCR= 0.0	138	AP= 5.6000	139	EP1= 0.0	140	EP2= 0.0
141	AERO= 0.0	142	VYW = 0.0	143	OMXW= 0.0	144	OMZW= 0.0	145	PHOA= 0.0
146	CYP = 0.0	147	CYR = 0.0	148	CZAL= 0.0	149	CZQ = 0.0	150	CLP = 0.0
151	CLR = 0.0	152	CMAL= 0.0	153	CMQ = 0.0	154	CNP = 0.0	155	CNR = 0.0
156	SF = 0.0	157	VLEN= 0.0	158	REWV= 0.0	159	= 0.0	160	= 0.0
161	= 0.0	162	= 0.0	163	= 0.0	164	= 0.0	165	= 0.0
166	= 0.0	167	= 0.0	168	= 0.0	169	SN1= 72.000	170	SNS = 72.000
171	SNS1= 72.000	172	SNSW= 2.0000	173	DIST= 0.0	174	PL = 0.0	175	TSCP= 0.25000
176	= 0.0	177	= 0.0	178	= 0.0	179	= 1.0000	180	PASS= 4.0000
181	= 1.0000	182	SI1= 0.20000	183	SI2= 0.20000	184	SI3= 0.20000	185	SI4= 0.20000
186	= 0.0	187	= 0.0	188	= 0.0	189	= 0.0	190	= 0.0
191	= 0.0	192	MTGB= 1.0000	193	DCSW= 0.0	194	LDF= 0.0	195	LDRF= 0.0
196	EK1=-0.25000	197	EK2= 0.25000	198	BMPL= 0.0	199	BMPS= 0.0	200	BMPH= 1.5000
201	XB= 0.0	202	APF1= 1.0000	203	APF2= 0.0	204	APR1= 1.0000	205	APR2= 0.0
206	MUSF= 0.75000	207	MUSR= 0.75000	208	RCON= 0.30000E-01	209	= 1.0000	210	= 0.0
211	= 0.0	212	= 0.0	213	= 0.0	214	= 0.0	215	= 0.0
216	= 0.0	217	= 0.0	218	= 0.0	219	FLE1= 1.55000	220	FLE2=-1.55000
221	THE1= 3.5000	222	THE2= 3.5000	223	= 0.0	224	= 0.0	225	= 0.0
226	= 0.0	227	= 0.0	228	= 0.0	229	= 0.0	230	= 0.0
231	H1= 2160.0	232	H2= 2160.0	233	LAMD= 0.0	234	AKF1= 164.50	235	AKF2= 164.50
236	AKF3= 400.00	237	AKF4= 400.00	238	BR1= 1.0000	239	BR2= 1.0000	240	BR3= 1.0000
241	BR4= 1.0000	242	KCF= 0.0	243	KCR= 0.0	244	KSR= 0.0	245	RB1=-0.32100E-04
246	RB2=-0.20000E-02	247	RB3= 0.91700	248	RB4=-0.19191E-07	249	AFK1=-0.48000E-03	250	AFK2= 0.48000E-03
251	AFK3= 0.0	252	ARK1=-0.48000E-03	253	ARK2= 0.48000E-03	254	ARK3= 0.0	255	DFC0= 0.0
256	DFC1= 0.0	257	DFC2= 0.0	258	DFC3= 0.0	259	DRC0= 0.0	260	DFC1= 0.0
261	DRC2= 0.0	262	DRC3= 0.0	263	CP0F= 0.0	264	CP1F= 0.0	265	CP2F= 0.0
266	CP0R= 0.0	267	CP1R= 0.0	268	CP2R= 0.0	269	CR0F= 0.0	270	CR1F= 0.0
271	CR2F= 0.0	272	CR0R= 0.0	273	CR1R= 0.0	274	CR2R= 0.0	275	= 0.0
276	= 0.0	277	BMPN= 0.0	278	TQB0= 0.0	279	TQB1= 0.0	280	= 0.0
281	= 1.0000	282	= 1.0000	283	= 0.0	284	HFC= 8.0500	285	HRC= 0.0
286	DRSW= 0.0	287	AXLE= 1.0000	288	DUAL= 0.0	289	WHEL= 4.0000	290	FBT = 0.28400
291	RA0 = 202.42	292	RA1 = 10.313	293	RA2 = 7376.0	294	RA3 = 0.21540	295	RA4 = -1200.0

PARAMETER VALUES - MODEL C - VEHICLE MODEL * WHITE TRUCK (UNLOADED)

1	PS= 22.210	2	MUE= 4.4120	3	PHI= 1.3440	4	ZF= 23.900	5	ZR= 23.900
6	A= 47.160	7	B= 108.84	8	TF= 79.90	9	TR= 71.250	10	TSR= 38.250
11	IX= 22257.	12	IY= 50011.	13	IZ= 63428.	14	IXZ= 0.0	15	IR= 4458.0
16	CF= 0.0	17	RF= 0.0	18	CFPR= 950.00	19	KF= 1300.0	20	LAMF= 1.0000
21	OMFC= -4.0000	22	OMFT= 4.0000	23	CR= 0.0	24	RR= 0.0	25	CRPF= 2200.0
26	KR= 5000.0	27	LAMR= 1.0000	28	OMRC= -4.0000	29	OMRT= 4.0000	30	KRS= 0.14000
31	RW= 20.500	32	SFSF= 0.60000E-01	33	FDT= 0.50000	34	AS= 819.54	35	A1= 8.2380
36	A2= 16915.	37	A3= 0.0	38	A4= 1.0000	39	TIR = 64.650	40	TOR = 77.850
41	KSC= 8000.0	42	NG= 30.000	43	LAFC= 3.0000	44	LAFT= 10.000	45	LARC= 3.0000
46	LART= 10.000	47	IFW= 27.000	48	IR = 3745.0	49	IWF= 206.00	50	IWR= 462.00
51	IDR= 1.5000	52	ARR= 4.0000	53	TSF = 32.500	54	KFS =-0.27000	55	PI= 0.0
56	YSA1= 10.000	57	YSA2= -10.000	58	PHS1= 0.0	59	PHS2= 0.0	60	CTSW= 1.0000
61	IDF= 0.0	62	ARF= 0.0	63	P-IN= 0.0	64	Q-IN= 0.0	65	R-IN= 0.0
66	U-IN= 45.000	67	V-IN= 0.0	68	W-IN= 0.0	69	X-IN= 0.0	70	Y-IN= 0.0
71	Z-IN= -44.074	72	THIN=-0.10585	73	PHIN= 0.0	74	PSIN= 0.0	75	DT= 0.50000E-02
76	IN= 5.0000	77	KT1= 9400.0	78	KT2= 9400.0	79	KT3= 9400.0	80	KT4= 9400.0
81	RPS1= 0.0	82	RPS2= 0.0	83	RPS3= 0.0	84	RPS4= 0.0	85	R1=-0.72000E-05
86	R2=-0.10000E-02	87	R3= 0.0	88	R4= 1.0000	89	D1DT= 0.0	90	D2DT= 0.0
91	D3DT= 0.0	92	DELF= 0.0	93	DELR= 0.0	94	DEL3= 0.0	95	PHDT= 0.0
96	PHI2= 0.0	97	DFW1= 0.0	98	DFW2= 0.0	99	U1PR= 0.0	100	U2PR= 0.0
101	U3PR= 0.0	102	U4PR= 0.0	103	S1PR= 0.0	104	S2PR= 0.0	105	S3PR= 0.0
106	S4PR= 0.0	107	PPRT= 1.0000	108	FREC= 0.40000	109	RWSF= 25.000	110	TOMX= 0.0
111	KTO= 0.0	112	VC= 0.0	113	MTSW= 0.0	114	DSWM= 150.00	115	TST= 1.0000
116	DSLP= 1.0000	117	CGAM= 3.0000	118	CS= 3.0000	119	TOP= 0.0	120	TDF= 0.0
121	PFL= 600.00	122	T1= 0.0	123	DSW= 0.0	124	= 0.0	125	ISW= 0.0
126	SW15= 0.0	127	P0SW= 0.0	128	VTPS= 3.0000	129	VHTP= 0.0	130	ANCR= 0.78000E-01
131	FSP= 0.0	132	KSL1= 0.15000E 06	133	KSL2= 0.15000E 06	134	AA1= 7.0000	135	AA2= 7.0000
136	CCR= 11.000	137	CFCP= 120.00	138	AP= 7.0000	139	FP1= 0.0	140	FP2= 0.0
141	AFPO= 0.0	142	VYW = 0.0	143	OMXW= 0.0	144	OMZW= 0.0	145	PHOA= 0.0
146	CYP = 0.0	147	CYR = 0.0	148	CZAL= 0.0	149	CZQ = 0.0	150	CLP = 0.0
151	CLR = 0.0	152	CMAL= 0.0	153	CMQ = 0.0	154	CNP = 0.0	155	CNR = 0.0
156	SF = 0.0	157	VLFN= 0.0	158	RFWV= 0.0	159	= 0.0	160	= 0.0
161	= 0.0	162	= 0.0	163	= 0.0	164	= 0.0	165	= 0.0
166	= 0.0	167	= 0.0	168	= 0.0	169	SNT= 75.000	170	SNSC= 75.000
171	SNS1= 75.000	172	SNSW= 2.0000	173	DIST= 0.0	174	PL = 0.0	175	TSCP= 0.25000
176	= 0.0	177	= 0.0	178	= 0.0	179	= 0.0	180	PASS= 4.0000
181	= 0.0	182	S11= 0.20000	183	S12= 0.20000	184	S13= 0.20000	185	S14= 0.20000
186	= 0.0	187	= 0.0	188	= 0.0	189	= 0.0	190	= 0.0
191	= 0.0	192	MTOR= 1.0000	193	DCSW= 0.0	194	LDF= 0.0	195	LDRF= 0.0
196	FK1= 0.0	197	FK2= 0.0	198	PMPL= 0.0	199	PMPS= 0.0	200	PMPH= 1.5000
201	XB= 0.0	202	APF1= 0.92000	203	APF2= 0.0	204	APR1= 0.92000	205	APR2= 0.0
206	MUSF= 0.70000	207	MUSR= 0.70000	208	BCON= 0.30000E-01	209	= 1.0000	210	= 0.0
211	= 0.0	212	= 0.0	213	= 0.0	214	= 0.0	215	= 0.0
216	= 0.0	217	= 0.0	218	= 0.0	219	FFF1= 0.0	220	FFF2= 0.0
221	THF1= 0.0	222	THF2= 0.0	223	= 0.0	224	= 0.0	225	= 0.0
226	= 0.0	227	= 0.0	228	= 0.0	229	= 0.0	230	= 0.0
231	H1= 400.00	232	H2= 400.00	233	LAMD= 0.0	234	AKF1= 1300.0	235	AKF2= 1300.0
236	AKF3= 5000.0	237	AKF4= 5000.0	238	BR1= 1.0000	239	BR2= 1.0000	240	BR3= 1.0000
241	BR4= 1.0000	242	KCF= 0.0	243	KCR= 0.0	244	KSR= 0.0	245	BB1=-0.72000E-05
246	BB2=-0.10000E-02	247	BB3= 0.85010	248	BB4= 0.0	249	AFK1=-0.36720E-03	250	AFK2= 0.36000E-03
251	AFK3= 0.0	252	ARK1=-0.36720E-03	253	ARK2= 0.36000E-03	254	ARK3= 0.0	255	OFC0= 0.0
256	OFC1= 0.0	257	OFC2= 0.0	258	OFC3= 0.0	259	ORC0= 0.0	260	ORC1= 0.0
261	ORC2= 0.0	262	ORC3= 0.0	263	CP0F= 0.0	264	CP1F= 0.0	265	CP2F= 0.0
266	CP0R= 0.0	267	CP1R= 0.0	268	CP2R= 0.0	269	CR0F= 0.0	270	CR1F= 0.0
271	CR2F= 0.0	272	CR0R= 0.0	273	CR1R= 0.0	274	CR2R= 0.0	275	= 0.0
276	= 0.0	277	BMPN= 0.0	278	TOP0= 0.0	279	TOR1= 0.0	280	= 0.0
281	= 0.0	282	= 0.0	283	= 0.0	284	HFC= 0.0	285	HRC= 0.0
286	DRSW= 0.0	287	AXLE= 0.0	288	DUAL= 1.0000	289	WFEL= 6.0000	290	ROT = 0.50000
291	RA0 = 819.54	292	RA1 = 8.2380	293	RA2 = 16915.	294	RA3 = 0.0	295	RA4 = 1.0000

Table A-7

PARAMETER VALUES - MODEL C - VEHICLE MODEL * WHITE TRUCK (LOADED)

1	PS= 65.500	2	MDF= 4.5120	3	NDS= 5.5000	4	ZF= 32.000	5	ZR= 31.500
6	A= 104.42	7	B= 51.576	8	IF= 79.5	9	TF= 71.25	10	TSR= 36.250
11	IX= 40509.	12	IY= 0.22181E 06	13	IZ= 0.22151E 06	14	IXZ= 0.0	15	IR= 4456.0
16	CF= 0.0	17	RF= 0.0	18	CFFF= 500.00	19	KF= 15000.0	20	LAMF= 1.0000
21	LMFC= -4.0000	22	LMFI= 4.0000	23	CF= 0.0	24	RF= 0.0	25	CFPR= 2200.0
26	KR= 5000.0	27	LAMR= 1.0000	28	LMRC= -4.0000	29	LMRI= 4.0000	30	KRS= [illegible]
31	RW= 20.500	32	SFSF= 0.60000E-01	33	FCT= 0.0000	34	AC= 819.54	35	AI= 0.2380
36	A2= 16915.	37	A3= 0.0	38	A4= 1.0000	39	TTP = 64.650	40	TCR = 77.850
41	KSC= 8000.0	42	SS= 30.000	43	LAFC= [illegible]	44	LAFT= 17.000	45	LAFC= 36.000
46	LART= 1.0000	47	IFW= 27.000	48	IF = 2745.0	49	IWF= 206.00	50	IWR= 462.00
51	IPP= 1.5000	52	ARR= 6.0000	53	ISS = 32.500	54	KFS =-0.27000	55	PI= 0.0
56	YSA1= 10.000	57	YSA2= -10.000	58	PHS1= 0.0	59	PHS2= 0.0	60	CISW= 1.0000
61	ICF= 0.0	62	APF= 0.0	63	P-IN= 0.0	64	Q-IN= 0.0	65	R-IN= 0.0
66	U-IN= 40.000	67	V-IN= 0.0	68	W-IN= 0.0	69	X-IN= 0.0	70	Y-IN= 0.0
71	Z-IN= -51.649	72	THIN= 0.17185	73	PFIN= 0.0	74	PSIN= 0.0	75	DT= 0.50000E-02
76	TN= 5.0000	77	KT1= 9400.0	78	KT2= 9400.0	79	KT3= 9400.0	80	KT4= 9400.0
81	KPS1= 0.0	82	KPS2= 0.0	83	KPS3= 0.0	84	KPS4= 0.0	85	B1=-0.72000E-05
86	B2=-0.10000E-02	87	B3= 0.05010	88	B4= 0.0	89	D1DT= 0.0	90	D2DT= 0.0
91	D3DT= 0.0	92	DFLF= 1.1200	93	DFLR= 1.1200	94	DFL3= 0.0	95	PHDT= 0.0
96	PHIR= 0.0	97	DFW1= 0.0	98	DFW2= 0.0	99	U1PR= 0.0	100	U2PR= 0.0
101	U3PR= 0.0	102	U4PR= 0.0	103	S1PR= 0.0	104	S2PR= 0.0	105	S3PR= 0.0
106	S4PR= 0.0	107	PPAI= 1.0000	108	PPED= 0.40000	109	RWSF= 25.000	110	TUMX= 0.0
111	KTU= 0.0	112	VC= 0.0	113	MTSW= 0.0	114	DSWR= 150.00	115	TST= 1.0000
116	LSLP= 1.0000	117	CGAM= 5.0000	118	CS= 3.0000	119	TUR= 0.0	120	TUF= 0.0
121	PFL= 600.00	122	TI= 0.0	123	DSW= 0.0	124	= 0.0	125	ISW= 0.0
126	SWIS= 0.0	127	FWSW= 0.0	128	VTPS= 3.0000	129	VHTP= 0.0	130	AMCK= 0.78000E-01
131	FCP= 0.0	132	KSL1= 0.15000E 06	133	KSL2= 0.15000E 06	134	AA1= 7.0000	135	AA2= 7.0000
136	CCR= 11.000	137	CFCR= 120.00	138	AP= 7.0000	139	EP1= 0.0	140	EP2= 0.0
141	AERO= 0.0	142	VYW = 0.0	143	GMXW= 0.0	144	GMZW= 0.0	145	RHOA= 0.0
146	CYP = 0.0	147	CYR = 0.0	148	CZAL= 0.0	149	CZL = 0.0	150	CLP = 0.0
151	CLR = 0.0	152	CMAL= 0.0	153	CML = 0.0	154	CNP = 0.0	155	CNR = 0.0
156	SF = 0.0	157	VLEN= 0.0	158	REWV= 0.0	159	= 0.0	160	= 0.0
161	= 0.0	162	= 0.0	163	= 0.0	164	= 0.0	165	= 0.0
166	= 0.0	167	= 0.0	168	= 0.0	169	SNT= 75.000	170	SNSW= 75.000
171	SNS1= 75.000	172	SNSW= 1.0000	173	DIST= 0.0	174	PL = 0.0	175	TSCP= 0.25000
176	= 0.0	177	= 0.0	178	= 0.0	179	= 0.0	180	PASS= 4.0000
181	= 0.0	182	SI1= 0.20000	183	SI2= 0.20000	184	SI3= 0.20000	185	SI4= 0.20000
186	= 0.0	187	= 0.0	188	= 0.0	189	= 0.0	190	= 0.0
191	= 0.0	192	MIQ= 1.0000	193	DCSW= 0.0	194	LDF= 0.0	195	LDRF= 0.0
196	FK1= 0.0	197	FK2= 0.0	198	PMFL= 0.0	199	FMPS= 0.0	200	FMPF= 1.5000
201	XB= 0.0	202	APF1= 0.92000	203	APF2= 0.0	204	APR1= 0.92000	205	APR2= 0.0
206	MUSF= 0.70000	207	MUSR= 0.70000	208	ACCN= 0.50000E-01	209	= 1.0000	210	= 0.0
211	= 0.0	212	= 0.0	213	= 0.0	214	= 0.0	215	= 0.0
216	= 0.0	217	= 0.0	218	= 0.0	219	FEF1= 0.0	220	FEE2= 0.0
221	THI1= 0.0	222	THI2= 0.0	223	= 0.0	224	= 0.0	225	= 0.0
226	= 0.0	227	= 0.0	228	= 0.0	229	= 0.0	230	= 0.0
231	L1= 400.00	232	L2= 400.00	233	LAND= 0.0	234	AKF1= 1500.0	235	AKF2= 1500.0
236	AKF3= 1500.0	237	AKF4= 1500.0	238	BR1= 1.0000	239	BR2= 1.0000	240	BR3= 1.0000
241	BR4= 1.0000	242	KCF= 0.0	243	KCR= 0.0	244	KSR= 0.0	245	PB1=-0.72000E-05
246	PB2=-0.10000E-02	247	PB3= 0.05010	248	PB4= 0.0	249	AFK1=-0.36720E-03	250	AFK2= 0.36000E-03
251	AFK3= 0.0	252	AKK1=-0.36720E-03	253	AKK2= 0.36000E-03	254	AKK3= 0.0	255	OFC0= 0.0
256	OFC1= 0.0	257	OFC2= 0.0	258	OFC3= 0.0	259	ORC = 0.0	260	ORC1= 0.0
261	ORC2= 0.0	262	ORC3= 0.0	263	CPCF= 0.0	264	CP1F= 0.0	265	CP2F= 0.0
266	CPCR= 0.0	267	CP1R= 0.0	268	CP2R= 0.0	269	CKOF= 0.0	270	CP1F= 0.0
271	CK2F= 0.0	272	CKOR= 0.0	273	CK1R= 0.0	274	CK2R= 0.0	275	= 0.0
276	= 0.0	277	BMPV= 0.0	278	TCP= 0.0	279	TCP1= 0.0	280	= 0.0
281	= 0.0	282	= 0.0	283	= 0.0	284	HFC= 0.0	285	HFC= 0.0
286	IRSW= 0.0	287	AKLS= 0.0	288	TOAL= 1.0000	289	WEEL= 6.0000	290	PCT = 0.50000
291	RA0 = 819.54	292	RA1 = 0.2380	293	RA2 = 16915.	294	RA3 = 0.0	295	RA4 = 1.0000

PARAMETER VALUES - MODEL C - VEHICLE MODEL = INTERCITY BUS (12 AXLE)

1	MS=	47.670	2	MUF=	4.5100	3	MUR=	5.3700	4	ZF=	27.000	5	ZR=	27.000					
6	A=	172.50	7	B=	87.450	8	TF=	79.000	9	TR=	66.500	10	TSP=	31.250					
11	IX=	65900.	12	IY=	0.11089E 07	13	IZ=	0.11055E 07	14	IXZ=	0.0	15	IR=	4458.0					
16	CF=	9.5000	17	RF=	0.0	18	CFPR=	0.0	19	KF=	550.00	20	LAMF=	1.0000					
21	OMFC=	-1.0000	22	OMFT=	4.2500	23	CR=	19.000	24	RR=	0.21600E 06	25	CRPR=	0.0					
26	KR=	1100.0	27	LAMR=	1.0000	28	CMRC=	-1.0000	29	OMRT=	4.2500	30	KRS=	0.0					
31	RM=	22.000	32	SFSF=	0.15000	33	FOT=	0.50000	34	AO=	3054.0	35	A1=	9.1600					
36	A2=	20004.	37	A3=	0.0	38	A4=	1.0000	39	TIR =	54.000	40	TOR =	79.000					
41	KSC=	8000.0	42	NG=	30.000	43	LAFC=	2.0000	44	LAFT=	10.000	45	LARC=	2.0000					
46	LART=	10.000	47	IFW=	27.000	48	IF =	3748.0	49	INF=	600.00	50	IWR=	900.00					
51	IDR=	1.5000	52	ARR=	4.0000	53	TSF =	45.000	54	KFS =	0.0	55	PT=	1.2000					
56	YSA1=	5.0000	57	YSA2=	-5.0000	58	PHS1=	-0.10000E 00	59	PHS2=	0.10000E 00	60	CTSW=	1.0000					
61	IDF=	0.0	62	ARF=	0.0	63	P-IN=	0.0	64	Q-IN=	0.0	65	R-IN=	0.0					
66	U-IN=	40.000	67	V-IN=	0.0	68	W-IN=	0.0	69	X-IN=	0.0	70	Y-IN=	0.0					
71	Z-IN=	-48.406	72	THIN=	-0.15889E-01	73	PHIN=	0.0	74	PSIN=	0.0	75	DT=	0.50000E-02					
76	TN=	5.0000	77	KT1=	5500.0	78	KT2=	5500.0	79	KT3=	5500.0	80	KT4=	5500.0					
81	RPS1=	0.0	82	RPS2=	0.0	83	RPS3=	0.0	84	RPS4=	0.0	85	B1=	0.0					
86	B2=	0.0	87	B3=	0.84200	88	B4=	0.0	89	D1DT=	0.0	90	D2DT=	0.0					
91	D3DT=	0.0	92	DELF=	0.0	93	DELR=	0.0	94	DEL3=	0.0	95	PHDT=	0.0					
96	PHIR=	0.0	97	DFW1=	0.0	98	DFW2=	0.0	99	U1PR=	0.0	100	U2PR=	0.0					
101	U3PR=	0.0	102	U4PR=	0.0	103	S1PR=	0.0	104	S2PR=	0.0	105	S3PR=	0.0					
106	S4PR=	0.0	107	PPRT=	1.0000	108	FREQ=	0.40000	109	RWSF=	25.000	110	TQMX=	0.0					
111	KTQ=	0.0	112	VC=	0.0	113	MTSW=	0.0	114	DSWM=	150.00	115	TST=	1.0000					
116	DSLP=	1.0000	117	CGAM=	3.0000	118	CS=	3.0000	119	TQR=	0.0	120	TQF=	0.0					
121	PFL=	600.00	122	T1=	0.0	123	DSW=	0.0	124	=	0.0	125	ISW5=	0.0					
126	SW15=	0.0	127	PQSW=	0.0	128	VTPS=	3.0000	129	VHTP=	0.0	130	AMCR=	0.78000E-01					
131	ESP=	0.0	132	KSL1=	0.15000E 06	133	KSL2=	0.15000E 06	134	AA1=	13.000	135	AA2=	13.000					
136	CCR=	40.000	137	CFCR=	0.0	138	AP=	13.000	139	EP1=	0.0	140	EP2=	0.0					
141	AERO=	0.0	142	VYW =	0.0	143	CMXW=	0.0	144	CMZW=	0.0	145	RHOA=	0.0					
146	CYP =	0.0	147	CYR =	0.0	148	CZAL=	0.0	149	CZQ =	0.0	150	CLP =	0.0					
151	CLR =	0.0	152	CMAL=	0.0	153	CMQ =	0.0	154	CNP =	0.0	155	CNR =	0.0					
156	SF =	0.0	157	VLEN=	0.0	158	REWV=	0.0	159	=	0.0	160	=	0.0					
161	=	0.0	162	=	0.0	163	=	0.0	164	=	0.0	165	=	0.0					
166	=	0.0	167	=	0.0	168	=	0.0	169	SNT=	75.000	170	SNS0=	75.000					
171	SNS1=	75.000	172	SNSW=	2.0000	173	DIST=	0.0	174	PL =	0.0	175	TSCP=	0.25000					
176	=	0.0	177	=	0.0	178	=	0.0	179	=	0.0	180	PASS=	4.0000					
181	=	0.0	182	SI1=	0.20000	183	SI2=	0.20000	184	SI3=	0.20000	185	SI4=	0.20000					
186	=	0.0	187	=	0.0	188	=	0.0	189	=	0.0	190	=	0.0					
191	=	0.0	192	MTQB=	1.0000	193	DCSW=	0.0	194	LDF=	0.0	195	LDRF=	0.0					
196	EK1=	0.0	197	EK2=	0.0	198	BMPL=	0.0	199	BMPS=	0.0	200	BMPH=	1.5000					
201	XB=	0.0	202	APF1=	1.0000	203	APF2=	0.0	204	APR1=	1.0000	205	APR2=	0.0					
206	MUSF=	0.68000	207	MUSR=	0.68000	208	BCON=	0.30000E-01	209	=	1.0000	210	=	0.0					
211	=	0.0	212	=	0.0	213	=	0.0	214	=	0.0	215	=	0.0					
216	=	0.0	217	=	0.0	218	=	0.0	219	FEE1=	0.0	220	FEE2=	0.0					
221	THE1=	0.0	222	THE2=	0.0	223	=	0.0	224	=	0.0	225	=	0.0					
226	=	0.0	227	=	0.0	228	=	0.0	229	=	0.0	230	=	0.0					
231	H1=	2160.0	232	H2=	2160.0	233	LAMD=	0.0	234	AKF1=	550.00	235	AKF2=	550.00					
236	AKF3=	1100.0	237	AKF4=	1100.0	238	BR1=	1.0000	239	BR2=	1.0000	240	BR3=	1.0000					
241	BR4=	1.0000	242	KCF=	0.0	243	KCR=	0.0	244	KSR=	0.0	245	RB1=	0.0					
246	RB2=	0.0	247	RB3=	0.84200	248	RB4=	0.0	249	AFK1=	-0.36000E-03	250	AFK2=	0.40800E-03					
251	AFK3=	0.0	252	AFK1=	-0.36000E-03	253	AFK2=	0.40800E-03	254	AFK3=	0.0	255	OFC0=	0.0					
256	OFC1=	0.0	257	OFC2=	0.0	258	OFC3=	0.0	259	ORC0=	0.0	260	ORC1=	0.0					
261	ORC2=	0.0	262	ORC3=	0.0	263	CP0F=	0.0	264	CP1F=	0.0	265	CP2F=	0.0					
266	CP0R=	0.0	267	CP1R=	0.0	268	CP2R=	0.0	269	CR0F=	0.0	270	CR1F=	0.0					
271	CR2F=	0.0	272	CR0R=	0.0	273	CR1R=	0.0	274	CR2R=	0.0	275	=	0.0					
276	=	0.0	277	BMPN=	0.0	278	TQB0=	0.0	279	TQB1=	0.0	280	=	0.0					
281	=	0.0	282	=	0.0	283	=	0.0	284	HFC=	0.0	285	HRC=	0.0					
286	DRSW=	0.0	287	AXLE=	0.0	288	DUAL=	1.0000	289	WEEL=	6.0000	290	ROT =	0.50000					
291	RA0 =	3054.0	292	RA1 =	9.1600	293	RA2 =	20004.	294	RA3 =	0.0	295	RA4 =	1.0000					

Table A-9

PARAMETER VALUES – MODEL C – VEHICLE MODEL 4 INTERCITY BUS (LOADED)

1	MS= [illegible]	2	MIF= [illegible]	3	[illegible]	4	ZF= 23.670	5	ZR= 23.670
6	A= [illegible]	7	[illegible]	8	[illegible]	9	IP= [illegible]	10	TSP= 51.250
11	IY= 75770.	12	TY= [illegible]	13	[illegible]	14	IXZ= 0.0	15	IR= [illegible]
16	CF= 9.5000	17	[illegible] 0.0	18	[illegible]	19	KF= [illegible]	20	LAMF= 1.0000
21	CMFC=-0.70000	22	CMFT= 0.40000	23	CR= [illegible]	24	[illegible] 0.21600E 06	25	CRPR= 0.0
26	KP= 2000.0	27	LAMR= 1.0000	28	CMRC= [illegible]	29	CMRT= 1.2000	30	KRS= 0.55000E-01
31	PW= [illegible]	32	SFSR= [illegible]	33	[illegible]	34	AF= 3054.0	35	A1= 9.1600
36	A2= 20004.	37	A3= 0.0	38	A4= 1.0000	39	TIP= [illegible]	40	TCP= 79.000
41	KSC= 6000.0	42	SS= 30.000	43	LARC= [illegible]	44	LAFT= [illegible]	45	LARC= 1.7000
46	LAST= 0.70000	47	IEW= 27.000	48	IR= [illegible]	49	IWF= [illegible]	50	IWF= 400.00
51	IDR= 1.5000	52	APR= 4.0000	53	TSR= [illegible]	54	KFS= 0.0	55	PT= 1.2000
56	YSA1= [illegible]	57	YSA2= [illegible]	58	PHS1=-0.10000E 00	59	PHS2= 0.10000E 00	60	CTSW= 1.0000
61	IDF= 0.0	62	ARF= 0.0	63	P-IN= 0.0	64	Q-IN= 0.0	65	R-IN= 0.0
66	U-IN= 40.000	67	V-IN= 0.0	68	W-IN= 0.0	69	X-IN= 0.0	70	Y-IN= 0.0
71	Z-IN= -54.773	72	THIN=[illegible]E-01	73	PHIN= 0.0	74	PSIN= 0.0	75	DT= 0.50000E-02
76	TN= 5.0000	77	KT1= 5500.0	78	KT2= 5500.0	79	KT3= 5500.0	80	KT4= 5500.0
81	FPS1= 0.0	82	RPS2= 0.0	83	RPS3= 0.0	84	RPS4= 0.0	85	R1= 0.0
86	R2= 0.0	87	R3= 0.84200	88	R4= 0.0	89	DIDT= 0.0	90	DRDT= 0.0
91	D2DT= 0.0	92	DELF= 0.0	93	DELR= 0.0	94	DEL3= 0.0	95	PHDT= 0.0
96	PHIR= 0.0	97	DEW1= 0.0	98	DEW2= 0.0	99	U1PR= 0.0	100	U2PR= 0.0
101	U3PR= 0.0	102	U4PR= 0.0	103	S1PR= 0.0	104	S2PR= 0.0	105	S3PR= 0.0
106	S4PR= 0.0	107	PPRT= 1.0000	108	FRFC= 0.40000	109	PWSF= 25.000	110	TOMX= 0.0
111	KTO= 0.0	112	VC= 0.0	113	MTSW= 0.0	114	DSWM= 150.00	115	TSI= 1.0000
116	ESLP= 1.0000	117	CGAM= 3.0000	118	CS= [illegible]	119	TOF= 0.0	120	TOF= 0.0
121	PFL= 600.00	122	T1= 0.0	123	DSW= 0.0	124	= 0.0	125	ISW5= 0.0
126	SW1S= 0.0	127	POSW= 0.0	128	VTPS= [illegible]	129	VHTP= [illegible]	130	AMCR= 0.76000E-01
131	ESP= 0.0	132	KSL1= 0.15000E 06	133	KSL2= 0.15000E 06	134	AA1= 13.000	135	AA2= 13.000
136	CCP= 40.000	137	CHCR= 0.0	138	AP= 13.000	139	EP1= 0.0	140	EP2= 0.0
141	AERO= 0.0	142	VYW = 0.0	143	OMXN= 0.0	144	OMZW= 0.0	145	RHOA= 0.0
146	CYP = 0.0	147	CYR = 0.0	148	CZAL= 0.0	149	CZQ = 0.0	150	CLP = 0.0
151	CLP = 0.0	152	CMAL= 0.0	153	CMQ = 0.0	154	CNP = 0.0	155	CNR = 0.0
156	SF = 0.0	157	VLEN= 0.0	158	REWV= 0.0	159	= 0.0	160	= 0.0
161	= 0.0	162	= 0.0	163	= 0.0	164	= 0.0	165	= 0.0
166	= 0.0	167	= 0.0	168	= 0.0	169	SNT= 75.000	170	SNSC= 75.000
171	SNS1= 75.000	172	SNSW= 2.0000	173	DIST= 0.0	174	PL = 0.0	175	TSCP= 0.25000
176	= 0.0	177	= 0.0	178	= 0.0	179	= 0.0	180	PASS= 4.0000
181	= 0.0	182	SI1= 0.20000	183	SI2= 0.20000	184	SI3= 0.20000	185	SI4= 0.20000
186	= 0.0	187	= 0.0	188	= 0.0	189	= 0.0	190	= 0.0
191	= 0.0	192	MTGB= 1.0000	193	PCSW= 0.0	194	LDF= 0.0	195	LDRF= 0.0
196	FK1= 0.0	197	EK2= 0.0	198	PMPL= 0.0	199	PMPS= 0.0	200	PMPF= 1.5000
201	XF= 0.0	202	APF1= 1.0000	203	APF2= 0.0	204	APR1= 1.0000	205	APR2= 0.0
206	MISF= 0.65000	207	MISR= 0.65000	208	FCCN= 0.20000E-01	209	= 1.0000	210	= 0.0
211	= 0.0	212	= 0.0	213	= 0.0	214	= 0.0	215	= 0.0
216	= 0.0	217	= 0.0	218	= 0.0	219	FFF1= 0.0	220	FFF2= 0.0
221	THF1= 0.0	222	THF2= 0.0	223	= 0.0	224	= 0.0	225	= 0.0
226	= 0.0	227	= 0.0	228	= 0.0	229	0.0	230	= 0.0
231	H1= 2160.0	232	H2= 2160.0	233	LAMP= 0.0	234	AKF1= 1700.0	235	AKF2= 1700.0
236	AKF3= 2000.0	237	AKF4= 2000.0	238	RR1= 1.0000	239	RR2= 1.0000	240	RR3= 1.0000
241	RR4= 1.0000	242	KCF= 0.0	243	KCR= 0.0	244	KSR= 0.0	245	RA1= 0.0
246	RF2= 0.0	247	RR3= 0.84200	248	RR4= 0.0	249	AFK1=-0.36000E-03	250	AFK2= 0.40600E-03
251	AFK3= 0.0	252	ARK1=-0.36000E-03	253	ARK2= 0.40600E-03	254	ARK3= 0.0	255	DFCC= 0.0
256	CFC1= 0.0	257	DFC2= 0.0	258	DFC3= 0.0	259	DRCC= 0.0	260	DRC1= 0.0
261	DRC2= 0.0	262	DRC3= 0.0	263	CPFF= 0.0	264	CP1F= 0.0	265	CP2F= 0.0
266	CPCR= 0.0	267	CP1R= 0.0	268	CP2R= 0.0	269	CRCF= 0.0	270	CR1F= 0.0
271	CR2F= 0.0	272	CRCR= 0.0	273	CR1R= 0.0	274	CR2R= 0.0	275	= 0.0
276	= 0.0	277	LMPN= 0.0	278	TOL = [illegible]	279	TOS1= 0.0	280	= 0.0
281	= 0.0	282	= 0.0	283	= 0.0	284	HFC= 0.0	285	HRC= 0.0
286	DRSW= 0.0	287	AXLE= 0.0	288	QUAL= 1.0000	289	WFFL= 6.0000	290	PCT = 0.50000
291	RA0 = 3054.0	292	RA1 = 9.1600	293	RA2 = [illegible]	294	RA3 = 0.0	295	RA4 = 1.0000

SYMBOLS AND DEFINITIONS OF THE PROGRAM PARAMETERS

Parameter Number	Symbol: Table	Symbol: Equation	Definition or Function (Units)
001	MS	M_S	Total sprung mass (lb/in/sec^2)
002	MUF	M_{UF}	Total front unsprung mass (lb/in/sec^2)
003	MUR	M_{UR}	Total rear unsprung mass (lb/in/sec^2)
004	ZF	Z_F	Static distance between c.g. of sprung mass and spin axis of front wheels in z-direction (in)
005	ZR	Z_R	Static distance between c.g. of sprung mass and spin axis of rear wheels in z-direction (in)
006	A	a	Distance between c.g. of sprung mass and spin axis of front wheels in x-direction (in)
007	B	b	Distance between c.g. of sprung mass and spin axis of rear wheels in x-direction (in)
008	TF	T_F	Front tread width (in)
009	TR	T_R	Rear tread width (in)
010	TS	T_S	Distance between rear axle spring mounts in y-direction (in)
011	IX	I_X	Roll moment of inertia of sprung mass (lb-in-sec^2)
012	IY	I_Y	Pitch moment of inertia of sprung mass (lb-in-sec^2)
013	IZ	I_Z	Yaw moment of inertia of sprung mass (lb-in-sec^2)

Symbols and Definitions of the Program Parameters (cont'd.)

Parameter Number	Symbol: Table	Symbol: Equation	Definition or Function (Units)
014	IXZ	I_{XZ}	Product of inertia of sprung mass (lb-in-sec^2)
015	IR	I_R	Roll moment of inertia of rear unsprung mass, exclude zero for computational purposes (lb-in-sec^2)
016	CF		Viscous damping coefficient for a single front wheel (lb-in-sec) (initialization)
017	RF	R_F	Auxiliary roll stiffness in front suspension (in-lb/radian)
018	CFPR	C'_F	Coulomb damping at each front wheel (lb)
019	KF	K_F	Front suspension spring rate (lb/in)
020	LAMF	λ_F	Front spring rate proportionality factor (initialization)
021	OMFC	Ω_{FC}	Suspension deflection for initial front wheel contact with compression bump stop (in)
022	OMFT	Ω_{FT}	Suspension deflection for initial front wheel contact with rebound bump stop (in)
023	CR		Viscous damping coefficient for a single rear wheel (lb-in-sec) (initialization)
024	RR	R_R	Auxiliary roll stiffness in rear suspension (in-lb/radian)
025	CRPR	C'_R	Coulomb damping at each rear wheel (lb)
026	KR	K_R	Rear suspension spring rate (lb/in)
027	LAMR	λ_R	Rear spring rate proportionality factor (initialization)

Symbols and Definitions of the Program Parameters (cont'd.)

Parameter Number	Symbol: Table	Symbol: Equation	Definition or Function (Units)
028	OMRC	Ω_{RC}	Suspension deflection for initial rear wheel contact with compression bump stop (in)
029	OMRT	Ω_{RT}	Suspension deflection for initial rear wheel contact with rebound bump stop (in)
030	KRS	K_{RS}	Rear roll steer gain (rad/rad), (solid axle)
031	RW	R_w	Undeflected tire radius (in)
032			Unassigned
033	AOMT	$A\Omega_T$	Multiple of tire stiffness where cornering stiffness is constant, front wheels
034	A0	A_0	Constant coefficient in cornering stiffness function, front wheels
035	A1	A_1	Linear coefficient in tire cornering stiffness function, front wheels
036	A2	A_2	Quadratic coefficient in tire cornering stiffness function, front wheels
037	A3	A_3	Linear coefficient in tire camber stiffness function, front wheels
038	A4	A_4	Quadratic coefficient in tire camber stiffness function, front wheels
039 - 040			Unassigned
041	KSC	K_{SC}	Steering column-gear flexibility (in-lb/radian)

Symbols and Definitions of the Program Parameters (cont'd.)

Parameter Number	Symbol: Table	Symbol: Equation	Definition or Function (Units)
042	NG	N_G	Gear ratio of steering gear box
043	LAFC	λ_{FC}	Front spring rate proportionality factor at compression bump stop
044	LAFT	λ_{FT}	Front spring rate proportionality factor at rebound bump stop
045	LARC	λ_{RC}	Rear spring rate proportionality factor at compression bump stop
046	LART	λ_{RT}	Rear spring rate proportionality factor at rebound bump stop
047	IFW	I_{FW}	Moment of inertia of front wheel about the king pin axis (in-lb-sec^2)
048			Unassigned
049	IWF	I_{WF}	Moment of inertia of front wheel about its spin axis (in-lb-sec^2)
050	IWR	I_{WR}	Moment of inertia of rear wheel about its spin axis (in-lb-sec^2)
051	ID	I_D	Moment of inertia of drive line about its spin axis (in-lb-sec^2)
052	AR	$\overline{AR}$	Drive axle ratio
053 - 054			Unassigned

Symbols and Definitions of the Program Parameters (cont'd.)

Parameter Number	Symbol: Table	Symbol: Equation	Definition or Function (Units)
055	PT	$\overline{PT}$	Front wheel caster trail (in)
056	YSA1	y_{SA1}	Distance between kingpin axis and wheel center line, measured along wheel spin axis, right front (in)
057	YSA2	y_{SA2}	Distance between kingpin axis and wheel center line, measured along wheel spin axis, left front (in)
058	PHS1	ϕ_{SA1}	Kingpin inclination angle, right front (radian)
059	PHS2	ϕ_{SA2}	Kingpin inclination angle, left front (radian)
060	CTSW		Caster trail switch: 060 = 1, constant; = 0, function
061 - 062			Unassigned
063 - 074			Initial conditions: p,q,r,u,v,w,x,y,z,θ,ϕ,ψ. Note that z_0 and θ_0 are computed values at t=0 and need not be specified.
075	DT		Integration step size (sec)
076	TN		Maximum run time (sec)
077 - 078	KTI	K_{Ti}	Tire spring rate, front wheels (lb/in)
079 - 080	KTI	K_{Ti}	Tire spring rate, rear wheels (lb/in)
081 - 084	RPSI	RPS_i	Initial wheel rotation rates computed at t=0 (rad/sec)
085	B1	B_1	Load term coefficient of lateral friction coefficient, front tire (1/lb)

Symbols and Definitions of the Program Parameters (cont'd.)

Parameter Number	Symbol: Table	Symbol: Equation	Definition or Function (Units)
086	B2	B_2	Velocity term coefficient of lateral friction coefficient, front tire (1/mph)
087	B3	B_3	Constant term of lateral friction coefficient, front tire (dimensionless)
088	B4	B_4	Quadratic load term coefficient of lateral friction coefficient, front tire ($1/lb^2$)
089 - 091			Initial conditions: $\dot{\delta}_i, \delta_i, \dot{\phi}_R, \delta_{FWi}, \mu_{Xi}, S_i$
092	DELF	δ_{FIN}	Static displacement change in front suspension due to vehicle load configuration (in)
093	DELR	δ_{RIN}	Static displacement change in rear suspension due to vehicle load configuration (in)
094 - 106			Initial conditions: $\dot{\delta}_i, \delta_i, \dot{\phi}_R, \delta_{FWi}, \mu_{Xi}, S_i$
107	PPRT		Parameter table, print control: 107 = 1, print; = 0, no print
108 - 109			Unassigned
110	TQMX		Maximum available drive torque (in-lb)
111	KTQ	K_{TQ}	Drive torque gain factor (in-lb)/(in/sec)
112	VC	V_C	Commanded velocity (mph)
113	MTSW		Multiplier on front wheel aligning torque, M_{Ti}

Symbols and Definitions of the Program Parameters (cont'd.)

Parameter Number	Symbol: Table	Symbol: Equation	Definition or Function (Units)
114	DSWM	δ_{SW}	Maximum steering wheel angle (degrees), (except sinusoidal steer)
115	TST		Initial time of steer (sec), (except sinusoidal steer)
116	DSLP		Time to achieve maximum steer angle, equivalent to steer rate, exclude zero (sec), (except sinusoidal steer)
117	CGAM		Initial time of brake application (sec), (except drastic brake and steer)
118	CS		Initial time of brake application (sec), (except drastic brake and steer)
119	TQR	$\overline{TQ}_{Bi}$	Rear wheel brake torque (in-lb)
120	TQF	$\overline{TQ}_{Bi}$	Front wheel brake torque (in-lb)
121	PFL		Applied brake pressure (psi)
122	T1		Drive torque control (sec)
123	DSW		Sinusoidal steer amplitude (degrees)
124	TSW		Duration of sinusoidal steer (sec)
125	ISW5		VHTP sinusoidal steer enable code: 125 = 1, enable; = 0, disable
126	SW15		VHTP roll over enable code: 126 = 1, enable; = 0, disable
127	PQSW		Equation suppress option, 127 = 0, none; 1, $\dot{p} = 0$, 2, $\dot{q} = 0$; 3, $\dot{p} = \dot{q} = 0$

Symbols and Definitions of the Program Parameters (cont'd.)

Parameter Number	Symbol: Table	Symbol: Equation	Definition or Function (Units)
128	VTPS		VHTP switch
129	VHTP		VHTP index
130	AMCR	M_{CR}	Mass of steering system connecting rod (lb-sec^2/in)
131	ESP	ϵ_{SP}	Free play in steering gear box (rad)
132	KSL1	K_{SL1}	Steering linkage flexibility, right front wheel (in-lbs/radian)
133	KSL2	K_{SL2}	Steering linkage flexibility, left front wheel (in-lb/radian)
134 - 135	AAI	a_{Li}	Length of steering linkage arms (in)
136	CCR	C_{CR}	Viscous damping coefficient of steering system connecting rod (lb/in/sec)
137	CFCR	C_{FCR}	Coulomb damping of steering system connecting rod (lb)
138	AP	a_P	Length of Pitman arm (in)
139 - 140	EPI	ϵ_{Pi}	Free play in steer of front wheel (rad)
141 - 142	ERRI		Auxiliary roll stiffness play
143 - 144	AMLI	M_{1i}	Unbalanced wheel mass (lb-sec^2/in)
145	RRIM	R_{RIM}	Wheel rim radius (in)
146	RWR	R_{WR}	Wheel rim width (in)

Symbols and Definitions of the Program Parameters (cont'd.)

Parameter Number	Symbol: Table	Symbol: Equation	Definition or Function (Units)
147 - 168			Unassigned
169	SNT		Tire data surface skid number
170	SNS0		Simulated vehicle surface skid number
171	SNS1		Simulated vehicle surface skid number
172	SNSW		Skid patch switch: 172 = 2, disable; 1, front approach; 0, side approach
173	DIST		Initial distance between car and skid patch (in)
174	PL		Skid patch length (in)
175	TSCP		Computer time scale factor
176 - 179			Unassigned
180	PASS		Number of passes through integration routine
181			Unassigned
182 - 185	SII	SI_i	Wheel slip ratio at which peak braking coefficient of friction occurs
186 - 191			Unassigned
192	MTQB		Brake force rate, exclude zero for computational purposes (psi/sec)
193	DRSW		Driver control switch: 193 = 0, disable; 1, enable

Symbols and Definitions of the Program Parameters (cont'd.)

Parameter Number	Symbol: Table	Symbol: Equation	Definition or Function (Units)
194	LDF		Lateral displacement feedback gain (deg/in), 193 = 1
195	LDRF		Lateral displacement rate feedback gain (deg/in/sec), 193 = 1
196 - 197	EKI	ϵ_{Ki}	Static front wheel toe bias angles (degrees)
198	BMPL		Length of single road bump (in)
199	BMPS		Distance between road bumps (in)
200	BMPH		Road bump height (in)
201	XB		Initial distance from car to first bump (in)
202	APF1	P_{BF1}	Front tire peak braking coefficient of friction, constant term (dimensionless)
203	APF2	P_{BF2}	Front tire peak braking coefficient of friction, linear term (1/lb)
204	APR1	P_{BR1}	Rear tire peak braking coefficient of friction, constant term (dimensionless)
205	APR2	P_{BR2}	Rear tire peak braking coefficient of friction, linear term (1/lb)
206	MUSF	μ_{SF}	Front tire sliding coefficient of friction
207	MUSR	μ_{SR}	Rear tire sliding coefficient of friction
208 - 218			Unassigned

Symbols and Definitions of the Program Parameters (cont'd.)

Parameter Number	Symbol: Table	Symbol: Equation	Definition or Function (Units)
219 - 220	FEEI	$\Delta\phi_i$	Front wheel camber bias angles (degrees)
221 - 222	THEI	$\Delta\theta_i$	Front wheel caster bias angles (degrees)
223 - 230			Unassigned
231 - 232	HI	H_i	Viscous damping derivative in front wheel (lb/in/sec)
233			Unassigned
234 - 235	AKFI	K_{Fi}	Front suspension spring rates (lb/in)
236 - 237	AKFJ	K_{Ri}	Rear suspension spring rates (lb/in)
238 - 241	BRI	λ_{Bi}	Brake torque multiplier for wheel i
242	KCF	K_{CF}	Front lateral force compliance camber coefficient (rad/lb)
243	KCR	K_{CR}	Rear lateral force compliance camber coefficient (rad/lb)
244	KSR	K_{SR}	Rear aligning torque compliance steer coefficient (rad/in-lb)
245	RB1	RB_1	Load term coefficient of lateral friction coefficient, rear tire (1/lb)
246	RB2	RB_2	Velocity term coefficient of lateral friction coefficient, rear tire (1/mph)

Symbols and Definitions of the Program Parameters (cont'd.)

Parameter Number	Symbol: Table	Symbol: Equation	Definition or Function (Units)
247	RB3	RB_3	Constant term of lateral friction coefficient, rear tire (dimensionless)
248	RB4	RB_4	Quadratic load term coefficient of lateral friction coefficient, rear tire ($1/lb^2$)
249	AFK1	A_{F1}	Aligning torque coefficient, front tire ($in\text{-}lb/lb^2$)
250	AFK2	A_{F2}	Aligning torque coefficient, front tire ($in\text{-}lb/lb^2$)
251	AFK3	A_{F3}	Aligning torque coefficient, front tire (in-lb/lb sq root (rad))
252	ARK1	A_{R1}	Aligning torque coefficient, rear tire ($in\text{-}lb/lb^2$)
253	ARK2	A_{R2}	Aligning torque coefficient, rear tire ($in\text{-}lb/lb^2$)
254	ARK3	A_{R3}	Aligning torque coefficient, rear tire (in-lb/lb sq root (rad))
255	OFC0	OF_0	Overturning moment coefficient, front tire (in-lb)
256	OFC1	OF_1	Overturning moment coefficient, front tire ($in\text{-}lb/lb^2$)
257	OFC2	OF_2	Overturning moment coefficient, front tire ($in\text{-}lb/lb^2\text{-}rad$)
258	OFC3	OF_3	Overturning moment coefficient, front tire (in-lb/lb-rad)
259	ORC0	OR_0	Overturning moment coefficient, rear tire (in-lb)
260	ORC1	OR_1	Overturning moment coefficient, rear tire ($in\text{-}lb/lb^2$)

Symbols and Definitions of the Program Parameters (cont'd.)

Parameter Number	Symbol: Table	Symbol: Equation	Definition or Function (Units)
261	ORC2	OR_2	Overturning moment coefficient, rear tire (in-lb/lb^2-rad)
262	ORC3	OR_3	Overturning moment coefficient, rear tire (in-lb/lb-rad)
263	CP0F	P_{F0}	Anti-pitch coefficient, front suspension (dimensionless)
264	CP1F	P_{F1}	Anti-pitch coefficient, front suspension, (1/in)
265	CP2F	P_{F2}	Anti-pitch coefficient, front suspension, (1/in^2)
266	CP0R	P_{R0}	Anti-pitch coefficient, rear suspension (dimensionless)
267	CP1R	P_{R1}	Anti-pitch coefficient, rear suspension (1/in)
268	CP2R	P_{R2}	Anti-pitch coefficient, rear suspension (1/in^2)
269	CR0F	R_{F0}	Anti-roll coefficient, front suspension (dimensionless)
270	CR1F	R_{F1}	Anti-roll coefficient, front suspension (1/in)
271	CR2F	R_{F2}	Anti-roll coefficient, front suspension (1/in^2)
272	CR0R	R_{R0}	Anti-roll coefficient, rear suspension (dimensionless)
273	CR1R	R_{R1}	Anti-roll coefficient, rear suspension (1/in)
274	CR2R	R_{R2}	Anti-roll coefficient, rear suspension (1/in^2)
275 - 276			Unassigned
277	BMPN		Number of bumps in bump grid

Symbols and Definitions of the Program Parameters (cont'd.)

Parameter Number	Symbol: Table	Symbol: Equation	Definition or Function (Units)
278	TQB0		Time of brake application in combined drastic brake and steer VHTP
279	TQB1		Time of brake release in combined drastic brake and steer VHTP
280 - 283			Unassigned
284	HFC	h_{FC}	Distance between ground and the roll center of the front suspension (in)
285	HRC	h_{RC}	Distance between center of rear axle and the roll center of the rear suspension (in)
286			Unassigned
287	AXLE		Solid rear axle/split rear axle option code, solid=1, split=2
288 - 289			Unassigned
290	ROMT	$R\Omega_T$	Multiple of maximum tire load where cornering stiffness is constant, rear wheels
291	RA0	RA_0	Constant coefficient in tire cornering stiffness, rear wheels
292	RA1	RA_1	Linear coefficient in tire cornering stiffness function, rear wheels
293	RA2	RA_2	Quadratic coefficient in tire cornering stiffness function, rear wheels

Symbols and Definitions of the Program Parameters (cont'd.)

Parameter Number	Symbol		Definition or Function (Units)
	Table	Equation	
294	RA3	RA_3	Linear coefficient in tire camber stiffness function, rear wheels
295	RA4	RA_4	Quadratic coefficient in tire camber stiffness function, rear wheels

REFERENCES

A-1. Bernard, J.E., Winkler, C.B., and Fancher, P.S. A Computer Based Mathematical Method for Predicting the Directional Response of Trucks and Tractor-Trailers. Phase II , Highway Safety Research Institute, Univ. of Michigan, June 1, 1973.

A-2. Wier, D.H., et al. Analysis of Truck and Bus Handling. Vol. II, Final Report for Contract No. DOT-HS-242-2-421, prepared for National Highway Traffic Safety Administration, June 1974.

A-3. "Super Cushion-Air Springs." Goodyear Tire and Rubber Co., Catalogue #821-947-174 dated July 1971.

A-4. Summer Conference Notes on "Motor Vehicle Performance Measurement and Prediction." Highway Safety Research Institute, Univ. of Michigan, July 22-26, 1974.

A-5. Rasmussen, R.E. "Typical Vehicle Parameters for Dynamic Studies." General Motors Proving Ground, A-2542, April, 1970.

A-6. Bohn, P.F. and Keenan, R. J. Hybrid Computer Vehicle Handling Program. Final Report to National Highway Traffic Safety Administration for Contract No. DOT-HS-213-3-695, Applied Physics Laboratory, Johns Hopkins University, July 1974.

APPENDIX B

TIRE TESTING FACILITIES

B.1 Flat-Bed Tire Tester

The HSRI flat-bed tire tester, shown earlier in Figure 2.1, provides precise laboratory measurements of the mechanical properties of standing, rolling, and slipping tires. It can accommodate tires up to 44 in. OD with vertical loads to 10,000 lb. The slip angle is adjustable in 1-degree increments from 0 ± 30 degrees and in 15-degree increments out to + 90 degrees. Camber angles can be varied from -10 to +20 degrees in 1-degree increments. The test wheel is powered by a 13,000 ft-lb hydraulic system which is driven independently of the flat-bed table to create longitudinal slip conditions.

The machine is instrumented to measure the three force and three moment components developed by the tire, in addition to test wheel drive torque (T), rolling height (R_h), and wheel angular velocity (ω). The positions of the six load cells used to measure the forces and moments are shown in Figure B.1.

The bed surface is 100 grit tungsten carbide bonded directly to the aluminum table with no intervening paper or glue. The bed velocity is 2.11 ft/s or 1.44 mph. Thus the flat-bed machine is useful for exploring the small slip or "elastic" mechanical properties of tires, which are essentially speed independent, and for measuring the ultimate force and moment capabilities of tires at higher slip conditions. The magnitude of these large slip forces and moments will be considerably lower at highway velocities.

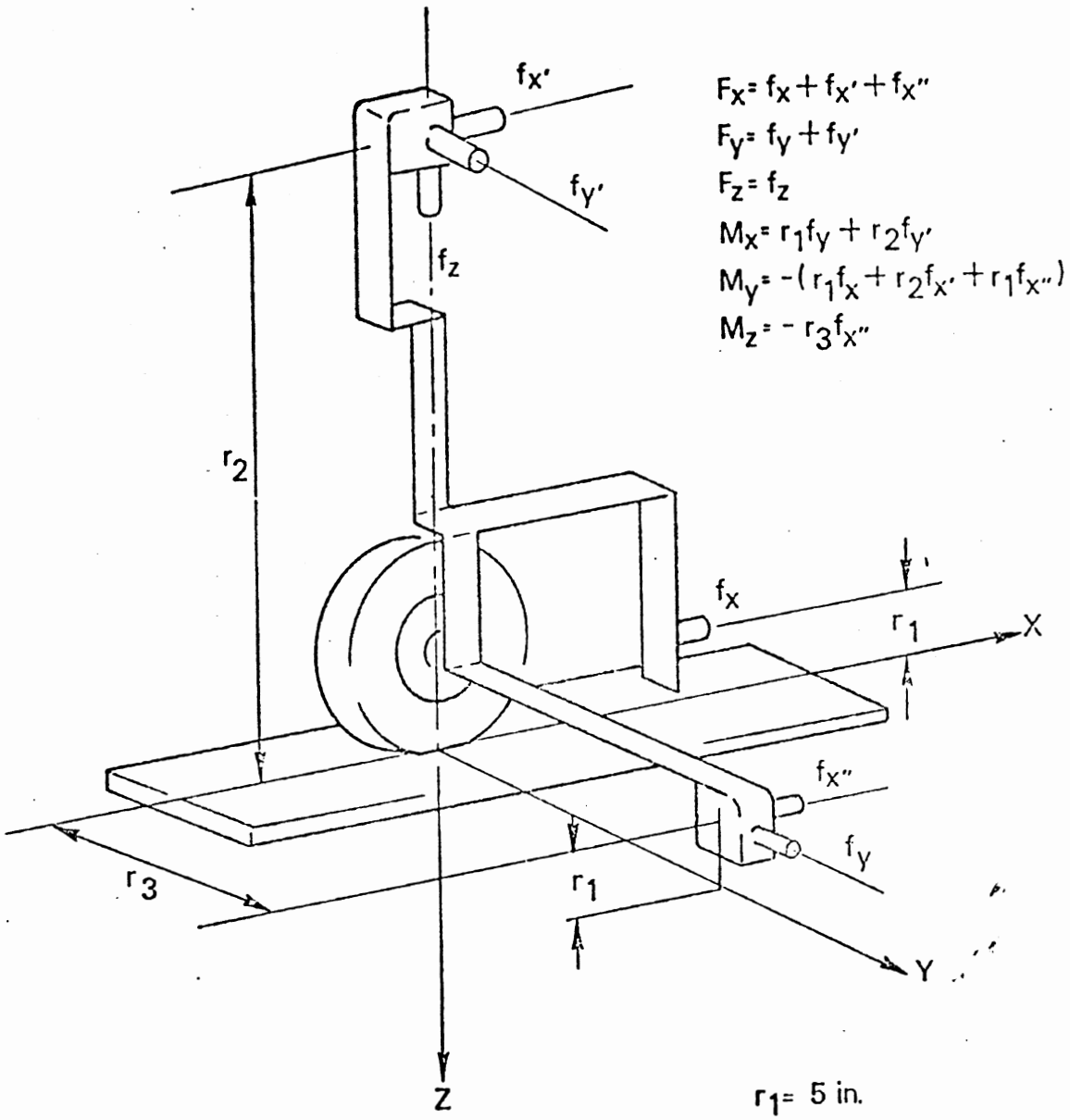

Figure B.1. Location of Force Transducer on Test Wheel Frame.

B.2 Mobile Truck Tire Dynamometer

The HSRI Mobile Truck Tire Dynamometer consists of a tractor, semi-trailer vehicle which permits investigation of either longitudinal or lateral traction characteristics of heavy truck tires. The system, shown previously in Figure 2.2, permits measurement of longitudinal properties by way of the trailer-configured dynamometer as it is towed and serviced by the instrumented tractor. Mounted on the same tractor is a structure supporting a lateral traction measurement system, as diagrammed in the plan view of Figure B.2. Each test system is basically designed to expose a truck tire specimen to a set of operating conditions which cover the full range of possible loads, velocities, longitudinal or angular slip, and pavements such as can be encountered under either normal or emergency situations on the highway.

The longitudinal traction dynamometer, shown in Figure B.3, is a welded trailer structure of pipe and plate sections, designed for economy of construction and for stiffness. The test wheel is situated approximately at the trailer c.g. position and is supported by a parallelogram suspension, shown in Figure B.4. The parallelogram linkage suspension provides kinematic isolation of forces while assuring a zero inclination (camber) of the test wheel plane. The use of an air spring loading mechanism permits a controllable vertical load condition and a low spring rate coupling between the foundation vehicle and the test wheel.

The basic design principle behind air spring loading, then, is that the machine incorporates a relatively "soft" loading member (which is also virtually frictionless) and thereby attains features which serve to enhance the quality of the vertical load condition which is imposed upon the test tire. With such a mechanism, it is then straightforward to obtain precision selections of vertical load through the use of commercially available precision regulators.

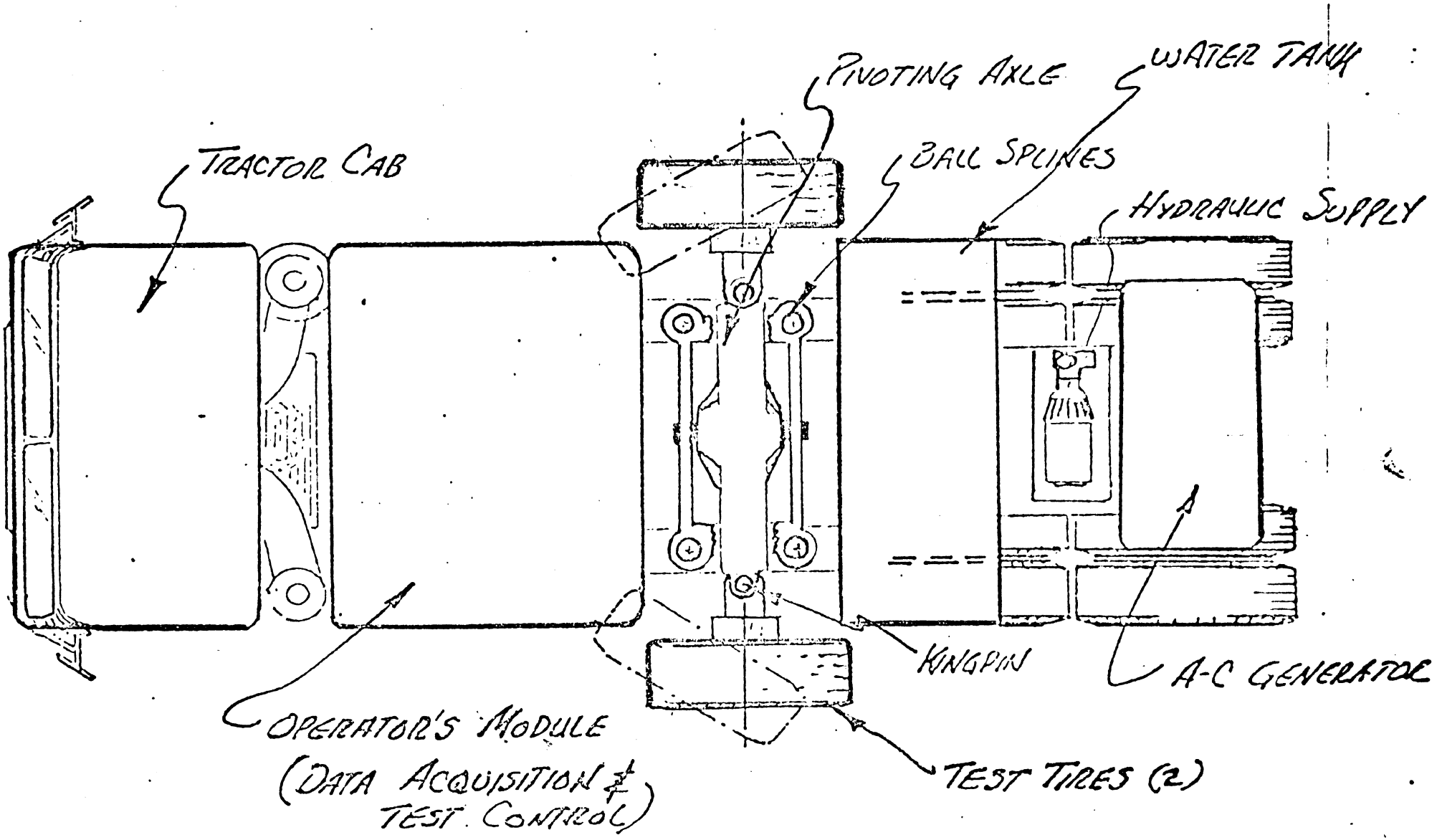

Figure B.2. Plan View of Mobile Truck Tire Side Force Dynamometer

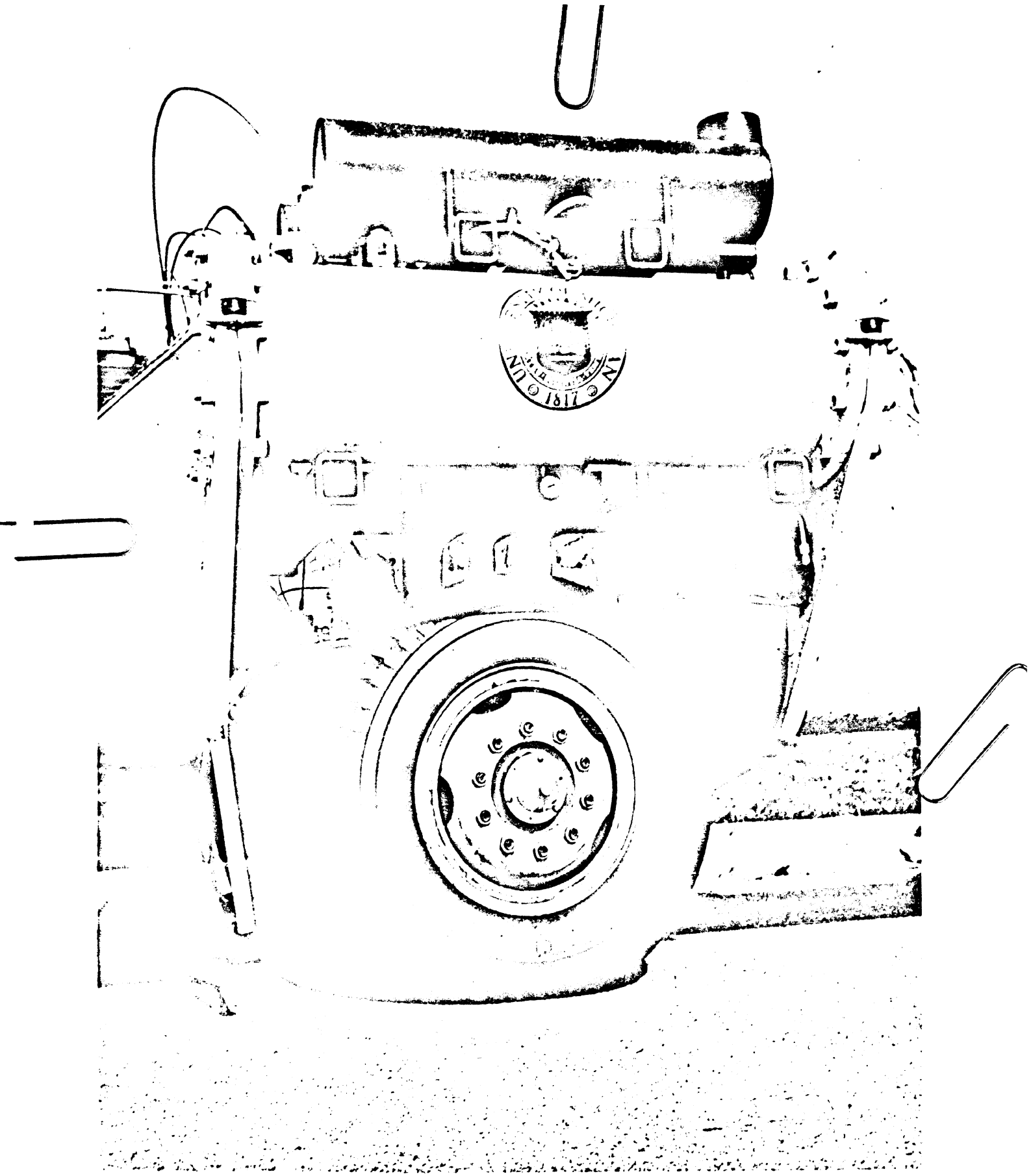

Figure B.3. Test wheel mounted on the longitudinal traction dynamometer.

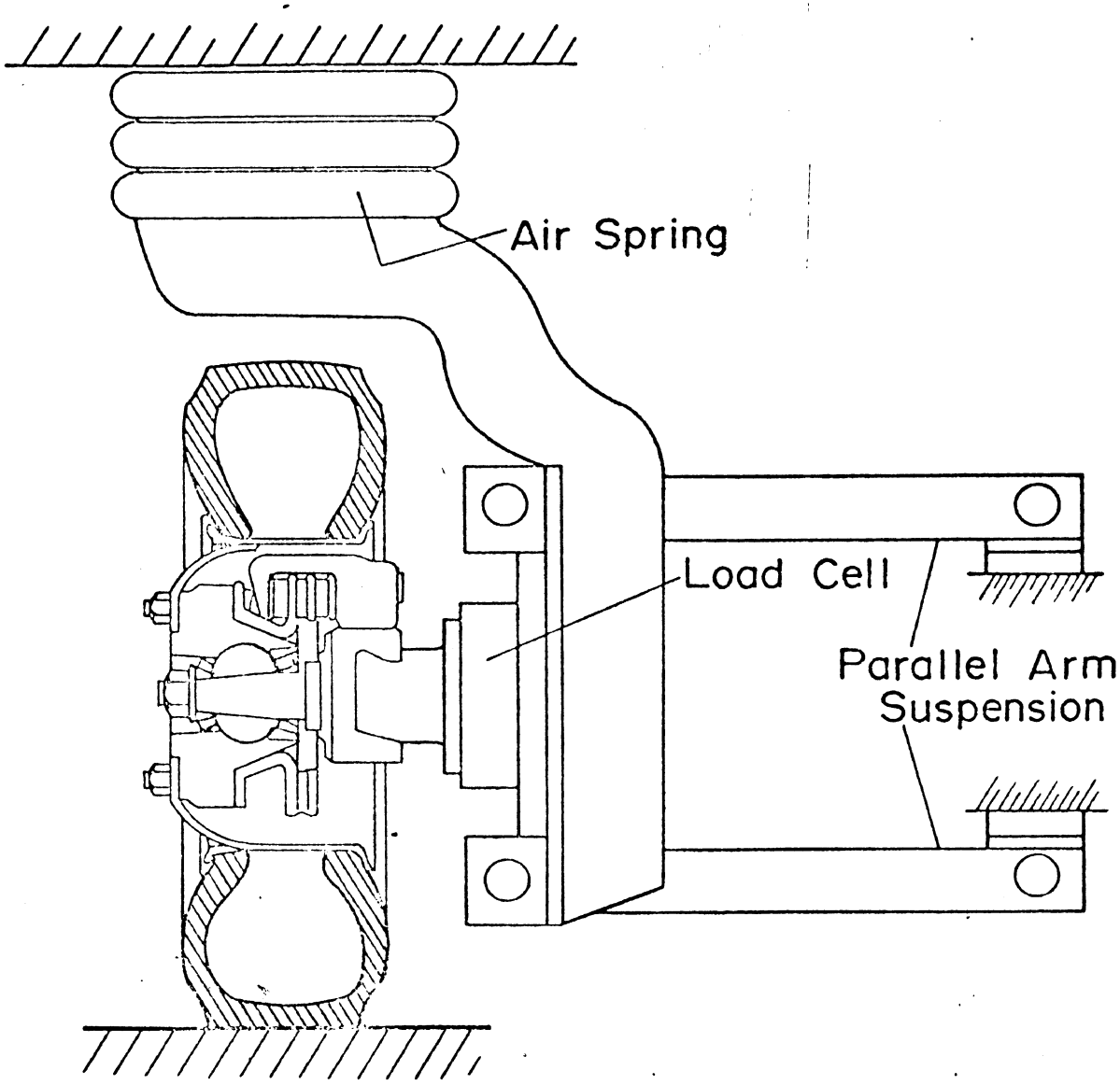

Figure B.4. Test wheel suspension.

The test trailer is capable of mounting any light or heavy truck tire which is:

a) less than 46 inches in free diameter, and

b) 18 inches or less in maximum section width.

Tires can be loaded to a maximum level of 20,000 lb., although, to date, brake torque limitations have prevented the lockup of tires on high friction surfaces at loads exceeding about 15,500 lbs.

The lateral traction dynamometer, shown schematically in Figure B.5, mounts two tire samples on opposing steerable spindles outboard of the tractor's wheel tracks. The two tires are "toed-in" together by an electrohydraulic servo system covering a slip angle range from -1° to +30°.

The test wheel spindles are mounted upon a solid cross-axle which is constrained by a single longitudinal pivot pin. The pin itself is fastened within a cage which can move only vertically, as constrained by a set of four ball-spline bearings. The vertically-"floating" cage is then loaded through inflation of a set of air springs.

The "pivot axle" arrangement provides for a load equalization between both tires while also providing a higher frequency response to road profile irregularities which are uncorrelated, side to side. The "floating cage" provides the needed kinematic isolation of the vertical load from forces in the ground plane by virtue of its rectilinear antifriction constraints. The air spring loading configuration again provides for precision load selection while incorporating a low spring rate coupling between the unsprung mass(es) and the foundation vehicle.

The system permits mounting of any light or heavy truck tire which is less than 48" in diameter and 18" in cross-section width. The measurement of tire force and moment conditions is achieved by way of a serial multicomponent load cell which transduces lateral and vertical force components as well as aligning moment.

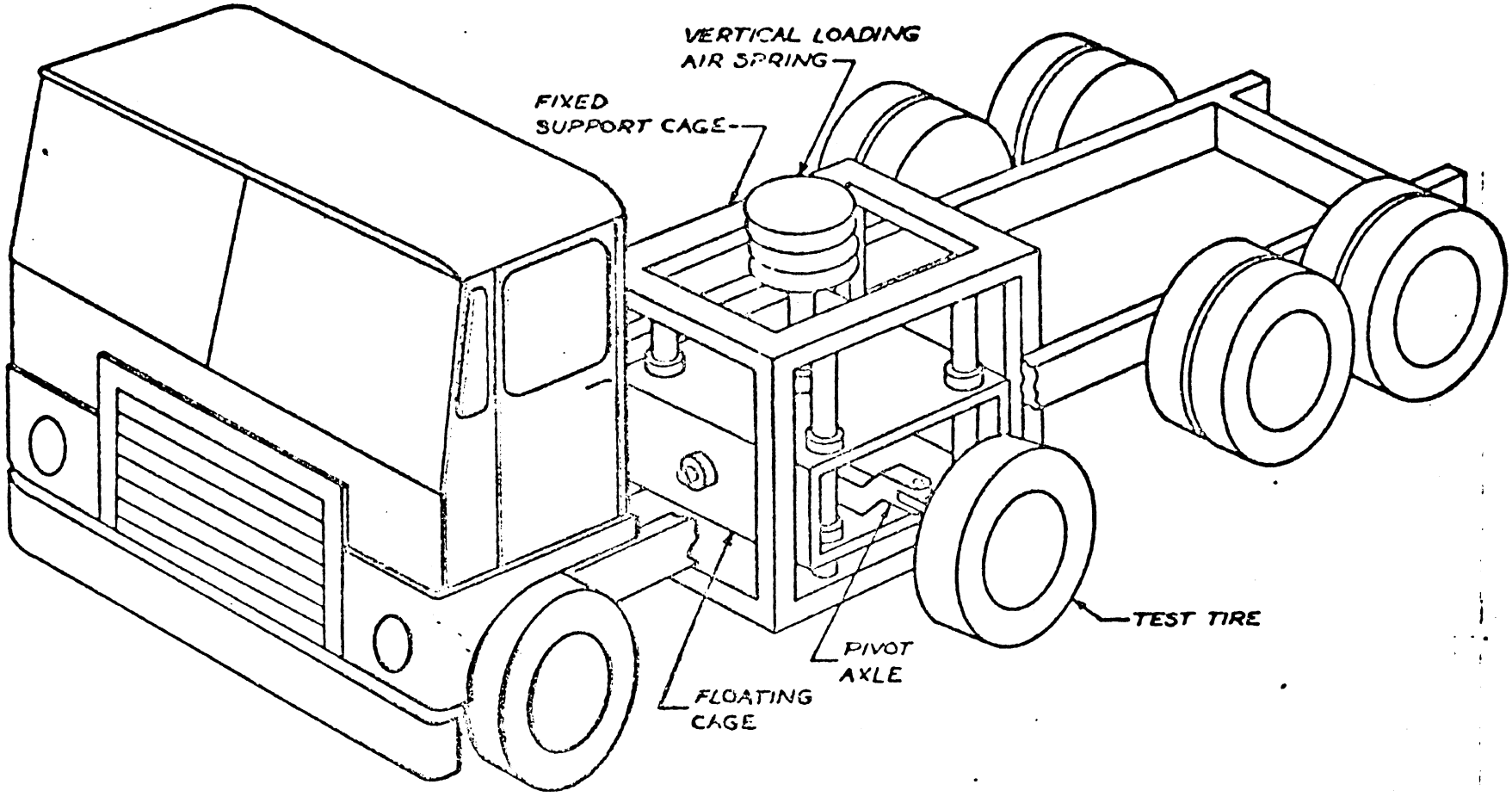

Figure B.5. Major Components of the Side Force Dynamometer Assembly.

Data signals from either the longitudinal or lateral test apparatuses are conditioned and recorded within a tractor-mounted module. The module serves as a self-contained data acquisition laboratory as well as the operator's station for selecting and initiating test control functions. As shown in Figure B.6., the operator's module provides an array of hard-wired electrical controls in addition to certain pneumatic and hydraulic control elements.

B.3 TIRF Test Facility

A dimensional view of the TIRF facility is shown in Figure B.7. The primary features of the machine are as follows.

B.3.1 Tire Positioning System. The tire, wheel, force sensing balance and hydraulic motor to drive or brake the tire are mounted in the movable upper head. The head provides steer, camber and vertical motions to the tire. These motions (as well as vertical loading) are servo controlled and are programmable for maximizing test efficiency. The ranges of the position variables, the rates at which they may be adjusted, and other information are shown in Table B.1.

Table B.1

TIRF CAPABILITIES

CHARACTERISTIC	RANGE
TIRE SLIP ANGLE (α)	$\pm 30^{o}$
TIRE CAMBER ANGLE (γ)	$+28, -30^{o}$
TIRE SLIP ANGLE, RATE ($\dot{\alpha}$)	10^{o}/sec
TIRE CAMBER ANGLE RATE ($\dot{\gamma}$)	$> 3.5^{o}$/sec
TIRE LOAD RATE (L)	2000 lb/sec/2"/sec
SIMULATED ROAD SPEED (V)	0-200 mph
TIRE OUTSIDE DIAMETER	46" MAX.
TIRE TREAD WIDTH	24" MAX.
BELT WIDTH	28"

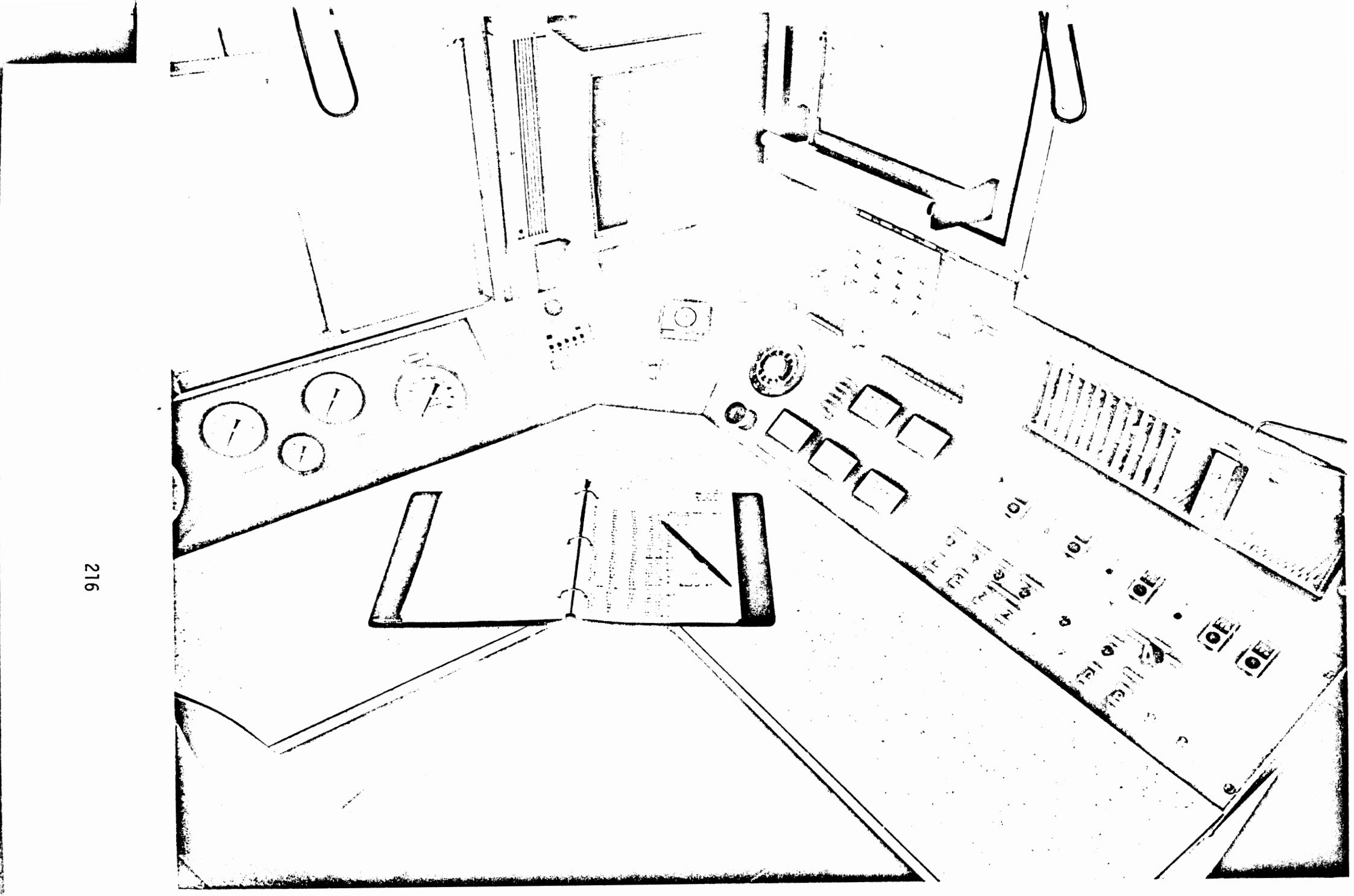

Figure B.6. Data acquisition module.

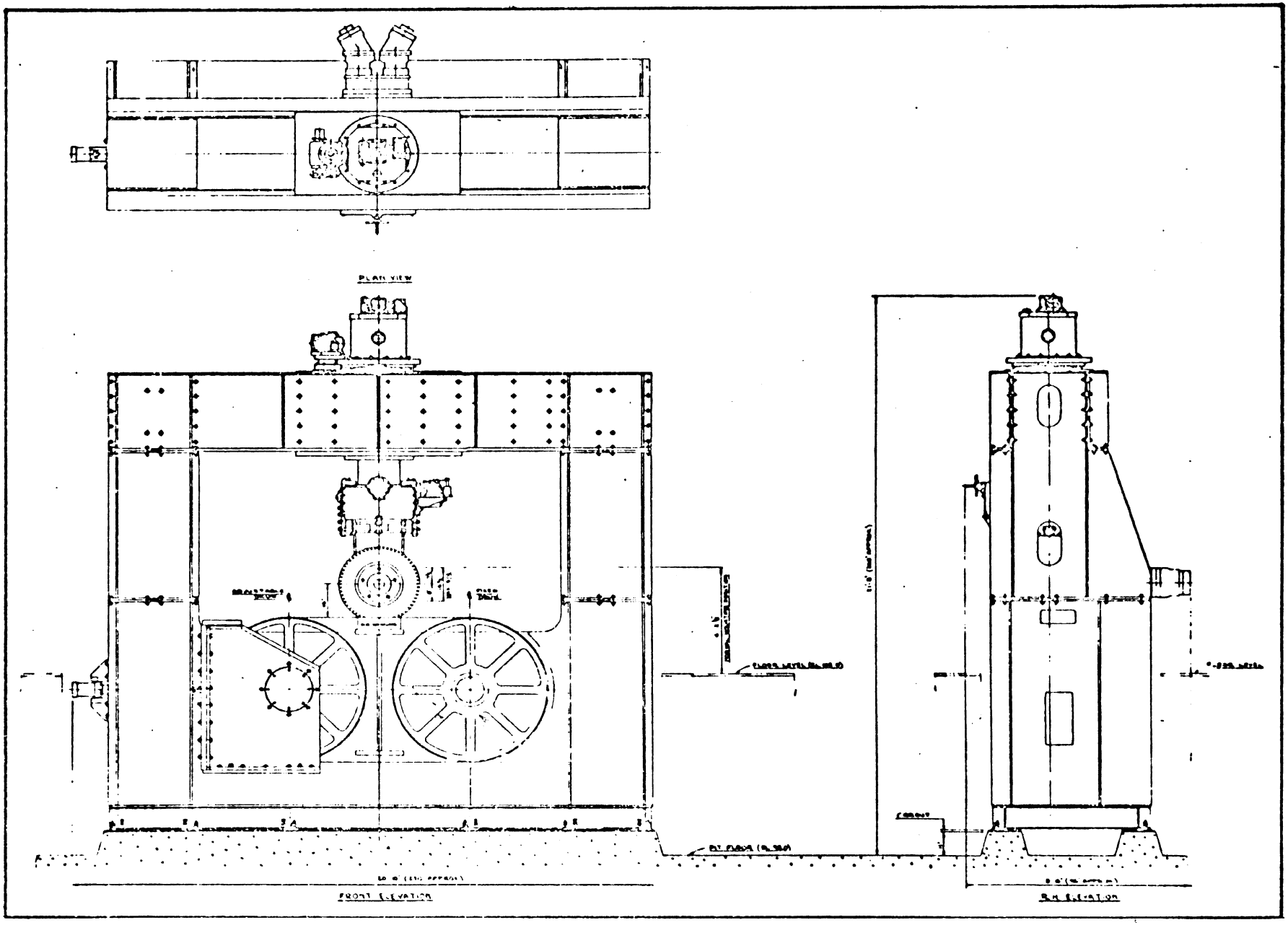

Figure B.7. TIRE RESEARCH MACHINE

B.3.2 Roadway. The 28-inch-wide roadways are made up of stainless steel belts covered with materials which simulate the surface texture and frictional properties of actual road surfaces. The belts are maintained flat to within 1 to 2 mils under the tire patch by the restraint provided by an air bearing pad which is beneath the belt in the tire patch region. The roadway is driven by one of the two 67 in. diameter drums over which it runs. Sufficient power is available so full locked-wheel braking of passenger car-size tires may be accomplished. The road speed is servo controlled; it may be programmed to be constant or varied.

The surfaces usually used are "Safety Walk."* These surfaces have excellent microtexture giving a wet skid number** of about 60 in the untreated condition. The surfaces are honed to reduce the wet skid number to lower values (typically surfaces of skid number 50 and 30 are used).

B.3.3 Tire-Wheel Drive. A drive system which is independent of the roadway drive is attached to the tire-wheel shaft. This separate drive allows full variation of tire slip both in the braking and driving modes. The tire slip ratio, referenced to road speed, is under servo control.

B.3.4 Balance System. A six-component strain gauge balance surrounds the wheel drive shaft. Three orthogonal forces and three corresponding moments are measured through this system. A fourth moment, torque, is sensed by a torque link in the wheel drive shaft. The load ranges of the basic passenger car and truck tire balances are shown in Table B.2. Transfer of forces and moments from the balance axis-system to the conventional SAE location at the tire-roadway interface is in the data reduction computer program.

---

*Manufactured by the 3M Company.

**At 40 mph and 0.020" water depth using the ASTM E-501 Standard Pavement Traction Tire.

Table B.2

BALANCE SYSTEM CAPABILITY

COMPONENT	PASSENGER CAR TIRE BALANCE	TRUCK TIRE BALANCE
TIRE LOAD (L)	4000 lb	12,000 lb
TIRE TRACTIVE FORCE	±4000 lb	9000 lb
TIRE SIDE FORCE	±4000 lb	8000 lb
TIRE SELF ALIGNING TORQUE	±500 lb ft	1000 lb ft
TIRE OVERTURNING MOMENT	±1000 lb ft	2000 lb ft
TIRE ROLLING RESISTANCE MOMENT	±200 lb ft	400 lb ft

B.3.5 System Operation.

Data Acquisition Program (DAP) Control

The data acquisition program (DAP) is a software system which controls machine operation and logs data during tests. DAP controls test operations by means of discrete setpoints which are generated in the computer by the program. These setpoints are sent to the machine servos which respond and establish tire test conditions. After the setpoints are sent to the servos, a delay time is provided which starts after the machine variables have reached a steady-state value within predetermined tolerances. This allows the system to stabilize before data are taken. After data are taken, the next set of test conditions is established and testing continues.

One or two variables can be changed during DAP testing. The other test parameters are kept fixed throughout the test. Up to twenty data points can be used for each variable in a run.

A data reduction program is used to operate on the raw data collected during testing. These new data are reduced to forces and moments in the proper axis system and all variables are scaled

to produce quantities with engineering units. Raw and reduced data are temporarily stored in a disc file. Both reduced and raw data can be transferred to magnetic tape and maintained as a permanent record.

Reduced data points can be listed, plotted, and curves can be fitted to the points. All of the standard Calspan plots can be generated from DAP test data.

Data lists and plots are displayed on the oscilloscope screen of a CRT console. Hard copies of this information can be made off this display.

Continuous Sampling Program (CSP) Control

The continuous sampling program (CSP) is a software system which controls machine operation and continuously logs data during tests. Test variables can be constant or changed at rapid rates. One or all variables can be changed during a test. Data can be sampled at rates up to 100 samples per second. Pauses are used so that data can be logged during desired intervals of the test.

CSP testing can be conducted quickly which in turn reduces tire wear during severe tests. The high rate of data sampling also permits limited dynamic measurements to be made during testing.

Two parameter plots of data can be made. Carpet and family plots of test data cannot be made with this program at the present time. CSP data will also reflect time effects if tire characteristics are a function of the rate of change of testing variables.

Data reduction is accomplished in a manner similar to that employed in DAP testing.